ASPECTS OF FERMI ARCS AND SURFACES FROM THE PERSPECTIVE OF GAUGE-GRAVITY DUALITY

A
Thesis Submitted
in Partial Fulfillment of the Requirements
for the Degree of
DOCTOR OF PHILOSOPHY

By

WADBOR WAHLANG

Under the Supervision of

Dr. Sayan Chakrabarti

Department of Physics
Indian Institute of Technology Guwahati
Guwahati 781 039, Assam, India

To **Batrity**

who can read most of the text in this thesis, but will probably not understand much of its meaning;

and

to **Papa**

who cannot read or understand any of the text in this thesis, but filled with lots of love and appreciation for my work.

Declaration

I hereby declare that the thesis entitled "**Aspects of Fermi arcs and surfaces from the perspective of Gauge-Gravity Duality**", submitted by me to the *Indian Institute of Technology Guwahati*, for the award of the degree of Doctor of Philosophy, are original except where specific reference is made to the work of others and is carried out by me under the supervision of Dr Sayan Chakrabarti. The content of this thesis, in full or in parts, have not been submitted to any other University or Institute for the award of any degree or diploma.

Signed: ______________________________

Wadbor Wahlang
Roll No. 146121025
Department of Physics,
Indian Institute of Technology Guwahati,
Guwahati, Assam-781039, India.

Date: ______________________________

Certificate

This is to certify that the thesis entitled "**Aspects of Fermi arcs and surfaces from the perspective of Gauge-Gravity Duality**", submitted by **Wadbor Wahlang**, a research scholar in the *Department of Physics*, *Indian Institute of Technology Guwahati*, for the award of the degree of Doctor of Philosophy, is a record of an original research work carried out by him under my supervision and guidance. The thesis has fulfilled all requirements as per the regulations of the institute and in my opinion has reached the standard needed for submission. The results embodied in this thesis have not been submitted to any other University or Institute for the award of any degree or diploma.

Signed: ________________________________

Supervisor: Dr. Sayan Chakrabarti
Department of Physics,
Indian Institute of Technology Guwahati,
Guwahati-781039, Assam, India.

Date: ________________________________

List of Publications

Articles included in the Thesis :

1. S. Chakrabarti, and D. Maity, **W. Wahlang**, " Probing the holographic Fermi arc with scalar field: numerical and analytical study", *Journal of High Energy Physics* **07** (2019), 037. doi:10.1007/JHEP07(2019)037, arXiv:1902.08826 [hep-th].
2. S. Chakrabarti, and D. Maity, **W. Wahlang**, "Studying the holographic Fermi surface in the scalar induced anisotropic background", *Physics Letters B* **827** (2022), 136990. doi:10.1016/j.physletb.2022.136990, arXiv:2108.10043 [hep-th].
3. **W. Wahlang**, "Evolution of holographic Fermi surface from non-minimal couplings," *European Physical Journal C* (2022). doi:10.1140/epjc/s10052-022-10304-1, arXiv:2112.05097 [hep-th].
4. S. Chakrabarti, and D. Maity, **W. Wahlang**, "A note on the effects of magnetic field on holographic fermions with dipole-like coupling", Submitted to Journal arXiv: 2204.06756 [hep-th].

Outside Thesis :

1. **W. Wahlang**, Piyush A. Jeena and S. Chakrabarti, "Quasinormal modes of scalar and Dirac perturbations of Bardeen de Sitter black holes", *International Journal of Modern Physics D*, **26** (2017) no.14, 1750160. doi:10.1142/S0218271817501607, arXiv:1703.04286 [gr-qc].

Conferences and Talks :

◇ XXI **DAE - BRNS High Energy Physics Symposium** at Indian Institute of Technology, Guwahati - 2014.

◇ IAGRG - **The Era of Gravitational Waves** at Indian Institute of Technology, Guwahati - 2017.

◇ XXIII **DAE - BRNS High Energy Physics Symposium** at Indian Institute of Technology, Madras - 2018.

◇ IAGRG - **New Eras in Cosmology and Multi-messenger Astronomy** at Birla Institute of Technology and Science Pilani, Hyderabad - 2019.

◇ Talk given at Indian Institute of Technology, Madras - 2019.

Acknowledgements

At the very end of my journey as a PhD student, I would like to express my deepest gratitude to the following people who have helped and accompanied me over many years, both at home and at the Indian Institute of Technology, Guwahati.

First and foremost, I am indebted to my supervisor, Dr S.K. Chakrabarti, and my mentor, Dr D. Maity, for teaching me and boosting my interest in my research. This thesis would not have been possible without their scientific ideas, advice, and tons of patience. I would also like to express my sincere thanks to all the DPPC members for their questions, advice, and constructive criticism, which led to many improvements in the subject and communication skills.

Secondly, I would not be in this position today had it not been for the immense love, patience, and care I received from my wife, Batrity Khongwar. Also, I extend my gratitude to my parents and uncle for the faith and support they gave me throughout my years. I am very grateful to John McGreevy, Askar Illiasov, Alexander Krikun, and Tomas Andrade for helping me with numerical computation. Thanks to Matteo Baggioli for teaching me various important elements of AdS/CFT and for an illuminating discussion on the subject at IIT Madras.

Last but not least, I am grateful to my fellow PhD students, my juniors, seniors, batchmates, the faculty, office and technical staff at IIT Guwahati. They have made my experience more enjoyable. I could not forget the tasty dinner and the tea sessions we had with them, during which we shared our interests and had many stimulating conversations. I would also like to thank my family and friends for their encouragement, endless love and support, and for always keeping my spirits up. I could thank many more people, but time, space, and modesty compel me to stop here.

Sincerely,

WADBOR WAHLANG

Abstract

Despite several efforts, strongly correlated systems still pose as one of the most challenging conundrums in theoretical physics. The difficulty in modelling and solving the problems has grown even more after the discovery of high-temperature superconductors, topological insulators, Dirac and Weyl's semimetals. Experimental results on these materials have revealed many intriguing phenomena such as pseudo-gap phase and Fermi arcs, which we have very little understanding theoretically. These systems are not suitable to be described by conventional perturbative approaches. In the present thesis, we used an alternative method with a non-perturbative tool provided by the gauge-gravity duality, allowing us to access the strongly coupled regime.

With the motivation to understand the underlying mechanism that gives rise to these peculiar phenomena, we proposed several holographic models by exploring the symmetries of either the background geometry in the bulk or at the boundary. By computing the fermions spectral function, we primarily explore the properties of the Fermi surface and Fermi arcs in certain strongly coupled systems of interests. Our results revealed some interesting features that are closely related to those that are seen in real materials from condensed matter experiments.

Contents

List of Figures

Chapter 1

Introduction and Motivation

1.1 Preview of the thesis

This thesis emerged from an attempt to provide theoretical models to understand some phenomena encountered in strongly correlated systems by using gauge/gravity duality as a mathematical framework. Compiling together different parts of this thesis was undoubtedly a challenging task. Nevertheless, I will try my best to provide a step-by-step guide for the reader through all its contents and orientation. Beginning with section 1.2, we briefly introduce condensed matter physics by discussing a few concepts such as doping, Fermi surface, Fermi arcs, phase transition, and the phase diagram for various temperatures and doping ranges. Furthermore, we will discuss the challenges faced by condensed matter theorists to understand strongly coupled systems. For example, there is no existing theoretical model that provides a complete description of the underlying mechanism for the high T_c superconductors (HTSC) (superconductors with higher transition temperatures). The same is true for the non-conventional materials or non-Fermi liquid, the presence of Fermi arcs in the pseudogap phase, and the new topological materials, Dirac and Weyl's semimetals. Addressing some of these challenges are the main objectives of this thesis. It is to be mentioned here that strongly coupled systems are not suitable to be described using standard perturbative techniques. However, the one area in physics that we find many such strongly coupled phenomena are in the realm of condensed matter system.

On the other hand AdS/CFT correspondence, which was conjectured by J.M Maldacena [1] in order to describe the quantum nature of gravity, has provided a completely new outlook and prescription to understand strongly coupled quantum field theories (QFTs). In a more general formulation and context, the above correspondence is also known as the **gauge-gravity duality**, which can be used as a tool for understanding such systems by using a dual gravitational description. This description turns out to be much simpler than the original strongly coupled system. In recent times, a lot of works are going on where this duality is used to study different new phases of matter which are strongly coupled.

With this in mind, we discuss in Section 1.3 the basic concepts of gauge-gravity duality followed by a brief introduction to the structure and symmetries of anti-de Sitter (AdS) spacetime and few basic building blocks and symmetries related to conformal field theory (CFT). *Gauge/Gravity duality* or simply *Holography* provides a one to one relation or mapping between the gravity theory in AdS spacetime and CFT on its boudary [2]. This conjecture is the main mathematical tool used in the various chapters of this thesis. In sections 1.4 and 1.5 of this chapter, we provide some essential preliminary steps to calculate the observables on the boundary theory (CFT that lives on the boundary of AdS) using the methods of AdS/CFT correspondence. In particular we have chosen the scalar and fermionic fields as our examples and computed the one$-$point function and Green's function.

In Chapter 2, we set the stage by reviewing few pioneering works, which are based on the holographic principle. In the first example, we will present some of the important calculations to compute the retarded Green's function and subsequently the spectral function. We will discuss about the evolution of non-Fermi liquid behaviour from holography in the strongly correlated fermionic system [3]. Secondly, we will review the steps to compute the conductivity as discussed in [4] and then compare them with the results from real condensed matter systems. In the final example, we review an application of AdS/CFT to the evolution of Fermi arcs from the Mott insulator [5], which is closely related to the works presented in this thesis. The main purpose of these introductory chapters will be to do a literature survey of the existing field and familiarise ourselves with the techniques used in both analytical and numerical computations. As a disclaimer, none of the discussions on condensed matter systems or AdS/CFT are detailed and complete. I only discuss the areas in brief which will be helpful to understand the rest of the thesis.

This will be followed by Chapter 3 which is based on our work [6]. In this chapter, we discuss the Fermi arcs which are disconnected contours of the Fermi surface observed in the pseudogap phase of high-temperature superconductors. Since our aim is to understand the pseudo-gap phenomena, we study a holographic Fermionic system coupled with a massive scalar field in a Reissner–Nordström AdS black hole background. Depending on the boundary condition on the scalar field mode, we discuss two possible scenarios. When the scalar condenses below a critical temperature T_c, the Fermi surface is deformed and eventually the Fermi arcs appear when the system undergoes a transition from normal phase to pseudogap phase. Hence T_c can be reminiscent of the well-known cross over temperature T^* in cuprate superconductors, below which pseudogap appears at constant doping. In the second scenario, the bulk scalar develops a non-normalizable profile at arbitrary temperature for a non-zero source at the boundary. Therefore, we can tune the Fermi spectrum by tuning a dual-source at the boundary. The dual-source in this case can be reminiscent of hole doping in the real cuprate superconductors. For both cases, we have studied the Fermi spectrum and observed an anisotropic gap in the spectral function depending on the model parameter and studied the properties of Fermi arcs across different phases.

In Chapters 4 and 5, we study the nature of the Fermi surface and its evolution by tuning different types of non minimal dipole and dipole-like couplings in the bulk. These two chapters are based respectively on our works [7, 8]. We further introduce translational symmetry breaking complex scalar field, which is assumed to couple with the holographic fermions. The symmetry breaking background induced by the scalar field is known as Q-lattice [10]. We calculate the fermionic spectral function, which captures the low energy behaviour of the system. By tuning the parameters and the non-normalizable component of the scalar field, we observed interesting phenomena such as spectral weight transfer and Fermi surface smearing, which has already been reported in various real condensed matter experiments.

Chapter 6 discusses our work [9] and is devoted to the study of the effects of the magnetic field in the presence of modified dipole couplings [11, 13]. We consider a fermion field with interaction terms in the AdS_4 dyonic black hole background. We found that the system can be reduced to a non magnetic one with the momentum being quantized into Landau levels n. By tuning the coupling parameter, we study its effect on the Fermi level and the quasiparticle width. We found an interesting scaling relation between the decay width and the coupling parameter, with a universal scaling exponent which is independent of the levels n. Finally, in Chapter 7 we summarize our results and findings based on the works done so far by me and discuss the future plans and directions which can be taken up from here.

1.2 Condensed matter background

In general, condensed matter systems are finite density systems. The questions asked in this branch of physics is mostly related to the following: how does a system behave when we gather large amount of matter together? Condensed matter systems are those when one considers large densities such that the wave function for each building constituent overlap or when one considers system at very low temperatures where quantum effects start appearing.

The main purpose of this section is to introduce the reader to different aspects of condensed matter problems in the many-body systems. Firstly, the study of strongly correlated systems is one of the most active field of research in both experiment and theory. This is because of the presence of many intriguing phenomena, such as the high T_c superconductors, non-Fermi liquid behaviours, pseudogap phases, to name a few. Secondly, the field theoretic approach towards studying strongly correlated systems related to condensed matter faces difficulty in the sense that the standard perturbative approaches play almost no or limited role. In order to understand such systems and to make a way to apply gauge/gravity duality, we need to briefly discuss the condensed matter systems. But before turning into the strongly correlated phenomena, let us first understand the basic. Consider the free electrons gas in three dimensions [17] obeying Pauli's exclusion principle where the filling of the ground state in momentum space is such that all the single-particle states inside a sphere with radius k_F are filled, while the state outside are empty. The surface of this sphere with constant energy (referred as the Fermi energy), is called the *Fermi surface* (FS), and the energy is given by $\epsilon_F = k_F^2/2m$ (in units of $\hbar = 1$) as depicted in Figure 1.1. If one starts filling a state just outside the FS or removes a fermion from a filled state just inside the FS, low energy excitations of particles and holes are produced respectively. The low energy excitations outside the FS are gapless, and have a linear dispersion relation of the form $\epsilon(k) = v_F(k - k_F)$, where v_F is the Fermi velocity given by $v_F = k_F/m$. The sign of $(k - k_F)$ will dictate the excitation energy for holes and particles.

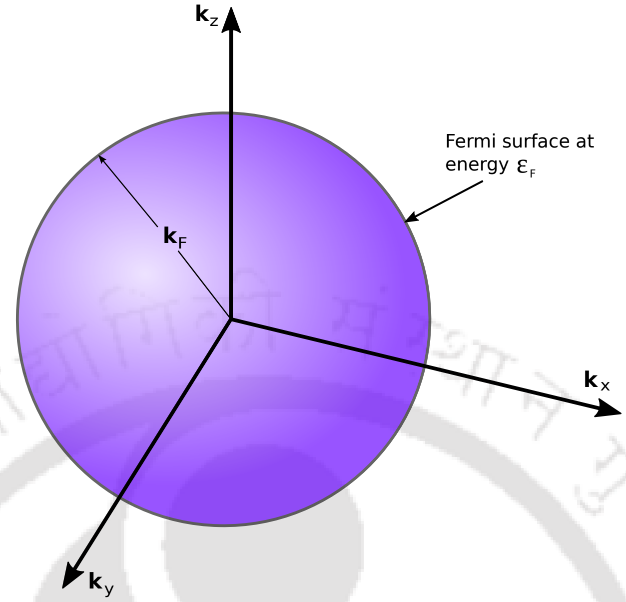

Figure 1.1: Filling of the ground state of a free electrons system with occupied orbitals inside a sphere of radius k_F, where $\epsilon_F = k_F^2/2m$ is the energy of an electron having a wavevector k_F.

In a more advanced language that is used to describe the strongly coupled quantum many-body systems, these excitations manifests itself as a pole in the complex frequency plane of the retarded Green's function G_R of the electron operator $\hat{c}_{k\sigma}(t)$. Let us briefly discuss this important concept of Green's function method used in describing the many-body physics which is based on the formalism known as second quantisation [18]. It is worth mentioning here that we will be using this Green's function method a lot in various chapters of this thesis. We begin with the definition of retarded Green's function, which is given by the thermal expectation values of the creation and annihilation operators, $\hat{c}^\dagger(t)$ and $\hat{c}(t)$ obeying the (anti-)commutation relation

$$\{\hat{c}_a\,,\,\hat{c}_b^\dagger\} \;=\; \hat{c}_a\,\hat{c}_b^\dagger + \hat{c}_a^\dagger\,\hat{c}_b \;=\; \delta_{ab}\,, \quad \text{fermions} \tag{1.1}$$

$$\left[\hat{c}_a\,,\,\hat{c}_b^\dagger\right] \;=\; \hat{c}_a\,\hat{c}_b^\dagger - \hat{c}_a^\dagger\,\hat{c}_b \;=\; \delta_{ab}\,, \quad \text{bosons} \tag{1.2}$$

Since we will focus only on fermions in this thesis, therefore we only mention the retarded Green's function G^R related to the fermions, which is given by

$$\begin{aligned} G^R_{ab}\,(t,t') &= -\,i\,\theta(t-t')\langle\,\{\hat{c}_a(t),\hat{c}^\dagger_b(t')\}\,\rangle \quad \text{for} \;\; t>t' \\ &= \theta(t-t')\left[-i\,\langle\,\hat{c}_a(t)\;\hat{c}^\dagger_b(t')\,\rangle\;-i\,\langle\,\hat{c}^\dagger_b(t')\;\hat{c}_a(t)\,\rangle\right] \\ &= \theta(t-t')\,[\,G^>_{ab}\;-\;G^<_{ab}\,]\,. \end{aligned} \tag{1.3}$$

where, $\theta(t)$ is the Heaviside step function, and $G^>$ and $G^<$ are called greater and lesser Green's functions defined as [18]

$$G^>_{ab} \;=\; -i\,\langle\,\hat{c}_a(t)\;\hat{c}^\dagger_b(t')\,\rangle \quad \text{and} \quad G^<_{ab} \;=\; +i\,\langle\,\hat{c}^\dagger_b(t')\;\hat{c}_a(t)\,\rangle$$

The physical interpretation in these definition is the probability that if we put an electron to the many particle system in a state 'b' at time t' then we can take out an electron from a state 'a' at time t. Note that the electron taken out need not have to be the same electron. Consider a system with time-translation invariance where the Hamiltonian $\hat{H}$ has no time dependence. Then the Green's function G^R_{ab} must depend only in the time difference $(t-t')$ i.e., $G^R_{ab}(t,t') \;\equiv\; G^R_{ab}(t-t')$. This shows that the Green's function corresponds to a correlation function involving operators acting at time t and t'. Since the correlation depends only on the time difference, we can choose $t'=0$, giving $G^R_{ab}\,(t) \;=\; -i\,\theta(t)\langle\;\{\hat{c}_a(t),\hat{c}^\dagger_b(0)\}\;\rangle$, the definition of greater and lesser Green's function remain the same with $t'=0$.

Using the above formalism, let us consider a Hamiltonian for free electrons

$$\hat{H} \;=\; \sum_{k\sigma} \epsilon_{k\sigma}\, c^\dagger_{k\sigma} c_{k\sigma} \tag{1.4}$$

where, $\epsilon_{k\sigma}$ is the energy level corresponding to the quantum numbers k and σ (momentum and spins). For this Hamiltonian one can work out the greater and lesser Green's function, which gives

$$G^<\,(k,t) \;=\; i\,F(\epsilon_k)\;e^{-i\,\epsilon_k\,t} \tag{1.5}$$

$$G^>\,(k,t) \;=\; -i\,(1-F(\epsilon_k))\;e^{-i\,\epsilon_k\,t} \tag{1.6}$$

with $F(\epsilon_k)$ being the Fermi-Dirac distribution function which gives the occupation number of particles. From these expressions, we see that if $G^>$ gives the population of electrons, then $G^<$ should give the population of holes in a complementary way of counting things. In the frequency domain, the full retarded Green's function can be obtained by Fourier transforming $G^<$ and $G^>$. Using equation (1.3) with $t' = 0$, we get

$$G_R(k,\omega) = -i\int_{-\infty}^{\infty} dt\,\theta(t)\,e^{i\omega t}\,e^{-i\,\epsilon_k\,t-\eta\,t} = \frac{1}{\omega - \epsilon_k + i\eta} \quad \text{for } \eta \to 0^+ \,. \tag{1.7}$$

Now one can define a quantity A, known as the spectral function given by

$$A\,(k,\omega) \;=\; -2\,\mathrm{Im}\,G_R(k,\omega) \;=\; 2\pi\,\delta(\omega\;-\;\epsilon_k), \tag{1.8}$$

which gives the density of states. From this definition, we see that for free electrons, the spectral function gives a delta function, which indicates a peak at $\omega = \epsilon_k$. This peak is an excitation at a state k when an electron with energy equal to ω is added.

In the presence of interactions, the form of the spectral function changes from a delta function to a broadened profile due to interactions involving energy exchange which could be electron-phonon, electron-electron interactions etc. To get a better picture of this, consider a Green's function that decays in time, with τ as the characteristic decay time given by

$$G_R(k,t) \sim -i\,\theta(t)e^{-i\,\epsilon_k\,t}e^{-t/\tau}, \tag{1.9}$$

then the spectral function would be of the form

$$A(k,\omega) \;=\; \frac{2/\tau}{(\omega-\epsilon_k)^2 + (1/\tau)^2}\;. \tag{1.10}$$

This spectral function has a Lorentzian shape, which is peaked and centered at $\omega = \epsilon_k$, whose width and height equals to τ^{-1} and 2τ respectively.

When we take the interaction into account, *Landau's Fermi liquid (FL) theory* is one of the most successful theories that provides deeper understanding of different states of matter, such as normal metals, superconductors and superfluids. It is based on weakly interacting fermions filling up a Fermi surface, similar to non interacting fermions discussed above, but with an assumption that the excitation produced by putting a particle into the system can be described by a particle with long lifetime called a quasiparticle with an effective mass m^*.

Starting from a single particle retarded Green's function, in the presence of interaction, the expression from equation (1.7) in general can be written as

$$G_R(\omega,k) \;=\; \frac{1}{\omega-\epsilon_k-\Sigma(\omega,k)}, \tag{1.11}$$

where, ϵ_k is the free electron energy as mentioned above, but now measured with respect to the chemical potential μ given as $\epsilon_k = k^2/2m \;\; - \mu$ and Σ is the fermion self-energy that should be solved by including all possible Feynman diagrams, which in general is impossible to do. Even approximation methods are non trivial and lots of technicality will be involved in doing so. For this reason we do not discuss it here. To see the quasiparticle nature from the general retarded Green's function in equation (1.11), one has to look near the Fermi energy for k values where the real part of the energy vanishes i.e., $\epsilon_{k_F} + \mathrm{Re}\Sigma(0,k_F) = 0$. Let us rewrite G_R as follows

$$G_R(\omega,k) \;=\; \frac{1}{\omega-[\epsilon_k+\mathrm{Re}\Sigma(\omega,k)]-i\;\mathrm{Im}\Sigma(\omega,k)}\;. \tag{1.12}$$

In the low energy limit, near $k = k_F$, we can expand G_R to get

$$G_R(\omega,k) \;=\; \frac{Z}{\omega-\tilde{\epsilon}_k+i/2\tau_k(\omega)}, \tag{1.13}$$

where, Z is the renormalization constant, which is a measure of the quasiparticle weight, also known as residue, $\tau_k(\omega)$ is related to the imaginary part of self energy and $\tilde{\epsilon}_k$ is the effective energy given by

$$\tilde{\epsilon}_k = \frac{k_F}{m^*}\,(k-k_F) \;=\; v_F(k-k_F)\;, \tag{1.14}$$

where m^* is the effective mass. To obtain a connection from (1.13) to those of non interacting systems, one can apply some approximation. For example, in the limit of low temperatures with long lifetime, near $k = k_F$, one gets the spectral functions as

$$A(\omega,k) \;=\; \frac{Z/\tau_k}{(\omega-\tilde{\epsilon}_k)^2+1/4\tau_k^2(\omega)} \;\approx\; 2\pi\,Z\,\delta(\omega-\tilde{\epsilon}_k). \tag{1.15}$$

Again, this equation shows that the spectral function is Lorentzian, which is peaked at $\omega = \tilde{\epsilon}_k$ and its width equals $\tau_k^{-1}(\omega)$, which is analogous to the pole in free electron gas. On evaluating the self energy near the Fermi surface using the approximation discussed in [18], one finds that $\tau_k^{-1}(\omega) \sim \epsilon_k^2 = \omega^2$. With the spectral function in (1.15), there is a problem that the spectral function does not obey the sum rule, which is given by

$$\int_{-\infty}^{\infty} \frac{d\omega}{2\pi} A(\omega, k) = 1 , \tag{1.16}$$

and its integral equals to Z. This means that quasiparticles cannot be the full part of the spectral function and we must have other contribution with a weight of $1 - Z$ to obey the sum rule. For detail discussion on this and on other transport properties related to Fermi liquid theory we refer the readers to [18].

Since the concept of quasiparticle is still very powerful under these approximations, one can develop a more general low energy theory, independently of the microscopic details of the system. Fermi liquid theory predicts the temperature dependence of resistivity to be quadratic i.e., $\rho \sim T^2$, which indeed is true for most metals. On the other hand, the linear dependence of specific heat on temperature was another common phenomena predicted by this theory. The breakdown and drawbacks of Fermi liquid theory were noticed in the early 80s since the discovery of the phenomenon of high-temperature superconductivity. For the normal state of high T_c cuprates (oxides of copper), experiments showed that a Fermi surface still exists and the expression in (1.11) still holds, but the

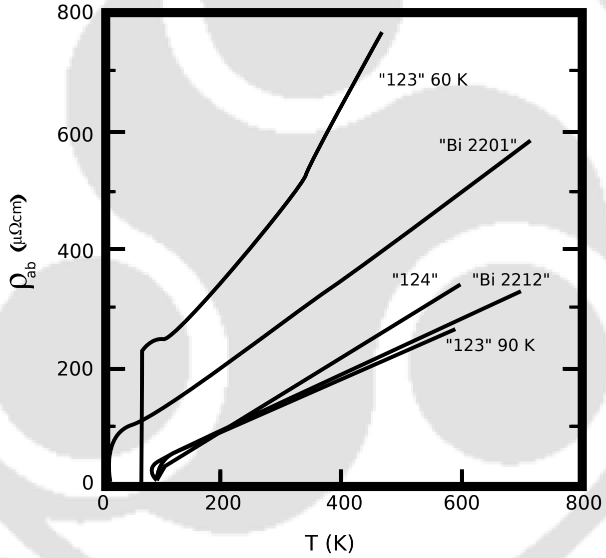

Figure 1.2: Sketch of resistivity as a function of temperature for various high temperature superconductors. Original plot can be found here [19].

self energy is given by [20]

$$\Sigma(\omega, k) \;\approx\; c\,\omega\,\log\,\omega \;+\; d\,\omega \tag{1.17}$$

where c is real and d complex. This behaviour of self energy was later experimentally verified in [21]. We see that the system seems to possess gapless excitations with a dispersion relation $\omega = v_F(k - k_F)$ and the width $\tau_k^{-1}(\omega)$ is now proportional to ω and not ω^2, which is different in comparison to that of Fermi liquid. Further, in case of high T_c superconductors, the resistivity was experimentally found to vary linearly with temperature (i.e., $\rho \;\sim\; T$) as shown in Figure 1.2. The incompatibility of FL theory in these scenarios shows that we need a more sophisticated theory that can account for the strongly correlated electrons. In the recent years, there has been considerable amount of progress on various aspects of strongly coupled system and yet the problems related to such systems still persist. One of the successful theories, such as the BCS theory of superconductors [22] also have not been able to fully understood the high T_c superconductors. Apart from the deviation in the resistivity from Fermi liquid prediction, the presence of the mysterious pseudogap phase in the underdoped region of high T_c- superconductors (see Figure 1.3), the disconnected Fermi surface known as Fermi arcs and other strange transport properties in these materials keep adding up to the existing problems. It may be noted that the available fast modern computing machinery for heavy numerical simulation of "density-matrix renormalisation group" (DMRG) and "dynamical mean-field theory" (DMFT) computation methods have their own strength and limitations. Further, since these phenomena are very much dependent on temperature and doping (adding holes or electrons), various transport properties can be altered by either tuning the temperature or by the process of doping which is materials dependent. By varying the temperature and doping, especially at very low temperature, we get different phases. We illustrate the phase diagram of the cuprate high-temperature superconductors below in Figure 1.3.

Let us briefly discuss the temperature (T) and doping parameter ($\mathbf{x}$) phase diagram in Figure 1.3. In the far left of underdoped region, we have the anti-ferromagnetic phase and the Mott insulator[1] at zero and near zero doping. This phase is an insulator due to jamming effect impelled by strong electron correlations. The electron spin in various atomic sites point in opposite directions in this phase. While on the overdoped region in the far

---

[1] Mott insulators represents the class of materials which are supposed to conduct electricity according to the band theory, but turn out to be insulator at low temperature.

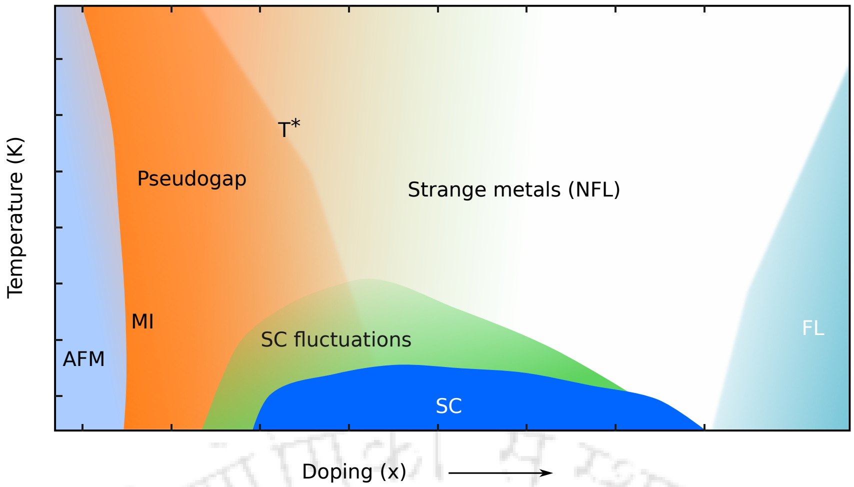

FIGURE 1.3: Pictorial representation of a phase diagram in temperature vs doping plane. The abbreviations here are FL: Fermi Liquid, NFL: Non-Fermi liquid, MI: Mott Insulator, AFM: Anti ferromagnets, SC: Superconductors.

right, shaded with blue we have the normal metals or the Fermi liquid. Because at higher doping, the localised electrons due to strong coulomb repulsion can move freely to become normal metals. In the middle dome with optimal doping, we have superconductors (SC) ranging from very low to higher temperatures. Surrounding the superconducting phase highlighted in green, we have the superconducting fluctuations, which is a disordered non-superconducting phase with no coherence Cooper pairs. Above SC phase at higher temperatures we have the class of strange metals or non-Fermi liquid. This phase cannot be described by the Fermi liquid theory (hence the name non-Fermi liquid) that we have discussed above and are characterized by linear dependence of resistivity on temperature T at high temperature as shown in Figure 1.2. In between the superconducting dome and the AFM, we have the so-called *pseudogap* phase [27] characterized by the crossover temperature T^{*}, which is the temperature corresponding to the onset of energy gap suppression in the density of states as indicated by experimental results in Figure 1.4(A). It is the most mysterious and interesting phase at the same time to explore, because we have very little understanding about it. Further, the pseudogap seems to have emerge from the superconducting state when one increases the temperature. Finding a mechanism that connects these different regions is quite a challenging task. Since the breakdown of Fermi liquid theory, which is based on the concept of quasi-particles and the presence of a well defined FS in momentum space has left us with many problems to solve. The spectrum in the pseudogap and the strange metals does not have a well-defined quasiparticle; the question now is, what do we even mean by FS in these regions? We shall discuss more on the specific problems and potential explanation in the later chapters. Because of these strange phenomena observed in high T_c superconductivity in the cuprates and other compounds, it has drawn the attention not only to condensed matter community, but also to Holographers [2]. For discussion from the perspective of holography on these phenomena, see [23] for a review.

It is worth mentioning that apart from the strange properties in the cuprates, we also have a new class of materials such as the Topological insulators, Dirac and Weyl's semimetals [86–90], which also have shown various intriguing phenomena such as Fermi arcs [28–30, 30, 31]. In this thesis, we will try to understand the mysteries in the pseudogap phase where the spectral function is gapped and consequently the Fermi arcs are observed (see Figure 1.4).

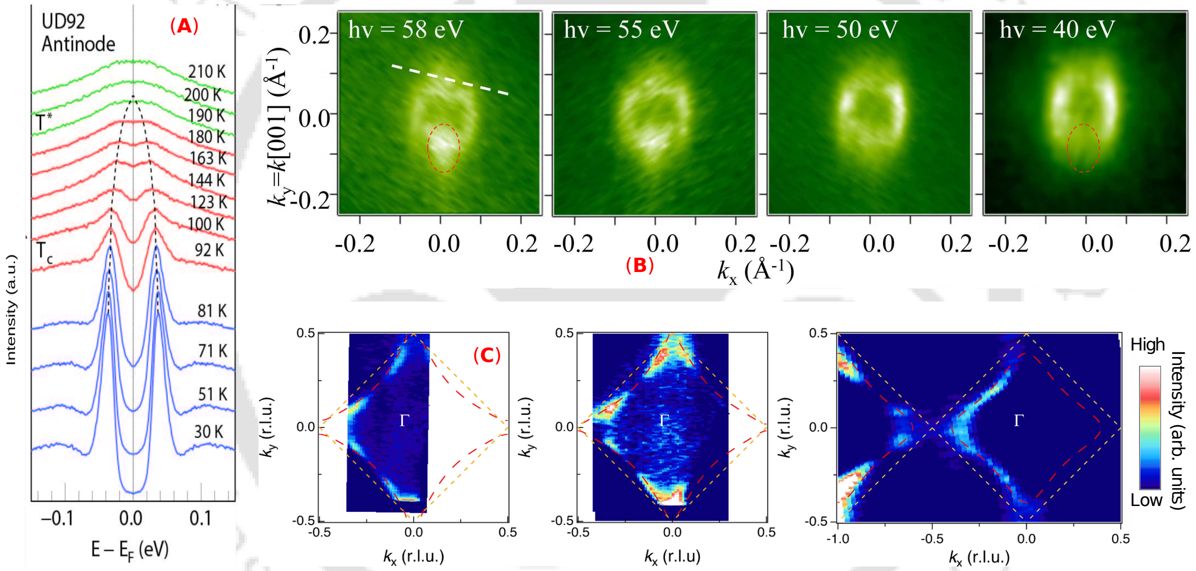

FIGURE 1.4: **A**: Spectral function vs energy, closing of the superconducting gap accur at T^* which is the crossover temperature. **B** & **C**: Example of fermi arcs seen in topological semimetal and HTSC ($La_{2-x}Sr_xCuO_4$). Plots taken from [25, 30, 31].

Towards that direction, we would like to first briefly discuss about the Angle Resolved Photoemission Spectroscopy(ARPES) experiment (for a detailed review we refer the readers to [24–27]). The ARPES set up is a powerful tool with high energy and momentum resolution, which is based on the phenomenon of the photoelectric effect. Following [26], we illustrate the basic setup in Figure 1.5. In the ARPES experiment, an incoming photon falls on the sample where it is absorbed. In case the energy of the absorbed photon is

---

[2] refer to the people that are using the AdS/CFT correspondence or Holographic duality to study these strongly correlated systems.

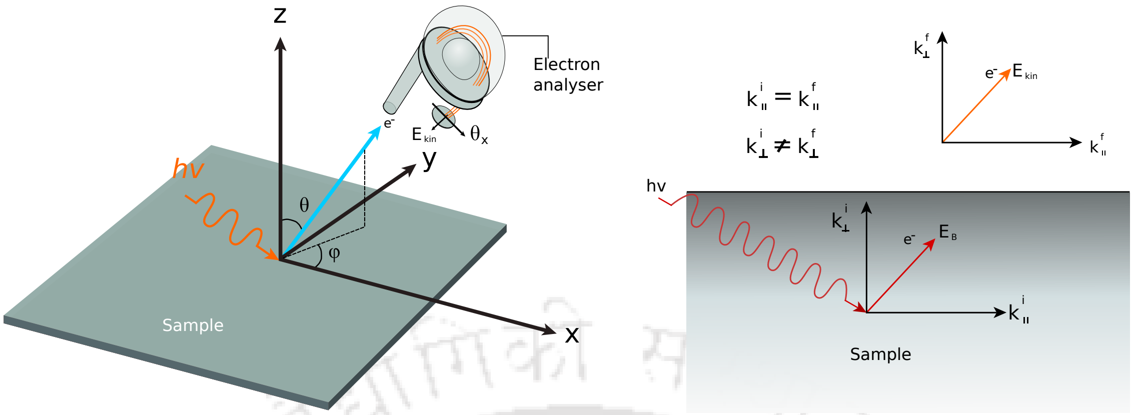

FIGURE 1.5: Basic geometry of angle resolved photoemission spectroscopy (ARPES) measurements. Here E_B is the binding energy and photon energy is $h\nu$, and E_{kin} is the kinetic enery of the electron ejected by the photon.

more than the work function Φ of the sample materials, photoelectrons are emitted and they can escape into the vaccuum. These emitted electrons captured in a specific energy range and solid angle are analysed. Using the principle of conservation of energy and momentum, information regarding the electron's initial momentum, energy and underlying electronic structure can be extracted. In case of many body systems, such technique can provide useful insight into many body physics. ARPES has provided useful information about the physics of many types of materials like high T_c superconductor cuprates, colossal magnetoresistive manganites etc. It is used to probe the electronic structure of the materials especially to study the surface properties.

The ARPES photoemission intensity is given by the following mathematical expression:

$$I(\omega, k) \;=\; I_0(k, \nu, \vec{A})\, A(k, \omega)\, f(\omega, T) \tag{1.18}$$

where, $A(k,\omega)$ is the spectral function, $f(\omega, T)$ is the Fermi Dirac distribution function and I_0 is the photoemission matrix element, which describes the transition from the initial state to the final state. Under the sudden approximation, ARPES data has been interpreted as a direct measure of the single particle spectral function $A(k,\omega)$. The spectral function, as mentioned earlier is one of the most fundamental objects in the study of many body theory that provides energy and momentum space information about the single particle states. In general the spectral function can be written in terms of the self energy encoding the information about the particle's interaction with the rest of the system. The real part of self energy captures the physical self energy while the inverse of the imaginary part is a measure of the particle's life time.

From the theoretical perspective one can get the spectral function from the retarded Green's function as discussed above. Since the spectral function can be mapped directly to experiments, therefore it is the most relevant quantity of interest needed to be extracted when solving the problems of strongly correlated systems using AdS/CFT correspondence.

1.3 The holographic principle

The holographic principle means the equivalent description of two different theories. The concept of duality is very common in physics. Electromagnetic duality and wave-particle duality are a few classic examples.

In understanding the problems mentioned in the previous section, we will take the help of a powerful duality known as the AdS/CFT conjecture. This represents a duality between a quantum field theory in $d-$ dimensions and a theory of gravity in $(d+1)-$dimensions. Since the number of dimensions of the two completely different theories does not match, one is one dimension less than the other, therefore, the theory is termed the "holographic theory". The important feature of this approach is that when one side is strongly coupled, the other is not, and vice-versa. Also, it needs to be emphasized that the degrees of freedom on both sides are completely different. While one side contains dynamical gravity, the other one is expressed on a fixed background.

The concept of holography was first realized in the context of black holes thermodynamics. Black holes (BH) arise as solutions to Einstein's field equations. These solutions are plagued with singularities, but these singularities are hidden by event horizons, from where nothing can escape classically. It turns out that there is a profound connection between BHs and thermodynamics. It was shown by Hawking and Bekenstein [32, 33] that BHs have entropy, which is directly proportional to the area of the horizon given by

$$S_{BH} = \frac{A}{4\ell_p^2}\,, \tag{1.19}$$

where A is the BH horizon area, ℓ_p is Planck length and we have chosen the Boltzmann's constant $k_B = 1$. Consequently, it also turned out that BH obey the laws of thermodynamics. From Einstein's equations one can prove that BHs obey the first law of thermodynamics

$$dM = \frac{\kappa}{8\pi} A \,, \tag{1.20}$$

where, κ is the surface gravity representing the gravitational acceleration of an object at the surface of the horizon. However, one important factor is still absent: the temperature. In order to relate to thermodynamics, we need to write $dM = T\, dS_{BH}$. The question is whether BHs possess temperature too. Again, Hawking [34] used a semiclassical approach and showed that BHs emit black body radiation due to quantum fluctuation at the horizon, and the temperature of such radiation is $T = \kappa/2\pi$, thereby satisfying the first law. Not only this but in 1972, Bekenstein [33] proposed the second law of thermodynamics with the following relation

$$\Delta\, (S_{BH} + S_0) = \Delta\, S_{total} \geq 0 \tag{1.21}$$

which means that the entropy never decreases. Here, S_0 is the entropy of the outside system, constituting together the total entropy. The generalized second law (1.21) gives us the first hint of holography as was initially proposed by 't Hooft [35] and Susskind [36]. The idea is the following: in any system where gravity is absent, the number of degrees N_{dof} is related to the volume V as $N_{dof} \sim e^V$. This immediately gives the statistical entropy $S \sim \ln N_{dof}$, which is proportional to the volume $V \sim L^d$ of the system in question in $d-$dimensions. However, in the presence of gravity, the entropy is proportional to the horizon's area instead of being proportional to the volume. This led to the initial concept and formulation of a holographic principle (for review, see [37]). In our case, we will try to understand the duality where gravity in $(d+1)-$dimensions will have the same number of degrees of freedom as a field theory in $d-$dimensions.

For detail and more recent reviews on the holographic principle in connection to the gauge-gravity duality, we suggest the reader to these references [23, 43–46]. Before jumping into the mathematical details in mapping various quantities from both theories, we shall begin with a brief discussion on AdS/CFT correspondence. The plan will be to introduce to the duality by discussing Anti-de-Sitter (AdS) spacetime and conformal field theory (CFT) separately and then relate them.

1.3.1 The anti-de Sitter space

The anti-de Sitter spacetime (AdS) is a spacetime which is maximally symmetric with constant negative curvature. Spacetimes are best classified by their symmetries. This means that one should look for coordinate transformation that leave the metric invariant. To each symmetry, one can associate a Killing vector. Under a general coordinate transformation $\delta x^a = \xi^a(x)$, the metric transforms as

$$\delta g_{ik} = \nabla_k \xi_i \; + \; \nabla_i \xi_k \;, \tag{1.22}$$

A Killing vector obeys the condition $\nabla_k \xi_i \; + \; \nabla_i \xi_k \; = \; 0$. Now, a spacetime having maximum number of symmetries will have the most number of Killing vectors. For example in $d-$spacetime dimensions, a symmetric metric will have $d(d+1)/2$ independent elements and hence there will be $d(d+1)/2$ independent Killing equations. In such cases, there will be at most $d(d+1)/2$ Killing vectors. Spacetime with such number of Killing vectors are called maximally symmetric. The Killing vectors themselves form a group. Maximally symmetric spacetimes are defined by Riemann tensor of the form

$$R_{ijkl} \; = \; k \left(g_{ik} \, g_{jl} \; - \; g_{il} \, g_{jk} \right) \,, \tag{1.23}$$

where k is a constant. Because of this the Ricci scalar R also turns out to be a constant. Such metric spaces are also known as constant curvature spaces. All such spacetimes are solutions of Einstein's equation with a cosmological constant:

$$R_{ab} - \frac{1}{2} \left(R - 2\Lambda \right) g_{ab} \; = \; 8\pi G \, T_{ab} \; . \tag{1.24}$$

$\Lambda > 0$ corresponds to de-Sitter space, $\Lambda = 0$ to Minkowski space and $\Lambda < 0$ to anti-de-Sitter space. AdS spacetime can be represented as a hyperboloid embedded into a higher dimensional Minkowski space. Let us consider the AdS$_{d+1}$ spacetime embedded in a $(d+2)-$dimensional Minkowski space. The constraint equation of the embedding space is given by:

$$-L^2 \; = \; X^A X^B \, \eta_{AB} \; , \quad X^{-1} > 0 \tag{1.25}$$

the parameter L is the length scale of the geometry and can be thought of as the "radius" of the hyperboloid. Here $A\,, B \;=\; -1, 0, 1, ..., d$. The flat Minkowski metric signature is taken as $(-1, 1, 1, ..)$, while $\eta_{-1-1} = -1$, $\eta_{\mu\nu} = \delta_{\,\mu\nu}$ and $\eta_{-1\mu} = 0$ with $\mu = 0, 1, ..., d$. The AdS metric, is then represented by

$$ds^2 \;=\; dX^A dX^B \,\eta_{\,AB} \;, \tag{1.26}$$

if one takes X^μ as AdS coordinates and X^{-1} is given by (1.25). Now introducing the following set of coordinates

$$x^0 \;=\; \frac{L^2}{X^0 + X^{-1}} \;, \quad x^i \;=\; \frac{X^i\, x^0}{L} = \frac{L\, X^i}{X^0 + X^{-1}} \;, \tag{1.27}$$

with $i = 1, \ldots, d$ and the domain in the new variables is given by $0 < x^0 < \infty, x^i \,\epsilon\, \mathbb{R}$. Then the above metric (1.26) becomes

$$ds^2 \;=\; \frac{L^2}{(x^0)^2}\,\delta_{\,\mu\nu} dx^\mu dx^\nu . \tag{1.28}$$

We can see from this metric that AdS$_{d+1}$ do not have a boundary, but it is useful for practical pusposes to consider the boundary of the coordinate patch which are the conformally compactified Euclidean space at $x^0 = 0$ and the point $x^0 = \infty$, known as AdS horizon.

Let us briefly discuss the symmetry group of AdS following [47]. The AdS space is invariant under transformations of the embedding Minkowski space of the form $(X')^A \;=\; \Lambda^A{}_B\, X^B$, where the matrix Λ is of $(d+2)\times(d+2)$ dimensions and satisfies $\Lambda^T \eta\, \Lambda \;=\; \eta$ and $\Lambda^{-1}_{-1} > 0$. These matrices form a group which can be divided into two subsets, the first one is the Lie group $SO(d+1, 1)$, while the other is represented by $I \times SO(d+1, 1)$, with I as an inversion. In what follows, we shall show that matrix Λ belongs to the Lie group $SO(d+1, 1)$. Under infinitesimal coordinate transformation, $\Lambda \;\approx\; 1 + J$, we have

$$\delta\, X^A \;=\; J^A_B\, X^B \;=\; \frac{1}{2}\omega^{CD} (J_{CD})^A_{\;B}\, X^B \;, \tag{1.29}$$

where the generators $(J_{CD})^A_{\;B} \;=\; \delta^A_C\, \eta_{DB} \;-\; \delta^A_D\, \eta_{CB}$ form the usual basis of $SO(d+1, 1)$ algebra and satisfies the commutation relations $[J_{AB}, J_{CD}] = \eta_{\,AB} J_{BC} +$ permutations.

Introducing the conformal basis of $SO(d+1,1)$ which is given by

$$\begin{aligned} D &= M_{-10}\,, \quad K_i \;=\; M_{0i} \;+\; M_{-1i}\,, \\ L_{ij} &= M_{ij}\,, \quad P_i \;=\; M_{0i} \;-\; M_{-1i}\,. \end{aligned} \tag{1.30}$$

Now in the above conformal basis, the matrix J in (1.29) can be written in the following form.

$$\frac{1}{2}\omega^{AB}\,J_{AB} \;=\; a\,D \;+\; b^i\,K_i \;+\; c^i\,P_i \;+\; \frac{1}{2}\,\omega^{ij}\,L_{ij}\,, \tag{1.31}$$

where a, b and c are given by

$$a \;=\; \omega^{-10}\,, \quad b^i \;=\; \frac{1}{2}\left(\omega^{0i} \;+\; \omega^{-1i}\right)\,, \quad c^i \;=\; \frac{1}{2}\left(\omega^{0i} \;-\; \omega^{-1i}\right)\,. \tag{1.32}$$

Using equations (1.27) and (1.29), one can show that the Killing vectors under a symmetry transformation for the infinitesimal change in coordinate x^μ is given by

$$\begin{aligned} \delta\,x^0 &= -a\,x^0 - 2\,x^0\,\frac{b_i\,x^i}{L} \\ \delta\,x^i &= -a\,x^i - L\,c^i \;+\; \omega^{ij}\,x_j \;+\; \frac{b^i\,x^2}{L} \;-\; 2\,x^i\,\frac{b_j\,x^j}{L}. \end{aligned} \tag{1.33}$$

Further, one can show using the commutation relations $[J_{AB}, J_{CD}]$ and equation (1.30) that the elements D, K_i, L_{ij} and P_i satisfy the usual commutation relations of the conformal algebra given by

$$[D\,, P_i] \;=\; -P_i\,, \quad [D\,, K_i] \;=\; K_i\,, \tag{1.34}$$

$$[L_{i,j}\,, P_k] \;=\; \delta_{jk}\,P_i - \delta_{ik}\,P_j\,, \quad [L_{i,j}\,, K_k] \;=\; \delta_{jk}\,K_i - \delta_{ik}\,K_j\,, \tag{1.35}$$

$$[P_i\,, K_j] \;=\; 2\,(\delta_{ij}\,D \;-\; L_{ij})\,, \quad [L_{i,j}\,, L_{kl}] \;=\; \delta_{il}\,L_{jk} + \delta_{jk}\,L_{il} \;-\; \delta_{ik}\,L_{jl} - \delta_{jl}\,L_{ik}\,, \tag{1.36}$$

$$[P_i\,, P_j] \;=\; [K_i\,, K_j] \;=\; [D\,, L_{ij}] \;= 0\,. \tag{1.37}$$

Apart from the conformal algebra, there are different coordinates to describe this spacetimes; we will look at some sets of these coordinates. As an example, consider the AdS$_2$ spacetime embedded into a flat spacetime. First let us look at the hyperbolic global coordinates system (τ, ρ)

$$X^{-1} = L\cosh\rho\cos\tau \ , \ X^0 = L\cosh\rho\sin\tau \ , \ X^1 = L\sinh\rho \ . \tag{1.38}$$

One can easily generalize this to higher dimensions. Notice that the coordinate τ is periodic with a periodicity of 2π. The AdS$_2$ metric from (1.26) in these coordinates becomes

$$ds^2 = L^2\left(-\cosh^2 d\tau^2 + d\rho^2\right) . \tag{1.39}$$

We see that now the AdS embedded in a flat spacetime has only one timelike direction. Moreover, the periodicity in τ is causally problematic, but one can get rid of this by unwrapping the timelike direction and consider only the covering space of AdS$_2$ with $-\infty < \tau < \infty$. This unwrapped spacetime is the AdS spacetime used when one talks in the context of AdS/CFT correspondence. Now let us see another coordinate (τ, θ) called as *conformal coordinates*, defined by $\tan\theta = \sinh\rho$. One can show that the AdS$_2$ metric becomes

$$ds^2 = \frac{L^2}{\cos^2\theta}\left(-d\tau^2 + d\rho^2\right) . \tag{1.40}$$

We see that this metric is conformally flat, meaning that the metric is rescaled by a factor. We show a sketch of the spacetime in Figure 1.6.

Lastly, let us look at the Poincaré coordinates (t, r, x^i), which we will be using in the subsequent chapters for our application. The coordinates are defined by

$$\begin{aligned} X^{-1} &= \frac{L\,r}{2}\left(\frac{1}{r^2} + 1 + x_i^2 - t^2\right) \ , \quad X^i = L\,r\,x^i \ , \\ X^{d+1} &= \frac{L\,r}{2}\left(\frac{1}{r^2} - 1 + x_i^2 - t^2\right) \ , \quad X^0 = L\,r\,t \, . \end{aligned}$$

then, the given AdS$_{d+1}$ metric in (1.26) transform to

$$ds^2 = L^2 r^2\left(-dt^2 + dx^{i\,2}\right) + \frac{L^2\,dr^2}{r^2} . \tag{1.41}$$

Sometimes it is more convenient to use the coordinate $r \equiv z^{-1}$, rather than the coordinate z, which we will learn more about in the later sections. Sometimes we refer these

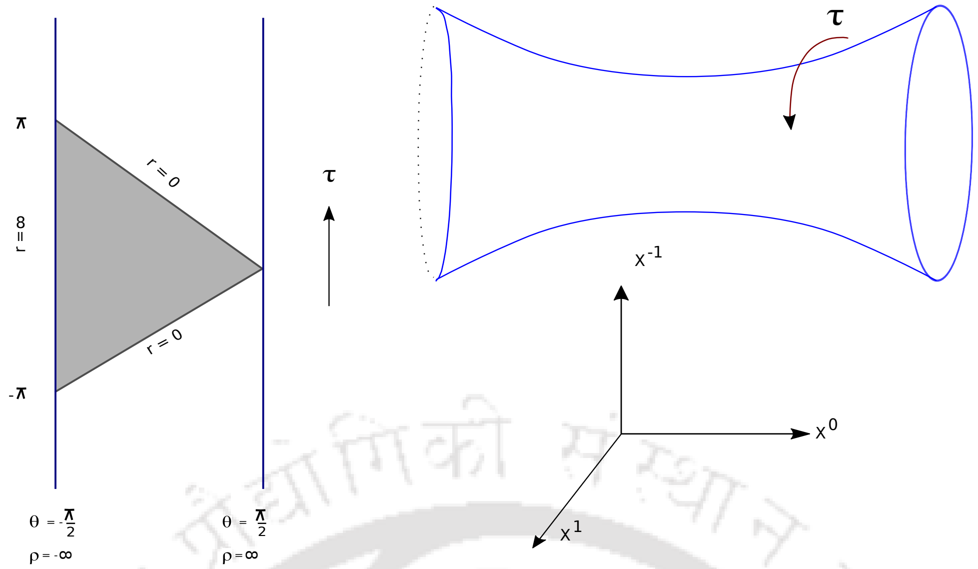

FIGURE 1.6: Right: Covering space of AdS_2 embedded into $\mathbb{R}^{2,1}$. Left: AdS_2 spacetime in conformal coordinates while the Poincaré coordinates cover only part of the full AdS spacetime.

coordinates as *Poincaré patch*. For Poincaré patch in terms of coordinate r, the boundary of AdS space is at $r \to \infty$ with $\mathbb{R}^d$ topology. The presence of the boundary means that in order to understand the physics in AdS, one has to specify the boundary conditions both at $r = 0$ and $r = \infty$. Thus in the context of AdS/CFT correspondence, these boundary conditions can be related to the mapping between the gravity theory and the dual field theory.

1.3.2 Basic Conformal Field Theory

A conformal field theory is a quantum field theory which is invariant under a group of symmetry called the conformal group. Conformal symmetry is a spacetime symmetry including scale invariance and Poincaré symmetry. Let us suppose $g_{\mu\nu}$ be the metric of some $d-$dimensional manifold whose coordinate is x^μ, a transformation $x \to x'$ which changes the metric tensor up to a scale factor as

$$g'_{\mu\nu}(x) \;=\; [\Omega(x)]^2 \; g_{\mu\nu}(x) \tag{1.42}$$

is called a conformal transformation. Based on these coordinate transformation one can define the transformation matrix

$$M^{\mu}_{\nu}(x) \; = \Omega(x)\, \frac{\partial\, x'^{\mu}}{\partial\, x^{\nu}} \tag{1.43}$$

and we can write

$$g'_{\nu\,\lambda}\,(x') = g'_{\mu\,\alpha}\,(x')\; M^{\mu}{}_{\nu}(x)\; M^{\alpha}{}_{\lambda}(x)\ . \tag{1.44}$$

which form a group. We can derive the infinitesimal generators of the conformal group by taking an infinitesimal coordinate transformation $x^{\mu} \to x^{\mu} + \epsilon^{\mu}$. As shown in the appendix A.1, ϵ^{μ} should have upto quadratic terms given by:

$$\epsilon_{\mu} \;\; = \;\; a_{\mu} + \, b_{\mu\nu}\, x^{\nu} + c_{\mu\,\nu\,\rho} x^{\nu} x^{\rho}\ . \tag{1.45}$$

Analysing the coefficients a, b, c, for higher dimensions $(d > 2)$ we have the transformations satisfying the following equations

$\epsilon^{\mu} = \lambda\, x^{\mu}$:	scale transformations
$\epsilon^{\mu} = a^{\mu}$:	translation
$\epsilon^{\mu} = \omega^{\mu}_{\ \nu}\, x^{\nu}$:	with antisymmetric ω corresponds to Lorentz transformations
$\epsilon^{\mu} = b^{\mu}\, x^{2} - 2\, x^{\mu}\, b\, x$:	special conformal transformations.

These transformations form a conformal group which is $SO(d+1,1)$ and consists of generators such as P_{μ} , $M_{\mu\nu}$ which correspond to translation and rotations. In addition to these, there are the generators of dilatations D and special conformal transformations K_{μ}. These generators obey the same algebra to that of AdS space, which we discussed in our previous section.

The important link between the fundamentals of AdS spaces and CFTs is built on the basis that the symmetry algebra of AdS$_{d+1}$ and the conformal algebra are both isomorphic to $SO(d+1,1)$. This provides a very important hint in the build up process of the duality between AdS and CFT. It also means that to every symmetry of AdS$_{d+1}$ correspond to a conformal symmetry acting on flat $d-$dimensional space. For example, consider a free scalar field in AdS$_{d+1}$ (for an elaborate discussion, see section 1.4) which can be written as:

$$\phi(x) \;=\; \int d^d y \Big[\frac{z}{(x-y)^2}\Big]^{\Delta} \phi_0(y) \tag{1.46}$$

where Δ is a constant depending on the scalar mass. Then one can perform a symmetry transformation $x' \to \lambda\, x$ which gives

$$\phi'(x') \;=\; \int d^d y \Big[\frac{z}{(x-y)^2}\Big]^{\Delta} \lambda^{d-\Delta} \phi'_0(\lambda\, y) \tag{1.47}$$

For scale invariant ϕ, we must have $\phi'(x') = \phi(x)$, then this implies

$$\phi'_0(\lambda\, y) \;=\; \lambda^{\Delta - d}\, \phi_0(y) \tag{1.48}$$

As a result, the boundary value of field ϕ with conformal dimension $d - \Delta$ coupled naturally to a conformal operator $\mathcal{O}$ with scaling dimension Δ through the integral $\int d^d x\, \phi_0(x) \mathcal{O}(x)$. Furthermore, equation (1.46) implies that ϕ_0 and $\mathcal{O}$ belongs in the AdS boundary and through a bulk-boundary propagator, a unique relationship is established between the AdS scalar field $\phi(x)$ and the field operator $\mathcal{O}(x)$.

1.3.3 The AdS/CFT Correspondence

The conjecture by Maldacena [1] is that in the large N limit, the $\mathcal{N} = 4$ supersymmetric Yang–Mills (SYM) theory with SU(N) gauge group and Yang-Mills coupling g_{YM} can be equivalently described by a type IIB superstring theory compactified on the AdS$_5 \times S^5$ background with string length $\ell_s = \sqrt{\alpha'}$ and g_s as a coupling constant. The relationship between these parameters of the two theories is given by [48]

$$4\pi\, g_s \;=\; g^2_{YM}\,, \quad L^4/\alpha'^2 \;=\; \lambda \;=\; g^2_{YM}\, N. \tag{1.49}$$

where, λ is the 't Hooft coupling. It is to be noted that the number of degrees of freedom in the bulk matches with the number of degrees of freedom at the boundary. This particular example that Maldacena derived is a limiting case of a type IIB string theory in (9+1)−dimensional spacetime with N D3−branes[3] stacked together. D−branes can be thought of as objects on which the open strings end. They can also be thought of as solitonic solutions of the low energy closed string theory equations of motion. At low energy, which

---

[3] For dertail description on D-branes and the AdS/CFT correspondence, see [50]

is below the string mass scale $1/\sqrt{\alpha'}$ or equivalently taking the string length $\ell_s \to 0$, the quantum gravity of closed strings reduces to classical supergravity. On the other hand, in the limit $N \to \infty$ and λ fixed but large, open string corresponds to the planar limit of $SU(N)$ gauge theory. Therefore, at low energy, the open and closed string descriptions reduce to $\mathcal{N} = 4$ super Yang-Mills theory and string theory on $\text{AdS}_5 \times S^5$. This duality is exciting because of its non-perturbative nature in string coupling g_s, just when the perturbative SYM calculation breaks down at large λ, we then have the classical type IIB supergravity solution which becomes useful. Up till date, we do not have a direct mathematical proof of this conjecture. However, [49] confirmed the equivalence of the two sides. They tested the gauge/gravity duality numerically by comparing the entropy of a black hole in the gauge theory with the entropy in a gravity theory including the quantum gravity correction.

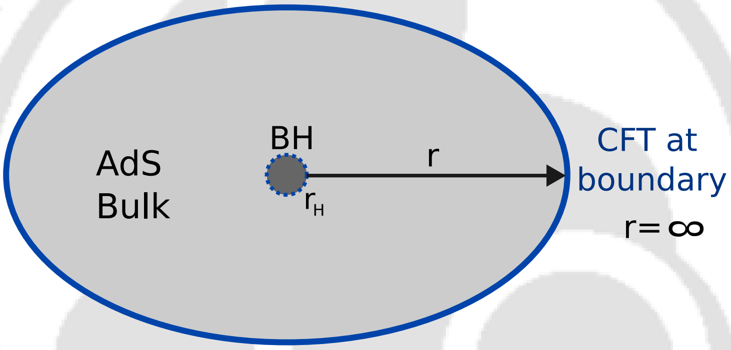

FIGURE 1.7: Cartoon of gravity theory that lives inside the bulk of AdS spacetime while the CFT is at the boundary at $r = \infty$. Here r_H is the horizon radius of the AdS−blackhole (BH) with r being the radial coordinate.

In order to understand the equivalence mentioned above, we need to formulate a dictionary between any fields ϕ in the supergravity theory and the operators $\mathcal{O}$ in conformal field theory side. After the conjecture by Maldacena, Gubser, Klebanov, Polyakov [51] and Witten [2] proposed a classical on-shell supergravity action, expressed in terms of given boundary values, with the effective action of SYM theory, where the supergravity boundary values now play the roles of generating currents. Witten further suggested that any field theory action on $(d+1)-$dimensional anti-de Sitter space gives rise to an effective action of a field theory on the $d-$dimensional boundary of AdS spacetime. The general relation is given by [2]

$$\int \mathcal{D}\phi \, e^{-\mathcal{S}[\phi]} = \left\langle \exp \int d^d x \, \mathcal{O}(x) \, \phi_0(x) \right\rangle \tag{1.50}$$

where, ϕ is the field in the bulk of AdS, $\mathcal{O}$ is the operator of the boundary conformal field theory and ϕ_0 is the boundary value of the field ϕ. Equation (1.50) is also known as $GKPW$ relation. In the strong coupling and large N limits, we do not really need to evaluate the full functional integral on the left hand side, but we can approximate by the classical on-shell action of an AdS field theory in terms of the field boundary values ϕ_0. Thus we can write (1.50) as

$$\mathcal{S}[\phi_0] \, = \mathcal{W}_{CFT}[\phi_0], \tag{1.51}$$

where, $\mathcal{W}_{CFT}[\phi_0]$ is the effective action in the CFT. However, when evaluating the gravity action on the left hand side of (1.51), it typically diverges and has to be renormalized following the procedure of holographic renormalization [52–54]. Thus, we have to replace by a renormalized version and rewrite (1.51) as

$$\mathcal{S}[\phi_0]_{ren} \, = \mathcal{W}_{CFT}[\phi_0]. \tag{1.52}$$

In general, to extract the correlation functions $\langle \mathcal{O}(x_1) \cdots \mathcal{O}(x_n) \rangle$ in the CFT side corresponding to the bulk fields (for examples: scalar field, guage field etc.), we have to take a functional derivatives of $\mathcal{W}_{CFT}(\phi)$:

$$\left\langle \prod_i \mathcal{O}(x_i) \right\rangle = -\prod_i \frac{\delta}{\delta\phi(x_i)} \log \mathcal{W}_{CFT}[\phi] \Big|_{\phi=0} \tag{1.53}$$

Note that we have to follow the same renormalization procedure mentioned above. In principle, using this relation we can derive all observables on the field theory side. In the next section we shall take a look at some concrete examples.

1.4 Scalar field in AdS spacetime

We shall study the simplest case of a bulk massive scalar field Φ in AdS which satisfies the Klein−Gordon equation of motion and compute the form of the two-point function. This example will be important for us when we discuss the effects of scalar field on the fermionic spectral function in Chapter 3. Let us consider the AdS$_{d+1}$ spacetime in

Euclidean signature[4] with the metric in Poincaré patch

$$ds^2 = \frac{L^2}{z^2}(-dt^2 + dz^2 + d\vec{x}^2);. \tag{1.54}$$

Taking the bulk scalar field action

$$S = -\frac{1}{2}\int d^{d+1}x\sqrt{-g}(g^{MN}\partial_M\Phi\partial_N\Phi + m^2\Phi)\ , \tag{1.55}$$

by Fourier transforming $\Phi(z,\vec{x}) = \frac{1}{(2\pi)^4}\int d^dk\, e^{ik.x}\,\tilde{\Phi}(z,k)$, the Klein-Gordon (KG) equation of motion then becomes:

$$z^{d+1}\,\partial_z\left(z^{1-d}\,\partial_z\tilde{\Phi}\right)\ -\ k^2\,z^2\,\tilde{\Phi}\ -\ m^2\,L^2\,\tilde{\Phi}\ =\ 0\ . \tag{1.56}$$

This equation can be solved in term of the Bessel's function. However, we are interested in the general structure of the two-point function by analysing the solution of KG equation near the AdS boundary $z = 0$. Asymptotically $(z \to 0)$, we can show from equation (1.56) that $\tilde{\Phi}$ behaves as:

$$\tilde{\Phi}(z) \approx A(k)\,z^{d-\Delta}\ +\ B(k)\,z^{\Delta}\ , \tag{1.57}$$

where $\Delta = \frac{d}{2} + \nu$, with $\nu\ =\ \sqrt{\frac{d^2}{4}\ +\ m^2\,L^2}$. As we have seen earlier, Δ is the dimension of the operator. We notice that Δ is real only if the expression under the square root in ν is non negative, the condition for the bound on the mass m is called *Breitenlohner-Freedman (BF) bound* given by

$$m^2L^2 \geq -\frac{d^2}{4}\ . \tag{1.58}$$

Since the scalar equation of motion is second order, the coefficients A and B in equation (1.57) can be taken as two independent boudary conditions. In equation (1.57), near the boundary, $z^{d-\Delta}$ is the leading term and z^{Δ} as the subleading. The coefficient $A(k)$ of the leading term near the boundary, in AdS/CFT terminology is known as the *source* that corresponds to the dual operator $\mathcal{O}$ of the CFT. The source is usually defined as

$$\phi(k) \approx \lim_{z\to 0} z^{\Delta-d}\,\tilde{\Phi}(z,k)\ . \tag{1.59}$$

---

[4] For Minkowski correlators see [55]

Conversely, we can write $\tilde{\Phi}(z,k) = z^{d-\Delta}\,\phi(k)$ at leading order. In the other hand, the sub-leading term $B(k)$ is known as the *response* or the expectation value. To perform the holographic renormalization [52, 53], which is adding counter terms to regularize the boundary action, when the BF bound (1.58) is satisfied. Fixing the boundary condition of A as the source and obtain B as the expectation value is usually referred as standard quantisation. If we allow the mass m^2 to approach the BF bound, the dimension of the gravity dual operator is $\Delta = d$. However, we know that some systems have operators with dimension smaller than this. In order to realize that, one has to lower m^2 values close to the BF bound. Then the role of A and B can be interchanged and this is known as alternative quantisation, we showed these scenarios in Figure 1.8.

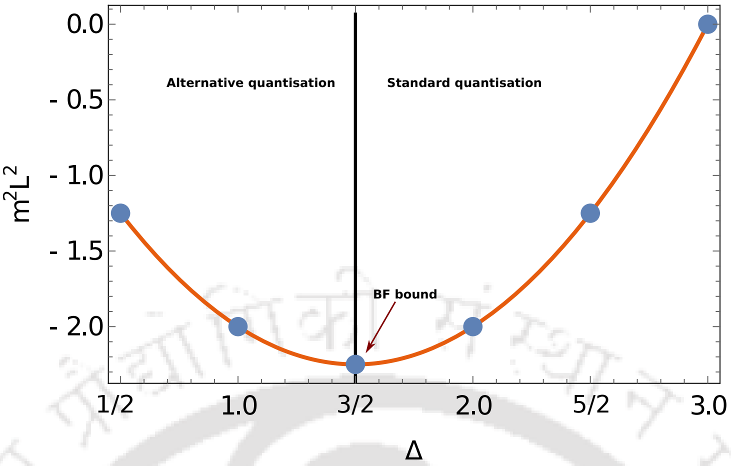

FIGURE 1.8: The plot of mass-squared of the gravity scalar versus the dimension Δ of the dual field theory operator $\mathcal{O}$ in $d = 3$ dimensions

For various m^2 values, we have different dual operators:

- For $m^2L^2 > 0$, for $\Delta > d$, the corresponding operator $\mathcal{O}$ is called an irrelevant operator.
- For $m^2L^2 = 0$, then $\Delta = d$, the corresponding operator $\mathcal{O}$ is called marginal operator.
- For $m^2L^2 < 0$ but in the range $-d^2/4 < m^2L^2 < 0$, the dual operator is called relevant.

Following the standard quantisation, we can identify the source and its corresponding dual operator. The next step would be to calculate the correlator or two point function of the boundary theory. Let us start from the basic field theory calculation. It is known to us that the field theory path integral representation of the one-point function with a source can be written as

$$\langle \mathcal{O}(x)\rangle_\phi \;=\; \int [D\psi]\, \mathcal{O}(x)\, e^{S_E[\psi]+\int d^d y\, \phi(y)\mathcal{O}(y)}\ , \tag{1.60}$$

where ψ is some field of the CFT. Upto linear order (1.60) can be expanded as

$$\langle \mathcal{O}(x)\rangle_\phi \;=\; \langle \mathcal{O}(x)\rangle_{\phi=0} + \int d^d y\, \langle \mathcal{O}(x)\, \mathcal{O}(y)\rangle\, \phi(y) + \cdots\ . \tag{1.61}$$

Now, we can define the Euclidean two-point function or *Green's function* $G_E(x-y) = \langle \mathcal{O}(x)\, \mathcal{O}(y)\rangle$. Then, $\langle \mathcal{O}(x)\rangle_\phi$ measures the fluctuations of the observable away from the expectation value, *i.e.* the linear response of the system to the external perturbation and we can write:

$$\langle \mathcal{O}(x)\rangle_\phi \;=\; \int d^d y\, G_E(x-y)\, \phi(y)\ . \tag{1.62}$$

In momentum space this expression can be written as:

$$\langle \mathcal{O}(k)\rangle_\phi \;=\; G_E(k)\, \phi(k)\ , \tag{1.63}$$

thus, we can obtain the two-point function in momentum space by dividing the one-point function by the source

$$G_E(k) \;=\; \frac{\langle \mathcal{O}(k)\rangle_\phi}{\phi(k)}\ . \tag{1.64}$$

As discussed above, the source is given by $\phi = z^{\Delta-d}\ \Phi(z,x)$ as $z \to 0$, we have the following formula for the two-point function in momentum space:

$$G_E(k) \;=\; \lim_{z\to 0} z^{d-\Delta}\, \frac{\Pi^{(R)}(z,k)}{\phi(z,k)}\ , \tag{1.65}$$

where $\Pi^{(R)}$ is the renormalised conjugate momentum. Now to get the Green's function, we have to compute the quantity $\Pi^{(R)}$. But as we pointed out earlier that we have to properly renormalize the action to remove the diverging terms. This can be done by intuitively adding some counter term to cancel with the diverging term. In this case it is found that the counter term and the renormalized action is given by

$$S_{ct} \;=\; -\frac{\mathcal{C}}{2}\,(d-\Delta)\,L^{d-1}\int\frac{d^dk}{(2\pi)^d}\Big[\epsilon^{-2\nu}\,A(-k)\,A(k)\;+\;2\,A(-k)\,B(k)\Big]\;. \tag{1.66}$$

$$S^{(R)} \;=\; \frac{\mathcal{C}}{2}\,L^{d-1}\,(2\Delta-d)\int\frac{d^dk}{(2\pi)^d}\,A(-k)\,B(k)\;. \tag{1.67}$$

where $\mathcal{C}$ is a normalization constant (see these references [46, 56, 57] for detail calculation). Now the Green's function $G_E(k)$ is given by

$$G_E(k)\;=\;2\nu\,\mathcal{C}\,L^{d-1}\,\frac{B(k)}{A(k)}\;. \tag{1.68}$$

It is worth mentioning that if one solves the full scalar equation in terms of Bessel's function, we can prove that indeed Δ is the conformal dimension of the dual operator $\mathcal{O}$. This is a very neat example for understanding of AdS/CFT duality.

1.5 Fermion field in AdS spacetime

In this section, we review the methodology to compute the two-point function for the fermion field using AdS/CFT duality [58, 60]. In order to compute the retarded fermionic Green's function, we will follow the prescription of Liu and Iqbal [61]. Consider a boundary fermionic operator $\mathcal{O}$ whose gravity dual is a spinor field ψ in the bulk of AdS spacetime with Δ as the scaling dimension.

First we write down the action for the spinors in Euclidean signature as follows

$$S=-\int_M d^{d+1}x\sqrt{-g}\left(\bar{\psi}\Gamma^M D_M\psi-m\bar{\psi}\psi\right)\,, \tag{1.69}$$

with $\bar{\psi}=\psi^\dagger\Gamma^t$ and the covariant derivative $D_M=\partial_M+\frac{1}{4}\omega_{abM}\Gamma^{ab}$, ω_{abM} is the spin connection. The gamma matrices satisfies the Clifford algebra

$$\Gamma^{ab}=\frac{1}{2}\left[\Gamma^a,\Gamma^b\right]\quad,\ \left\{\Gamma^a,\Gamma^b\right\}=2\eta^{ab} \tag{1.70}$$

where, η_{ab} is a $(d+1)-$ dimensional Minkowski metric of signature $(-,+,+,...,+)$ and the capital letter M is the bulk spacetime indices, while small letters $a\,,b,..$ denote the tangent space indices. These two indices are connected through a choice of vielbein e^a_M, defined by

$$g_{MN} = e^a_M e^b_N \eta_{ab} \quad \text{or} \quad \eta_{\,ab} = g_{MN} e^M_a e^N_b \quad , \quad \Gamma^M = e^M_a \; \Gamma^a \; . \tag{1.71}$$

The choice of gamma matrices differs when d is odd and even. For now consider d to be odd and conveniently choose the following basis

$$\Gamma^\mu = \begin{pmatrix} 0 & \gamma^\mu \\ \gamma^\mu & 0 \end{pmatrix}, \quad \Gamma^r = \begin{pmatrix} 1 & 0 \\ 0 & -1 \end{pmatrix}. \tag{1.72}$$

Taking the bulk background spacetime metric of the form

$$ds^2 = g_{\mu\nu} dx^\mu dx^\nu + g_{rr} dr^2 \; , \tag{1.73}$$

where the metric coefficients asymptotically ($r \to \infty$) behave as

$$g_{tt}, \; g_{ii} \sim r^2, \quad g_{rr} \sim 1/r^2 \; , \tag{1.74}$$

where, the $d-$dimensional boundary is at $r \to \infty$. For the spinors, the AdS/CFT prescription for computing $n-$point functions of a quantum field theory from a classical supergravity action in Euclidean signature goes as

$$\left\langle \exp\left[\int d^d x \left(\bar{\chi}_0 \, \mathcal{O} + \bar{\mathcal{O}} \chi_0 \right) \right] \right\rangle_{QFT} = e^{-S_{gravity}[\chi_0, \bar{\chi}_0]}, \tag{1.75}$$

where $\chi_0 = \lim_{r\to\infty} r^{d-\Delta}\psi$. Our first goal now is to calculate the right hand side of equantion (1.75). Note that ψ and χ_0 are spinors of different spacetime dimensions, and will have a different number of components. The action for ψ, on the other hand, contains only one derivative and therefore implementing Dirichlet boundary conditions for a first order system is more tricky and will need a careful approach.

Decomposing the spinor into two components with eigenvalues of Γ^r, i.e., ± 1 .

$$\psi = \psi_+ + \psi_-, \quad \psi_\pm = \Gamma_\pm \psi, \quad \Gamma_\pm = \frac{1}{2} \left(1 \pm \Gamma^r \right), \tag{1.76}$$

The Dirac equation $\left[\Gamma^M D_M - m\right]\psi = 0$, becomes

$$\left[r\ \Gamma^r\partial_r + \frac{i}{r}\Gamma\ .\ k + \frac{d}{2}\ \Gamma^r - m\right]\begin{pmatrix}\psi_+\\ \psi_-\end{pmatrix} = 0, \tag{1.77}$$

where, $\Gamma\ .\ k = \gamma^\mu k_\mu$. Now examining the asymptotic behaviour of $\psi_\pm$ gives the following form

$$\psi_+(k,r) = A_0(k)r^{m-\frac{d}{2}} + B_0(k)r^{-\frac{d}{2}-m-1},\quad \psi_-(k,r) = C_0(k)r^{m-\frac{d}{2}-1} + D_0(k)r^{-\frac{d}{2}-m} \tag{1.78}$$

From this equation for $m \geq 0$, the leading term A_0 is the source for the dual operator $\mathcal{O}$ whose mass dimension $\Delta = \frac{d}{2} + m$. Thus, we can identify the source as

$$\lim_{r\to\infty} r^{\frac{d}{2}-m}\psi_+ = A_0 \ = \chi_0\ . \tag{1.79}$$

Because the Dirac equation is first order, the coefficients in (1.78) are not independent, which we can immediately see by plugging equation (1.78) back into equation of motion (1.77). We get the following relations among the coefficients

$$\begin{cases} B_0(k) = -\frac{i\,\gamma.k}{1+2m}D_0(k), \\ C_0(k) = -\frac{i\,\gamma.k}{1-2m}A_0(k). \end{cases} \tag{1.80}$$

Similar to the scalar field, the boundary counter term that must be added for a stationary action for the fermions is given by [60]

$$C_{ct} = -\int_{\partial M} d^dx\sqrt{gg^{rr}}\bar{\psi}_+\psi_- = -\int_{\partial M} d^dx\sqrt{gg^{rr}}\left(\bar{\psi}_-\delta\psi_+ + \delta\bar{\psi}_+\psi_-\right) \tag{1.81}$$

whose conjugate momenta Π is given by

$$\Pi_+ = -\sqrt{gg^{rr}}\ \bar{\psi}_-,\quad \Pi_- = -\sqrt{gg^{rr}}\ \bar{\psi}_+. \tag{1.82}$$

$$\Pi_+ = -\bar{C}_0(k)\ r^{\frac{d}{2}+m-1} - \bar{D}_0(k)\ r^{\frac{d}{2}-m},\quad \Pi_- = \bar{A}_0(k)\ r^{\frac{d}{2}+m} + \bar{B}_0(k)\ r^{\frac{d}{2}-m-1} \tag{1.83}$$

Then (1.78) and (1.79) result in $\langle\mathcal{O}\rangle_{A_0} = -\lim_{r\to\infty} r^{m-\frac{d}{2}}\Pi_+, = \bar{D}_0$. The source and the expectation value are related to each other by a matrix $\mathcal{S}$ as $D_0 = \mathcal{S}\,A_0$. Thus we get the Euclidean correlators given by:

$$G_E(k) = \mathcal{S}(k)\gamma^\tau. \tag{1.84}$$

The retarded Green's function in Lorentzian signature is $G_R(k) = i\mathcal{S}(k)\gamma^t$. The factor γ^τ comes from the fact that the correlators $G_E = \langle \mathcal{O}\mathcal{O}^\dagger \rangle$ but not $\langle \mathcal{O}\bar{\mathcal{O}} \rangle$.

In summary, to compute retarded correlators for fermionic operators, one has to find a solution for ψ by imposing the in-falling conditions at the horizon. Then we can expand ψ at the boundary $r \to \infty$, take the ratios of the coefficients and multiply with the appropriate gamma matrix.

So far we have discussed the general procedure for computing the Green's function for both scalar and spinors fields. However, one can follow the same methodology to other fields, for instance the gauge field A_μ, which will be discussed later. In the Chapter 2, we will review some application of AdS/CFT technique to discuss and calculate the spectral function that relates to actual condensed matter system, which we described at the beginning of this chapter. Also we shall compute the conductivity by perturbing the gauge field in the bulk which correspond to the current J_μ and compare the results from experiments to see the reliability of this approach.

There are many more examples that we can map from gravity theory in the bulk of AdS and the CFT at boundary that we have not discussed here. We list the correspondence between gravity in the bulk with field theory on the boundary in the table below 1.1 for a quick reference.

GRAVITY IN THE BULK	CFT IN THE BOUNDARY OF ADS
Classical GR	$N \longrightarrow \infty$ and strong coupling
Metric field $g_{\mu\nu}$	energy momentum tensor $T^{\mu\nu}$
Maxwell field A_μ	conserved Current J^μ.
Scalar field ϕ	order parameter/scalar operator.
Dirac field ψ	fermionic operator $\mathcal{O}_f$
Mass of the field	conformal dimension of the operator.
Spin/charge of the field	spin/charge of the operator.
Local isometry	global symmetry.
Boundary value and radial momentum of the field	source and vaccumn expectation value of the operator.
Instability and Hawking temperature of the Blackhole	phase transition and temperature.
Boundary value of the gauge field	chemical potential/charge density.

TABLE 1.1: The dictionary of AdS/CFT correspondence

Chapter 2

Applications: AdS/CFT in action

In order to familiarize with the methodology and apply in our work, let us review some of the pioneering works which are based on the *Holographic Principle*. In particular we will take a look at the articles [3–5]. We shall discuss and try to learn about the holographic technique by performing all the analytical calculations and numerics involved. In this chapter and the subsequent chapters we will use mostly `Mathematica` for our numerical analyses and plotting. There are cases where we will use pre-built packages such as `EDCRGTCcode.m` and `diffgeo.m` for analytical calculation.

2.1 Example 1: Non-Fermi liquid behaviour from Holography

As our first example, we want to study a strongly coupled systems at finite charge density. In this particular simple model we identify a non-Fermi liquid behaviour which is a signature of strong interactions. In order to utilize the formalism of AdS/CFT duality, we have to fulfil certain requirements in the bulk of AdS to relate with the quantities in the field theory side. For a system with finite charge density, we need a charged black hole. Therefore, let us consider a conformal field theory (CFT) which is in $(2+1)$ dimensions that contain a fermionic charge with global $U(1)$ symmetry. In the gravity side, such a system is described by the Reissner–Nordström black hole in AdS$_4$. The mapping between fermionic operator in the CFT to gravity satisfies the relation $\boxed{m\,L = \Delta - 3/2}$, where Δ is a conformal dimension and L is known as AdS curvature radius. Now to identify the quasi-particle and non-Fermi liquid, we have to analyse the spectral function or the

Green's function discussed in our introduction, which can be extracted directly from the solution of Dirac equations for spinors ψ in the charged AdS black hole geometry using the method discussed in section 1.5 of Chapter 1.

2.1.1 Set-up of background geometry and fermionic action

Consider a charged Reissner–Nordström (RN) black hole with Einstein-Maxwell action in AdS$_4$ given by

$$S = \frac{1}{2\kappa^2}\int d^4x\sqrt{-g}\left(R - \frac{6}{L^2} - \frac{L^2}{g_F^2}F_{MN}F^{MN}\right) \tag{2.1}$$

where, R is Riemann scalar, and g_F^2 is an effective dimensionless gauge coupling, $\kappa^2 = 8\pi G$. The Maxwell's field is given by $F_{MN} = \partial_M A_N - \partial_N A_M$ with the gauge field A_M. The solution to the equations of motion obtained from the above action satisfies the following metric:

$$ds^2 = \frac{r^2}{L^2}(-f dt^2 + dx_i^2) + \frac{L^2 dr^2}{r^2 f} \tag{2.2}$$

with

$$f = 1 + \frac{Q^2}{r^4} - \frac{M}{r^3}\,, \qquad A_t = \mu\left(1 - \frac{r_h}{r}\right)\,, \qquad \mu \equiv \frac{g_F Q}{L^2 r_h}\,, \tag{2.3}$$

where r_h and μ are the black hole horizon radius and the chemical potential respectively. For convenience of fixing the horizon radius, we can perform a rescaling of the coordinates and parameters as follows:

$$r \to r_h\, r,\ (t,\vec{x}) \to \frac{L^2}{r_h}(t,\vec{x})\,,\ A_t \to \frac{r_h}{L^2},\ M \to M r_h^3,\ Q \to Q\, r_h^2\,, \tag{2.4}$$

then the above metric (2.2) now takes the following form:

$$\frac{ds^2}{L^2} = r^2(-f dt^2 + d\vec{x}^2) + \frac{dr^2}{r^2 f}\,, \tag{2.5}$$

with

$$f = 1 + \frac{Q^2}{r^4} - \frac{1+Q^2}{r^3},\ A_t = \mu\,(1 - \frac{1}{r}),\ \mu = g_F Q\,. \tag{2.6}$$

Now the horizon is at $r = 1$, and the black hole temperature is given by

$$T = -\frac{g'_{tt}(r)}{4\pi}\bigg|_{r=1} = \frac{1}{4\pi}\Big(3 - Q^2\Big) \tag{2.7}$$

We see that the zero temperature can be obtained by setting the black hole charge $Q = \sqrt{3}$. Near the horizon if we expand the metric coefficient as $f(r) \approx (3 - Q^2)(r-1) + (-6 + 4Q^2)(r-1)^2 + \cdots$, then for zero temperature, we have $f(r) \approx 6(r-1)^2$. Now if we define $\eta = \lambda \frac{1}{6(r-1)}$ and $t = \lambda^{-1}\tau$ as our new coordinates, the metric (2.5) reduces to

$$ds^2 = \frac{L_2^2}{\eta^2}\Big(-d\tau^2 + d\eta^2\Big) + L^2 d\vec{x}^2 \,, \tag{2.8}$$

which is $AdS_2 \times \mathbb{R}^2$ with the radius of AdS_2 being given by $L_2 = L/\sqrt{6}$. This metric will be important if we want to study the IR properties of the Green's function. With this background geometry, we can write the action for spinors and solve the Dirac equation to obtain the spectral function. The action for fermion field ψ is given by

$$S_{spinor} = i\int d^{3+1}x\sqrt{-g}\,\left(\bar{\psi}\Gamma^M D_M\psi - m\bar{\psi}\psi\ \right), \tag{2.9}$$

where , $\bar{\psi} = \psi^\dagger \Gamma^{\underline{t}}$, $D_M = \partial_M + \frac{1}{4}\omega_{abM}\Gamma^{ab} - iqA_M$, ω_{abM} is the spin connection. The indices M and a, b denote the bulk spacetime and tangent space indices, and μ, ν denote the indices along the boundary directions i.e, $M = (r, \mu)$. The gamma matrices obey the commutation relations $\{\Gamma^a, \Gamma^b\} = 2\eta^{ab}$, $\Gamma^{ab} = \frac{1}{2}[\Gamma^a, \Gamma^b]$ and $\Gamma^M = e^M_a\Gamma^a$, where e^M_a is a vielbein. Now the Dirac equation of motion for ψ from the action (2.9) is given by

$$(\Gamma^M D_M - m)\psi = 0 \,. \tag{2.10}$$

We can calculate the vielbeins that appears in the covariant derivative of the Dirac equations from the given metric (2.5), and one finds that the non-vanishing components of spin connections are given by :

$$\begin{aligned} e^r_{\underline{r}} &= \frac{1}{\sqrt{g_{rr}}} \ , \quad e^t_{\underline{t}} = \frac{1}{\sqrt{-g_{tt}}} \ , \quad e^x_{\underline{x}} = \frac{1}{\sqrt{g_{xx}}} \\ \omega_{\underline{t}\,\underline{r}} &= -\left(rf(r) + \frac{r^2 f'(r)}{2}\right)dt \ , \ \omega_{\underline{r}\,\underline{x}} = -r\sqrt{f(r)}dx \,. \end{aligned}$$

Now we can simplify the Dirac equation (2.10) by writing $\psi = \begin{pmatrix} \psi_+ \\ \psi_- \end{pmatrix}$ and choose the following basis:

$$\mathit{\Gamma}^{\underline{r}} = \begin{pmatrix} 1 & 0 \\ 0 & -1 \end{pmatrix}, \quad \mathit{\Gamma}^{\underline{\mu}} = \begin{pmatrix} -i & 0 \\ 0 & i \end{pmatrix}. \tag{2.11}$$

The Dirac equation then simplifies to,

$$\left[\sqrt{\frac{g_{xx}}{g_{rr}}}\left(\Gamma^{\underline{r}}\partial_r - m\sqrt{g_{rr}} + \frac{\sqrt{g_{rr}}}{4}\,(S.C)\right) + \sqrt{\frac{g_{xx}}{-g_{tt}}}\,\Gamma^{\underline{t}}\,(\partial_t - iqA_t) + \Gamma^{\underline{x}}\partial_x\right]\psi = 0\,, \tag{2.12}$$

where, $S.C = e_{\underline{t}}^{t}\Gamma^{\underline{t}}\omega_{\underline{t}\,\underline{r}}\Gamma^{\underline{t}\,\underline{r}} + e_{\underline{x}}^{x}\Gamma^{\underline{x}}\omega_{\underline{r}\,\underline{x}}\Gamma^{\underline{r}\,\underline{x}}$. Since it is more convenient to work in Fourier space, we will Fourier transform the spinor ψ and simultaneously remove the spin connection by rescaling $\psi_\pm = (r^4 f)^{-\frac{1}{4}} e^{-i\omega t + k_i x^i}\phi_\pm$. Then we can write in compact form as

$$\sqrt{\frac{g_{xx}}{g_{rr}}}\left(\partial_r - m\sqrt{g_{rr}}\right)\phi\pm = \mp i K_\mu \gamma^\mu \phi_\mp\,, \tag{2.13}$$

$$\text{where,} \qquad K_\mu(r) = (-u(r), k_i), \quad u(r) = \sqrt{\frac{g_{xx}}{-g_{tt}}}\left(\omega + \mu_q(1 - \frac{1}{r})\right).$$

Now, equation (2.13) near the AdS boundary (i.e., $r \to \infty$) have the following form:

$$\begin{aligned} &(r^2\partial_r - m\,r)\,\phi_+ = -i\gamma.k\,\phi_-\,, \quad (r^2\partial_r + m\,r)\,\phi_- = +i\gamma.k\,\phi_+\,, \\ \Rightarrow \qquad &\phi_+ = -i\frac{\gamma.k\,(r^2\partial_r + m\,r)}{k^2}\,\phi_-\,, \quad \phi_- = +i\frac{\gamma.k\,(r^2\partial_r - m\,r)}{k^2}\,\phi_+\,, \end{aligned} \tag{2.14}$$

which can be the decoupled to give

$$A(-m)\,A(m)\phi_\pm = k^2\phi_\pm \ \ ; \ A(m) = r^2\partial_r - m\,r \ \ , A(-m) = r^2\partial_r + m\,r \tag{2.15}$$

This equation can be analytically solved using Bessel functions. However, we are not going to do that here. By examining the fields $\phi_\pm$ for $r \to \infty$ they have the following behaviour:

$$\phi_+ = Ar^m + Br^{-m-1}, \quad \phi_- = Cr^{m-1} + Dr^{-m}\,. \tag{2.16}$$

When substituting back the above solution $\phi_\pm$ in equation (2.13), we get the following relations

$$C = \frac{i\gamma^\mu k_\mu}{2m-1}\, A\ , \quad B = \frac{i\gamma^\mu k_\mu}{2m+1}\, D, \tag{2.17}$$

where, $k_\mu = \Big(-(\omega+\mu_q), k_i\Big)$. As pointed out in our previous chapter, for standard quantization, the leading coefficient A is interpreted as the source of the dual operator in the boundary theory and D as the vaccumn expectation value (or vev in short) of the field. When $m \to -m$, we simply exchange the role of $\phi_\pm$ with $A \longleftrightarrow D$ and $B \longleftrightarrow C$. The coefficients A and D are related by matrix S as $D = \mathcal{S}A$, and hence the retarded Green's function G_R is now given by [61]

$$G_R = -i\mathcal{S}\gamma^{\underline{t}}. \tag{2.18}$$

In principle, we can extract the coefficient numerically by solving the Dirac equations and get the Green's function, but it is more efficient to solve the flow equations with two non-linear first order ODEs. By choosing the basis $\gamma^{\underline{t}} = i\sigma_2$,$\gamma^{\underline{x}} = \sigma_1$,$\gamma^{\underline{r}} = \sigma_3$ and due to the rotational symmetry, we set $k_2 = 0$, then one arrives with two sets of decoupled equations

$$\begin{aligned}\sqrt{\frac{g_{xx}}{g_{rr}}}(\partial_r \mp m\sqrt{g_{rr}})y_\pm &= \mp(k_1-u)z_\mp\ ,\\ \sqrt{\frac{g_{xx}}{g_{rr}}}(\partial_r \pm m\sqrt{g_{rr}})z_\mp &= \pm(k_1+u)y_\pm\ ,\end{aligned} \tag{2.19}$$

where $\phi_\pm$ is written as $\phi_\pm = \begin{pmatrix} y_\pm \\ z_\pm \end{pmatrix}$. From the above equations (2.19), we can derive the following flow equations

$$\sqrt{\frac{g_{xx}}{g_{rr}}}\partial_r\xi_\pm = -2m\sqrt{g_{xx}}\xi_\pm \mp (k_1 \mp u) \pm (k_1 \pm u)\xi_\pm^2\ , \tag{2.20}$$

where, $\xi_+ = i\,\frac{y_-}{z_+}$ and $\xi_- = -i\,\frac{z_-}{y_+}$. We then get the retarded Green's function written as

$$G_R = \lim_{\epsilon\to 0}\epsilon^{-2m}\begin{pmatrix} \xi_+ & 0 \\ 0 & \xi_- \end{pmatrix}\Bigg|_{r=\frac{1}{\epsilon}} \tag{2.21}$$

It is very important to chose the correct boundary conditions in order to solve equation (2.20). We have to impose the ingoing condition at the horizon and carefully check for $\omega \neq 0$ and $\omega = 0$ cases.

2.1.2 Boundary conditions

One way to get the boundary conditions is by expanding the equation (2.20) near the horizon ($r = 1$). Taking only the leading non-vanishing terms, we need to solve the quadratic equation in $\xi_\pm$ and get the boundary conditions as shown below. Another way is by starting from (2.19), putting $y_+ = e^{S(r)}$ for some function $S(r)$ and plugging back in the sets of equations (2.19) gives

$$z_- = \frac{(r^2\sqrt{f}S' - mr)}{-i(k-u)}e^S \quad \Rightarrow \partial_r z_- = \frac{S'(r^2\sqrt{f}S' - mr)}{-i(k-u)}e^S \, .$$

Further simplifications gives $S'(r) = \pm\frac{\sqrt{k^2+m^2r^2-u^2}}{r^2\sqrt{f}}$. At zero temperature and near the horizon, $\xi_- = \frac{-iz_-}{y_+}$ is simplified as

$$\begin{aligned} \xi_-|_{r\to1} &= i \qquad \text{for} \;\; \omega \neq 0 \, , \\ \xi_-|_{r\to1} &= \frac{m - \sqrt{k^2 + m^2 - \frac{\mu_q^2}{6} - i\epsilon}}{\frac{\mu_q}{\sqrt{6}} - k} \qquad \text{for} \;\; \omega = 0 \, , \end{aligned} \tag{2.22}$$

with $m^2 \longrightarrow m^2 - i\epsilon$. In the same way one can derive an expression for ξ_+ and in general

$$\xi_\pm|_{r\to1} = \frac{m - \sqrt{k^2 + m^2 - \frac{\mu_q^2}{6} - i\epsilon}}{\frac{\mu_q}{\sqrt{6}} \pm k} \qquad \text{for} \;\; \omega = 0 \, . \tag{2.23}$$

Now with these boundary conditions we are ready to solve equations (2.20). One can easily obtain the retarded Green's function and analyze its properties from the solutions of (2.20). For the numerical computation of the flow equation (2.20), see appendix B.1.

2.1.3 Analysis of the spectral function G_R

The spectral function is defined as $A(k,\omega) \equiv \mathrm{Im}\, G_R(k,\omega)$. Looking at equation (2.20), for $k \to -k$, we have $G_{22} \leftrightarrow G_{11}$. Similarly, for $q \to -q, \omega \to -\omega$, we get $G_{11}(\omega, k, -q) =$

$-G^{*}_{22}(-\omega,k,q)$. For $m=0$, from the flow equation, we have $\xi_{-}=-\frac{1}{\xi_{+}}$, which implies that $G_{22}=-\frac{1}{G_{11}}$. Also for $k=0,m=0$, we have $G_{11}(\omega)=G_{22}(\omega)=i$. From the

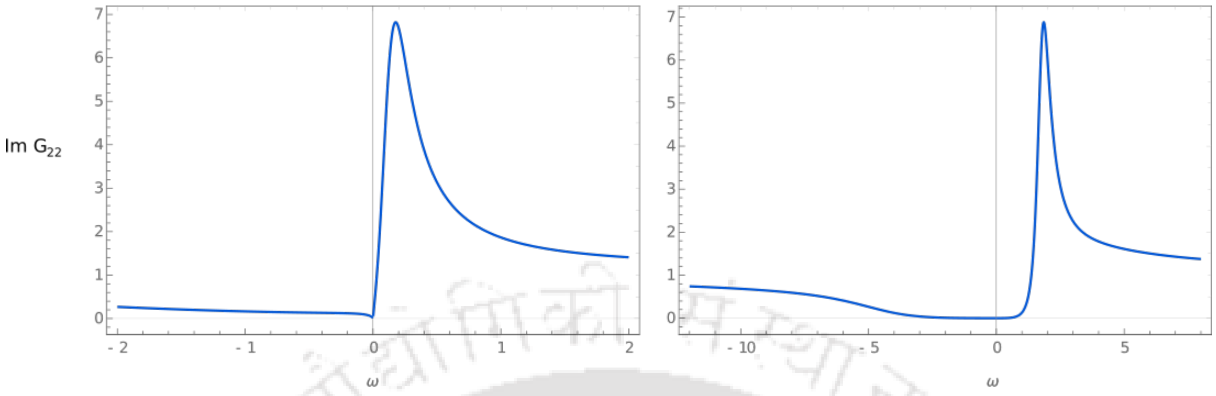

FIGURE 2.1: Plot of Im$G_{22}(\omega)$ at $k=1.2<\mu_q$ (left) and $k=3.0>\mu_q$ (right) for the parameters $m=0$, $q=1$ and $\mu_q=\sqrt{3}$.

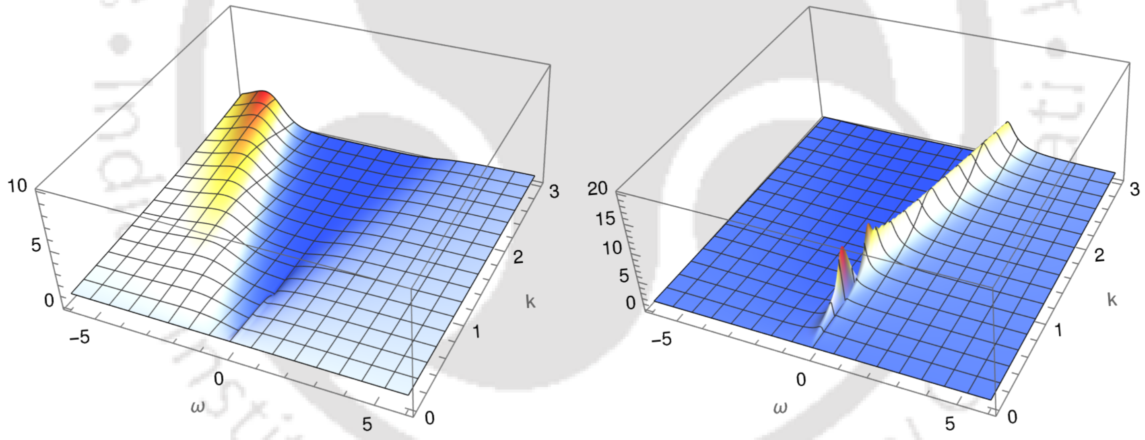

FIGURE 2.2: Three dimensional plot of Im $G_{11}(\omega,k)$ (left) and Im $G_{22}(\omega,k)$ (right) at temperature $T=0$ with the parameter $m=0$, $q=1$ and $\mu_q=\sqrt{3}$.

numerical solution of the flow equation (2.20), the spectral function approaches unity for large value of ω as can be seen from Figure 2.1 (right). Note that the on set of the peak is approximately around $\omega\approx1.2\approx k-\mu_q$, which corresponds to the divergence at $\omega=k$ in the vacuum Green's function which is given by [58, 59]

$$G_{11}(\omega,k)=-\sqrt{\frac{k-(\omega+i\epsilon)}{k+(\omega+i\epsilon)}},\quad G_{22}(\omega,k)=\sqrt{\frac{k+(\omega+i\epsilon)}{k-(\omega+i\epsilon)}}$$

Furthermore the spectral function is almost zero in the region where ω is between $(-k-\mu_q)$ and $(k+\mu_q)$ as that of vacuum. From Figures 2.1 and 2.2, we see that both ImG_{11} and ImG_{22} are positive which is a requirement from unitarity as these two quantities are related to the density of states which cannot be negative. Also the peak observed in Figure 2.2 (right) indicates the presence of a Fermi surface and near $k_F \approx 0.92$, there exists a quasiparticle like peak. One can analyse ImG_{22} peak with corresponding Fermi momentum k_F near the region of $k_\perp \equiv k - k_F$. As we can see from Figure 2.3 (left), clearly there is a quasiparticle peak at $\omega < 0$. When $k_\perp$ approaches zero, both the peak and bump approach $\omega = 0$ and their heights becomes large. Similarly for $k > k_F$ as shown in the right plot.

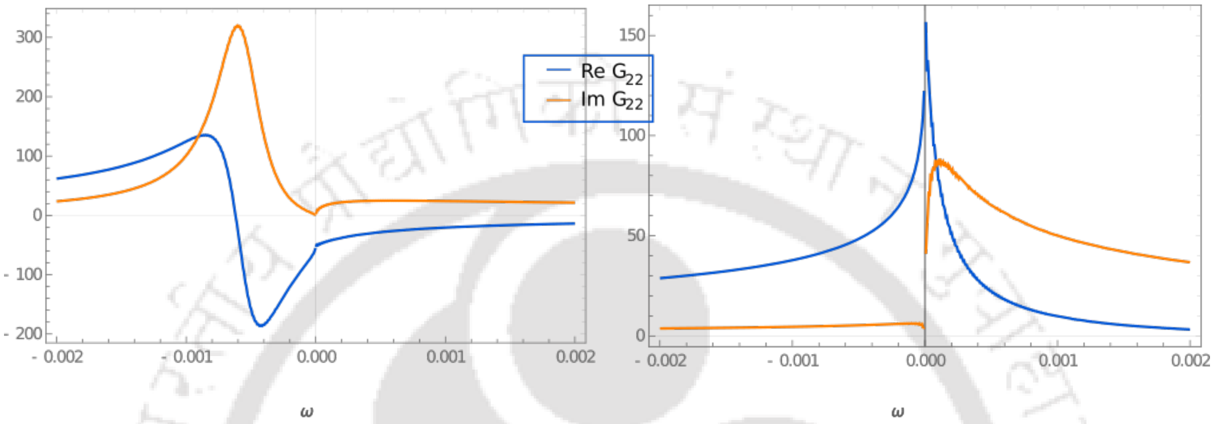

FIGURE 2.3: Plot of G_{22} vs ω (small omega values around zero) at $k = 0.90 < k_F$ (left) and $k = 0.925 > k_F$(right). Other parameters are same as in Figure 2.2.

Studying the scaling behaviour near the location of quasiparticle (denoted by $\omega_*(\kappa_\perp)$), the scaling goes as $\omega_*(\kappa_\perp) \sim k_\perp^z$ and the maximum height of ImG_{22} scales as

$$\mathrm{Im}G_{22}(\omega_*(\kappa_\perp), k_\perp) \sim k_\perp^{-\alpha} \, .$$

In the limit where $(k_\perp, \omega) \sim 0$, which is near the Fermi surface, Im$G_{22}(\omega, k_\perp)$ scales as

$$\mathrm{Im}G_{22}(\lambda^z \omega, \lambda k_\perp) = \lambda^{-\alpha} \mathrm{Im}G_{22}(\omega, k_\perp) \tag{2.24}$$

The scaling behaviour reveals the sharp Fermi surface with Fermi momentum k_F. However the scaling exponents are found to be $z = 2.09 \pm 0.01$ and $\alpha = 1.00 \pm 0.01$, which are different from those obtained in *Landau's* Fermi liquid where the scaling exponents are

$\alpha = z = 1$. It shows that our system exhibits non Fermi liquid properties. So in summary, by solving Dirac equation for the corresponding bulk spinor field in the charged RN AdS$_4$ black hole geometry, and after analysing the spectral function we found a non-Fermi liquid behaviour.

2.2 Example 2: Computation of conductivity

In this example, we shall illustrate how to compute the conductivity of strongly interacting quantum field theories that has a dual gravity theory in AdS spacetime. Though we will not be computing any conductivity in this thesis, it is useful to learn and check how effective is the holographic method. Previously, we learned that the gauge field A_M in the bulk is dual to the current density J_μ at the AdS boundary. RN black hole in AdS meets our requirement here. For what we are going to discuss, we refer the readers to the review [4] for details. Firstly let us recall the Ohm's Law from school that relate the potential difference to the current, but now in advanced concept we can generalize to the following form

$$\begin{pmatrix} \langle J_x \rangle \\ \langle Q_x \rangle \end{pmatrix} = \begin{pmatrix} \sigma & \alpha T \\ \alpha T & \bar{\kappa} T \end{pmatrix} \begin{pmatrix} E_x \\ -(\nabla_x T)/T \end{pmatrix}, \tag{2.25}$$

where we have two currents J_x and Q_x, with the current $Q_x = T_{tx} - \mu J_x$ sourced by a thermal gradient. Here T_{tx} appears by variation of the Einstein-Maxwell action, μ is the chemical potential at the boundary, $-(\nabla_x T)/T$ and E_x are the temperature gradient and Electric field applied respectively. Now we have three conductivities: electrical (σ), thermal ($\bar{\kappa}$) and thermoelectric (α). Further manipulation with the variational calculus, one obtains the following equations

$$\begin{pmatrix} \langle J_x \rangle \\ \langle Q_x \rangle \end{pmatrix} = \begin{pmatrix} \sigma & \alpha T \\ \alpha T & \bar{\kappa} T \end{pmatrix} \begin{pmatrix} i\omega(\delta A_x + \mu\, \delta g_{tx}) \\ i\omega\delta\, g_{tx} \end{pmatrix}. \tag{2.26}$$

Let us concentrate only with the electrical conductivity (σ). Now if we assume an external oscillating electric field $E(\omega)$ as the source and, $J(\omega)$ as the current due to the electric field $E(\omega)$ (the fields are in Fourier space with momentum $k = 0$), then the conductivity is given by:

$$\sigma(\omega) = -i\,\frac{G^R_{J_x J_x}(\omega)}{\omega} = \frac{J_x(\omega)}{E_x(\omega)}\,. \tag{2.27}$$

where $G^R_{J_x J_x}$ is a response function and we usually call it the Green's function. We see from (2.26) that in order to calculate the conductivity σ we have to perturb the bulk equations of motion with respect to δA_x and δg_{tx}. For a 4−dimensional RN-AdS black hole, an equation for computing the conductivity as shown in the appendix B.2 (using `Mathematica`) is given by

$$\delta A_x \left(\frac{\omega^2}{f(z)} - z^2 {A'_t}^2 \right) + \delta A'_x \, f'(z) + f(z) \, \delta A''_x = 0 \,, \tag{2.28}$$

where $f(z)$ comes from the metric and A'_t is just a constant. Finally since the Green's function $G^R_{J_x J_x}$ is the ratio of coefficient from the leading and sub-leading term, if we expand δA_x near the boundary

$$\delta A_x = \delta A_{x(0)} + z \, \delta A_{x(1)} + \cdots \,, \tag{2.29}$$

The conductivity can be obtained with the following formula

$$\sigma(\omega) = -i \, \frac{\delta A_{x(1)}}{\omega \, \delta A_{x(0)}} \bigg|_{z \longrightarrow 0} \tag{2.30}$$

2.2.1 Numerics and some results

To obtain the electrical conductivity $\sigma(\omega)$, we need to solve the differential equation (2.28) numerically. Firstly, near the horizon we have to take the in-falling boundary conditions. For convenience, we remove the near-horizon oscillations from the field A_x by defining

$$A_x(z) = f(z)^{-i\omega/(4\pi T)} \, a_x(z). \tag{2.31}$$

Then we expand $a_x(z) \sim 1 + a_1 \, (z-1) + a_2 \, (z-1)^2 + \cdots$ near the horizon $z = 1$. These coefficients a_1, a_2 can be solved by substituting this expansion back in the equation of motion for a_x. Once we specify the boundary condition at the horizon we can numerically integrate equation (2.28) from the horizon to the boundary using `NDSolve` with shooting method[1], the in-build Mathematica function, and extract the leading and sub-leading terms at the boundary to obtain the conductivity σ using the formula given in equation 2.30 and we showed the results in Figure 2.4.

---

[1] Mathematica notebook can be found here.

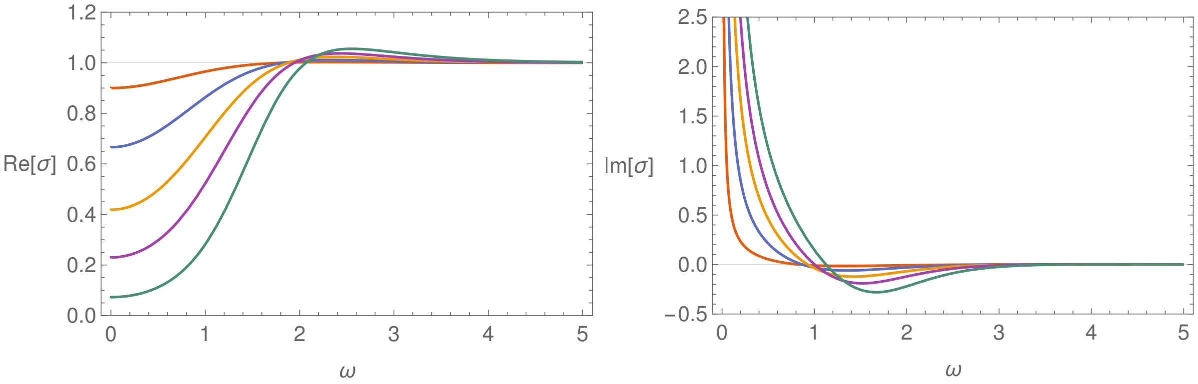

FIGURE 2.4: Plots of the electrical conductivity (σ) versus frequency obtained by using the AdS/CFT prescription. Different coloured curves are for different values of the chemical potential (μ) at a particular fixed temperature.

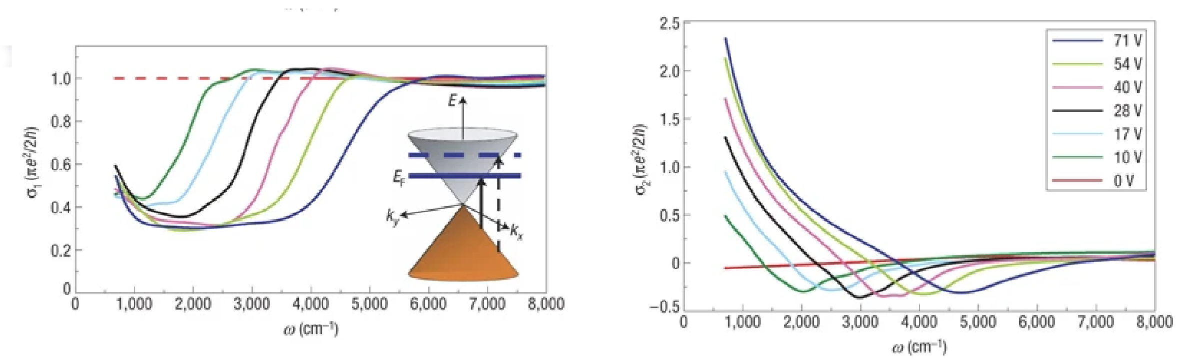

FIGURE 2.5: These two plots are from experimental data. The real (left) and imaginary (right) parts of the electrical conductivity obtained from the experiments performed on graphene. Here, different colours correspond to different values of the gate voltage. Plots are taken from [62].

When we compare the results in Figure 2.4 with some of the experimental results in Figure 2.5 performed in graphene [62], it is interesting to see the behaviour in conductivity is very close to the results obtained using AdS/CFT duality. For detailed explanations we refer the reader to this article [4] by S. Hartnoll. Another interesting comparison is between the observed experimental power law behaviour in the optical conductivity in the strange metal phase of high temperatures superconductors [63] with the optical conductivity computed numerically through the holographic principle for a strongly coupled system in the presence of an ionic lattice [38].

2.3 Example 3: Holographic Fermi arcs

Our previous example shows that a non-Fermi liquid behaviour is observed by considering only a massive Dirac action in RN AdS$_4$ black hole. Based on the results in [3], Vanacore et. al. in [5] attempted to use the same holographic framework to explain the origin and properties of the Fermi arcs, which are not well understood by weakly coupled physics. Since the high temperature (high T_c) superconductors start off their lives from the Mott insulators and not from Fermi liquid, their goal is to work out the formation of Fermi arcs from Mott insulator that appeared in the high T_c-superconductor cuprates. Motivated by the work in [11], which was further studied in more detail in [12, 13] that one can add a non-minimal Pauli coupling term such as $-ip\bar{\psi}\not{F}\psi$ with the following action:

$$S_{fermion} = \int d^4x\sqrt{-g}i\bar{\psi}\left(\not{D} - m - ip\not{F}\right)\psi \; . \tag{2.32}$$

When such an interaction term is added, they found that spectral weight is transferred between bands and the emergence of a gap in the fermion density of states. This dynamic formation of a gap and spectral weight transfer possesses the characteristics of Mott insulators. Also, it was observed that the coupling provides a shift in fermion momenta depending on the boundary chemical potential but only the fermion frequencies. Several other phenomena, such as the crossing of the dominant pole spectrum in low energy limit from the regimes of Fermi liquid, marginal and non-Fermi liquid and extend up to a gapped phase. The opening in the energy gap when the strength of the coupling parameter p is large and positive is due to the collapse of the quasi-particle. However, it was realized in [14] that the gapped spectrum arises from the presence of both poles and zero or *pole-zeros* duality. For the coupling term considered in (2.32), the spectrum exhibit only zeros for large positive p and only poles at large negative p. Thus, the diminishing of the spectral weight is due to zeros. To better understand this mechanism of pole-zeros duality, let us discuss this briefly. Starting from Fermi liquid theory, the quasi-particle is a pole in the retarded Green's function G_R. So the location of the pole is given by

$$G_R^{-1}(\omega = 0, k = k_F) = 0 \; , \tag{2.33}$$

which dictates the Fermi surface and dispersion. Furthermore, for weakly-coupled interactions, the real component of the Green's function, G_R, must change signs and is only possible through the pole, and via Luttinger's theorem [15], by integrating over the positive region of G_R one obtains the particle density. Now for an interacting theory, the Green's function is modified and given by

$$G_R^{-1}(\omega, k) = G_0^{-1}(\omega, k) + \sum(\omega, k), \tag{2.34}$$

where, G_0 is the non-interacting Green's function. The presence a zero in (2.34) would come from a divergent self-energy and it is this divergent that restricts the crossing between bands from the Fermi energy leading to Mottness. In fact, the condition for Mottness is specified by the eigenvalues of the matrix G_R, represented by its determinant as,

$$\det G_R(\omega = 0, k = k_L) = 0 \ . \tag{2.35}$$

To see the poles structure from the expression in (2.34), near the Fermi surface we can expand as

$$G_R^{-1}(\omega, k) \sim k - k_F - \omega/v_F - \Sigma(\omega, k) \tag{2.36}$$

where, the self-energy $\Sigma(\omega, k)$ is given by [16]

$$\Sigma(\omega, k) \sim c\,\omega^{2\nu_k^{\pm}} \quad , \quad 6\nu_k^2 = k^2 - \frac{q^2}{2} \ , \tag{2.37}$$

As pointed out above, now depending on the scaling dimension $\nu_k < 1/2$ that appeared in the self energy, the pole of G_R corresponds to an unstable quasi-particle identified as a non-Fermi fluid. When $\nu_k = 1/2$, the excitations are that of marginal Fermi fluid. But for $\nu_k > 1/2$ the dispersion relation is linear and thus it will corresponds to Fermi fluid. Finally, when ν_k is imaginary we have "log oscillatory" solutions.

Coming back to our main discussion, the dipole coupling strength p given in (2.32) plays the role of an order parameter in Mott physics. In the above model from the language of Green's function, the pole is the signature of the Fermi and non-Fermi liquids, while zeroes correspond to the Mott insulating phase. If the poles and zeroes coexist, that would be the pseudo-gap phase. Now, from the perspective of symmetry breaking, the presence of such Pauli's term in the action (2.32) breaks the chiral symmetry in the bulk due to the presence of a non-zero anticommutator with the generator of chiral rotations i.e., $\{\Gamma_{ab}, \Gamma_5\} \neq 0$, which is connected to the mechanism for mass generation. Since the Pauli's term only generates a gap for large and positive values of p; there would be no such restriction if the gap were a result of the loss of chiral symmetry. In the scaling dimension of the dual boundary operators, for positive coupling constant p, it will increase the exponent converting poles to zeros to cause the gap. In the minimal model [64], the gap generated by the Dirac mass m is due to the same reason, but the gapping emerges without changing the coupling between bulk fermions and the boundary charge. Even if the bulk and the boundary have different dimensions, they do share fermion charges and the time coordinates, which in turn share charge conjugation and time reversal symmetries. So chiral symmetry breaking in the bulk should be reflected in discrete symmetries of the boundary theory. Extending to lattice models in flat space, the combination of particle-hole and time-reversal symmetry is reflected as chiral symmetry. Thus, to generate Mott-type gaps in a holographic model, we need to break one of these symmetries.

Since the pseudogap is not a completely gapped phase, one expects that holographic models for Fermi arcs still preserve bulk chiral symmetry. Therefore, by exploiting the pole-zero duality in the Pauli's coupling, adding a Pauli's coupling that could have both zeroes and a pole in the spectral function is one way to get the Fermi arcs. For these reasons, the proposed model for a bulk fermion is given by the following action:

$$S_{fermion} = \int d^4x\sqrt{-g}i\bar{\psi}\left(\not{D} - m - i\wp\,\mathbf{\Gamma}\not{F}\right)\psi\ , \tag{2.38}$$

where, $\mathbf{\Gamma} = \Gamma^{\underline{r}}\Gamma^{\underline{t}}\left(\hat{n}.\vec{\Gamma}\right)$, $\not{D} = e^M_c\,\Gamma^c\left(\partial_M + \frac{1}{4}\omega^{ab}_M\Gamma_{ab} - iqA_M\right)$, $\not{F} = \frac{1}{2}\Gamma^{ab}e^M_a e^N_b F_{MN}$, with e^M_a , ω^{ab}_M are the vielbeins and spin connections respectively. The difference between the model (2.38) and the dipole coupling in (2.32) is the presence of $\mathbf{\Gamma}$ which restores the chiral symmetry broken by the dipole coupling. On the other hand, the presence of $\mathbf{\Gamma}$ breaks the rotational and Lorentz symmetries of the boundary theory. This absent of boundary rotational invariance is important to model anisotropic phenomena such as the Fermi arcs. In the above model (2.38), the breaking of parity is along the unit vector $\hat{n}$.

The Dirac equation of motion is given by

$$\left(\not{D} - m - i\wp\Gamma\not{F}\right)\psi = 0\ , \tag{2.39}$$

$$\{e_c^M\Gamma^c(\partial_M + \frac{1}{4}\omega_M^{ab}\Gamma_{ab} - iqA_M) - m - i\wp\,\Gamma\tfrac{1}{2}\Gamma^{ab}e_a^M e_b^N F_{MN}\}\psi = 0\ . \tag{2.40}$$

The indices $M, N..$ and $a, b..$ have same meaning as in our first example. The metric background in this case, were chosen to be the Schwarzchild−AdS in 4−dimensions with Poincaré patch given by

$$ds^2 = \frac{r^2}{L^2}(-f(r)dt^2 + d\mathbf{x}^2) + \frac{L^2dr^2}{r^2f(r)}\ , \tag{2.41}$$

with $f(r) = 1 - \left(\frac{r_0}{r}\right)^3$, r_0 is the horizon radius and the temperature is given by

$$T = 3r_0/4\pi L^2$$

Here $A_M = \mu\left(1 - \frac{r_0}{r}\right)dt$, where, $\mu = Qr_0/L^2$. The non-vanishing spin connections are

$$\omega_t^{\underline{t}\,\underline{r}} = \frac{r^2}{L^2}\left(\frac{f(r)}{r} + \frac{f'(r)}{2}\right) \quad \text{and} \quad \omega_x^{\underline{x}\,\underline{r}} = -\frac{r\sqrt{f(r)}}{L^2}\ , \tag{2.42}$$

and the non-zero term from $\not{F}$ is $\begin{pmatrix} \sigma_2 & 0 \\ 0 & \sigma_2 \end{pmatrix}\frac{\mu r_0}{r^2}$. Evaluating the term containing the spin connection gives

$$e_c^M\Gamma^c\frac{1}{4}\omega_M^{ab}\Gamma_{ab} = \frac{r^2\sqrt{f(r)}}{L^2}\begin{pmatrix} \frac{6f(r)+rf(r)}{4rf(r)} & 0 \\ 0 & \frac{6f(r)+rf(r)}{4rf(r)} \end{pmatrix}\ . \tag{2.43}$$

Now writing $\psi = (\psi_1, \psi_2)^T$ with the following basis

$$\Gamma^{\underline{r}} = \begin{pmatrix} -\sigma_3 & 0 \\ 0 & -\sigma_3 \end{pmatrix},\ \Gamma^{\underline{t}} = \begin{pmatrix} i\sigma_1 & 0 \\ 0 & i\sigma_1 \end{pmatrix},\ \Gamma^{\underline{1}} = \begin{pmatrix} -\sigma_2 & 0 \\ 0 & \sigma_2 \end{pmatrix},\ \Gamma^{\underline{2}} = \begin{pmatrix} 0 & \sigma_2 \\ \sigma_2 & 0 \end{pmatrix} \tag{2.44}$$

On simplification of equation (2.39) one arrives with two coupled equations with the non-minimal coupling rescaled as $\wp \to \wp L$

$$\frac{r^2\sqrt{f}}{L^2}\left(\partial_r - \frac{6f(r)+rf(r)}{4rf(r)}\right)\psi_1 = \left(-\frac{\sigma_2}{\sqrt{f}}(\partial_t - iqA_t) + i\sigma_1\partial_1 - \frac{r}{L}\sigma_3 m + \sigma_1\wp\mu\frac{r_0}{r}\right)\psi_1$$
$$- i\sigma_1\partial_2\psi_2\ , \tag{2.45}$$

$$\frac{r^2\sqrt{f}}{L^2}\left(\partial_r - \frac{6f(r)+rf(r)}{4rf(r)}\right)\psi_2 = \left(-\frac{\sigma_2}{\sqrt{f}}(\partial_t - iqA_t) - i\sigma_1\partial_1 - \frac{r}{L}\sigma_3 m - \sigma_1\wp\mu\frac{r_0}{r}\right)\psi_2 - i\sigma_1\partial_2\psi_1 \,. \tag{2.46}$$

Following the same technique as before, to remove the term from spin connection, we Fourier transform the bulk spinors and simultaneously rescale

$$\psi_{1,2}(r,x) = r^{\frac{3}{2}} f^{\frac{1}{4}} e^{-i\omega t+ikx}\psi_{1,2}(r,k).$$

Now the Dirac equations (2.45) and (2.46) above can be packed into a single equation given by

$$\frac{r^2\sqrt{f}}{L^2}\partial_r\psi_j = i\frac{\sigma_2}{\sqrt{f}}\left(\omega + q\mu(1-\frac{r_0}{r})\right)\psi_j - \sigma_3\frac{r}{L}m\psi_j - (-1)^j\sigma_1(\wp\mu\frac{r_0}{r} - k_1)\psi_j + \sigma_1 k_2\psi_i \quad, i\neq j \tag{2.47}$$

The asymtotic solutions of equation (2.47) when r approaches infinity have the following form

$$\psi_j = \left(b_j(k)\, r^{-mL},\ a_j(k)\, r^{mL}\right)^T,\ \ j=\{1,2\}\,. \tag{2.48}$$

By choosing $A=(a_1,a_2)^T$ as the source and $B=(b_1,b_2)^T$ as expectation value, A and B are related by the matrix S given by $B=SA$. The Green's function is now calculated as $G(\omega,k) = -iS\gamma^{\underline{t}}$. Here $\gamma^{\underline{t}} = i\sigma_1$ is the appropriate boundary Dirac matrix in the basis chosen above. But similar to our first example, it is convenient to solve the flow equation. For $\omega \neq 0$, we expand the Dirac Equation (2.47) near horizon ($r=r_0$) to get

$$\frac{3(r-r_0)}{\omega L^2}\partial_r\begin{pmatrix}\psi_1\\ \psi_2\end{pmatrix} = \begin{pmatrix} i\sigma_2 & 0\\ 0 & i\sigma_2\end{pmatrix}\begin{pmatrix}\psi_1\\ \psi_2\end{pmatrix}. \tag{2.49}$$

Writing the bulk spinors as $\psi_j = (\beta_j,\alpha_j)^T$, the infalling solutions ξ^I,ξ^{II} are given by

$$\begin{aligned} \xi^I &= (i,1,0,0)^T \quad , \ \beta_1^I = i,\ \alpha_1^I = 1,\ \beta_2^I = \alpha_2^I = 0\,,\\ \xi^{II} &= (0,0,i,1)^T \quad , \ \beta_1^{II} = \alpha_1^{II} = 0, \beta_2^{II} = i, \alpha_2^{II} = 1. \end{aligned} \tag{2.50}$$

To derive the matrix flow equation, we define the following matrices as in [64]

$$Y = \begin{pmatrix}\beta_1^I & \beta_1^{II}\\ \beta_2^I & \beta_2^{II}\end{pmatrix},\ Z = \begin{pmatrix}\alpha_1^I & \alpha_1^{II}\\ \alpha_2^I & \alpha_2^{II}\end{pmatrix},\ G = YZ^{-1}\,. \tag{2.51}$$

By combining equation (2.47) and (2.51) keeping in mind the infalling solution (2.50), we get the following flow equation

$$\frac{r^2}{L^2}\sqrt{f}\partial_r G = M_+ - GM_- G \ , \quad M_\pm = \begin{pmatrix} \pm v_\pm(r) - k_x & k_y \\ k_y & \pm v_\mp(r) + k_x \end{pmatrix} \ , \tag{2.52}$$

where,

$$v_\pm(r) = \frac{1}{\sqrt{f(r)}}(\omega + qA_t(r)) \pm \wp\mu\frac{r_0}{r}. \tag{2.53}$$

The infalling boundary condition to solve equation (2.52) is obtained from (2.50) given by:

$$\lim_{r\to r_0} G = \begin{pmatrix} i & 0 \\ 0 & i \end{pmatrix}. \tag{2.54}$$

2.3.1 Numerical Results

By solving equation (2.52) numerically[2] with boundary condition (2.50), we defined the spectral function as follows

$$A(\omega, k_x, k_y) = \mathrm{Tr}\left(\mathrm{Im}G(\omega, k_x, k_y)\right) \ . \tag{2.55}$$

We plotted the results below in Figure 2.6. Breaking of rotational symmetry at the boundary by unit vector $\hat{n}$ is very important to model the anisotropic nature of Fermi arcs. While from similar model [11, 13] given in equation (2.32), for $m = 0$, the Fermi surface appears only for large negative values of p and there is a gap for large positive value of p. If we look in terms of fermion boundary Green's function $G_{ij}(\omega, k)$, the Fermi surface shows up at two poles k_F and $-k_F$ with k_F depending on the background geometry. However, the interaction in (2.38) preserves the functional form of the coupling and the pole/zero structure of both blocks but inverts G_{11} along $\hat{n}$ axis. In the $\hat{n}$ frame, the pole which was once at k_F, becomes zero at $-k_F$, and when $G_{22}(0, k_F; p)$ and $G_{11}(0, k_F; -p)$ have negligible spectral weight, the Fermi surface gaps at k_F.

The plots in Figure 2.6 indicates that when the non-minimal interaction is turned off the Fermi surface closes, but when the interaction is switched on there is suppression

---

[2] see Appendix B.3 for the numerical routine implemented in `Mathematica` software.

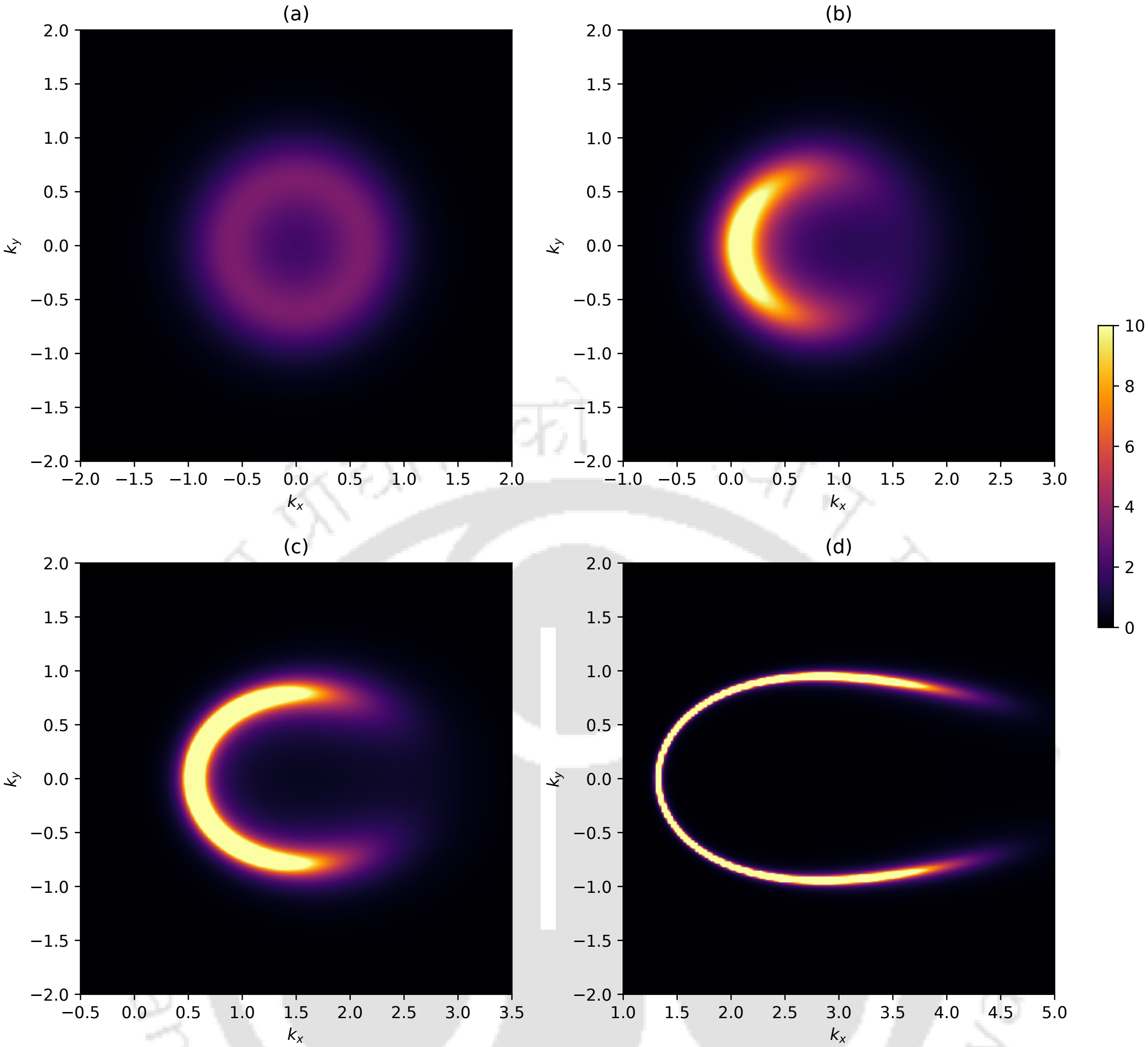

FIGURE 2.6: Fermionic spectral functions $A(\omega, k_x, k_y)$, at $\omega = 10^{-3} + i\delta$, $\delta = 10^{-6}$. Panel (a) – (d), in the fermi arc model with coupling of $\wp = 0, 1, 2$ and 4 for the parameters $Q = \sqrt{3}, r_0 = L = q = 1$ and $m = 0$ respectively.

on the spectral function on the right half of the Fermi surface and the left side gets enhanced. This continues for larger positive value of $\wp$ to show an arc-like spectrum and if we reverse the sign of $\wp$ the enhancement and suppression also gets reversed i.e.,the left side is suppressed and right gets enhanced. Thus, the bulk interaction in this model can provide a gapless spectra in the boundary dual and as we have seen it achieves the pole/zero duality [14] and Fermi arcs phenomena just by introducing a non-minimal interaction as mediator.

Chapter 3

Probing the Holographic Fermi Arc with scalar field

In our previous introductory chapters, we have highlighted many of the unsolved interesting phenomena that exists in strongly correlated systems. We also discussed about the holographic principle, which has evolved as a tool to describe the strongly coupled systems which otherwise were hard to study in a general perturbative approach. It relates the physics behind strongly interacting quantum systems to that of weakly interacting gravitational theory with one dimension higher, which was first used in the context of $\mathcal{N} = 4$ SYM theories [1, 2] and afterwards, it was realised that it could be of great help to model the real-world systems. Accordingly, applications towards strongly coupled systems in quantum chromodynamics were studied in great detail and also being used as a framework to understand non-linear hydrodynamics [65], Fermi liquid behavior [66, 67], transport phenomena [68], high temperature superconductors [69–71] to name a few. Most of these applications are towards exploring condensed matter systems. Interested readers are referred to the articles [4, 23, 72–74] for detailed reviews. It is therefore safe to say that the holographic principle has become an extremely powerful method to study strongly-correlated systems, be it in high energy physics or in condensed matter theory. One of the important aspects of condensed matter systems is to understand fermionic system in strong coupling regime. A quantity of interest in strongly coupled condensed matter systems, which can be computed using holography, is the spectral function of the fermions, as we have discussed in great details in Chapter 1, which in turn is proportional to the imaginary part of the fermionic retarded two-point correlation function. A lot of works were done in this regard in the literature [3, 66, 75], where the Dirac equation for a charged probe fermion propagating in a gravitational background is analysed. Many interesting and emergent phenomena seems to emerge out of these retarded two-point function of the dual fermionic operator in the boundary theory.

The discovery of superconductivity, on the other hand, in the LaBaCuO ceramics at 30 K by Bednorz and Müller [76] in 1986 has opened the era of high-T_c superconductivity. Prior to this, the phenomena of superconductivity had been confined to very low temperatures. This unexpected result prompted intense activity in the field of ceramic oxides, both in the experimental as well as theoretical front. These ceramic oxides have a superconducting phase with an order parameter having d-wave symmetry. This phase exists for the hole-doped material over 5% range of doping. However the material behaves like an antiferromagetic Mott insulator for very low doping. These two states are connected by an unconventional phase known as the pseudo-gap. Angle Resolved Photoemission Spectroscopy (ARPES) [77] has found the presence of a truncated Fermi surface in the pseudo-gap phase and this truncated Fermi surface in the momentum space is termed as a Fermi Arc [78–80, 82, 165]. As we pointed out in the introduction, this phenomenon remains a mystery, mostly because of the unconventional electronic properties of the normal state of the superconductor. As is well known, Landau's theory of metals predicts continuous closed Fermi surfaces and does not explain the observed truncated surfaces in momentum space when holes are doped into the copper-oxide plane. The arc is intermediate between the d-wave node of the superconductor and the complete Fermi surface of the normal state of the superconductor. On top of that, the arc appears to be formed by a closing of the energy gap of the superconducting state when temperature is increased above T_c.

Also the deviation from the standard Landau's theory of metal is generally taken into account in two different types of explanations [5]. It is shown that some type of order can set in [91] to give rise to a Fermi pocket with momentum dependent spectral intensity. This intensity can be extremely small (almost close to zero) for some range of momenta, giving rise to the discontinuity of the Fermi surface and thereby generating an arc-like structure in the momentum space. Secondly, the phenomenon was tried to be explained keeping the inherent strong coupling nature of the problem in mind, in which zeros of the single-particle electronic Green function, caused essentially by a divergent self-energy [92, 93] are the reasons for the vanishing of the surface. It is important to note that Fermi arcs have been obtained phenomenologically [92] and numerically [94] from the point of view of condensed matter physics, as well as there have been holographic description of it too [95, 96]. In these holographic descriptions, the arcs were obtained by condensing the fermions anisotropically into p-wave or d-wave superconducting states, but these does not describe the cuprates in the pseudo-gap phase.

It is well known that one can implement the holographic prescription in different ways for finite density fermionic system. In this work, we follow the program described in [5], where, the action for a bulk gravitational system is supplemented with fermionic fields which act as source to a fermionic operator at the boundary of AdS. It has been shown [66] already that a simple canonical fermion field in the Reissner-Nordström AdS$_4$ black hole background can give rise to both Fermi liquid and non-Fermi liquid behavior at the boundary. Although, this kind of constructions [66, 67] can give rise to gapped spectra depending upon the bulk fermion mass, it is very difficult to produce pseudo-gap spectrum without invoking any new coupling. One possible mechanism of obtaining pseudo-gap proposed by Vanacore et. al. [5] is by considering a non-minimal fermion and gauge field interaction.

So in this chapter, we generalize and most importantly dynamically generate the aforementioned fermion-gauge interaction by introducing another neutral scalar field and study its effect on the Fermi arc. This whole chapter is based on our published work [6]. We will consider two different scenarios. Firstly, the scalar field in the bulk can act as a neutral order parameter field giving rise to transition from normal to pseudogap phase. The phase transition temperature of this scalar field may be identified with the well known crossover temperature T^* in the high-T_c superconducting phase diagram, below which effects of electronic pairing correlations become significant[97, 98]. Therefore, in the holographic model this scalar field under consideration could be related to the pairing phase fluctuation from the dual field theory point of view. However, to confirm such claim we need to have detailed study on this issue. In the second scenario corresponding to the scalar field, we assume the existence of a dual tuning scalar operator which controls the pseudo-gap phase. From our discussion, it appears that the same neutral scalar field is responsible for both the aforementioned mechanisms. However, strictly speaking this is not the case. Even though the theory of scalar field looks same for both the mechanisms, in principle they are different. The difference can be easily understood if we consider the mass of the scalar field to be above AdS_2 Breitenlohner-Freedman (BF) bound $m_\Phi > -3/2$. The scalar field satisfying this condition will not condensate at any temperature. Therefore, the first mechanism will not be realisable for this system at all. Detail field theoretical understanding of these two scenarios could be an important topic of further research.

This Chapter consists various sections: in section 3.1 and 3.2 we will present a very brief discussion of the background geometry and the scalar field solution followed by section 3.3 where we discuss the fermionic Lagrangian. We present our numerical results, with a discussion on the energy gap in the spectral function and analytical discussion of the spectral function in sections 3.4, 3.5 and 3.6 respectively. Finally, in section 3.7 we conclude the Chapter with a brief discussion.

3.1 Review of Background Geometry and Action

Taking the simplest action coupled to gravity in AdS_4 with real massive scalar and gauge field

$$\mathcal{S} = \frac{1}{2\kappa^2}\int d^4x\sqrt{-g}\left[\mathcal{R} + \frac{6}{L^2} - \frac{1}{4}F^2 + \frac{1}{\lambda}\left(-\frac{1}{2}g^{\mu\nu}\nabla_\mu\Phi\nabla_\nu\Phi - V(\Phi)\right)\right] \tag{3.1}$$

with L the AdS curvature radius and $F = dA$. Here λ is a coupling constant and the potential $V(\Phi)$ is given by

$$V(\Phi) = \frac{1}{4L^2}\left(\Phi^2 + m_\Phi^2 L^2\right)^2 - \frac{m_\Phi^4 L^2}{4}.$$

The main motivation of choosing the above form of the potential is to have a non trivial scalar field solution, where m_Φ is scalar field mass. In this work we will neglect the effects of backreaction from the scalar field by taking λ to be large but include the effects of the gauge field leading to our electrically charged AdS black hole. For a detailed discussion the reader is referred to [99]. The equations of motion obtained from action (3.1) are

$$\begin{aligned} &R_{\mu\nu} - \frac{1}{2}g_{\mu\nu}R - \frac{3g_{\mu\nu}}{L^2} = \frac{1}{2}F_{\mu\lambda}F_\nu^\lambda - \frac{1}{8}g_{\mu\nu}F^2 + \nabla_\mu\Phi\nabla_\nu\Phi + g_{\mu\nu}\left(-\frac{1}{2}\nabla_\rho\Phi\nabla^\rho\Phi - V(\Phi)\right), \\ &\frac{1}{\sqrt{-g}}\nabla_\mu\left(\sqrt{-g}g^{\mu\nu}\nabla_\nu\Phi\right) - \frac{1}{L^2}(\Phi^2 + m_\Phi^2 L^2)\,\Phi = 0. \end{aligned} \tag{3.2}$$

On the other hand, it is well known that black holes are the simplest objects in general relativity. Assumption of rotational symmetry leads to the fact that the geometry of the black hole is fully specified by its mass and charge, independent of other details of the system. Systems which are of relevance in condensed matter physics are mostly finite density systems, with temperature much smaller than the chemical potential. These type of systems in the gravity side are described by black holes having charges. We will therefore, choose a familiar Reissner Nordström (RN) AdS_4 black hole as our background geometry with $\Phi = 0$. The general AdS_4 metric is given by the following line element:

$$\frac{ds^2}{L^2} = -g_{tt}dt^2 + g_{rr}dr^2 + g_{xx}dx^2 + g_{yy}dy^2 \,. \tag{3.3}$$

For RN-AdS$_4$, the metric coefficients are given by

$$g_{tt} = r^2 f(r) \ , \ g_{rr} = r^{-2} f^{-1}(r) \text{ and } g_{xx} = g_{yy} = r^2,$$

where, after rescaling, the horizon is at $r = 1$ and all coordinates are dimensionless. The metric function and the $U(1)$ gauge field A_t are given by:

$$f = 1 + \frac{3\gamma}{r^4} - \frac{1+3\gamma}{r^3}, \ A_t = \mu(1 - \frac{1}{r})dt.$$

Here, we expressed the chemical potential [99], as $\mu \equiv \sqrt{3}\gamma^{\frac{1}{2}}$ and the black hole temperature as $T = \frac{3}{4\pi}(1-\gamma)$. The parameter γ ranges from 0 to 1 and it controls the temperature and chemical potential of the system. For $\gamma = 1$, we have the extremal black hole with $T = 0$, and for $\gamma = 0$, we have finite temperature system with zero chemical potential ($\mu = 0$) and hence zero charge density on the dual field theory.

3.2 Scalar Field Solution

As we have already described, the scalar field in our model plays very distinct role in controlling the properties of Fermi arc. Properties of solution of such a field in the RN black hole background is well studied. For completeness let us discuss about the important behaviour of it. The radial equation of motion for $\Phi(r)$ is given by

$$\Phi''(r) + \left(\frac{f'}{f} + \frac{4}{r}\right)\Phi'(r) - \frac{(\Phi(r)^2 + m_\Phi^2 L^2)}{r^2 f}\Phi(r) = 0. \tag{3.4}$$

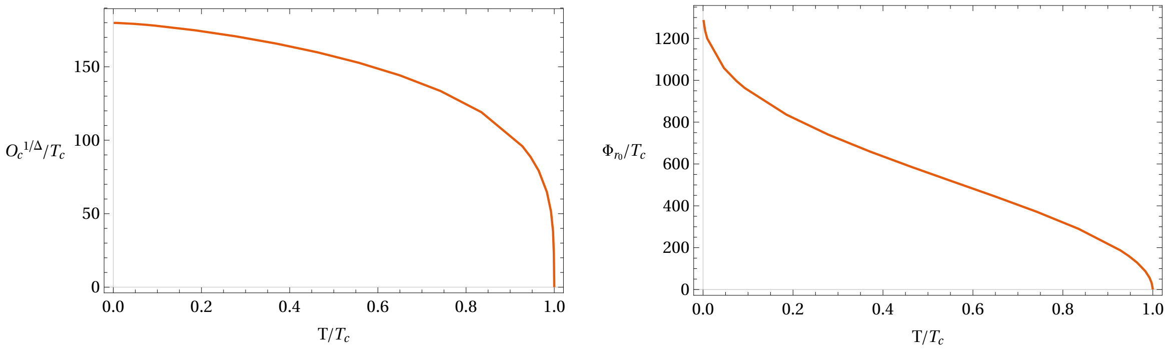

FIGURE 3.1: Plot of Condensate O_c (left) and horizon value of Φ (right) vs temperature (T/T_c) with $O_s = 0$. Here $m_\Phi^2 = -21/10$ and $T_c \approx$0.001078. We also found that T_c decreases when m_Φ^2 approach the BF bound.

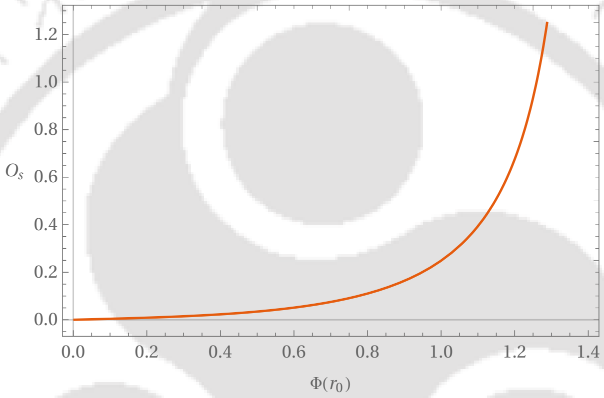

FIGURE 3.2: Plot of source O_s vshorizon value of $\Phi(r_0)$ for $T > T_c$.

From this, the asymptotic behaviour of Φ can be written as

$$\lim_{r\to\infty} \Phi(r) = \frac{O_s}{r^{3-\Delta}} + \frac{O_c}{r^{\Delta}}, \tag{3.5}$$

where $\Delta = 3/2 + \sqrt{9/4 + m_\Phi^2 L^2}$ is identified with the scaling dimension of the dual field theory operator. In the above expression, we set $L = 1$. As has already been emphasised, one of our goal is to study the evolution of fermionic spectral function across the phase transition, we therefore chose the mass of the scalar field within BF bound $-\frac{9}{4} < m_\Phi^2 < -\frac{3}{2}$. This essentially violates the AdS_2 BF bound near the horizon at zero temperature. For normal quantisation we interpret O_s as the source and O_c as response. From equation (3.5) we can write

$$\begin{aligned} \lim_{r\to\infty} \Phi(r) &= O_s\, r^{\Delta-3} + O_c\, r^{-\Delta}\,, \\ \lim_{r\to\infty} r\Phi'(r) &= O_s(\Delta-3)\, r^{\Delta-3} - O_c\, \Delta\, r^{-\Delta}. \end{aligned} \tag{3.6}$$

Solving for O_s & O_c we get

$$O_s = \lim_{r\to\infty}\left[\frac{r^{3-\Delta}\left(\Delta\,\Phi(r) + r\,\Phi'(r)\right)}{2\Delta-3}\right],$$
$$O_c = \lim_{r\to\infty}\left[\frac{r^{\Delta}\left((\Delta-3)\,\Phi(r) - r\,\Phi'(r)\right)}{2\Delta-3}\right].$$

Now, the constants O_s and O_c can be computed numerically. In order to solve the equation (3.4) we further expand $\Phi(r), f(r)$ near the horizon r_0 as

$$\Phi(r) \approx \Phi(r_0) + (r-r_0)\Phi'(r_0) + \frac{(r-r_0)^2}{2!}\Phi''(r_0) + \cdots,$$
$$f(r) \approx f(r_0) + (r-r_0)f'(r_0) + \frac{(r-r_0)^2}{2!}f''(r_0) + \cdots.$$

Using the above series expansion into the equation (3.4) and demanding the regularity condition at the horizon, one obtains following constraints on the field at the horizon,

$$\Phi'(r_0) = \frac{(\Phi(r_0)^2 + m_\phi^2 L^2)}{r_0^2 f'(r_0)}\Phi(r_0).$$

Thus, the choice of $\Phi(r_0)$ will automatically fix $\Phi'(r_0)$, and we can obtain a complete solutions for $\Phi(r)$. As discussed we have considered two possibilities. By shooting from the horizon with the scalar field value $\Phi(r_0)$, we studied sourceless condition $O_s = 0$, which happens only below a critical temperature. For the other case, we studied with boundary source $O_s \neq 0$, at arbitrary temperature. Before we move on, let us understand the behaviour of the scalar field and its dual nature with respect to the near horizon CFT. We examine the AdS$_2$ behaviour of the scalar field in the limit $r \to r_0$ and $T \to 0$ by writing the scalar field as

$$\Phi = \Phi(r_0) + \Phi_1\,(r-r_0)^{\delta}. \tag{3.7}$$

It is the value of δ which controls the conformal dimension of the IR CFT dual operator. Therefore, by plugging into the equation of motion and solving the coefficients, we get

$$\delta_{\pm} = -\frac{1}{2} \pm \sqrt{\frac{1}{4} + L_2^2\left(3\Phi(r_0) + m_\Phi^2\right)} \tag{3.8}$$

with L_2 being the AdS$_2$ radius. Condition for the dual of the scalar field to be an irrelevant deformation [99] in the IR CFT is $\delta = \delta_+ > 0$. This is also consistent with the scalar field which is going to be constant, $\Phi(r_0)$, in the near horizon limit. Therefore, under this neutral scalar field, properties of the back reacted near horizon geometry will remain same. A more elaborate discussion on this back-reaction issue can be found in [99]. We have also checked this by our full numerical solution. Therefore, we will mainly focus on the probe limit of the scalar field which makes our discussion simpler towards understanding the main goal of our work. However, at this point we should mention that for a charged scalar field condensation such as for the holographic superconductor, the back-reaction near zero temperature has been proved to be very much important [100–103]. To this end let us emphasis again the reason for considering the scalar field. We will consider two possible scenarios while calculating the fermionic spectral function.

Case-I: For this case, we will consider the effect of scalar condensation on the Fermi surface. Therefore, we will consider those solutions of the scalar field, for which the boundary source O_s will be zero. By appropriately tuning the background temperature and the horizon value of the scalar field $\Phi(r_0)$, one gets the desired solution with the condition $O_s = 0$ and $O_c \neq 0$. In the left panel of Figure 3.1, we showed the conventional condensation of the boundary dual scalar operator below the critical temperature T_c. As mentioned, we study how this temperature dependent scalar field profile controls the properties of low energy behaviour of the holographic fermions at finite temperature. Our numerical computation gives $T_c \approx 0.001078$. What we will observe is that below this critical temperature, the holographic Fermi surface develops a pseudo-gap phase in its spectral function. It would be interesting to investigate the connection between our phase transition temperature T_c with the well known cross over temperature T^* in the high temperature superconductivity phase diagram. We have plotted the behaviour of the scalar field at the horizon with temperature in the right panel of Figure 3.1. Very close to $T{=}T_c$ by fitting O_c with $\delta_1(T_c - T)^\delta$, we found that the exponent $\delta = 0.49 \pm 0.005$ and the proportionality constant δ_1 is found to be $\delta_1 \approx 1.41$. Similarly, the behaviour of $\Phi(r_0)$ *vs* $\alpha_1(T_c - T)^\alpha$ gives the constant $\alpha_1 = 33.24$ and the exponent α to be 0.53 ± 0.02.

Case-II: For this case we will identify O_s as a tuning parameter and our goal would be to study the effect of this source on the boundary fermionic spectrum. Therefore, this source can be thought of as doping in the higher temperature superconductivity phase diagram. In Figure 3.2, we show how the boundary source changes depending upon the horizon value the bulk scalar field $\Phi(r_0)$. As it is the horizon value of the scalar field which controls the fermion-gauge coupling in the bulk spacetime, study of the effect of the source as a tuning parameter, on the boundary fermionic spectrum is an important aspect.

In the next section we shall examine the effects of this scalar field in the fermion spectral function and see how the Fermi surfaces and Fermi arcs evolve across the phase transition.

3.3 Fermion Lagrangian and Dirac equation

In holographic approach to fermionic systems, there can be a number of ways in which fermions are coupled to gravity and gauge fields. One such non-minimal coupling is dipole-coupling, which was introduced in [11]. Coupling between fermions with background condensation has been studied in [64]. In this work, the authors discuss effects of a superconducting condensate on holographic Fermi surfaces. They found stable quasi-particles with a gap using coupling between the fermion and condensate. In [11], fermions coupled to gauge fields via a dipole interaction in the bulk was studied. By varying the strength of the interaction, it was shown that a new band in the density of states can be generated where the spectral density is transferred between bands. Beyond a critical interaction strength, a gap opens up dynamically. The effects of a superconducting condensate on the holographic Fermi surfaces was studied in [64]. Choosing a suitable coupling between the fermion and the condensate, the work had shown that there exists stable quasi-particles with a gap. Further, finding similarities with the behaviour of the cuprates high temperature superconductor, it was found that a stable quasiparticle peak can appear in the condensed phase in the systems under study whose normal state is a non-Fermi liquid with no stable quasiparticle. fermions were also studied in an electrically-probed and asymptotically AdS-Schwarzschild spacetime [5]. The dual fermion two-point correlator was computed and the bulk interactions were shown to create anisotropic gaps in the Fermi surfaces of the boundary spectrum. Consequently, the chiral symmetry breaking Pauli coupling provided a holographic model for Fermi arcs.

Our goal of the present work would be to control the aforementioned coupling by a scalar field through condensation or by tuning the dual operator at the boundary. We will consider two different models as discussed above. The motivation to consider two different fermion-scalar models is to understand better the mechanism of observing the pseudo gap in the fermion spectral function. Further, it is an important question and still a debated issue in condensed matter physics that whether the Fermi arcs arise due to the partial gapping of the Fermi surface or due to the certain destruction of quasi-particles. In the holographic framework we will try to understand this question for both models.

3.3.1 Model-A

Firstly, we generalise [5] with similar action given by

$$\mathcal{S}^{(1)}_{Fermion} = \int d^4x\sqrt{-g}\, i\bar{\psi}\left(\not{D} - m - ip\,\mathbf{\Gamma}\Phi\not{F}\right)\psi \tag{3.9}$$

where the matrix factor, $\mathbf{\Gamma} = \Gamma^{\underline{r}}\Gamma^{\underline{t}}(\hat{n}\cdot\vec{\Gamma})$. Dirac equation of motion for ψ is

$$\left(\not{D} - m - ip\,\mathbf{\Gamma}\Phi(r)\not{F}\right)\psi = 0 \tag{3.10}$$

where,

$$\not{D} = e^{\mu}_{c}\Gamma^{c}\left(\partial_{\mu} + \frac{1}{4}\omega^{ab}_{\mu}\Gamma_{ab} - iqA_{\mu}\right) \quad , \quad \not{F} = \frac{1}{2}\Gamma^{ab}e^{\mu}_{a}e^{\nu}_{b}F_{\mu\nu}.$$

with $\vec{\Gamma} \equiv (\Gamma^{\underline{x}}, \Gamma^{\underline{y}})$. The parameter p is a Pauli coupling, $e^{\mu}_{a}, \omega^{ab}_{\mu}$ are vielbeins and spin connection. Here, $\{a, b\}$ are tangent space indices and $\{\mu, \nu\}$ are for the bulk. By choosing $\hat{n} = \hat{x}$ and the following form of the Dirac matrices

$$\Gamma^{\underline{r}} = \begin{pmatrix} -\sigma_3 & 0 \\ 0 & -\sigma_3 \end{pmatrix}, \qquad \Gamma^{\underline{t}} = \begin{pmatrix} i\sigma_1 & 0 \\ 0 & i\sigma_1 \end{pmatrix}$$

$$\Gamma^{\underline{x}} = \begin{pmatrix} -\sigma_2 & 0 \\ 0 & \sigma_2 \end{pmatrix}, \qquad \Gamma^{\underline{y}} = \begin{pmatrix} 0 & \sigma_2 \\ \sigma_2 & 0 \end{pmatrix} \tag{3.11}$$

For non trivial profile of the scalar field $p_{eff} = p\Phi$ plays the role of anisotropic coupling between fermion and gauge field. By choosing the following ansatz for the fermion field $\psi(r, \vec{x}_i) = (-gg^{rr})^{-\frac{1}{4}}e^{-i\omega t + ik.x}\tilde{\psi}(r, k)$, one can get rid of the spin connection, and finally the Dirac equation (3.10) transforms into,

$$\Big[\frac{1}{\sqrt{g_{rr}}}\Gamma^{\underline{r}}\partial_r + \frac{1}{\sqrt{-g_{tt}}}\Gamma^{\underline{t}}(-i\omega - iqA_t) + \Gamma^{\underline{x}}\frac{ik_x}{\sqrt{g_{xx}}} + \Gamma^{\underline{y}}\frac{ik_y}{\sqrt{g_{yy}}} \\ - m - ip\Phi\frac{\Gamma^{\underline{r}}\Gamma^{\underline{t}}\Gamma^{\underline{x}}}{\sqrt{-g_{tt}g_{rr}}}\Gamma^{\underline{r}}\Gamma^{\underline{t}}\partial_r A_t\Big]\tilde{\psi} = 0 \tag{3.12}$$

Considering the following component form of the fermion field, $\tilde{\psi} = \left(\tilde{\psi}_1, \tilde{\psi}_2\right)^T$, and ansatz for the background gauge field $A_\mu = A_t$ with all other components to zero, above equation can be further simplified to

$$\frac{1}{\sqrt{g_{rr}}}\partial_r\begin{pmatrix}\tilde{\psi}_1\\ \tilde{\psi}_2\end{pmatrix} = \frac{1}{\sqrt{-g_{tt}}}(\omega + qA_t)i\sigma_2 \otimes \begin{pmatrix}\tilde{\psi}_1\\ \tilde{\psi}_2\end{pmatrix} - m\sigma_3 \otimes \begin{pmatrix}\tilde{\psi}_1\\ \tilde{\psi}_2\end{pmatrix} \mp \frac{k_x}{\sqrt{g_{xx}}}\sigma_1 \otimes \begin{pmatrix}\tilde{\psi}_1\\ \tilde{\psi}_2\end{pmatrix} \\ \pm \frac{p\Phi}{\sqrt{-g_{tt}g_{rr}}}A_t'\sigma_1 \otimes \begin{pmatrix}\tilde{\psi}_1\\ \tilde{\psi}_2\end{pmatrix} + \frac{k_y}{\sqrt{g_{yy}}}\sigma_1 \otimes \begin{pmatrix}\tilde{\psi}_2\\ \tilde{\psi}_1\end{pmatrix} \tag{3.13}$$

The above equation (3.13), after inserting the background geometry (3.3) becomes

$$r^2\sqrt{f(r)}\partial_r\tilde{\psi}_I = \frac{i\sigma_2}{\sqrt{f(r)}}\left(\omega + q\mu\left(1 - \frac{r_0}{r}\right)\right)\tilde{\psi}_I \\ - \sigma_3 m r\tilde{\psi}_I - (-1)^I\sigma_1\left(p\Phi(r)\mu\frac{r_0}{r} - k_x\right)\tilde{\psi}_I + \sigma_1 k_y\tilde{\psi}_J. \tag{3.14}$$

The asymptotic solutions of (3.14) are given by

$$\tilde{\psi}_J = A_J(k)r^m + B_J(k)r^{-m}$$

In fact, we can numerically read off the coefficients A and B to obtain the green's functions, but alternative approach exists by solving the first order flow equation.

In equation (3.14) we see that with $k_y \neq 0$ the block diagonal form is lost, we now have mixing of various spinors components. Following the prescription used in [5, 64, 104] to extract the Green's function by using two sets of linearly independent boundary conditions are given by

$$\begin{pmatrix}\beta_1^I & \beta_1^{II}\\ \beta_2^I & \beta_2^{II}\end{pmatrix} = \begin{pmatrix}s_{11} & s_{12}\\ s_{21} & s_{22}\end{pmatrix}\begin{pmatrix}\alpha_1^I & \alpha_1^{II}\\ \alpha_2^I & \alpha_2^{II}\end{pmatrix}, \tag{3.15}$$

where we further expressed two component spinor as, $\tilde{\psi}_i = (\beta_i, \alpha_i)^T$. The retarded Green's function is defined as

$$G_R(\omega, \vec{k}) = -i \begin{pmatrix} s_{11} & s_{12} \\ s_{21} & s_{22} \end{pmatrix} \cdot \gamma^t, \tag{3.16}$$

with gamma matrices $\gamma^t = i\sigma_1$. The spectral function is defined as

$$A(\omega, \vec{k}) = Im\left[TrG_R(\omega, \vec{k})\right]. \tag{3.17}$$

Along with the definition given in (3.15) and from equation (3.13), we can derive the flow equation (see Appendix C.1) given by

$$\frac{1}{\sqrt{g_{rr}}}\partial_r G_R + 2mG_R = M_+ - G_R M_- G_R \tag{3.18}$$

where,

$$M_\pm = \begin{pmatrix} \pm W_\pm - \frac{k_x}{\sqrt{g_{xx}}} & \frac{k_y}{\sqrt{g_{yy}}} \\ \frac{k_y}{\sqrt{g_{yy}}} & \pm W_\mp + \frac{k_x}{\sqrt{g_{xx}}} \end{pmatrix}$$

with $W_\pm$ given by

$$W_\pm = \frac{1}{\sqrt{-g_{tt}}}(\omega + qA_t) \pm \frac{p\Phi}{\sqrt{g_{tt}g_{rr}}}A_t'. \tag{3.19}$$

Numerically we will integrate equation (3.18) from horizon ($r = r_0$) to infinity in order to compute the spectral function.The boundary condition for $\omega \neq 0$ is still in diagonal form given by

$$G_R(r_0) = \begin{pmatrix} i & 0 \\ 0 & i \end{pmatrix} \tag{3.20}$$

3.3.2 Model-B

Even though most of our discussions will be focused on the previous model, for completeness and comparison specifically in the context of energy gap in the spectral function, we consider the following dipole model generalising the work of [11] by coupling a scalar field as part of the controlling parameter

$$\mathcal{S}^{(2)}_{Fermion} = \int d^4x \sqrt{-g} i \bar{\psi} \left(\not{D} - m - ip\Phi \not{F} \right) \psi, \tag{3.21}$$

As shown in appendix C.3, the Green's function is given by

$$G_R(\omega, k) = \lim_{r \to \infty} \frac{1}{r^{2m}} \begin{pmatrix} \zeta_+ & 0 \\ 0 & \zeta_- \end{pmatrix} \tag{3.22}$$

The spectral function defined as

$$A(\omega, k_x) = Tr\left[Im\left(G_R(\omega, k_x) \right) \right]. \tag{3.23}$$

For AdS$_2$ Green's function we refer to Appendix C.4, which includes the finite temperature dependent scalar field and how it changes the IR CFT operators.

3.4 Numerical results and discussions

3.4.1 Across the phase transition: without source

As discussed above, we have two different kind of solution for the scalar field. In this subsection we will discuss case-I, when the scalar field condenses below a critical temperature T_c. Therefore, above T_c we will have free fermion with well defined Fermi surface. However below T_c we will have non-trivial properties of the fermion spectral function. In the left panel of Figure 3.4, we see the evolution Fermi surface from higher temperature to lower temperature across the critical temperature T_c. For $T > T_c$, scalar field does not condensate leading to the closed Fermi surface. We lowered the temperature, consequently, Fermi surface starts to develop anisotropic gap which we call pseudo-gap. Important to mention that even though our results may look similar to the one shown in [5], it is the evolution of Fermi arc with respect to the temperature below a critical value, which can be identified with the pseudo-gap region at constant doping for the cuprate superconductor. Important difference is the arc topology of the holographic Fermi arc compared to the d-wave symmetric Fermi arc of the real high temperature superconductor. Therefore, we need to further work on the issue of understanding the d-wave symmetric Fermi arc for our holographic system. Nonetheless, an important point to emphasise that understanding the pseudo-gap phenomena is still an active area of condensed matter research. It is interesting to re-emphasise that the holographic dual of our bulk scalar field can be interpreted as an incoherent phase fluctuation, which was proposed as a potential mechanism for the pseudo-gap phenomena [97]. We also plotted in Figure 3.4 the evolution of Fermi surface for higher p value which essentially changes the absolute strength of the gauge-fermion coupling. We will further explore on this in the future publication. From pole/zero duality perspective [14, 107], the appearance of the gap can be realised from the pole and zero in G_{11} and G_{22} which are the diagonal components in the Green's function. The effective coupling $p\Phi$ and the Γ matrix in the $\hat{n}$-momentum axis inverts the sign of Fermi momentum k_f for negative and positive p values. As a results of this the gap appear in either $-\mathbf{k}_f$ or at $\mathbf{k}_f$. As the Fermi surface is anisotropic, we now investigate how the magnitude of the Fermi momentum k_f changes as we go along the surface.

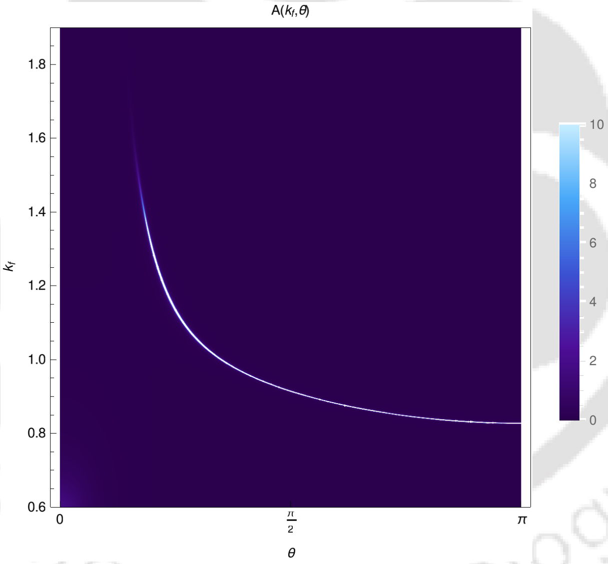

FIGURE 3.3: Plot of $A(k_f, \theta)$ in $\theta - k_f$. Here $p = 1.5$,$q = 1$, $m = 0$, $m_\Phi^2 = -21/10$ and at very small $T = 10^{-3}T_c$. In this plot we see the variation of k_f along θ direction.

In order to find k_f in k_x-k_y plane we will define k_x, k_y in terms of angle θ in $[k_x$-$k_y]$-plane as

$$k_x = k_f \, \sin\theta; \qquad k_y = k_f \, \cos\theta, \tag{3.24}$$

where k_f is the distance of the Fermi surface from the centre. In Table: 3.1, we tabulate different values of k_f in different directions (θ values) in the $k_x - k_y$ plane. Numerically

Table 3.1: Variation of k_f for different θ with p=1.5 and q=1.

k_f	θ
$\approx$1.5240	$\frac{\pi}{6}$
$\approx$1.0150	$\frac{\pi}{3}$
$\approx$0.9146	$\frac{\pi}{2}$
$\approx$0.83633	$\frac{5\pi}{6}$
$\approx$0.86388	$\frac{2\pi}{3}$
$\approx$0.84776	$\frac{3\pi}{4}$

we found that k_f is same for all angular coordinate for $T > T_c$. This is expected from the fact that in this limit the anisotropic gauge field and fermion coupling vanishes because of zero scalar field value. With the definition in equation (3.24), we plotted the spectral function in Figure 3.3.

3.4.2 At arbitrary temperature: with source

For case-II, as mentioned earlier we will consider the bulk scalar field with non-normalizable solution. Therefore, we have only one tuning parameter corresponding to the source of the dual operator which we tune to evolve the Fermi surface at a particular temperature. We have chosen two different value of p and the plots for the spectral function are shown in the Figure 3.5. For this particular case we do not have any critical temperature. For a fixed temperature of the system the Fermi surface evolves as we tune the boundary source, which essentially control the scalar field profile in bulk. For zero source we will obviously have closed spherical Fermi surface. In contrast to the previous case-I, the boundary tuning parameter of present case can be identified with the doping in the high temperature superconductor. Qualitatively we do not find much difference between the Fermi surface properties with increasing p as is clear from the Figure 3.4.

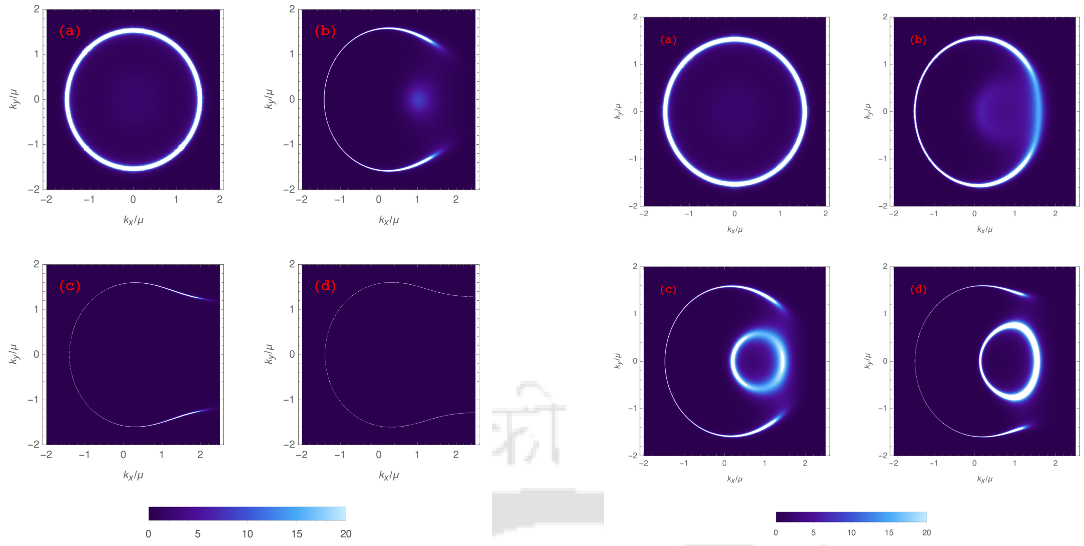

FIGURE 3.4: Density plot of spectral function $A(k_x, k_y)$ with small ω (=0.0001), q=1 and fixed p=2 (Left) p=0.92 (Right). The temperature of above plots from (a)-(d) are $0.99T_c, 0.55T_c, 0.18T_c$ and $10^{-3}T_c$ respectively.

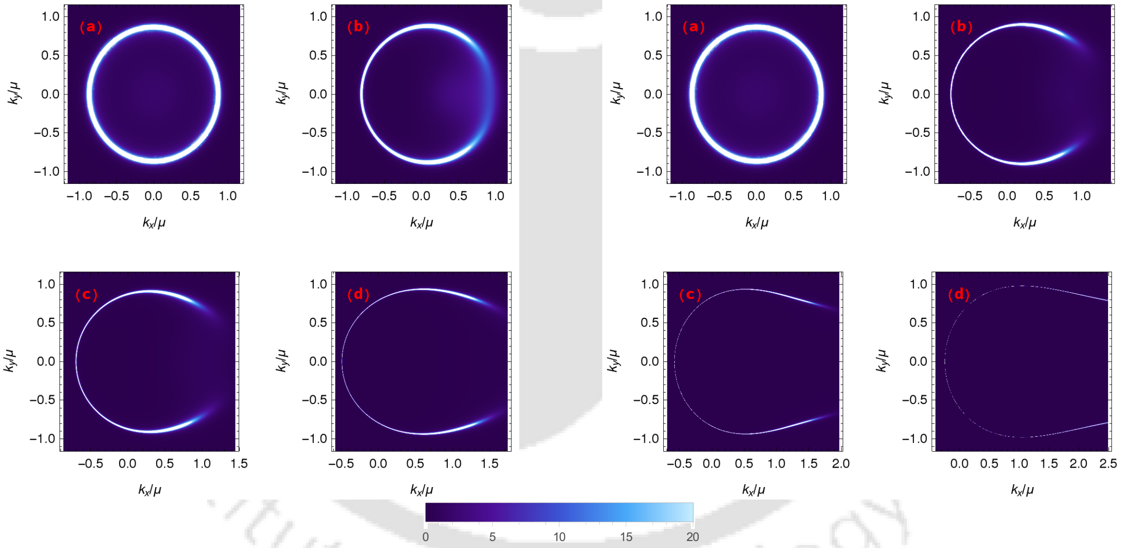

FIGURE 3.5: Plot of spectral function $A(k_x, k_y)$ for fixed temperature $T \approx 0.00238$, q=1 for $p = 1$(left) and $p = 2$(right). From [a-d] corresponds to $\Phi(r_0) = 0, 0.5, 1$ and 1.3 respectively.

3.5 Energy gap in the spectral function

In this section we consider an important question related to the existence of actual gap in the fermion spectral function. As already pointed out before, it is still a debated issue from the experimental point of view whether the Fermi arcs arise due to the partial gapping of the Fermi surface or due to the certain destruction of quasi-particles. Therefore, it is important to examine the situation for our holographic set up. We consider two different models-(A,B). Figure 3.6 illustrates the presence of the gap for model-B, which contains dipole type fermion-gauge interaction with scalar field dependent effective coupling parameter $p_{eff} = p\Phi$. For the usual no-scalar field dipole model described in [11] the energy gap has already been found out to be much wider than the present model. However, clearly the size of the gap increases with increasing p value. At this point, it is also important to note the symmetric nature of the energy gap for the dipole type coupling. On the other hand for the model-A, because of the parity breaking fermion-gauge coupling, we have already seen the anisotropic Fermi arc Figure 3.4, and that is indeed found to be translated into the anisotropic energy gap in the spectral function shown in Figure 3.7. For this plot we set $k_y = 0$ and $k_x = k$. Therefore, in the positive k direction we can clearly see the gap whose width is monotonically increasing with p value. Thus, in holographic pseudo-gap phase, the Fermi arcs seem to be intimately connected with the partial gapping of the Fermi surface. It would, therefore, be interesting to construct a holographic model where partial gapping is not occurring.

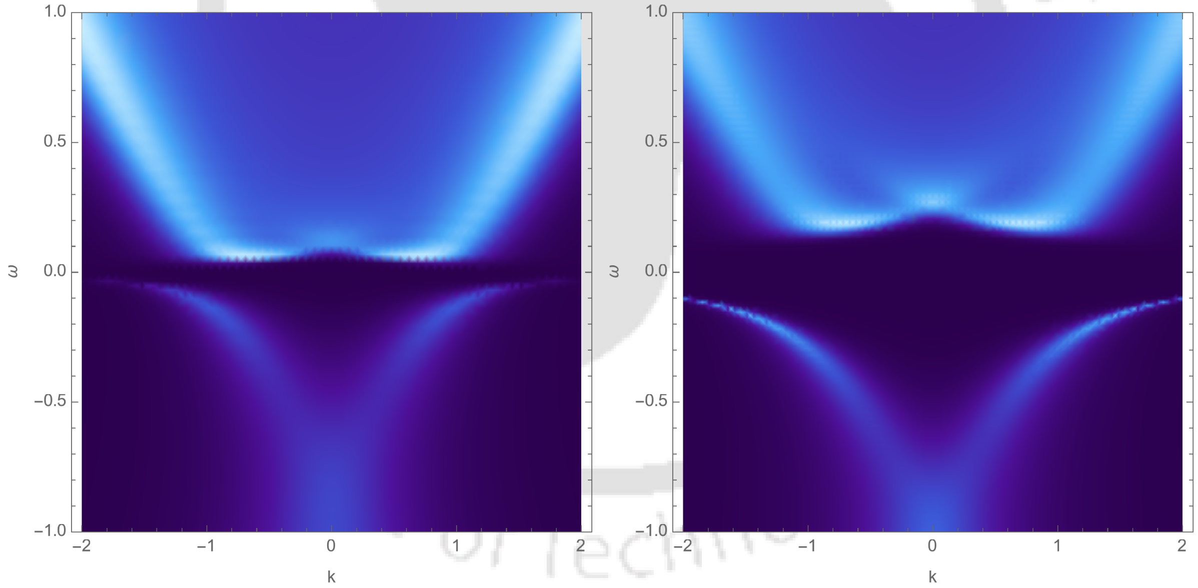

FIGURE 3.6: Spectral function $A(\omega, k)$ vs (ω, k) for model-B. Below T_c (≈ 0.001078), the opening of gap near $\omega = 0$ is seen along k_x direction for fixed $p = 5\,(left)$ and $p = 10\,(right)$, whereas above T_c the gap disappeared.

In our subsequent section we will try to understand the low energy properties of the Fermi surface for both the cases by considering the well known analytic technique in terms of AdS_2 fermionic spectral function.

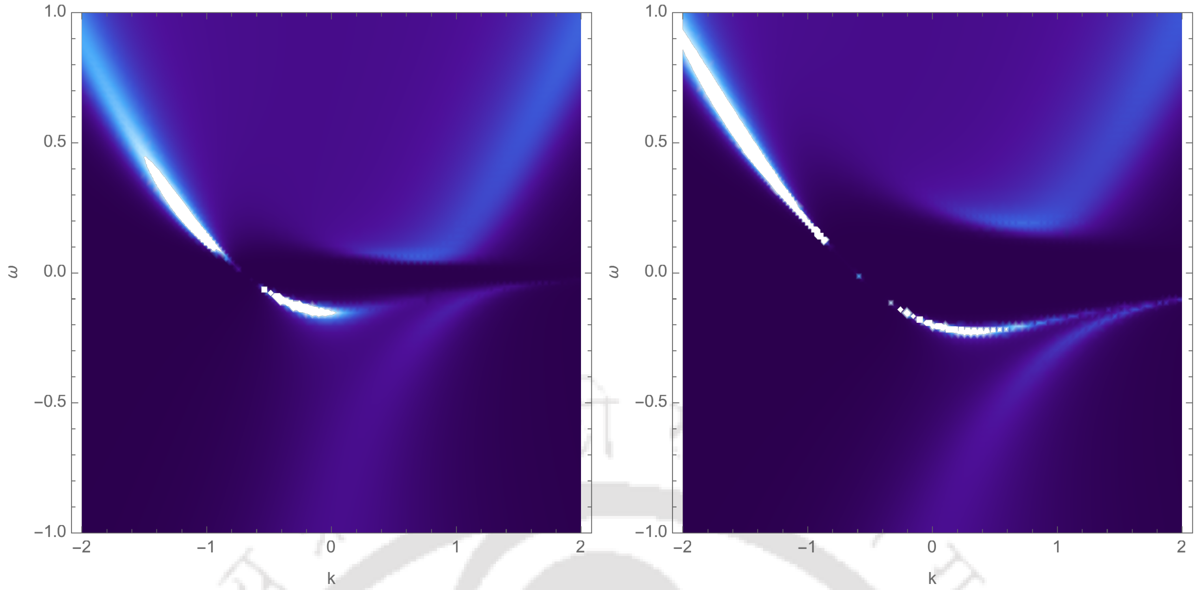

FIGURE 3.7: Spectral function $A(\omega, k)$ vs (ω, k) for action 3.9 for model-A. Below T_c, the opening of gap near $\omega = 0$ is seen along k_x direction for fixed $p = 5\,(left)$ and $p = 10\,(right)$.

3.6 Analytical study of Green's function at finite temperature

In this section we will try to understand how the scalar field enters into the Fermi arc dynamics using analytic treatment. We essentially follow the work of [66, 105] and pin point the contribution of the scalar field contribution. In the AdS$_2$ limit at temperature $T \to 0$, equation (3.14) takes the form (see appendix C.2)

$$-\zeta\partial_\zeta\tilde{\psi}_I = i\sigma_2\left(\omega\zeta + qe_d\right)\tilde{\psi}_I - \sigma_3 m L_2\tilde{\psi}_I - (-1)^I\sigma_1 L_2 m_k\tilde{\psi}_I + \sigma_1 L_2 k_y\tilde{\psi}_J \tag{3.25}$$

For finite temperature, the boundary Green's function is expressed as [106]

$$G_R = \frac{\tilde{B}_+ + \mathcal{G}_R T^{2\nu_k}\tilde{B}_-}{\tilde{A}_+ + \mathcal{G}_R T^{2\nu_k}\tilde{A}_-}, \tag{3.26}$$

where, $\tilde{B}_\pm$ and $\tilde{A}_\pm$ are all matrices. For small ω one can perturbatively expand $\tilde{B}_\pm$, $\tilde{A}_\pm$ in terms of ω. Where, the finite temperature AdS_2 Green's function is $\mathcal{G}_R$

$$\mathcal{G}_R(\omega, T) = c_k \ (4\pi T)^{2\nu_k} \tag{3.27}$$

where, c_k is a normalisation constant and $\nu_k = \sqrt{m^2 L_2^2 + m_k^2 L_2^2 + k_y^2 L_2^2 - q^2 e_d^2}$. Here, ν_k plays the role of conformal dimension of dual infrared conformal field theory operator. $L_2 = 1/\sqrt{6}$ is the AdS_2 radius in unit of AdS_4 radius L, and $m_k = (\Phi(r_0)\mu - k_x)$. We have already observed through our numerical calculation the anisotropic and temperature dependent behaviour of the Fermi surface. It is important to see that those behaviour is manifested into the expression for the conformal dimension ν_k through the scalar field condensation $\Phi(r_0)$, and component of Fermi momentum (k_x, k_y). Obviously, at low energy the boundary Green's function will be mainly controlled by $\mathcal{G}_R$. Fermi surface is associated with the zeros of $\tilde{A}_\pm$. Therefore at small energy and momentum near the Fermi surface $(|\vec{k}| = |k_f|)$ the Green's function can be expressed in the following form [106]

$$G_R = \frac{\tilde{H}_1}{k_\perp - \omega V_f^{-1} + D_3 T - \tilde{H}_2 T^{2\nu_{k_f}} \mathcal{F}_{k_f}(\nu_{k_f}, \frac{\omega}{T})}, \tag{3.28}$$

where $\mathcal{F}$ is given by

$$\mathcal{F}_{k_f} = \frac{\Gamma(\frac{1}{2} + \nu_{k_f} - \frac{i\omega}{2\pi T} + iqe_d)}{\Gamma(\frac{1}{2} - \nu_{k_f} - \frac{i\omega}{2\pi T} + iqe_d)}.$$

In (3.28), $\tilde{H}_1, V_f, \tilde{H}_2$ has the form as in [106] and D_3 is a constant which can be obtained by full numerical calculation.

Zero temperature limit: When $\frac{\omega}{T} \to \infty$(zero temperature), $\mathcal{F}$ behave as

$$\mathcal{F} \approx e^{-i\pi\upsilon_{k_f}} \left(\frac{\omega}{T}\right)^{2\nu_{k_f}},$$

which gives us back the zero temperature AdS_2 Green's function. The Fermi surface is defined by the pole of G_R expressed as

$$\det\left[k_\perp - \omega V_f^{-1} - \tilde{H}_2 e^{-i\pi\nu_{kf}} \omega^{2\nu_{k_f}}\right] = 0$$

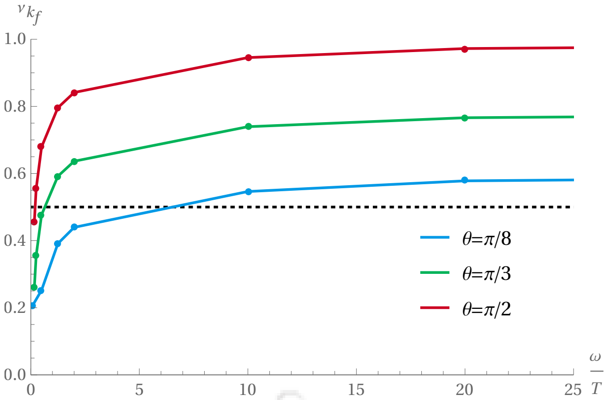

FIGURE 3.8: Plot of ν_{k_f} as a function of ω/T keeping ω fixed. Behaviour is in the condensed phase of the scalar field. We considered $p = 1, m = 0, q = 1$, dashed line corresponds to ν_{k_f}=1/2. It illustrates how ν_{k_f} changes for $\frac{\omega}{T} \to \infty$ as seen in AdS$_4$ Green's function. As we decrease T for fixed small ω, ν_{k_f} decreases below $\nu_{k_f} = 1/2$.

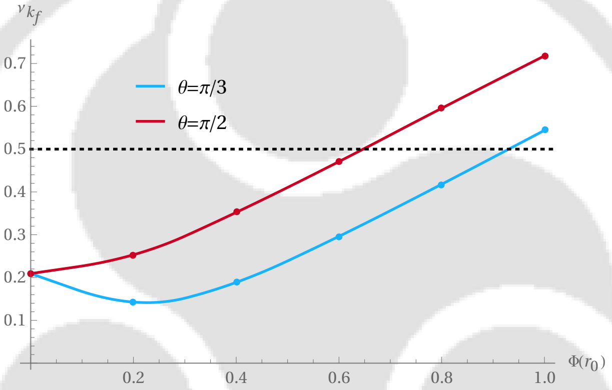

FIGURE 3.9: Plot of ν_{k_f} as a function of horizon value of the scalar field $\Phi(r_0)$ associated with non-zero source at the boundary. Temperature is fixed at $T = 0.00238$ for $q =$ 1,$m = 0, q = 1$ and dashed line is ν_{k_f}=1/2. Here, we take $m^2_\Phi = -1.4$, which is above the BF-bound to avoid the condensation of the scalar field.

The properties are usually measured by the dispersion relation near the Fermi surface which is the pole of the Greens's function,

$$\omega_p(k) \equiv \omega_*(k) - i\Omega(k)$$

The dispersion relations are parametrized as $\omega_*(k) \propto k_\perp^z$ and widths $\Omega_*(k) \propto k_\perp^\alpha$ [66]. The exponents are

$$z = \begin{cases} \frac{1}{2\nu_{k_f}} & \text{for } \nu_{k_f} < \frac{1}{2} \\ 1 & \text{for } \nu_{k_f} > \frac{1}{2} \end{cases} ; \ \alpha = \begin{cases} 1 & \text{for } \nu_{k_f} < \frac{1}{2} \\ 2\nu_{k_f} & \text{for } \nu_{k_f} > \frac{1}{2} \end{cases}$$

Our strategy will be the following: For the mechanism when the neutral scalar field condensates below the critical temperature which is very small, the black hole near horizon geometry can be approximated as AdS_2. Near zero temperature similar approximation can also be made for the other mechanism when the spectral function is controlled by the external source of dual scalar operator at the boundary. With this assumption in mind we consider the Green's function with the horizon value of the scalar field to be temperature dependent and show the evolution of Fermi arc with temperature. Considering mass of the fermion to be zero,

$$\begin{aligned}\nu_{k_f} &= \sqrt{{m_{k_f}}^2 L_2^2 + k_{y_f}^2 L_2^2 - q^2 e_d^2} \\ &= \sqrt{\frac{1}{6}\left[\Phi(r_0)\left(\Phi(r_0)\mu^2 - 2\mu k_f \cos\theta\right)\right] + k_f^2 - q^2 e_d^2} \qquad (3.29)\end{aligned}$$

It is clear and well known that $\nu_k = 1/2$ encodes the properties of marginal Fermi liquid which has been phenomenologically introduced to describe the strange metal phase of cuprate. From the above expression of ν_{k_f}, it is clear that it is the horizon value of the scalar field $\Phi(r_0)$ which controls the properties of the fermion spectral function. When the scalar field condensates below a critical temperature, ν_k naturally depends on the temperature through the scalar field value $\Phi(r_0)$ at the horizon. Therefore, below T_c as one decreases the temperature, $\Phi(r_0)$ increases and consequently the properties of the Fermi surface changes from Fermi liquid, $\nu_k > \frac{1}{2}$, with long-lived quasi-particles to non-Fermi liquid $\nu_k < \frac{1}{2}$ with well defined quasi-particles shown the Figure 3.8. The anisotropic nature of the Fermi surface can also be clearly observed. In the Figure 3.9, we have plotted ν_{k_f} in terms of explicit scalar field horizon value $\Phi(r_0)$ for a fixed temperature. For this case the horizon value depends on the external source at the holographic boundary. One can, therefore, clearly see the quantitative difference between the two mechanisms of controlling the fermionic spectral function.

3.7 Summary and Conclusions

Phenomena of pseudo-gap is an interesting area of condensed matter field in high temperature superconductivity. In the context of holographic method, one interesting mechanism of obtaining pseudo-gap was first proposed by Vanacore et. al. [5]. A non-minimal coupling between the fermion and gauge field has been introduced in the AdS bulk. By appropriately tuning this free coupling parameter p, anisotropic gap in the fermion spectral function is generated. In this chapter, we introduced a real scalar field whose non-zero profile modifies the aforementioned fermion-gauge interaction in terms of $p_{eff} = p\Phi$, and thereby controls the boundary Fermi surface. We have considered two possible scenarios of generating this coupling. In the first scenario, the scalar field in the bulk acts as a neutral order parameter field at the boundary which gives rise to a phase transition from normal phase to pseudo-gap phase at a critical temperature T_c. As emphasised before, this T_c can be identified with the well known crossover temperature T^* in the high-T_c superconducting phase diagram, below which pseudo-gap appears. For holographic fermions, parameter ν_k plays the role of operator dimension in the AdS_2, which controls the behaviour of the low energy fermions at the boundary. In our analysis, this ν_k depends on the scalar field value at the horizon. This in turn makes ν_k temperature dependent. We therefore, obtain the characteristic changes of the Fermi surface while changing the temperature below T_c shown in Figure 3.4. Because of strong anisotropic nature of the Fermi surface, we also discussed how the fermionic properties changes along the Fermi surface from normal ($\nu_k < 1/2$) to marginal ($\nu_k = 1/2$) and marginal to non-Fermi liquid ($\nu_k > 1/2$) for a given temperature shown in Figure 3.8. In the second scenario, we tune the non-minimal coupling p_{eff} by the dual boundary scalar operator as a source, which essentially corresponds to the non-normalisable solution of the bulk scalar field. Hence for this system we do not have any critical temperature. Therefore, we studied this case for a fixed temperature and tune the boundary source which can be identified with the doping in high temperature superconductor. However, detail study needs to be done to understand this identification.

Finally we examine an important question related to the existence of actual gap in the fermion spectral function. We consider two different holographic models-(A,B), associated with two different fermion-gauge coupling prescription. The Figure 3.6 and 3.7 illustrate the presence of the gap for both the models. For dipole type coupling the energy gap is symmetric in nature Figure 3.6, whereas for the other model it is anisotropic Figure 3.6 in accordance with the anisotropic Fermi arc Figure 3.4. Therefore, in holographic pseudo-gap phase, the Fermi arcs seem to be intimately connected with the partial gapping of the Fermi surface. It would, therefore, be interesting to construct a holographic model where partial gapping is not occurring.

Chapter 4

Studying the holographic Fermi surface in the scalar induced anisotropic background

---

In Chapter 3, we have applied the methodology of holographic principle, to study the emergence of Fermi arcs when one crosses from a normal to a pseudogap phase by changing the temperature of the system. These phases were understood in terms of condensation of the scalar field normalisable mode. In addition to the scalar field condensation we also consider the non-normalisable mode of the scalar field that can be interpreted as the doping parameter. Interestingly, with the dipole-like coupling to the bulk fermions, we found the Fermi arcs feature. Based on these results, we are curious about the behaviour of the fermionic spectral function if the bulk background geometry is anisotropic. One way to introduce such anisotropy is by breaking the translational symmetry. This will be the main goal of this Chapter. This Chapter is based on our published work [7], in which we study a similar class of holographic models, where the appearance of the Fermi arc is a generic feature. We will essentially generalize our previous construction [6], where the bulk dipole coupling and the bulk scalar field, which can break the translational symmetry in the boundary are coupled to the bulk fermions. We will be mostly looking at the evolution of the Fermi surface and their band structure, with particular emphasis on their observational significances.

Explicit translational symmetry breaking solutions of a holographically dual [10, 38–41] theory has been studied either by considering spatially periodic chemical potential at the boundary or especially periodic scalar field in the AdS background. The specific framework we will consider here is Q-lattice [10], where holographic lattice background is constructed by exploiting the solution of a complex scalar field in the bulk. Fermionic spectral function has been studied on the Q-lattice background [107] together with a dipole type of coupling in the fermion sector. It is to be noted that the secondary Fermi surfaces were noted long back in [42]. In that work, beginning with a dilatonic black hole derived from a truncation of type IIB supergravity, fermionic Green's function dual to massless fermions in the bulk were studied. It was shown that for not too small bulk fermion charges, there are Fermi surfaces. The Fermi momenta in this case are equally spaced, and there are a finite number of them, proportional to the charge of the bulk fermion. Similar studies using the anisotropic holographic backgrounds have been done in [135–138]. Our goal would be to look into the nature of the holographic Fermi surface evolution due to bulk coupling parameters which will correspond to different dual controlling operators.

Let us highlight the main contents of this chapter. In the next section, we briefly review the Q-lattice background solution, followed by section 4.2, where we write down the fermion's action and the equations of motion with our definition of the spectral function $A\left(\omega,\, \vec{k}\right)$. In section 4.3, we present the results for different scenarios for massless fermion and discuss each of them. For completeness, in section 4.4 we discuss the scenarios where by taking non-zero fermion mass. Finally, in the last section, we conclude with the interpretation of our results along with a brief discussion.

4.1 The background geometry

As has already been mentioned in the introduction, Fermi arc behaviour has been generically observed in two spatial dimension, we consider our holographic system to be in $(2+1)$ dimensions. Hence, we shall take a $(3+1)$-dimensional Einstein-Scalar-Maxwell system as a background set up,

$$\mathcal{S} = \frac{1}{\kappa^2}\int d^{3+1}x\sqrt{-g}\left[\mathcal{R} + \frac{6}{L^2} - \frac{1}{4}F^2 - |\partial\phi|^2 - m_\phi^2|\phi|^2\right] \tag{4.1}$$

where $\mathcal{R}$ is a Ricci scalar, L being the AdS radius which we will set to be unity later and, Maxwell's field strength $F = dA$, where d is the exterior derivative acting on the vector potential one form A. Finally, $\kappa^2 = 16\pi G$ is the effective reduced gravitational constant which we set to be unity too. As mentioned we consider a complex scalar field ϕ which will source the break down of translational invariance of the boundary field theory. From the above action (4.1) we have the following equations of motions

$$\begin{aligned}
&R_{\mu\nu} = \\
&g_{\mu\nu}\left(-3 + \frac{m_\phi^2}{2}|\phi|^2\right) + \partial_{(\mu}\phi\partial_{\nu)}\phi^* + \frac{1}{4}\left(2F_{\mu\nu}^2 - \frac{1}{2}g_{\mu\nu}F^2\right) \\
&\nabla_\mu F^{\mu\nu} = 0\,, \quad \left(\nabla^2 - m_\phi^2\right)\phi = 0.
\end{aligned} \tag{4.2}$$

We take the ansatz for the metric and the complex scalar field to be of the following form

$$ds^2 = -g_{tt}(z)\, dt^2 + g_{zz}(z)\, dz^2 + g_{xx}(z)\, dx^2 + g_{yy}(z)\, dy^2. \tag{4.3}$$

where,

$$\begin{aligned}
&g_{tt}(z) = \frac{U(z)}{z^2};\ g_{zz}(z) = \frac{U(z)^{-1}}{z^2};\ g_{xx}(z) = \frac{V_1(z)}{z^2}; \\
&g_{yy}(z) = \frac{V_2(z)}{z^2}, \quad A = (1-z)\, a(z)dt, \\
&U(z) \ = \ (1-z)\ u(z), \ \ \phi = e^{i\,k_1\,x + i\,k_2\,y}\ \chi(z)\,.
\end{aligned} \tag{4.4}$$

With the above choice of ansatz for the scalar field, the breaking of translational symmetry by the same scalar field is both in x and y directions. Here, u, V_1, V_2, a, χ are all functions of radial coordinate z and k_1, k_2 are constants interpreted as wave numbers of the lattice. From the above equation we have four second order coupled ODEs for V_1, V_2, a, χ and one first order for u. For a general mass m_ϕ^2, the complex scalar field near the AdS boundary ($z \longrightarrow 0$) behave as

$$\chi(z) \ = \ z^{\alpha_-}\,\chi^{(1)} \ + \ z^{\alpha_+}\,\chi^{(2)} \ + \ldots \tag{4.5}$$

where, $\alpha_\pm = 3/2 \pm \sqrt{9/4 + m_\phi^2}$. The leading term $\chi^{(1)}$ is associated with the source of the dual scalar operator in the boundary theory, whose dimension is $\Delta = 3 - \alpha_- = \alpha_+$. To this end we study in detail the case when, scalar field mass $m_\phi^2 = 0$, which corresponds to $\alpha_- = 0$ and the corresponding marginal dual scalar operator in the (2+1)- dimensional boundary theory. For building a numerical black hole solution, we solve these equations using the regularity conditions near the horizon $z = 1$ and, at the AdS boundary or UV, we assume the following series expansion,

$$
\begin{aligned}
& u = 1 + O(z)\ ,\ V_1 = 1 + O(z)\ ,\ V_2 = 1 + O(z)\ , \\
& a = \mu + O(z)
\end{aligned}
\tag{4.6}
$$

To solve the non-linear equations first, we linearize the ODEs by discretizing simultaneously both the equations of motions and the boundary conditions following [139, 140] and then use the iterative Newton-Raphson's (NR) method [141, 142] in Mathematica. Moreover for fixed m_ϕ^2, we found that the solutions are specified by 3-dimensionless parameters namely, T/μ, k/μ and $\chi^{(1)}/\mu^{\alpha_-}$. We notice that for very low temparature (small T/μ), NR method does not converge as it is sensitive to the initial guess values or seeds. We can overcome this by using the solutions at higher temparature as a seeds to achieve another solution at lower temparature. We illustrate the background solutions in Figure 4.1. We consider this as our numerical background in our subsequent analysis for the fermion spectral function. Most of our analysis will be for both fermion and scalar mass to be zero. In this sense our $(3+1)$ dimensional gravitational bulk contains Weyl fermion. Our goal would be to understand the fermion spectral function dual to those Weyl fermion. This could resemble the class of Weyl semi-metals in the real condensed matter systems as pointed out in the introduction.

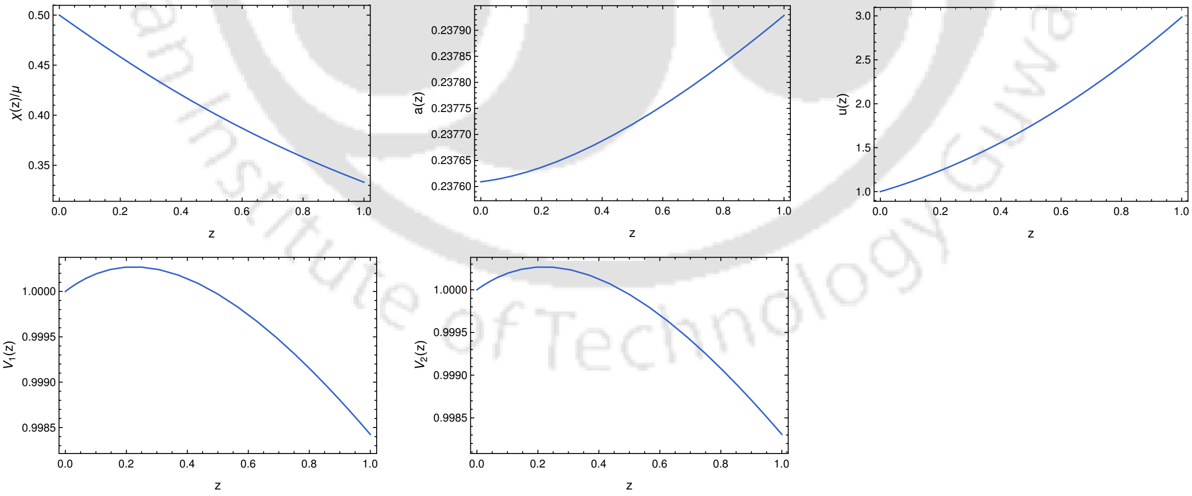

FIGURE 4.1: Q-lattice profile with $m_\phi^2 = -2$, for the parameters $T/\mu{=}1, \chi^{(1)}/\mu{=}0.5, k_1/\mu = 1$ and $k_2/\mu = 0$

4.2 Fermions: Action and the spectral function.

Now that we have the solutions of the background, we can write down the action for fermions with four non-trivial interaction terms given by

$$\mathcal{S}_{fer} = \int d^4x\sqrt{-g}i\bar{\psi}\Big(\not{D} - m_\psi - i\,\wp_1\not{F} - i\,\wp_2\,|\phi|^2\not{F}\Big)\psi\,. \tag{4.7}$$

with ϕ and m_ψ being the complex scalar field from the background and fermion mass respectively. We have considered two coupling parameters: one is simple dipole coupling parametrised by $\wp_1$ and another is similar to dipole type coupling with the scalar field parametrised by $\wp_2$. At this point, it is to be mentioned that these two types of couplings in the holographic context has already been studied in understanding the Mott-Insulator [11] transition or appearance of Fermi Arc [5]. One can interpret the Fermi arc in the present context as the emergence of Mottness anisotropically due to Lorentz violating couplings. In our previous work [6], we have further generalised and explored the influence of Lorentz violating dipole coupling on the fermionic spectral function adding a scalar field as a source term. We have constructed the solution associated with the transition from circular to arc like Fermi surface controlled by the scalar condensation in the bulk. In this chapter, we look into such system with two sets of couplings and also introduced one dimensional lattice in the boundary theory. For the present case, we will mostly concentrate on the simultaneous effect of those coupling parameters on the fermionic spectral function. Various symbols in (4.7) are given by:

$$\begin{aligned}\not{D} &= e^\mu_c\Gamma^c\left(\partial_\mu + \frac{1}{4}\omega^{ab}_\mu\Gamma_{ab} - iqA_\mu\right)\\ \not{F} &= \frac{1}{2}\Gamma^{ab}e^\mu_a e^\nu_b F_{\mu\nu}\,.\end{aligned}$$

where, e^μ_a, ω^{ab}_μ are the vielbeins and spin connection, q is the charge of the bulk fermions. The Dirac equation from the above action is given by:

$$\Big(\not{D} - m_\psi - i\,\wp_1\not{F} - i\,\wp_2\,|\phi|^2\not{F}\Big)\psi = 0. \tag{4.8}$$

In order to further simplify the Dirac equation, we choose the following gamma matrices

$$\Gamma^{\underline{z}} = \begin{pmatrix} -\sigma^3 & 0 \\ 0 & -\sigma^3 \end{pmatrix}, \quad \Gamma^{\underline{t}} = \begin{pmatrix} i\sigma^1 & 0 \\ 0 & i\sigma^1 \end{pmatrix},$$
$$\Gamma^{\underline{x}} = \begin{pmatrix} -\sigma^2 & 0 \\ 0 & \sigma^2 \end{pmatrix}, \quad \Gamma^{\underline{y}} = \begin{pmatrix} 0 & \sigma^2 \\ \sigma^2 & 0 \end{pmatrix} \tag{4.9}$$

Now, we can expand the Dirac equation as

$$\Big(e^{z}_{\underline{z}}\, \Gamma^{\underline{z}} \partial_z + S.C + e^{t}_{\underline{t}} (\Gamma^{\underline{t}} \partial_t - iqA_t) + e^{x}_{\underline{x}} \Gamma^{\underline{x}} \partial_x + e^{y}_{\underline{y}} \Gamma^{\underline{y}} \partial_y$$
$$- m_\psi - i\,\wp_1 \not{F} - i\,\wp_2\, |\phi|^2 \not{F} \Big)\, \psi = 0 \tag{4.10}$$

where $S.C$ is a contribution from the spin connection that can be cancelled by rescaling the field $\psi = (g_{tt} g_{xx} g_{yy})^{-\frac{1}{4}} e^{-i\omega t + ik_x x + ik_y y} \xi\,(z, \vec{k})$, where $\vec{k} \equiv (-\omega, k_x, k_y)$. Then we have

$$\Bigg(\frac{1}{\sqrt{g_{zz}(z)}}\, \Gamma^{\underline{z}}\, \partial_z + \frac{1}{\sqrt{-g_{tt}(z)}} \left(\Gamma^{\underline{t}}\, (-i\omega) - iqA_t \right) +$$
$$\frac{1}{\sqrt{g_{xx}(z)}}\, \Gamma^{\underline{x}}\, (ik_x) + \frac{1}{\sqrt{g_{yy}(z)}}\, \Gamma^{\underline{y}}\, (ik_y) - m_\psi +$$
$$\frac{\partial_z A_t}{\sqrt{-g_{zz}(z) g_{tt}(z)}} \left(-i\,\wp_1\, \Gamma^{\underline{z}\,\underline{t}} - i\,\wp_2\, |\phi|^2\, \Gamma^{\underline{z}\,\underline{t}} \right) \Bigg)\, \xi(z, \mathbf{k}) = 0 \tag{4.11}$$

Using the basis (4.9) and by writing the spinors $\xi = (\xi_1, \xi_2)^T$, on further splitting as $\xi_j = (\beta_j, \alpha_j)^T$, where $j = 1, 2$, we have the following radial equations

$$\left(\frac{1}{\sqrt{g_{zz}}} \partial_z \pm m_\psi \right) \begin{pmatrix} \beta_1 \\ \alpha_1 \end{pmatrix} \mp \frac{(\omega + qA_t)}{\sqrt{-g_{tt}(z)}} \begin{pmatrix} \alpha_1 \\ \beta_1 \end{pmatrix} + \frac{k_x}{\sqrt{g_{xx}}} \begin{pmatrix} \alpha_1 \\ \beta_1 \end{pmatrix}$$
$$- \frac{k_y}{\sqrt{g_{xx}}} \begin{pmatrix} \alpha_2 \\ \beta_2 \end{pmatrix} + \frac{\partial_z A_t}{\sqrt{-g_{zz} g_{tt}}} \left(\wp_1 + \wp_2\, |\phi|^2 \right) \begin{pmatrix} \alpha_1 \\ \beta_1 \end{pmatrix} = 0 \tag{4.12}$$

$$\left(\frac{1}{\sqrt{g_{zz}}}\partial_z \pm m_\psi\right)\begin{pmatrix}\beta_2\\ \alpha_2\end{pmatrix} \mp \frac{(\omega+qA_t)}{\sqrt{-g_{tt}(z)}}\begin{pmatrix}\alpha_2\\ \beta_2\end{pmatrix} - \frac{k_x}{\sqrt{g_{xx}}}\begin{pmatrix}\alpha_2\\ \beta_2\end{pmatrix}$$
$$-\frac{k_y}{\sqrt{g_{xx}}}\begin{pmatrix}\alpha_1\\ \beta_1\end{pmatrix} + \frac{\partial_z A_t}{\sqrt{-g_{zz}g_{tt}}}\left(\wp_1+\wp_2\,|\phi|^2\right)\begin{pmatrix}\alpha_2\\ \beta_2\end{pmatrix} = 0 \tag{4.13}$$

From these equations, we can expand near the horizon and one can find that the leading terms from the equations of motions are given by

$$\partial_z\begin{pmatrix}\beta_j(z,\vec{k})\\ \alpha_j(z,\vec{k})\end{pmatrix} \mp \frac{\omega}{4\pi T}\frac{1}{1-z}\begin{pmatrix}\alpha_j(z,\vec{k})\\ \beta_j(z,\vec{k})\end{pmatrix} = 0. \tag{4.14}$$

From this equation, we determine the in-falling boundary condition at the horizon for extracting the retarded Green's function at the AdS boundary, and the independent ingoing boundary condition should be imposed at the horizon, i.e.,

$$\begin{pmatrix}\beta_j(z,\vec{k})\\ \alpha_j(z,\vec{k})\end{pmatrix} \sim c_j(1-z)^{-\frac{i\omega}{4\pi T}}. \tag{4.15}$$

Furthermore, the asymptotic behaviour of the Dirac equations near the AdS boundary ($z \to 0$) has the following form

$$\begin{pmatrix}\beta_j\\ \alpha_j\end{pmatrix} \approx A_j z^{m_\psi}\begin{pmatrix}1\\ 0\end{pmatrix} + D_j z^{-m_\psi}\begin{pmatrix}0\\ 1\end{pmatrix}. \tag{4.16}$$

We can numerically read off the coefficients A and D to obtain the Green's functions. For the couplings considered here, we have a mixing of various spinorial components. We followed the usual prescription used in [5, 64, 104] to extract the Green's function by using two sets of linearly independent boundary conditions that are given by

$$\begin{pmatrix}\beta_1^I & \beta_1^{II}\\ \beta_2^I & \beta_2^{II}\end{pmatrix} = \begin{pmatrix}s_{11} & s_{12}\\ s_{21} & s_{22}\end{pmatrix}\begin{pmatrix}\alpha_1^I & \alpha_1^{II}\\ \alpha_2^I & \alpha_2^{II}\end{pmatrix}, \tag{4.17}$$

Now the retarded Green's function is defined as

$$G^R(\omega,k_x,k_y) = -i\begin{pmatrix}s_{11} & s_{12}\\ s_{21} & s_{22}\end{pmatrix}\cdot\gamma^t \tag{4.18}$$

with gamma matrices in our basis as $\gamma^t = i\sigma_1$. The observable quantity of interest, is the spectral function $A\,(\omega, k_x, k_y)$ which is given by

$$A\,(\omega\,, \vec{k}) = \mathrm{Im}\left[\mathrm{Tr}\, G^R(\omega\,, \vec{k})\right]. \tag{4.19}$$

where $\vec{k} \equiv (k_x, k_y)$ and $G^R(\omega\,, \vec{k})$ is the retarded Green's function. The properties of $A\,(\omega\,, \vec{k})$ is what we will study in our subsequent analysis.

4.3 Results and Discussion

As already emphasized thorough out the earlier sections, our goal would be to explore the behaviour of the Fermi surface considering various coupling $\wp_1\,, \wp_2$ in a systematic manner. We wish to discuss the properties of the Fermi surface close to zero temperature. Before we explore different possibilities, as a consistency check, we reproduce the result in Figure 4.3 obtained in [107, 135] assuming all the coupling parameters set to zero.

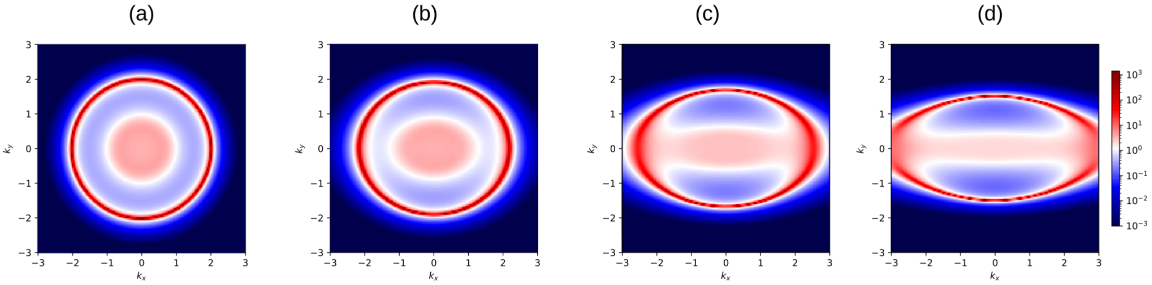

FIGURE 4.2: Spectral function $A\,(k_x, k_y)$ with all $\wp$'s set to zero. Panel (**a**) – (**d**) is for $\frac{\chi^{(1)}}{\mu^{\alpha_-}} = 0.2,\ 1.0,\ 2.0,\ 3.0$ respectively. Here $m_\psi = 0$, $q = 1$, background parameters $T/\mu = 0.009$, $k_1/\mu = 0.8$. and $k_2/\mu = 0$.

4.3.1 Symmetry broken along k_1 only

Firstly, let us set our background parameter $k_2 = 0$ and consider only k_1. The influence of the background scalar on the spectral function can be seen from Figure 4.2, $\chi^{(1)}$ represents the source of the dual boundary operator of the bulk scalar field. As we increase the strength of the boundary source term, the amplitude of the fermionic spectral

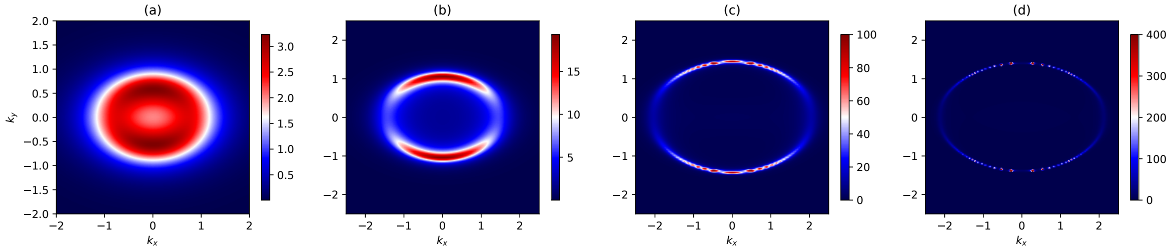

FIGURE 4.3: Density plot of the spectral function $A(k_x, k_y)$ with all couplings set to zero for the parameters $m_\psi = 0$ and $q = 1$. In panel (a) to (d) the background parameter $\chi^{(1)} = 2.0$, $k_1/\mu = 0.8$, $k_2/\mu = 0$, $m_\phi^2 = 0$ and $T/\mu = 0.09, 0.04, 0.02, \text{and}\, 0.009$ respectively. Clearly as we lowered the temperature the Fermi surface becomes very sharp.

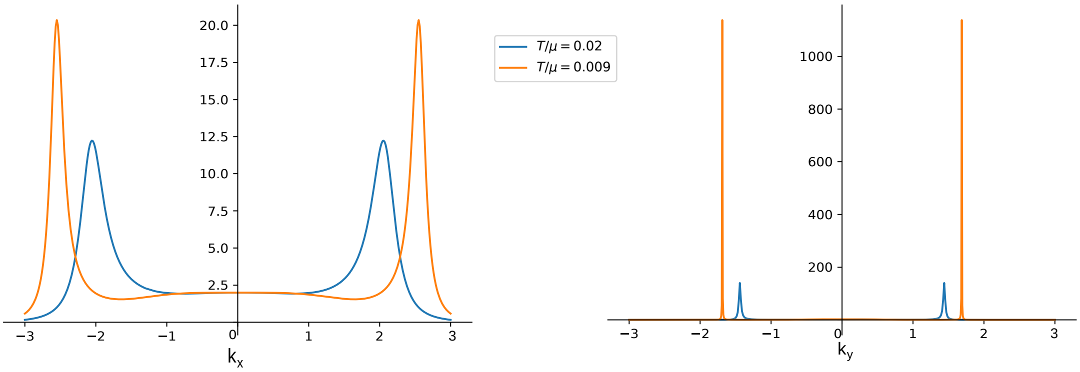

FIGURE 4.4: 2D slice along $k_y = 0$ (left) and $k_x = 0$ (right) of Figure 4.3 to compare the peaks for $T/\mu = 0.02$ (blue) and 0.009 (orange) respectively with other parameter values same as in Figure 4.3.

function reduces along k_x. Also in the limit of $\chi^{(1)} \to 0$, the spectrum reduces to the one observed in case of RN-AdS blackhole with a circular Fermi surface and no gap (see Figure 4.2 (a)). This suppression can be attributed to reducing a quasi-particle lifetime near the $k_x^F \simeq \pm 2$ point. From Figure 4.3 $((b) - (d))$, at low temperature one notices that, without any coupling terms, the spectral function gives rise to a stretched Fermi surface with its amplitude suppression along k_x-direction ($k_y = 0$), arising due to the broken translational symmetry along $x-$direction established by the background scalar field. Whereas, along k_y direction, the spectral function indicates the existence of the Fermi surface with a large density of states. Further, as one lowers the temperature, the peak of the Greens function increases, which essentially enhances the quasi-particle lifetime. On the other hand, turning on the pure dipole coupling $\wp_1 = 1$, the Fermi surface is completely destructed along $k_y = 0$ line giving rise to dipolar Fermi arcs Figure

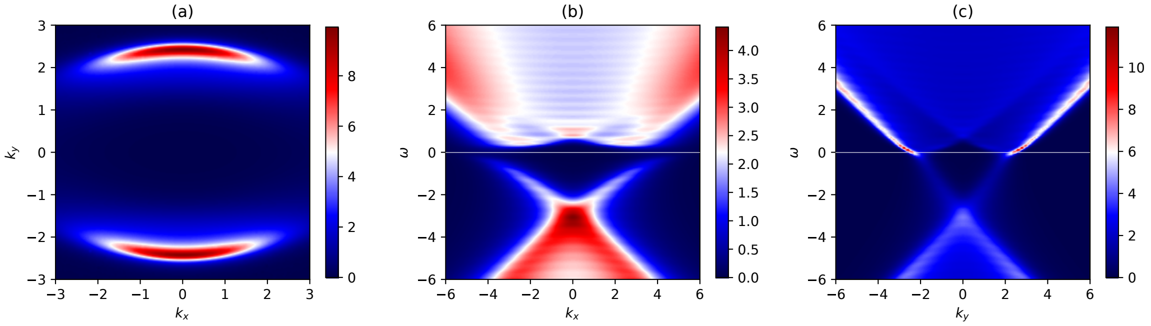

FIGURE 4.5: Panel (**a**): The fermionic spectral density in the $k_x - k_y$ space for $\wp_1 = 1$ near $\omega = 0$. Coupling $\wp_2$ set to zero. Panel (**b**)&(**c**): The energy-momentum distribution along k_x and k_y respectively. Here, the fermion mass $m_\psi = 0$ and charge $q = 1$ with background parameters $\chi^{(1)} = 2.0$, $k_1/\mu = 0.8$, $k_2/\mu = 0$, $m_\phi^2 = 0$ and $T/\mu = 0.02$. The thin white line is at $\omega = 0$ which is the Fermi level.

4.5(a). This destruction can be characterized by the opening of the energy gap that can be clearly observed from panel (*b*) of Figure 4.5. With this consistency check of present calculations with the previous works, we shall now examine the evolution of the spectral function or, in other words, the nature of the Fermi surface due to change of different controlling parameters such as coupling $(\wp_1, \wp_2)$, temperature (T/μ), and source strength $\chi^{(1)}$ of the scalar field at the boundary.

Controlling both the dipole couplings $(\wp_1, \wp_2)$**:** No special features appeared in the spectral function upon increasing the value of $\wp_1$, with $\wp_2 = 0$, except the known two Fermi arcs becoming more flattened (see [107]) and prominent. Similar behaviour is observed for the non-zero but positive value of $\wp_2$, which we chose not to discuss any further here. However, interesting behaviour of the spectral function emerges if the dipole coupling $\wp_2$ assumes a negative value, which is further controlled by the anisotropic scalar field profile in the background. The background anisotropic scalar field plays a crucial role in controlling the shape and the amplitude of the spectral function. As discussed, we will consider a complex scalar field in the bulk that will have a non-normalizable source at the boundary, which can be used as a tunable parameter. For this, we choose the mass of the scalar field to be $m_\phi = 0$, later on, we will comment on non-zero masses which are outside the AdS$_2$ BF bound. Nevertheless, as we independently increase the magnitude of the dipole coupling parameter $\wp_2$, a pair of Fermi surfaces emerges as shown in Figure 4.6. The appearance of multiple Fermi surfaces in holographic model was initially reported in [42] for spherically symmetric background. Also recently in [137, 138], more complicated background geometry were introduced while breaking translational invariance and Fermi arcs like features were observed triggered by the effective mass term and the lattice effects. The emergence of these pair of anisotropic Fermi surfaces are the interesting features of our results as they have been observed in the ARPES experiments in different real condensed matter systems such as Topological insulators (TI), recently discovered Dirac and Weyl semi-metals [83, 84]. For superconductivity, it is the pseudogap region in the phase diagram where the Fermi arc appears with a controlled doping concentration in a 2-dimensional layer of the superconducting sample, and it is connected to the suppression in the Spectral function. For the case of Dirac and Weyl semi-metals, Fermi arcs appear as surface states which converge at the two distinct Dirac points in the three-dimensional bulk. We also showed the presence of these gappedless surface states in the energy-band dispersion in Figure 4.8 with only coupling $\wp_2$ and in Figure 4.10 with the two couplings parameters $\wp_1$ and $\wp_2$. Further, from Figure 4.10, one can notice the existence of flat band near the Fermi surface. Interestingly such a highly flat band has been observed in the real condensed matter system, such as in the bilayer graphene [143]. The double Fermi arcs for our holographic system can be thought of as holographic surface states of a bulk material located in $(2+1)$ dimensional boundary of the AdS space [146].

Further observation in Figure 4.6 (e) at $T/\mu = 0.009$, though in the cuprates, the presence of a secondary Fermi surfaces is not yet known but here it shows that when these two surfaces crossed each other to formed a $d-$wave like structure Fermi surface. These phenomena have an interesting resemblance with the usual high-temperature superconductor as discussed in a recent solvable toy model using conventional method [147]. However, the shrinking of the Fermi surface in the radial momentum direction can be tied with the reduction of the available density of states for the system. This shrinking of the Fermi surface does happen in the pseudogap region for the high-temperature superconducting system as one decreases the temperature in the appropriate range of doping concentration.

The same behaviour of the Fermi surface can be observed by keeping fixed $\wp_2 = -0.2$, and controlling source at the boundary of the scalar field (see Figure 4.7). Therefore, the source identified by the non-normalizable part of the bulk scalar field $\chi^{(1)}$ can be thought of as a doping parameter in a certain boundary field theory. In the Figure 4.8, we plotted the evolution of energy band diagram in both k_x and k_y direction. It clearly captures the opening and closing of the energy gap depending on $\wp_2$ values specifically along k_y direction.

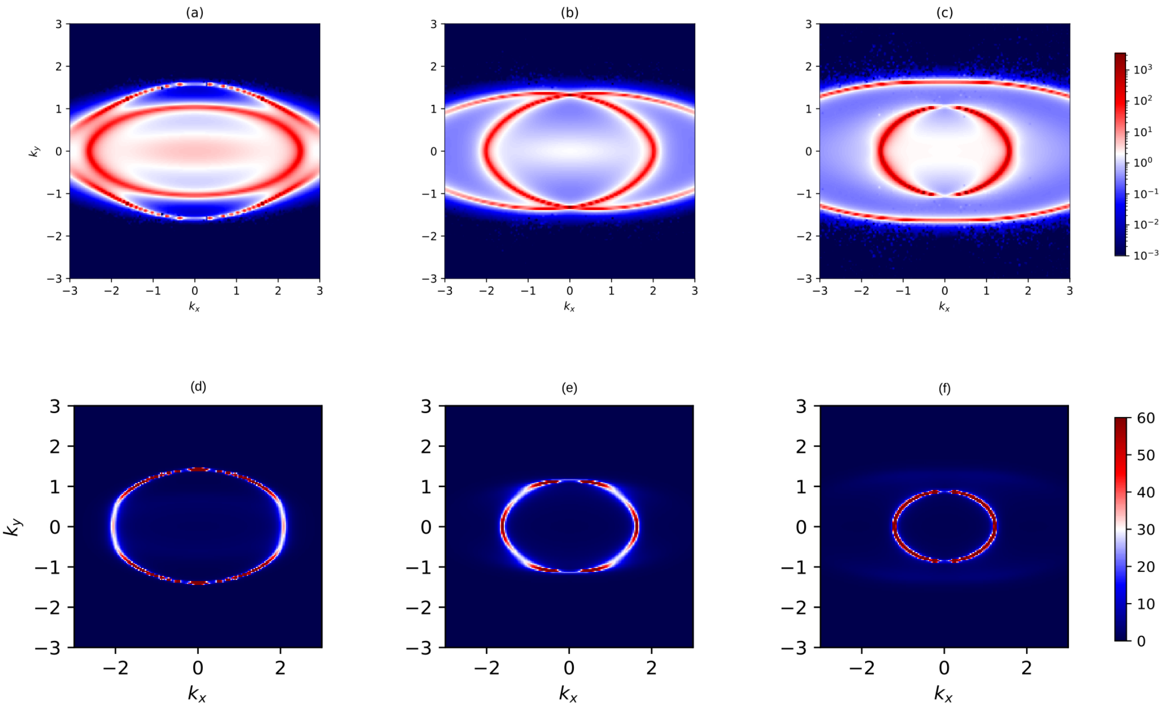

FIGURE 4.6: Spectral density $A\,(k_x, k_y)$ for $T/\mu = 0.001\,(\text{top})$ and $T/\mu = 0.009\,(\text{bottom})$ with $\chi^{(1)}/\mu^{\alpha_-} = 2.0$ and $k_1/\mu = 0.8$. $\wp_1$ is set to zero and $\wp_2$ is non-zero and $m_\psi = 0$, $q = 1$. Both the top and bottom panel from left to right $\wp_2 = [-0.1, -0.2, -0.3]$.

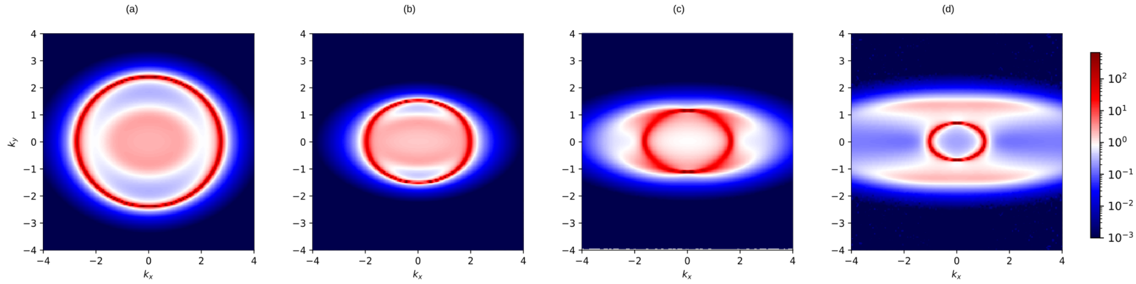

FIGURE 4.7: Plot of $A\,(k_x, k_y)$ with $\wp_2 = -0.2$ and $\wp_1 = 0$. Panel $(a) - (d)$ is for $\frac{\chi^{(1)}}{\mu^{\alpha_-}} = 1.0,\, 1.5,\, 2.0,\, 2.5$ respectively. Here, $m_\psi = 0$, $q = 1, k_1/\mu = 0.8, k_2/\mu = 0$, and $T/\mu = 0.009$.

So far, we have discussed about controlling the dipole coupling independently. Interesting behaviour of the Fermi surface also emerges (see Figure 4.9), once we turn on both the coupling parameters. We assume two sample values of $\wp_1 = 0.2,\, 0.5$, and vary $\wp_2$ across the range $(-0.2, -0.4)$ keeping the temperature fixed at $T/\mu = 0.009$, and background translational symmetry breaking parameter $k_1/\mu = 0.8$ same. What is observed is that for a given $\wp_1$, at a lower value of $\wp_2$, the outer dipolar Fermi arcs is sharp with an additional closed Fermi surface inside the arc. Interestingly with the increasing $\wp_2$, the outer Fermi arc is gradually disappearing along with the prominent appearance of the inner closed Fermi surface through the transfer of spectral weight from the outer to the inner one. Such transfer of spectral weight has been observed in the real condensed matter system [148] such as $La_{1-x}Sr_xMnO_3$. ARPES results on those materials shows the changes in the electronic structure across the metal-insulator transition, which is attributed to the gradual disappearance of the Fermi surface near the Mott-Insulator transition. The reason has been given due to transfer of spectral weight from the coherent band near the Fermi level to the lower Hubbard band. Such transfer of spectral weight can also be seen in our holographic energy band diagram shown in Figure 4.10. Furthermore, at lower $\wp_2$, $\omega = 0$ Fermi surface seems to be smeared over a large momentum range. This observation has striking similarities with the phenomena of Fermi surface smearing observed experimentally in disordered condensed matter system [149]. The role of bulk dipole parameters can be thought of as the strength of the disorderness in the boundary. As we increase $\wp_2$, the available smeared FS states specifically near $k = 0$ move toward

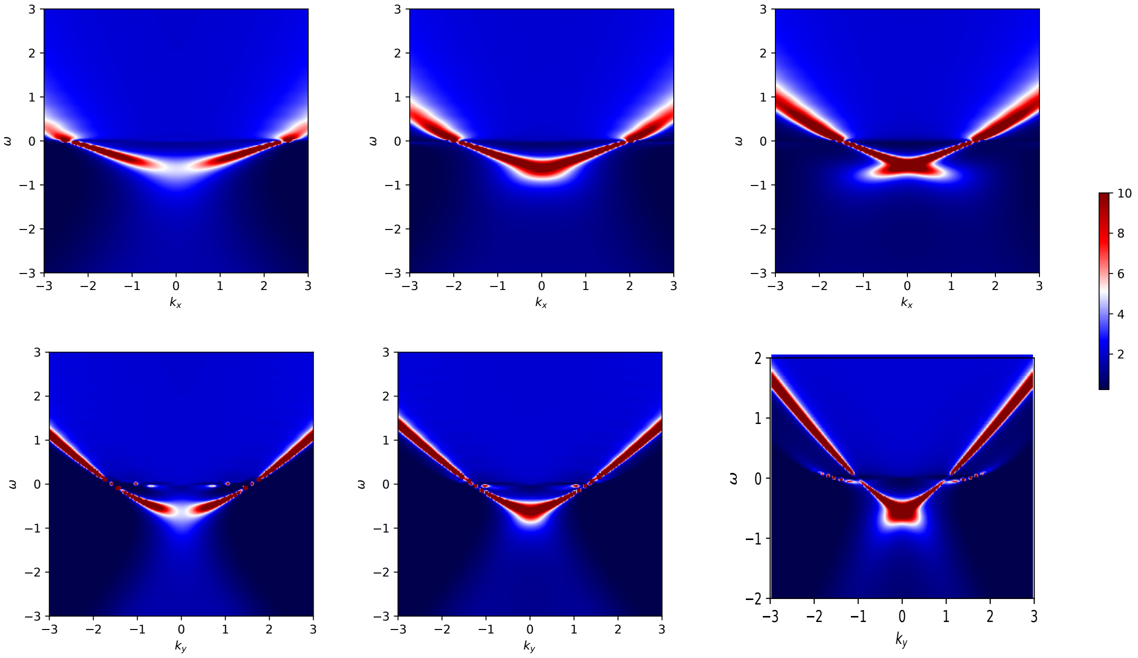

FIGURE 4.8: Spectral density $A(\omega, \vec{k})$ for $T/\mu = 0.001$ with $\chi^{(1)}/\mu^{\alpha_-} = 2.0$, $k_1/\mu = 0.8$ and $k_2/\mu = 0$. Here, parameter $\wp_1 = 0$ and $\wp_2$ is non-zero and $m_\psi = 0$, $q = 1$. In the top and bottom panel from left to right $\wp_2 = [-0.1, -0.2, -0.3]$.

the higher momentum state giving rise to specific Fermi momentum. The emergence of such multiple Fermi surfaces can also be understood from a different perspective that the boundary strongly coupled system contains different species of emergent fermionic degrees of freedom corresponding to their intrinsic properties, which must be coupled with the dual operators associated with bulk dipole couplings.

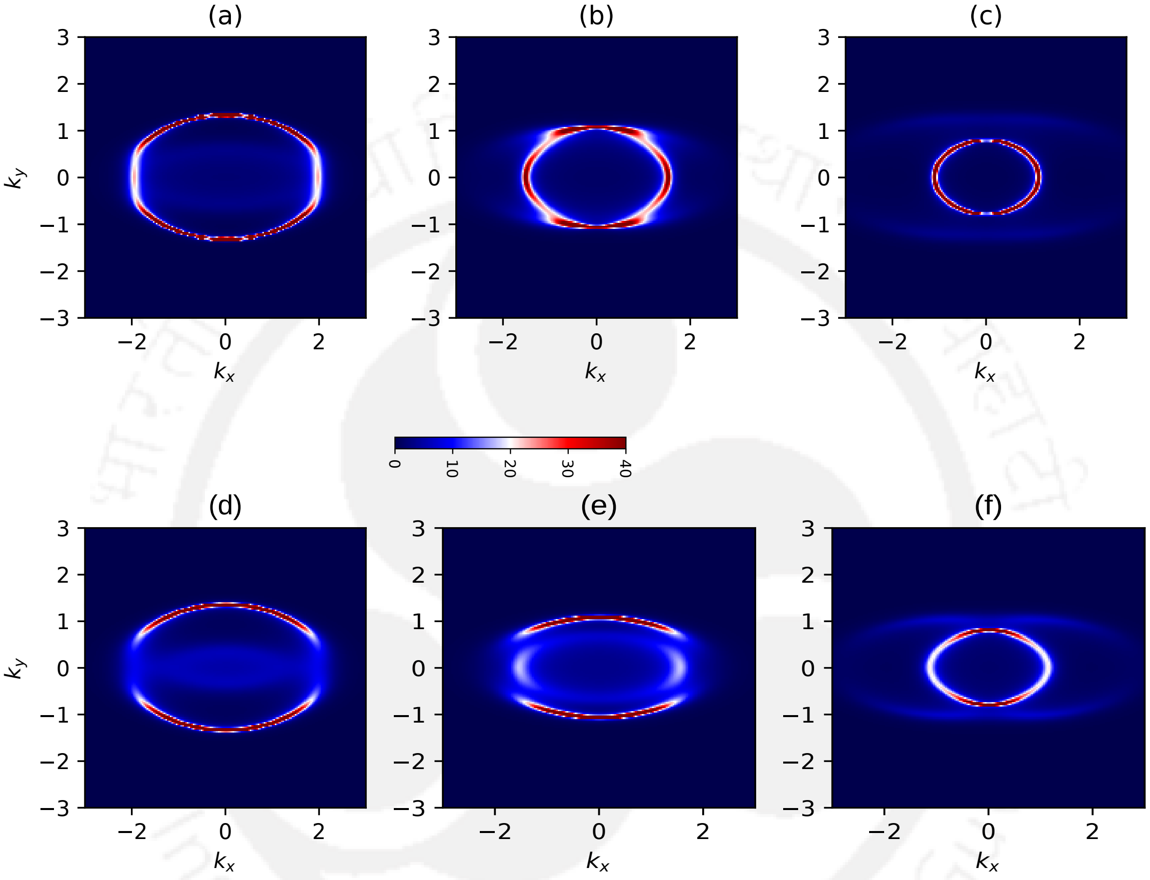

FIGURE 4.9: Spectral function $A\,(k_x, k_y)$ with $\wp_1$, $\wp_2$ set to non-zero and $m_\psi = 0$, $q = 1$, $T/\mu = 0.009$, $\frac{\chi^{(1)}}{\mu^{\alpha_-}} = 2.0$, $m_\phi^2 = 0$, $k_1/\mu = 0.8$ and $k_2/\mu = 0.0$. Panel (a)-(c) are for $[\,(\wp_1\,,\wp_2)\,] = [\,(0.2, -0.2), (0.2, -0.3), (0.2, -0.4)]$ and panel $(d) - (f)$ are for $[\,(\wp_1\,,\wp_2)\,] = [\,(0.5, -0.3), (0.5, -0.4), (0.5, -0.5)]$ respectively.

4.3.2 Symmetry broken in both k_1 and k_2 spatial direction

So far we have look into the scenario where translational symmetry is broken only in the $x-$direction. Now let us check what happens when symmetry is broken in both x and y spatial directions. As expected, when $k_2/k_1 > 1$, the gap along k_y now opens up as shown in the first panel of Figure 4.11. Similar interesting features were observed as shown in Figure 4.11 and Figure 4.12. On zooming in on the inner Fermi surface Figure 4.11(e-f), the spectral weight is suppressed in the opposite direction in comparison to that of the outer surface for smaller $\wp_2$ values. However, for $k_1 = k_2$ the Fermi surface is circular in shape as in the case of RN-AdS blackhole background. Furthermore, one can explore the interplay between the relative signs of $\wp_1$ and $\wp_2$ such that the two interaction terms can cancel each other either at the boundary or near the horizon. For instance, if we consider a solution with the background parameters $\chi^{(1)} = 2$, $T/\mu = 0.009$, $k_1/\mu = 0.8$, $k_2/\mu = 0.2$ and $m_\phi^2 = 0$, we can have the effective coupling $(\wp_1 + \wp_2|\phi|^2)$ to be zero, negative or positive for different $\wp_1$ and $\wp_2$ values. We have explored such a scenario in Figure 4.13 where the plots show the cases when $(\wp_1 + \wp_2|\phi|^2) \lesseqgtr 0$ going through the point $(\wp_1 + \wp_2|\phi|^2) = 0$. For fixed $\wp_2 = -0.1$ and varying $\wp_1$ such that the effective coupling becomes large positive value of we saw a gap spectrum similar to Figure 4.5(a)

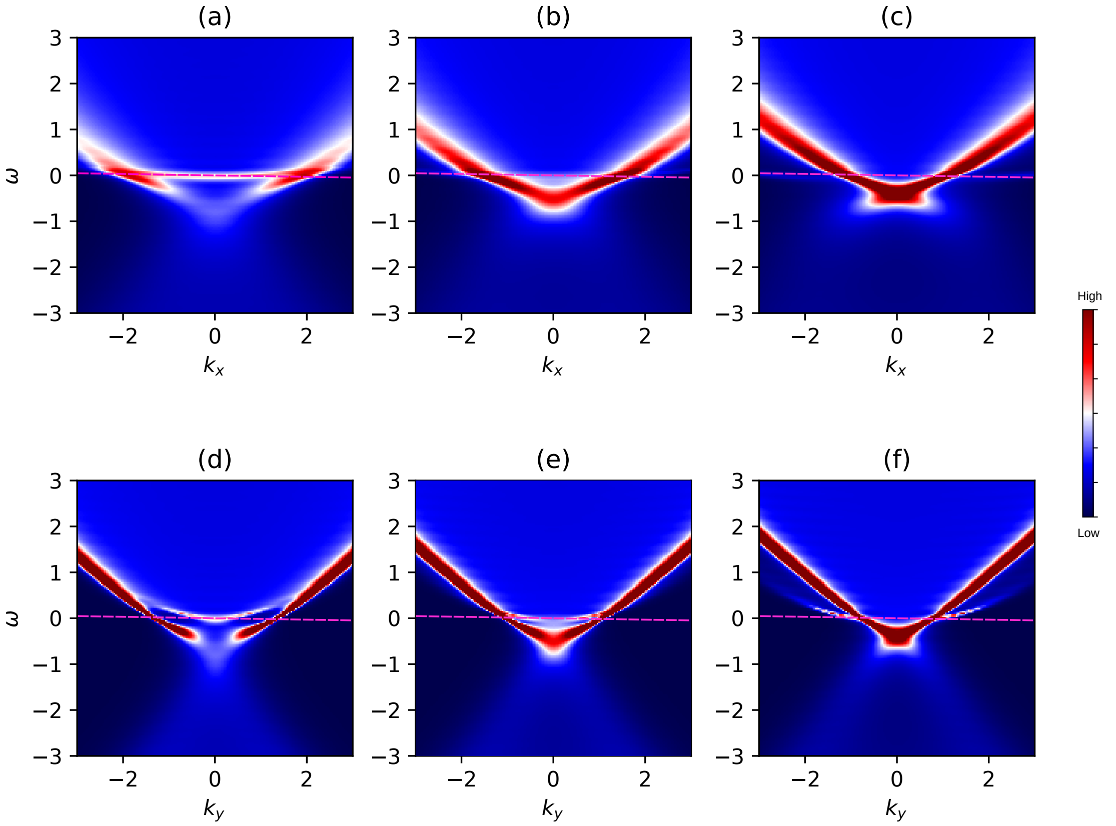

FIGURE 4.10: Energy-momentum dispersion with $\wp_1$, $\wp_2$ set to non-zero and $m_\psi = 0$, $q = 1$, $T/\mu = 0.009$, $m_\phi^2 = 0$, $k_1/\mu = 0.8$ and $k_2/\mu = 0$. Top and bottom panel are along $\omega - k_x$ and $\omega - k_y$ respectively. From left to right the parameters $[(\wp_1, \wp_2)] = [(0.5, -0.2), (0.5, -0.3), (0.5, -0.4)]$.

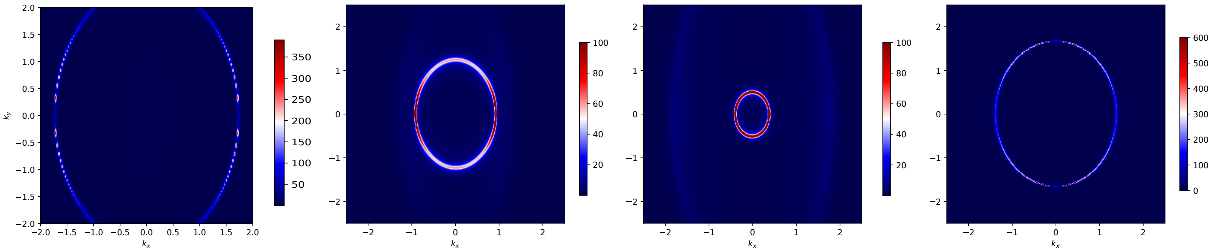

FIGURE 4.11: Spectral density with background parameters $T/\mu = 0.009$, $k_1/\mu = 0.2$, $k_2/\mu = 0.8$, $m_\phi^2 = 0$ and, $\chi^{(1)} = 2$. Here, the fermion mass $m_\psi = 0$, and charge $q = 1$. Left to right we vary $\wp_2 = 0, -0.3, -0.5,$ and -1.2 while fixing $\wp_1 = 0$. Right most panel showing a zoom in version of the inner Fermi surface.

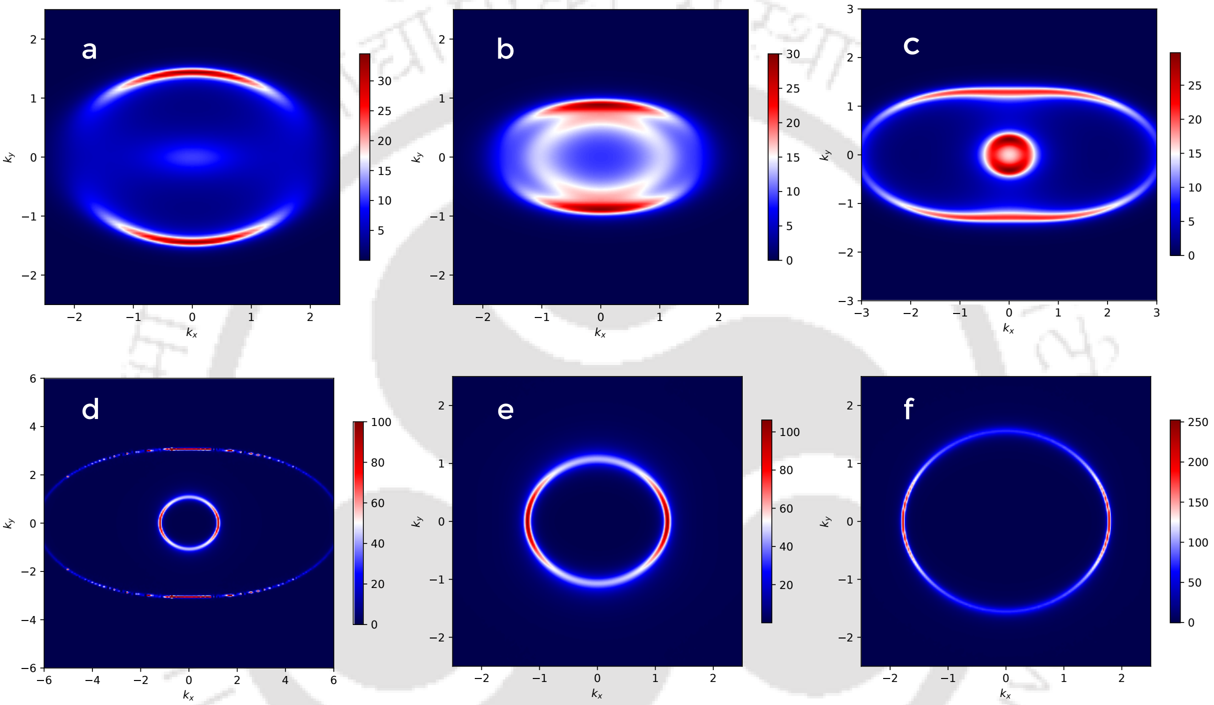

FIGURE 4.12: Spectral density with background parameters $T/\mu = 0.009$, $k_1/\mu = 0.8$, $k_2/\mu = 0.2$, $m_\phi^2 = 0$ and, $\chi^{(1)} = 2$. Here, the fermion mass $m_\psi = 0$, and charge $q = 1$. In the panel $(a) - (d)$ we vary $\wp_2 = -0.3, -0.5, -0.7, -1.2$ and fixing $\wp_1 = 0.5$. Panel (e): Zoom of the inner FS in (d) and (f) is a zoom version for $(\wp_1, \wp_2) = (0.5, -1.2)$ and $(0.5, -1.4)$ respectively.

and for large negative values, we observed the presence of secondary FS with the outer surface showing almost of negligible density.

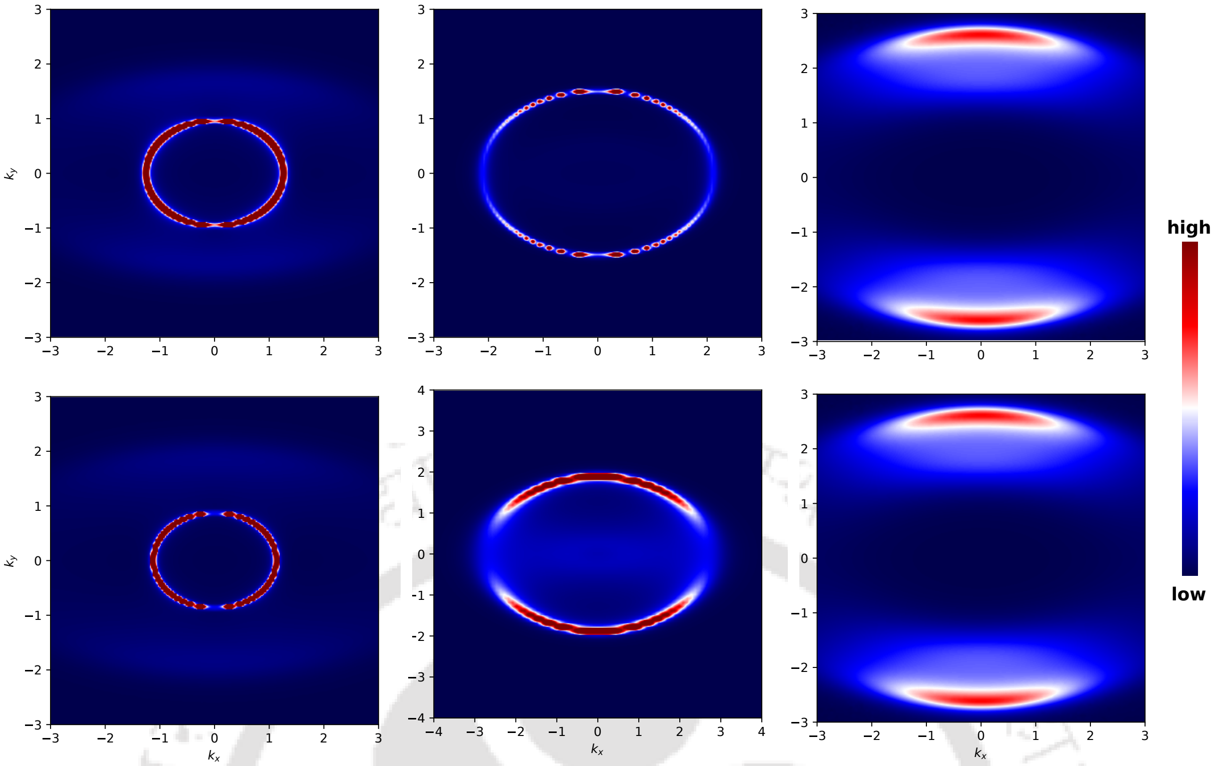

FIGURE 4.13: Spectral density with background parameters $T/\mu = 0.009$, $k_1/\mu = 0.8$, $k_2/\mu = 0.2$, $m_\phi^2 = 0$ and, $\chi^{(1)} = 2$. Here, the fermion mass $m_\psi = 0$, and charge $q = 1$. Top panel is for combination of $\wp_1$ and $\wp_2$ in the IR while bottom panel is for the UV. From left to right, the effective coupling is negative, zero and positive.

4.4 Effect of mass on the fermionic spectral function

For completeness, we also checked the case where fermion mass is non zero with $m_\psi = 1/4$ within the mass window $m_\psi < 1/2$, where we have the freedom to choose either the coefficient A_j or D_j as the sources for fermionic operators. We did not find any significant differences and interesting effects on the spectral function other than what we observed for massless fermions. Nonetheless we present some of the results in Figure 4.14.

On the other hand, when the scalar mass is within the BF bound $-9/4 \leq m_\phi^2 < 0$, for mass m_ϕ^2 close to $-9/4$, for example, $m_\phi^2 = -2$, the contribution from our coupling to the boundary fermionic spectral function was highly suppressed, however, when m_ϕ approaches zero, the effect is much more significant as we have seen from the results for $m_\phi^2 = 0$. We checked for $m_\phi^2 = -11/16$, which correspond to $\alpha_- = 1/4$ and $\alpha_+ = 11/4$, and we obtained similar results.

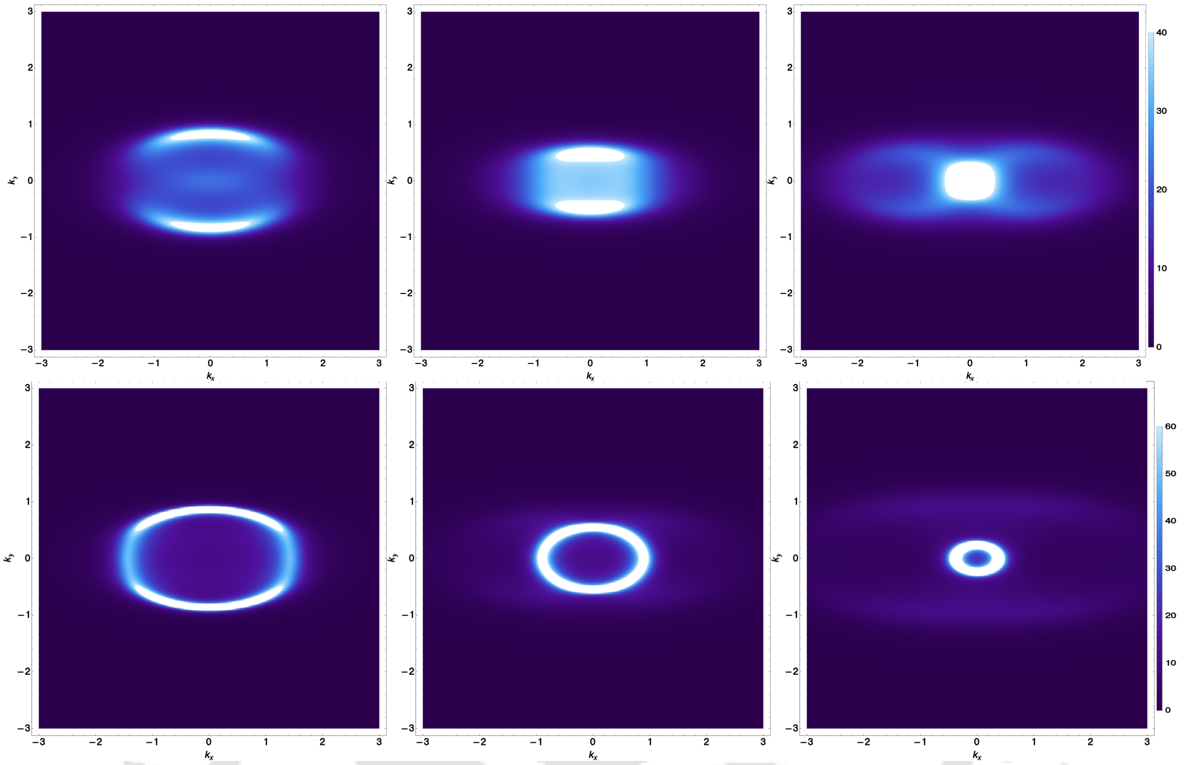

FIGURE 4.14: Spectral density with background parameters $T/\mu = 0.009$, $k_1/\mu = 0.8$, $k_2/\mu = 0$, $m_\phi^2 = 0$ and, $\chi^{(1)} = 2$. Here, the fermion mass $m_\psi = 1/4$, and charge $q = 1$. In the top panel we vary $\wp_2 = -0.1, -0.2, -0.3$ (left to right) and fixing $\wp_1 = 0.5$. In the bottom $\wp_1 = 0$ and $\wp_2 = -0.1, -0.2, -0.3$ from left to right.

4.5 Conclusion

We have considered the anisotropic lattice background, namely the Q-lattice, and explored the fermionic spectral function in detail by considering two specific fermion-gauge field couplings. In addition to the well-studied dipole coupling, we have also introduced the coupling containing the background scalar field $|\phi|^2$, which gives the interesting features.

In this Chapter, we adopt a similar generalisation considered in our previous constructions by considering both types of coupling into the fermionic spectral function. We further introduce the scalar field interaction with the fermion and introduced the discrete spatial translation symmetry in two dimensions on the boundary field theory. Apart from producing the anisotropic background, the non-normalizable mode of the scalar field plays the role of controlling the dipole coupling parameter in the bulk. We observed some interesting features on the spectral function due to $(\wp_1 + \wp_2|\phi|^2)$ coupling. The background is anisotropic without any Lorentz violation, and the spectral function passes through some interesting phases (see Figure 4.10), where phenomena like spectral transfer, Fermi surface smearing happen when simultaneously turning on both the couplings $(\wp_1, \wp_2)$.

Chapter 5

Evolution of holographic Fermi surface from non-minimal couplings

---

In our previous chapters, we proposed various holographic toy models. Our numerics revealed several interesting results, which are related to the Fermi arcs phenomena observed in strongly correlated condensed matter systems seen from ARPES experiments. We have also pointed out in our introduction of this thesis that in addition to the usual high T_c superconductors, other new classes of materials, such as topological Dirac and Weyl semi-metals [83–90] also shown to have the Fermi arcs feature. For detail review on this topic, see [26]. As mentioned earlier, the Fermi arcs appear as the surface states, which maybe because of the underlying symmetries or structure in the bulk of materials for Dirac and Weyl semi-metals. These unconventional electronic properties, which cannot be explained by known theories due to strong interaction and also suspected of being protected by some unknown symmetries, have led to a search for an alternative approach like AdS/CFT. In recent years, lots of experiments and theories have been performed and modelled to shed some light in understanding of the underlying mechanism behind these strange properties of the Fermi surface from the perspective of condensed matter physics [91–94] and other approaches like the holographic method. This is done by following the recent pioneering works [5, 11, 12, 95, 96], which began investigating the Fermi arc-like structures and the Mott transition, taking various classical gravity background as the bulk theory. The authors in [11, 12], considered a non minimal coupling of the form $p\bar{\psi}\not{F}\psi$, where the gauge field is coupled with the fermion field ψ. They observed a transfer of spectral weight between energy bands as the strength of the coupling p is increased, and also beyond certain critical value of p, a gap emerges in the spectral function, which are the key features of Mott physics in the condensed matter systems. Later in [5], by exploring symmetries of the system they proposed a similar modification of the coupling mentioned earlier and the Fermi-arcs features were seen.

Motivated by the features seen in these works [5, 11, 12], in this Chapter, we will study a holographic toy model similar to the one considered in our previous work [7], where we observed an evolution of a pair of Fermi arcs. Here, we will essentially extend our earlier approach by modifying the previous couplings with a different one [6], where the bulk dipole coupling is modified to break the rotational and Lorentz symmetries at the boundary. Our main objective here is to further study the evolution of the Fermi surface and their band structure in presence of the two couplings given in section 5.1. In this Chapter also, we will consider the same Q-lattice [10] as our holographic lattice background, which we have constructed in Chapter 4 with a complex scalar field that breaks the translational symmetry in the bulk. Recall that, in Chapter 4, we had studied the fermionic spectral function in the Q-lattice background with couplings of the form $p\bar{\psi}\,\not{F}\psi$ and $p\,\bar{\psi}\,\not{F}|\phi|^2\psi$. Given the anisotropic background it will be interesting to study the Fermi surface evolution due to fermions bulk couplings parameters given in equation (5.1) below.

We will organise the rest of our discussion in this chapter as follows: In section 5.1, we write down the fermion's action with our coupling terms and the equations of motion, leading to the spectral function $A\,(\omega,\,\vec{k})$ which is the most relevant quantity for our discussion—followed by section 5.2, where we present the numerical results with a discussion on each of them. In the last section, we summarise the results.

5.1 Fermions: Action and the spectral function.

We will consider the probe fermions along with the non minimal couplings in the background solutions discussed above and write down the action as

$$\mathcal{S}_\psi = \int d^4x\sqrt{-g}i\bar{\psi}\Big(\not{D} - m_\psi - i\,p_1\,|\phi|^2\not{F} - i\,p_2\,|\phi|^2\mathbf{\Gamma}\not{F}\Big)\psi \tag{5.1}$$

Here, the scalar field ϕ is the same discussed in the lattice solution and m_ψ is the fermion mass. Expanded expression of the symbols in (5.1) are given by:

$$\mathbf{\Gamma} = \Gamma^{\underline{z}}\Gamma^{\underline{t}}(\hat{n}.\vec{\Gamma}) \ , \qquad \not{D} = e^{\mu}_{c}\Gamma^{c}\left(\partial_\mu + \frac{1}{4}\omega^{ab}_{\mu}\Gamma_{ab} - iqA_\mu\right)$$

$$\not{F} = \frac{1}{2}\Gamma^{ab}e^{\mu}_{a}e^{\nu}_{b}F_{\mu\nu} \ .$$

where, $e^{\mu}_{a}, \omega^{ab}_{\mu}$ are the vielbeins and spin connection, q is the charge of the bulk fermions. The first coupling with controlling parameter p_1 is the same to what we studied in [7], however we include here to study the combine effects. While the second coupling parametrized by p_2 is similar the one studied in the evolution of Fermi Arc from Mott insusator [5] that breaks rotational and Lorentz symmetries of the boundary theory. We studied this type of coupling term in our previous chapter, involving a real scalar field that controls the transition from circular to arc like Fermi surface controlled by the scalar condensation in the bulk at low temperature.

The Dirac equation from the above action is given by:

$$\left(\not{D} - m_\psi - i\,p_1|\phi|^2\not{F} - i\,p_2\,|\phi|^2\mathbf{\Gamma}\not{F}\right)\psi = 0. \tag{5.2}$$

In order to further simplify the Dirac equation, we choose the following gamma matrices

$$\Gamma^{\underline{z}} = \begin{pmatrix} -\sigma^3 & 0 \\ 0 & -\sigma^3 \end{pmatrix}, \quad \Gamma^{\underline{t}} = \begin{pmatrix} i\sigma^1 & 0 \\ 0 & i\sigma^1 \end{pmatrix},$$
$$\Gamma^{\underline{x}} = \begin{pmatrix} -\sigma^2 & 0 \\ 0 & \sigma^2 \end{pmatrix} \quad , \quad \Gamma^{\underline{y}} = \begin{pmatrix} 0 & \sigma^2 \\ \sigma^2 & 0 \end{pmatrix} \tag{5.3}$$

Now, we can expand the Dirac equation (5.2) together with rescaling of the field $\psi = (g_{tt}g_{xx}g_{yy})^{-\frac{1}{4}}e^{-i\omega t + ik_x x + ik_y y}\xi\,(z,\vec{k})$, where the vector $\vec{k} \equiv (-\omega, k_x, k_y)$, we have

$$\begin{aligned}&\Bigg(\frac{1}{\sqrt{g_{zz}(z)}}\,\Gamma^{\underline{z}}\,\partial_z + \frac{1}{\sqrt{-g_{tt}(z)}}\,\left(\Gamma^{\underline{t}}\,(-i\omega) - iqA_t\right) + \\ &\frac{1}{\sqrt{g_{xx}(z)}}\,\Gamma^{\underline{x}}\,(ik_x) + \frac{1}{\sqrt{g_{yy}(z)}}\,\Gamma^{\underline{y}}\,(ik_y) - m_\psi + \\ &\frac{\partial_z A_t}{\sqrt{-g_{zz}(z)g_{tt}(z)}}\left(-i\,p_1\,|\phi|^2\,\Gamma^{\underline{z}\,\underline{t}} - i\,p_2\,|\phi|^2\,\mathbf{\Gamma}\,\Gamma^{\underline{z}\,\underline{t}}\right)\Bigg)\,\xi(z,\mathbf{k}) = 0\end{aligned} \tag{5.4}$$

Now using the basis (5.3) and by splitting the spinors $\xi = (\xi_1, \xi_2)^T$, and $\xi_j = (\beta_j, \alpha_j)^T$, with j taking values $j = 1, 2$, we get the following coupled radial equations

$$\begin{aligned}&\left(\frac{1}{\sqrt{g_{zz}}}\partial_z \pm m_\psi\right)\begin{pmatrix}\beta_1\\ \alpha_1\end{pmatrix} \mp \frac{(\omega + qA_t)}{\sqrt{-g_{tt}(z)}}\begin{pmatrix}\alpha_1\\ \beta_1\end{pmatrix} + \frac{k_x}{\sqrt{g_{xx}}}\begin{pmatrix}\alpha_1\\ \beta_1\end{pmatrix}\\ &- \frac{k_y}{\sqrt{g_{xx}}}\begin{pmatrix}\alpha_2\\ \beta_2\end{pmatrix} + \frac{\partial_z A_t}{\sqrt{-g_{zz}g_{tt}}}\left(p_1 \left|\phi\right|^2 - p_2 \left|\phi\right|^2\right)\begin{pmatrix}\alpha_1\\ \beta_1\end{pmatrix} = 0 \end{aligned} \tag{5.5}$$

$$\begin{aligned}&\left(\frac{1}{\sqrt{g_{zz}}}\partial_z \pm m_\psi\right)\begin{pmatrix}\beta_2\\ \alpha_2\end{pmatrix} \mp \frac{(\omega + qA_t)}{\sqrt{-g_{tt}(z)}}\begin{pmatrix}\alpha_2\\ \beta_2\end{pmatrix} - \frac{k_x}{\sqrt{g_{xx}}}\begin{pmatrix}\alpha_2\\ \beta_2\end{pmatrix}\\ &- \frac{k_y}{\sqrt{g_{xx}}}\begin{pmatrix}\alpha_1\\ \beta_1\end{pmatrix} + \frac{\partial_z A_t}{\sqrt{-g_{zz}g_{tt}}}\left(p_1 \left|\phi\right|^2 + p_2 \left|\phi\right|^2\right)\begin{pmatrix}\alpha_2\\ \beta_2\end{pmatrix} = 0 \end{aligned} \tag{5.6}$$

From now on, we follow the standard procedure of extracting the Green's function. One can expand these equations near the horizon ($z = 1$) to obtain the in-falling boundary condition given by

$$\begin{pmatrix}\beta_j(z, \vec{k})\\ \alpha_j(z, \vec{k})\end{pmatrix} \sim c_j(1 - z)^{-\frac{i\omega}{4\pi T}}. \tag{5.7}$$

Now to extract the boundary Green's function, one needs the asymptotic behaviour of the Dirac equations near the AdS boundary ($z \to 0$) to identify the source and the expectations values. In this case, the leading behaviour at the boundary is given by

$$\begin{pmatrix}\beta_j\\ \alpha_j\end{pmatrix} \approx a_j z^{m_\psi}\begin{pmatrix}1\\ 0\end{pmatrix} + b_j z^{-m_\psi}\begin{pmatrix}0\\ 1\end{pmatrix}. \tag{5.8}$$

We then followed the usual prescription used in [5, 64, 104] to obtain the Green's function by extracting the coefficients a_j and b_j and because the couplings considered here, we have a mixing of various spinorial components, thus we use two different sets of linearly independent boundary conditions that can be written in the form $B = SA$ and expanded as

$$\begin{pmatrix}\beta_1^I & \beta_1^{II}\\ \beta_2^I & \beta_2^{II}\end{pmatrix} = \begin{pmatrix}s_{11} & s_{12}\\ s_{21} & s_{22}\end{pmatrix}\begin{pmatrix}\alpha_1^I & \alpha_1^{II}\\ \alpha_2^I & \alpha_2^{II}\end{pmatrix}, \tag{5.9}$$

Now the retarded Green's function is defined as

$$G^R(\omega, k_x, k_y) = -i \begin{pmatrix} s_{11} & s_{12} \\ s_{21} & s_{22} \end{pmatrix} \cdot \gamma^t \tag{5.10}$$

with gamma matrices in our basis as $\gamma^t = i\sigma_1$. Now from the retarded Green's function we can get quantity of interest, i.e., the spectral function $A\,(\omega, k_x, k_y)$ given by

$$A(\omega\,,\vec{k}) = \mathrm{Im}\left[\mathrm{Tr}\, G^R(\omega\,,\vec{k})\right]. \tag{5.11}$$

where $\vec{k} \equiv (k_x, k_y)$. In the section that follows we will study the properties of $A\,(\omega\,,\vec{k})$. The importance of spectral function is that it directly relates to real condensed matter experiments.

5.2 Numerical Results and Discussion

In this section, we are going to look at the qualitative properties of the spectral function $A(\omega, \vec{k})$ defined above, which reflect on the nature of Fermi surface (FS) and the dispersion spectrum by varying the coupling $p_1\,, p_2$ and also the background parameters. For our numerical purposes, we defined the Fermi level with small offset from $\omega = 0$. In our previous work [7], we have explored the affects of temperature and the source $\chi^{(1)}$ on the Fermi surface with and without couplings, also more analysis on fermions spectral function due to the Q-lattice can be found in [107, 135]. Here we show the results only for scenarios when coupling parameters are non-vanishing.

As discussed previously, the complex scalar field can break translational invariance in both x and y directions, depending on k_1 and k_2. Let us first study for $k_2 = 0$ and consider only k_1. Assuming the background scalar mass is fixed $m_\phi^2 = 0$, then the leading constant $\chi^{(1)}$ which represents the source of the dual boundary operator of the bulk complex scalar field can be varied, and as we have seen in [7] and the references therein, as we increase the strength of the source, the weight of the spectral function reduces along k_x where translational symmetry is broken. Since the spectrum of our first couplings controlled by p_1 is known from our previous discussion in [7], we directly show the combined effects of p_1 and p_2 in Figure 5.1. One can immediately notice in Figure 5.1 that for low temperatures (bottom panel), the combined effects yield two arcs like spectrum, and the peak of FS is sharper in comparison to that of higher temperatures (top panel), where the inner arc vanishes. Further, the stretched Fermi surface that appeared in the spectral function because of the anisotropic background for large $\chi^{(1)}$ values, now its amplitude suppressed and is now more prominent along the negative k_x-direction especially at low temperatures, due to the second coupling. However, from previous analysis at lower temperatures, the effects of p_1 induces a second Fermi surface that is partially destroyed along $x-$direction which is the signature of second coupling. Whereas, along the k_y direction, the spectral function indicates the existence of a sharp Fermi surface with a large density of states. The sharp peak in the spectral function essentially indicates the presence of a stable quasi-particle with a longer lifetime. Similarly, from the energy-momentum dispersion shown in Figure 5.2, we see the presence of gapless spectra, which are anisotropic in nature, and the surface state induced by p_2 connecting the lower and upper band.

From the emergence of these interesting behaviour in the spectral function from our couplings p_1 and p_2, firstly we can think of the effects of the source $\chi^{(1)}$ as a doping parameter in the pseudogap region and secondly, for both the couplings, we know from the work in [5, 11, 14], the appearance of these Fermi arcs can be understood in the context of pole-zero duality. In terms of the two diagonal entries of the boundary fermion Green function $G_{ij}(\omega, \vec{k})$, the FS appears at two poles which exist at $G_{11}(\omega = 0, |k_f|)$ and $G_{22}(\omega = 0, -|k_f|)$. Now the presence of p_2 coupling, whenever the pole/zero of G_{11} coincides with zero/pole of G_{22}, we get a reduced spectral weight along $-k_x$ or $+k_x$ depending on the sign of p_2 that appears as Fermi arcs. The presence of these pairs of FS in the spectral function indicates that the scalar field plays a crucial role in not mixing the individual spectra of p_1 and p_2. Hence we eventually have two Fermi surfaces on changing p_1, p_2. Notice that in our plots, we choose the mass of scalar field to be $m_\phi = 0$, because for non-zero masses, the way our scalar field manifest itself in the coupling terms, its effects will be highly suppressed. However, we plotted for non-zero fermion mass in Figure 5.4. Again here for same charge q and background parameter we see a similar spectrum to that in the case of zero mass shown above. So far we have consider only k_1, now let us turn on k_2. As shown in our previous Chapter 4, depending on whether $k_1 > k_2$ or $k_1 < k_2$, the fermionic spectrum is gapped along k_x or k_y. We consider the case when $k_2 > k_1$ and the plots are shown in Figure 5.3. In the top panel we fixed $p_1 = 1$ and vary boundary source $\chi^{(1)}$ of the bulk scalar field ϕ. As the source $\chi^{(1)}$ is increased, in addition to being stretch

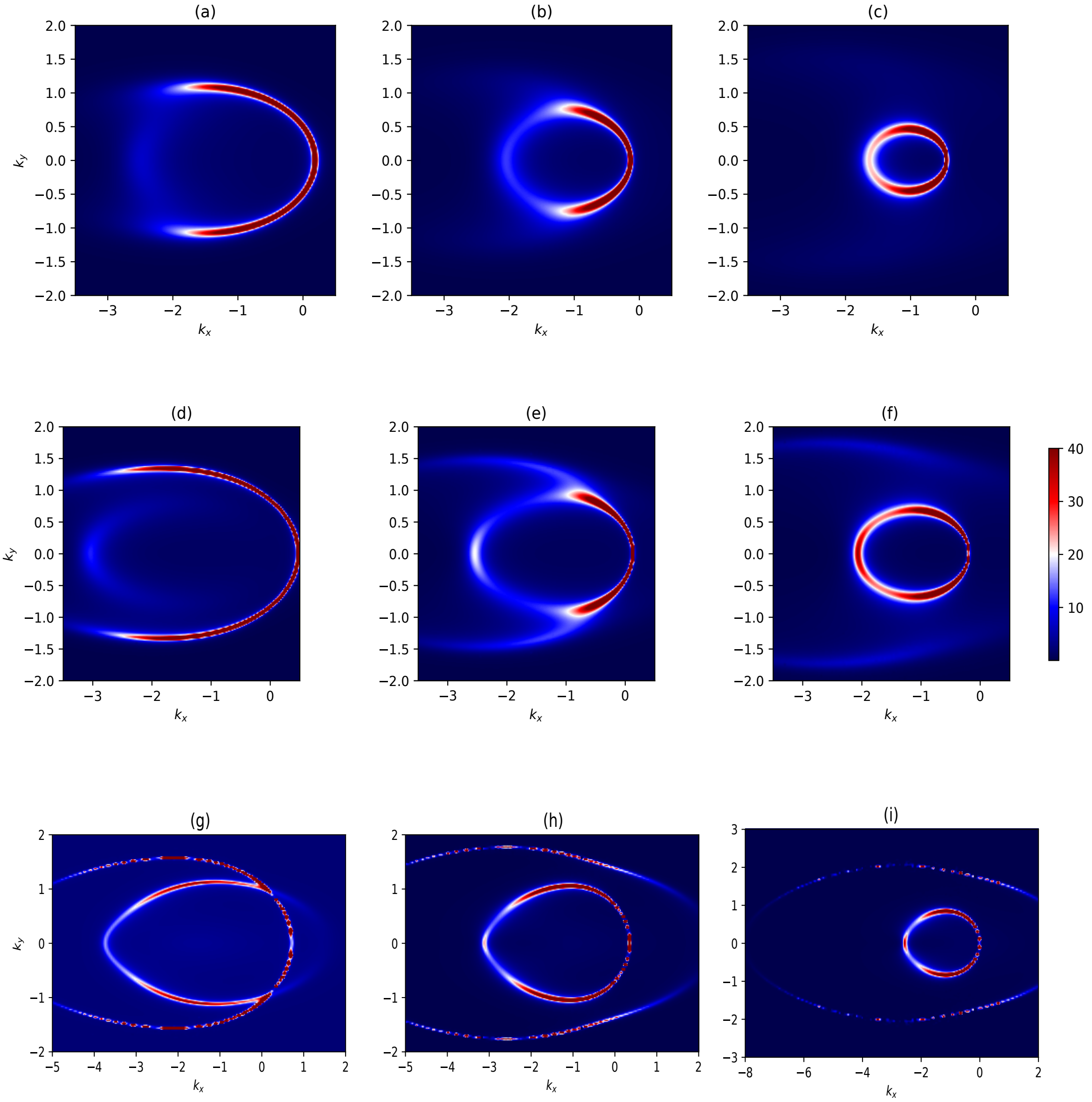

FIGURE 5.1: Density plot of $A\left(k_x, k_y\right)$ by varying the value of p_1. Here, we fixed $p_2 = 0.3$ and $m_\psi = 0$, $q = 1$. Left to right: are for $p_1 = -0.2\,, -0.3,\ -0.4,$. The top, middle and bottom panel correspond to $T/\mu = 0.02,\ 0.009,\ 0.001$ with $m_\phi^2 = 0$ and source $\chi^{(1)} = 2$ respectively.

from circular shape to an elliptical shape, we see an emergence of a second FS of smaller peaks. Some similarity is seen when we vary p_2 instead and fixing $\chi^{(1)} = 2$. Here also we observed a new kind of spectrum which is different from that observed in [5, 6] with similar couplings. It was earlier shown in [42] the presence of multiple FS in holographic model with no Fermi arcs and then recently in [137, 138], the Fermi features were seen triggered by the effective mass term and the lattice effects in their holographic models.

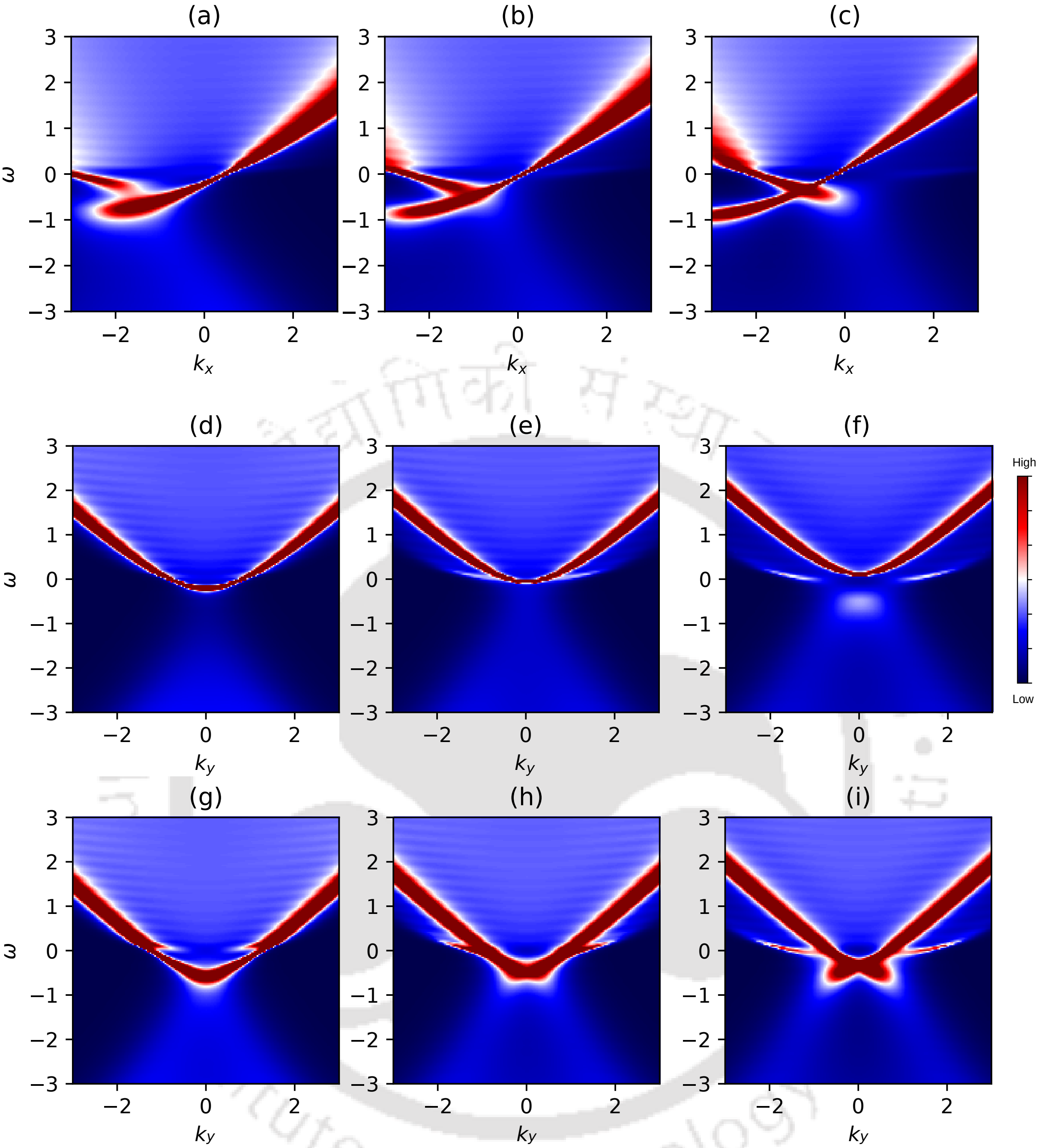

FIGURE 5.2: Energy-momentum dispersion with p_1, p_2 set to non-zero and $m_\psi = 0$, $q = 1$, $T/\mu = 0.009$, $m_\phi^2 = 0$, $k_1/\mu = 0.8$,and $k_2/\mu = 0$. Top and middle panel are along $\omega - k_x$ $(k_y = 0)$ and $\omega - k_y$ $(k_x = 0)$, while the bottom panel is along $\omega - k_y$ $(k_x = -1)$. From left to right the parameters $[\,(p_2\,, p_1)\,] = [\,(0.3, -0.2), (0.3, -0.3), (0.3, -0.4)]$ respectively.

It is to be noted here that though both our studies and theirs are somewhat similar in terms of the features in suppression of the spectral function and the Fermi surfaces, our couplings and the one considered in [137] should correspond to a different boundary field theory with a different kind of underlying mechanism. Moreover, the evolution of these

Fermi arcs without including superconductivity as discussed in [95, 96], could provide an interesting framework for studying the Fermi arcs in the pseudogap phase and cuprate superconductors.

Up till now, we have discussed only the spectra produced by the two couplings. Let us try to relate these results to real condensed matter systems. Firstly, the emergence of these pair of Fermi surfaces are mostly our interesting features out of our numerics as these kind of spectra have been observed in the ARPES experiments measuring the spectral function in real condensed matter systems such as those of Topological insulators (TI), Dirac and Weyl semi-metals [83, 84, 88]. Also, for superconductivity, these types of interactions terms provides us a holographic model in the pseudogap region in the phase diagram where these Fermi arcs are seen. They are connected through the suppression in the weight spectral function. Similar to our observation, the presence of these kind of arcs in pairs, was also discussed in a theoretical model in [147]. While in the case of Dirac and Weyl semi-metals, Fermi arcs emerges out as surface states which connect the two Dirac points in three-dimensional bulk crystals. From the energy band dispersion shown in Figure 5.2 in our models, we can see the presence of non-trivial gapless surface states that were also observed in experiments. Details discussion on these topics can be found in these articles [30, 86, 88, 151, 152] and references therein. Since our holographic system at the boundary is $(2+1)$ dimensions, we can think of these pairs of Fermi arcs as the surface states of a $(3+1)$ dimensional bulk material. Thus the observations from our holographic models are reminiscent to those of real materials in terms of the band spectrum and surface states known as Fermi arcs. There have been other holographic models also, such as those in [144–146], which attempted to address these interesting and rich phenomena observed in topological insulators and semi-metals.

5.3 Conclusion

In this Chapter, we have studied the fermion spectral function $A(\omega, \vec{k})$ in anisotropic Q-lattice background where, the probe fermion is coupled with two non-minimal dipole-type couplings. We discussed some of the interesting features produced by the couplings. Our observation of the spectral function from the numerics of our holographic models seems to encode the unconventional properties that was observed in real condensed matter systems,

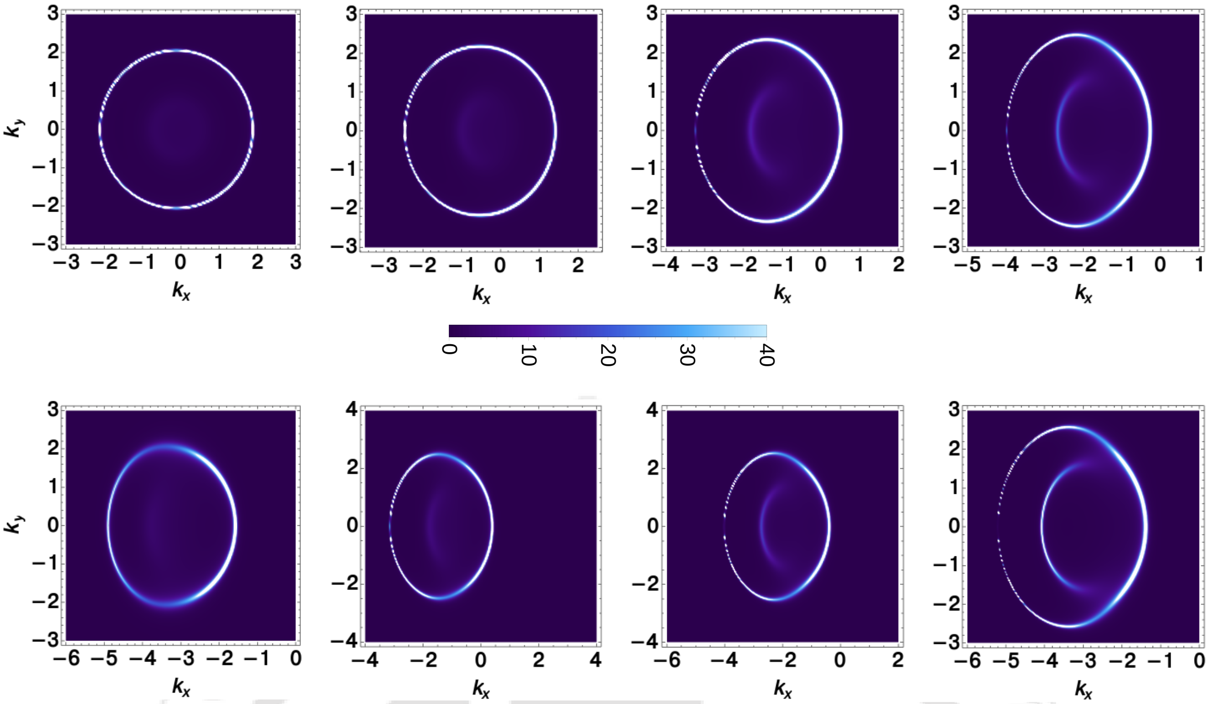

FIGURE 5.3: Here we plotted the spectral density with fermion mass $m_\psi = 0$ and charge $q = 1$. In the top panel we fixed $T/\mu = 0.009$, coupling $p_2 = 1.$ and vary source $\chi^{(1)} = (0.5, 1.0, 1.5, 1.8)$ with $k_1/\mu = 0.2$, $k_2/\mu = 0.8$, and $m_\phi^2 = 0$ respectively. In the bottom panel, we vary the coupling p_2 taking values $p_2 = 0.1, 0.5, 0.8, 1.2$ while we fixed $\chi^{(1)} = 2$.

such as the gapless spectra in the energy-momentum dispersion and the presence of Fermi arcs, also the appearance of doubled FS connecting the two nodes seen in Dirac-Weyl semimetals and topological insulators. Though we are not in anyway claiming that our models to represent the exact condensed matter systems, however we hope that in future, this kind of holographic approach might give us some hints in understanding the strongly coupled systems.

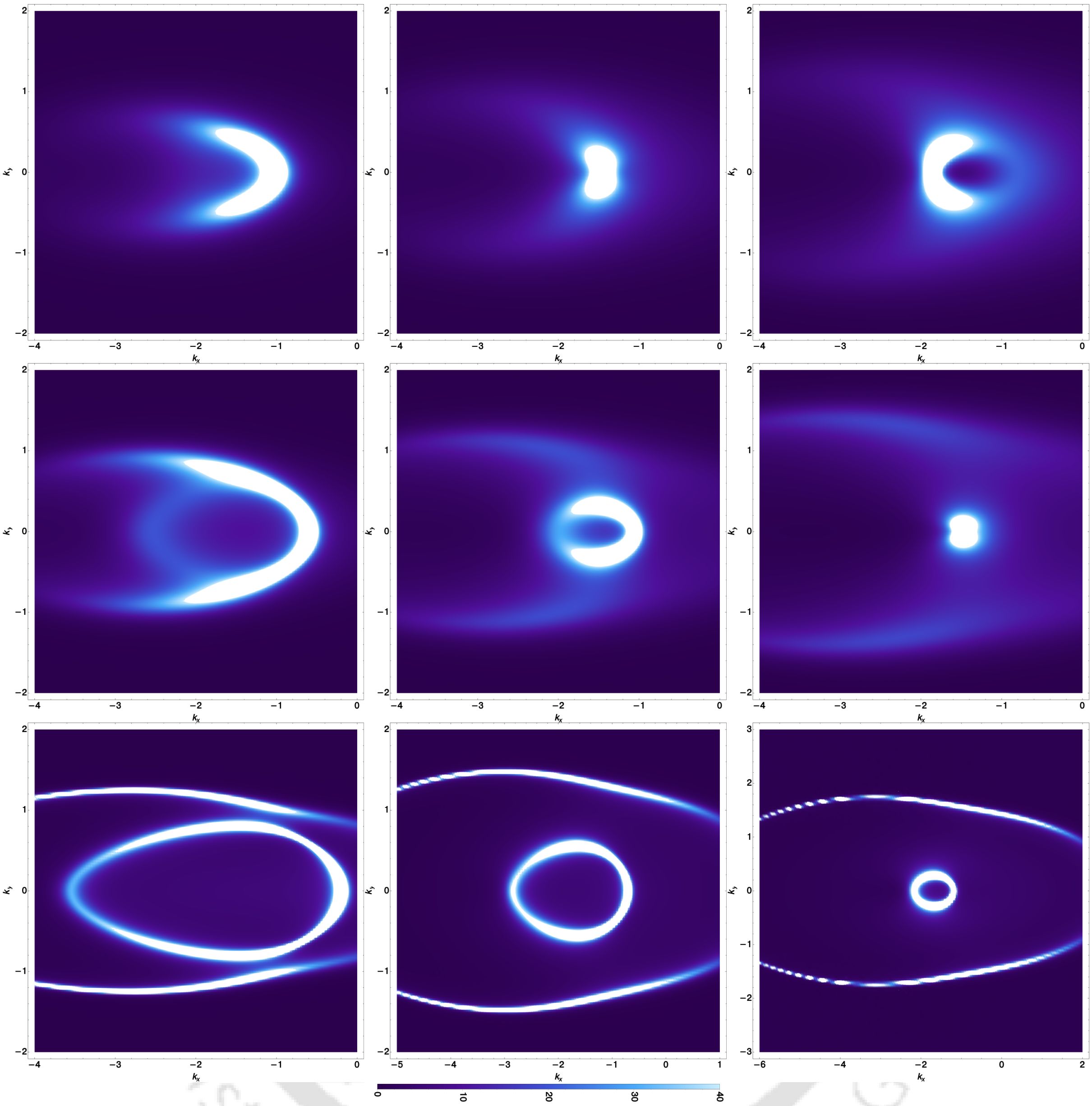

FIGURE 5.4: Here we plotted the spectral density for non-zero fermion mass $m_\psi = 1/4$ and charge $q = 1$ with the background parameters $T/\mu = 0.02, 0.009, 0.001$ (top to bottom), $k_1/\mu = 0.8, k_2/\mu = 0$, $m_\phi^2 = 0$ and $\chi^{(1)} = 2$ respectively. We fixed the coupling parameters $p_2 = 0.3$ and vary $p_1 = -0.2, -0.3, -0.4$.

Chapter 6

A note on the effects of magnetic field to holographic fermions with dipole like coupling

---

So far we have discussed the fermionic spectral function in the presence of different types of interaction terms as non-minimal couplings to the bulk fermions, and all of our background geometry are non magnetic. Therefore, it would be interesting and important to also study a probe fermion which are placed in the bulk geometry containing magnetic field. Thus, this chapter is dedicated to such studies. We shall take those types of coupling terms that we have studied in our previous chapters generalised to a background with magnetic charge. The rest of this Chapter will be based on our recent work [9].

The holographic study of the fermionic systems at a finite charge density has shown to exhibit the interesting behaviour of non-Fermi liquid using simple probe fermions in an extremal AdS black hole geometry [3, 66, 105]. Recently, more complicated models were also proposed, with extra symmetries included in the background gravity in order to mimic the real condensed matter system at the boundary where the observables, like the spectral function, can be extracted [159–165]. But some have introduce a coupling directly to the probe fermions fields in the bulk. One such coupling is the dipole coupling which has been used to study the dynamical gap in Mott physics [11, 13].

In this Chapter, we are going to extend such studies where a magnetic field is present. Only few works [157, 167, 168] have been done towards the study of holographic fermionic system in a non-zero magnetic field. In our study, we will explore just a tiny portion from the vastness of possibilities in this topic. We consider a non-minimal dipole-like coupling taking the dyonic AdS black hole as our background geometry. The motivation for choosing a dyonic black hole is to have both magnetic and electric charged, which correspond to a $(2+1)$ dimensional boundary CFT with a non-zero chemical potential and a magnetic field. For this, we introduce a probe fermion with a coupling in this geometry to study the properties of the spectral functions which is the most relevant quantity directly related to condensed matter experiments.

In Section 6.1 we will discuss the set up of a background geometry which is the dyonic black hole solution and further parametrize the solution parameters to arrive at the conditions for zero and non-zero temperature. In Section 6.2 we discuss the fermionic action and the non-minimal coupling in the background geometry followed by solution to the Dirac equations and the spectral function. In Section 6.3, we discuss and comment on our findings of the results and finally in Section 6.4 we summarize with some discussion of possible future directions and final thoughts.

6.1 Review of the Background geometry

In order to study the affect of magnetic field on the probe fermions field, we will consider a dyonic black hole that has both electric and magnetic charges in AdS_4 spacetime. The most general Maxwell-Einstein action with a negative cosmological constant in 4-dimensions can be written as:

$$S = \frac{1}{\kappa^2}\int d^4x\sqrt{-g}\left[\mathcal{R} - \frac{6}{R^2} - \frac{R^2}{g_F^2}F_{MN}F^{MN}\right] \tag{6.1}$$

Here $\mathcal{R}$ is the Ricci scalar and R is the radius of the AdS spacetime. From the given action, the solution to the Einstein equations in a metric form is given by

$$\frac{ds^2}{R^2} = r^2\Big[-f(r)dt^2 + dx^2 + dy^2\Big] + \frac{dr^2}{r^2 f(r)} \tag{6.2}$$

$$f(r) = 1 + \frac{h^2+\mu^2}{r^4} - \frac{(1+(h^2+\mu^2))}{r^3}\,. \tag{6.3}$$

with components of the gauge fields given by

$$A_y = A_r = 0,\ A_t(r) = \mu(1 - 1/r),\ A_x(y) = -h\,y. \tag{6.4}$$

where μ is the chemical potential of the system and h is the magnetic field strength, and the temperature of the system is $T = \frac{1}{4\pi}\Big(3 - (\mu^2 + h^2)\Big)$. The condition for zero temperature is given by

$$h^2 + \mu^2 = 3. \tag{6.5}$$

The relevant dimensionless parameter related to the strength of the magnetic field is $H = h/\mu = \frac{h}{\sqrt{3-h^2}}$ which goes from zero to infinity.

6.2 Fermion action

We will consider a bulk Dirac fermion field ψ coupled to a non-minimal coupling as a probe to the system. The action for ψ is given by

$$S_\psi = \frac{1}{\kappa^2}\int d^4x\sqrt{-g}i\,\bar{\psi}\left(\not{D}\,\psi - m\,\psi - i\wp\left(\not{F} + \tilde{\not{F}}\right)\psi\right). \tag{6.6}$$

where $\not{D}$, $\not{F}$ and $\tilde{\not{F}}$ stands for

$$\begin{aligned} \not{D} &= e^M_{\ a}\Gamma^a\Big[\partial_M + \frac{1}{8}\omega^{ab}_M[\Gamma_a,\Gamma_b] - iqA_M\Big], \\ \not{F} &= \frac{1}{2}\Gamma^{ab}e^M_a\, e^N_b\, F_{MN},\ \tilde{\not{F}} = \frac{1}{4}\Gamma^{cd}\epsilon_{cdab}e^a_M\, e^b_N\, F^{MN}. \end{aligned} \tag{6.7}$$

Here $e^M_{\ a}$ is the inverse vielbein, $\omega^{ab}_{\ \ M}$ is the spin-connection and q is the fermion charge. The fermionic operator $\hat{\mathcal{O}}$ at the boundary is dual to the field ψ in the bulk, and its conformal dimension Δ is mapped to spinors ψ with mass m as

$$\Delta = m + \frac{3}{2}. \tag{6.8}$$

The Dirac equation from the above action is given by:

$$(\not{D} - m - i\wp\not{F} - i\wp\tilde{\not{F}}\,)\,\psi = 0 \tag{6.9}$$

which can be written in the form

$$\Big(Z(r) + Y(y)\Big)\,\psi = 0, \tag{6.10}$$

where,

$$\begin{aligned} Z(r) =& \sqrt{\frac{g_{ii}}{g_{rr}}}\,\Gamma^{\underline{r}}\,(\partial_r + S_p) - m\,\sqrt{g_{ii}} + \Gamma^{\underline{t}}\sqrt{\frac{g_{ii}}{-g_{tt}}}\,(\partial_t - iqA_t) \\ & - i\wp\,\Gamma^{\underline{rt}}\left(\partial_r A_t\sqrt{\frac{g_{ii}}{-g_{tt}g_{rr}}} + \frac{h}{\sqrt{g_{ii}}}\right) \\ & - i\wp\Gamma^{\underline{xy}}\left(\frac{h}{\sqrt{g_{ii}}} + \partial_r A_t\sqrt{\frac{g_{ii}}{-g_{tt}g_{rr}}}\right). \\ Y(y) =& \Gamma^{\underline{x}}(\partial_x - iqA_x) + \Gamma^{\underline{y}}\partial_y. \end{aligned} \tag{6.11}$$

The term S_p in $Z(r)$ is the contribution from the spin connection. If we now perform a Fourier transform along (t, x), then $\partial_t \to -i\omega,\ \partial_x \to ik_x$ and also we can remove the S_p by rescaling the spinors $\psi = (-gg^{rr})^{-\frac{1}{4}}\Psi$. Then we have $Z(r),\ Y(y)$ as

$$\begin{aligned} Z(r) =& \sqrt{\frac{g_{ii}}{g_{rr}}}\,\Gamma^{\underline{r}}\,\partial_r - m\sqrt{g_{ii}} + \Gamma^{t}\sqrt{\frac{g_{ii}}{-g_{tt}}}\,(-i\omega - iqA_t) \\ & - i\wp\,\Gamma^{\underline{rt}}\,P(r) - i\wp\Gamma^{\underline{xy}}\,P(z)\,, \\ Y(y) =& \Gamma^{\underline{x}}\cdot(i\,k_x - iqA_x) + \Gamma^{\underline{y}}\cdot\partial_y. \end{aligned} \tag{6.12}$$

where, $P(r) = \frac{(h+\mu)}{r}$. For convenience, we will choose the following Gamma matrices:

$$\Gamma^{\underline{r}} = \begin{pmatrix} \mathbb{1} & 0 \\ 0 & -\mathbb{1} \end{pmatrix},\ \Gamma^{\underline{t}} = \begin{pmatrix} 0 & i\sigma_3 \\ i\sigma_3 & 0 \end{pmatrix},$$

$$\Gamma^{\underline{x}} = \begin{pmatrix} 0 & \sigma_1 \\ \sigma_1 & 0 \end{pmatrix},\ \Gamma^{\underline{y}} = \begin{pmatrix} 0 & \sigma_2 \\ \sigma_2 & 0 \end{pmatrix}.$$

Then we have

$$Z\,(r) = \begin{pmatrix} \mathcal{D}_r^- & i\sigma_3\,V_+ \\ i\sigma_3\,V_- & -\mathcal{D}_r^+ \end{pmatrix},$$

$$Y\,(y) = \begin{pmatrix} 0 & \sigma_1\mathcal{C}_y + \sigma_2\partial_y \\ \sigma_1\mathcal{C}_y + \sigma_2\partial_y & 0 \end{pmatrix},$$

where

$$
\begin{aligned}
\mathcal{D}_r^{\pm} &= \sqrt{\frac{g_{ii}}{g_{rr}}}\,\partial_r \ \pm m\,\sqrt{g_{ii}} \ + \wp\, P(r)\,\sigma_3\,, \ \ \mathcal{C}_y = i(k_x + qhy)\ , \\
V_{\pm} &= -i\left(\sqrt{\frac{g_{ii}}{-g_{tt}}}\,(\omega + qA_t) \ \pm\ \wp\, P(r)\right)\ .
\end{aligned}
\tag{6.13}
$$

Clearly, the matrices Z and Y do not commute. However, it is possible to find a constant matrix $\mathcal{M}$ such that $[\mathcal{M}Z, \mathcal{M}Y] = 0$ and then look for common eigenvectors of $\mathcal{M}Z$ and $\mathcal{M}Y$ as they are commuting Hermitian operators. The transformation matrix statisfies the following relations:

$$
\begin{aligned}
&\left\{\mathcal{M}, \Gamma^{\underline{r}}\right\} = 0\,, \quad \left\{\mathcal{M}, \Gamma^{\underline{t}}\right\} = 0\,, \quad \left[\mathcal{M}, \Gamma^{\underline{x}}\right] = 0\,, \\
&\left[\mathcal{M}, \Gamma^{\underline{y}}\right] = 0\,, \quad \left[\mathcal{M}, \Gamma^{\underline{x}\,\underline{y}}\right] = 0\,, \quad \left[\mathcal{M}, \Gamma^{\underline{r}\,\underline{t}}\right] = 0\,.
\end{aligned}
$$

It turns out that a convenience choice for $\mathcal{M}$ is $\begin{pmatrix} 0 & \sigma_3 \\ -\sigma_3 & 0 \end{pmatrix}$. In order to separate the variables, one can multiply (6.10) by $\mathcal{M}$ from the left to have

$$
\begin{aligned}
\mathcal{M}\, Z &= \begin{pmatrix} i\,V_{-} & -\sigma_3\mathcal{D}_r^{+} \\ -\sigma_3 D_r^{-} & -i\,V_{+} \end{pmatrix}, \\
\mathcal{M}\, Y &= \begin{pmatrix} \sigma_3(\sigma_1\mathcal{C}_y + \sigma_2\partial_y) & 0 \\ 0 & -\sigma_3(\sigma_1\mathcal{C}_y + \sigma_2\partial_y) \end{pmatrix}.
\end{aligned}
$$

Now we can look for solutions of the eigenvalue equation of the form

$$
\mathcal{M}Z\Psi = -\mathcal{M}Y\Psi = \lambda\Psi. \tag{6.14}
$$

with real λ. Writing $\Psi = (\Psi_+\,, \Psi_-)^T$. First we solve the y dependent part of the above equation, which is identical to that of a massless free fermion in $(2+1)$ dimensions

$$
\mathcal{M}Y\Psi = \begin{pmatrix} \sigma_3(\sigma_1\mathcal{C}_y + \sigma_2\partial_y)\Psi_+ \\ -\sigma_3(\sigma_1\mathcal{C}_y + \sigma_2\partial_y)\Psi_- \end{pmatrix} = -\lambda \begin{pmatrix} \Psi_+ \\ \Psi_- \end{pmatrix}. \tag{6.15}
$$

or,

$$
U_1\Psi_+ \ = \ -\lambda\,\Psi_+ \text{ and } U_2\Psi_- \ = \ -\lambda\,\Psi_- \tag{6.16}
$$

where $U_{1,2} = \pm\sigma_3(\sigma_1\mathcal{C}_y + \sigma_2\partial_y)$. For the Ψ_+ part, let us left multiply U_1, then

$$U_1\,U_1\Psi_+ \;=\; -\,U_1\,\lambda\,\Psi_+ \;=\; -\lambda\,U_1\Psi_+ \;=\; -\lambda(-\lambda\Psi_+) \tag{6.17}$$

$$\implies\; [\sigma_3(\sigma_1\mathcal{C}_y + \sigma_2\partial_y)]\,[\sigma_3(\sigma_1\mathcal{C}_y + \sigma_2\partial_y)]\,\Psi_+ = \lambda^2\Psi_+ . \tag{6.18}$$

On further simplification (6.18) gives

$$\partial_y^2\,\Psi_+ + (\lambda^2 + C_y^2 - i\sigma_3 C_y')\Psi_+ = 0\,. \tag{6.19}$$

Now separating the variables r and y as $\Psi_+ = \Big(Z_1(r)Y_1(y), Z_2(r)Y_2(y)\Big)^T$, and noting equation (6.19) does not depend on r, one can set $Z_1 = Z_2$, leading to

$$-\partial_y^2\,Y_{1,2} + T_\pm(y)\,Y_{1,2} = 0, \tag{6.20}$$

where $T_\pm(y) = -(\lambda^2 + C_y^2 \mp iC_y') = (k_x + qh\,y)^2 - \lambda^2 \mp qh$, which is similar to a simple harmonic oscillator differential equation. To see this more explicitly, let us define $\tilde{x} = \sqrt{qh}\,(y + \frac{k_x}{qh})$. Then we have

$$-\partial_{\tilde{x}}^2\,Y_{1,2} + \tilde{x}^2 Y_{1,2} = \left(\frac{\lambda^2}{qh} \pm 1\right) Y_{1,2}. \tag{6.21}$$

These equations do not have the form of the standard Hermite differential equation that arises in the case of harmonic oscillator problem. But on rescaling $Y_{1,2} = e^{-\frac{\tilde{x}^2}{2}}\,Y_{1,2}(\tilde{x})$, we have

$$\partial_{\tilde{x}}^2\,Y_{1,2} - \tilde{x}\,\partial_{\tilde{x}}\,Y_{1,2} + (E^\pm - 1)\,.Y_{1,2} = 0$$

Therefore by setting $E^\pm - 1 = 2n$, where n denotes the Landau levels, the eigenvalues and eigenvectors are given by

$$\begin{aligned} E_n &= \frac{1}{2}\left(\frac{\lambda^2}{qh} \pm 1\right) = n + \frac{1}{2}, \quad n = 0, 1, 2, \ldots \\ Y_{1,2} &= N_n e^{-\tilde{x}^2/2} H_n(\tilde{x}) \equiv I_n(\tilde{x}), \end{aligned} \tag{6.22}$$

where N_n is a normalization constant. By substituting this solution back into the first order equations for Ψ_+ assuming the same eigenvalues we get

$$\Psi_+ = \begin{pmatrix} I_n(\tilde{x})\ Z_1 \\ -iI_{n-1}(\tilde{x})\ Z_1 \end{pmatrix}, \tag{6.23}$$

whose eigenvalues are $\lambda_n = \sqrt{2nqh}$, $n = 0, 1, 2, \cdots$. For completeness, we define $I_{-1}(\tilde{x}) = 0$. Together with the expression for Ψ_-, which can be obtained in a similar fashion, we have

$$\Psi = \begin{pmatrix} I_n(\tilde{x})\ Z_1 \\ -iI_{n-1}(\tilde{x})\ Z_1 \\ I_n(\tilde{x})\ Z_2 \\ iI_{n-1}(\tilde{x})\ Z_2 \end{pmatrix}. \tag{6.24}$$

Another independent solution comes from the values corresponding to $-\lambda_n$, i.e.

$$\mathcal{M}\, Z\, \tilde{\Psi} = -\mathcal{M}\, Y\, \tilde{\Psi} = -\lambda_n \tilde{\Psi}\ . \tag{6.25}$$

Proceeding in a similar way, we get

$$\tilde{\Psi} = \begin{pmatrix} -i\ I_n\ \tilde{Z}_1 \\ I_{n-1}\ \tilde{Z}_1 \\ -i\ I_n\ \tilde{Z}_2 \\ -I_{n-1}\ \tilde{Z}_2 \end{pmatrix}. \tag{6.26}$$

The equations for Z_i and $\bar{Z}_i$ are respectively,

$$
\begin{aligned}
\left(\sqrt{\frac{g_{ii}}{g_{rr}}}\partial_r - m\sqrt{g_{ii}} \pm \wp\, P(r)\right) Z_1 &= -(i\,V_+ + \lambda_n) Z_2\ ,\\
\left(\sqrt{\frac{g_{ii}}{g_{rr}}}\partial_r + m\sqrt{g_{ii}} \pm \wp\, P(r)\right) Z_2 &= \ (i\,V_- - \lambda_n) Z_1\ ,\\
\left(\sqrt{\frac{g_{ii}}{g_{rr}}}\partial_r - m\sqrt{g_{ii}} \pm \wp\, P(r)\right) \tilde{Z}_1 &= -(i\,V_+ - \lambda_n) \tilde{Z}_2\ ,\\
\left(\sqrt{\frac{g_{ii}}{g_{rr}}}\partial_r + m\sqrt{g_{ii}} \pm \wp\, P(r)\right) \tilde{Z}_2 &= \ (i\,V_- + \lambda_n) \tilde{Z}_1\ .
\end{aligned}
\tag{6.27}
$$

To derive the flow equation and the Green's function, we follow the construction from [157, 168], by writing the general solution as linear combination of both (6.24) for λ_n and (6.26) for $(-\lambda_n)$ as follows

$$
\begin{aligned}
\Psi = \sum_n \Psi^{(n)},\quad \Psi^{(n)} &= \Psi^{(\lambda_n)} + \Psi'^{(-\lambda_n)}\\
&= \begin{pmatrix} iZ_1^{(n)} e_1^{(n)} \\ Z_2^{(n)} e_2^{(n)} \end{pmatrix} + \begin{pmatrix} -i\bar{Z}_1^{(n)} e_2^{(n)} \\ -\bar{Z}_2^{(n)} e_1^{(n)} \end{pmatrix},
\end{aligned}
\tag{6.28}
$$

where, $e_1^{(n)}$ and $e_2^{(n)}$ are the basis spinors. In terms of the above Hermite polynomials, the basis spinors are given by

$$
e_1^{(n)} = \begin{pmatrix} iI_n(\tilde{x}) \\ I_{n-1}(\tilde{x}) \end{pmatrix},\quad e_2^{(n)} = \begin{pmatrix} I_n(\tilde{x}) \\ iI_{n-1}(\tilde{x}) \end{pmatrix},\qquad n \geq 1.
\tag{6.29}
$$

Using the orthonormality of Hermite polynomials from the y dependent equations one can construct the retarded Green's function which is given by [3, 168]

$$
G_R^{(n)} = -iS^{(n)}\gamma^t = \begin{pmatrix} -\frac{Z_2^{(n)}}{Z_1^{(n)}} & 0 \\ 0 & \frac{\bar{Z}_2^{(n)}}{\bar{Z}_1^{(n)}} \end{pmatrix}.
\tag{6.30}
$$

Then the spectral function A is

$$A^{(n)} \sim \mathrm{Im}\left(-\frac{Z_2^{(n)}}{Z_1^{(n)}} + \frac{\bar{Z}_2^{(n)}}{\bar{Z}_1^{(n)}}\right). \tag{6.31}$$

By defining $G_{11}^{(n)} = \frac{Z_2^{(n)}}{Z_1^{(n)}}, G_{22}^{(n)} = \frac{\bar{Z}_2^{(n)}}{\bar{Z}_1^{(n)}}$, and combining with equation (6.27), we get the following flow equations

$$\begin{aligned}
\sqrt{\frac{g_{ii}}{g_{rr}}}\partial_r G_{11}^{(n)} &= -2m\sqrt{g_{ii}}\,G_{11}^{(n)} + (i\,V_- - \lambda_n) \\
&\quad + (i\,V_+ + \lambda_n)(G_{11}^{(n)})^2\,, \\
\sqrt{\frac{g_{ii}}{g_{rr}}}\partial_r G_{22}^{(n)} &= -2m\sqrt{g_{ii}}\,G_{22}^{(n)} + (i\,V_- + \lambda_n) \\
&\quad + (i\,V_+ - \lambda_n)(G_{22}^{(n)})^2\,.
\end{aligned} \tag{6.32}$$

These two equations are exactly the same equations appearing in equation (14) of [13] with $G_{11}^{(n)} \sim \xi_+$, $G_{22}^{(n)} \sim \xi_-$, $\lambda_n \sim k$. Surprisingly, the magnetic field h from the dual $\tilde{\not{F}}$ does not appear in the flow equations explicitly. We will analyse both the Green's function and the spectral function, which is given by

$$A^n(\omega, \lambda_n) = \mathrm{Im}\,(G_{11}^{(n)} + G_{22}^{(n)}). \tag{6.33}$$

6.3 Results and Discussion

In this section we will mainly focus on the magnetic field's effect and the effect of the dipole coupling on the Fermi level and the quasiparticle's nature. At this stage, we would like to mention a few observations before studying the properties of the spectral function with the effects of a dipole parameter $\wp$. Firstly, we noticed from the flow equation (6.32), the role of momentum k discussed in [3] is now replaced by λ_n which is discrete because of the levels n. For zero temperature analysis, it is convenient to write the blackhole charge $Q = \sqrt{3-h^2}$ in terms of h, and then define the effective charge of the system as $q_s = q_0\sqrt{1-\frac{h^2}{3}}$, such that q_0 will be the total charge in the absence of a magnetic field. One can map back to a non magnetic system by taking the limit $h \to 0$ and $n \to \infty$, and plotting ImG_{22} as a function of ω shown in Figure 6.1 below. This plot approximately matches with the results of [3].

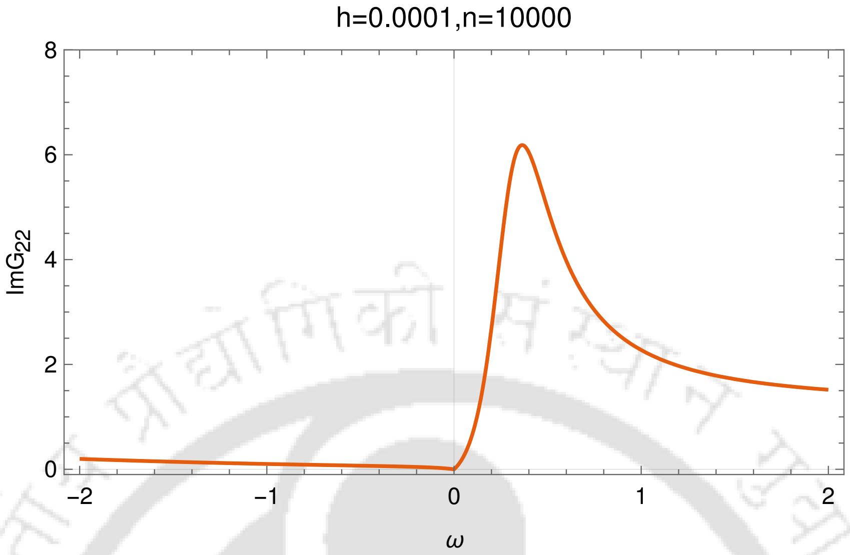

FIGURE 6.1: Zero temperature Im G_{22} for $m = 0$ and $q_0 = 1, \wp = 0$. In the limit of $h \to 0$ and $n \to \infty$.

6.3.1 Effects of the dipole coupling

Since, the effective momentum λ_n is discrete depending on the level n, before taking into account the detailed contribution from the constant coupling parameter $\wp$, we discuss the case with $\wp = 0$. Towards that direction we first look at the behaviour of ImG_{22} as function of magnetic field h at zero temperature. Figure 6.2 (left panel), shows the discreteness in the spectrum, which are unique in the presence of a magnetic field. For every discrete n values, there is a corresponding pole, which peaks whenever the effective momentum $k_{\text{eff}} = \sqrt{2qnh}$ equals the Fermi momentum k_F. Also for larger n, the poles are moving towards smaller h and the spacing between these poles decreases. Other interesting features without the coupling terms were studied in details by the authors in [157, 167, 168]. However we are interested for the case when our coupling is non-zero. Though, extensive studies have been done for holographic fermions with dipole coupling for non dyonic background, here we generalize the discussion for a dyonic black hole. As a quick preview, from Figure 6.2 (right panel), we see that by turning on the dipole parameter $\wp = 0.5$, the pole's height reduces significantly even for the same magnetic field strength keeping the discrete nature of Im G_{22} intact.

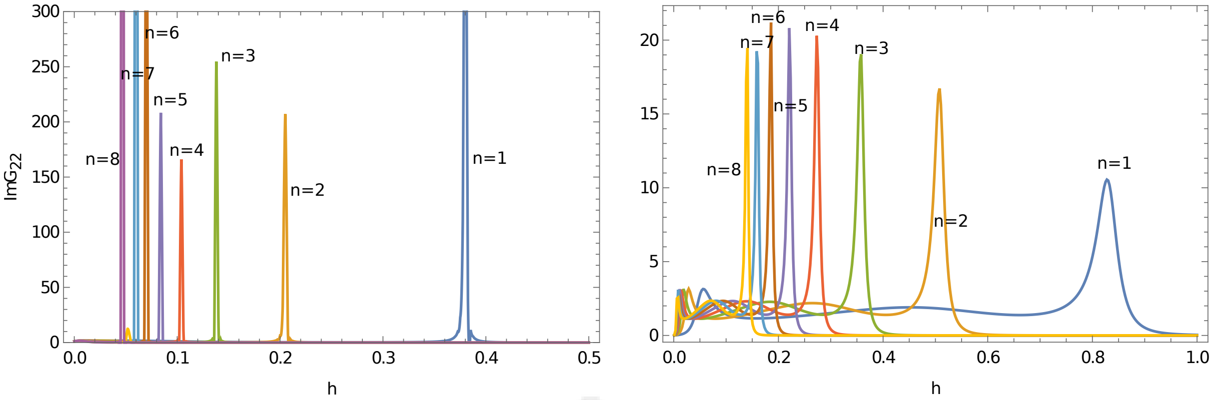

FIGURE 6.2: Left: Plot of $\operatorname{Im} \mathrm{G}_{22}$ for zero temperature, the poles near $\omega = 0$ is clearly visible for $n = 1, 2, 3...$ levels at different field strength h with $m = 0$ and $q_0 = 1, \wp = 0$. Right: Here, $\wp = 0.5$ and the height of quasi particle decreases.

Further, taking a particular level n, we study the decay width Γ of a quasiparticle, which in turn gives the life-time τ by a relation $\tau \sim \Gamma^{-1}$. In Figure 6.3, we showed the variation of the decay width versus the coupling constant $\wp$ for the levels $n = 1, 2$ and 3. The plot indicates that the width Γ is increasing as we increase $\wp$. This means that the quasiparticle lifetime decreases with increasing $\wp$. By performing a non linear fit on the decay width data obtained from Figure 6.3, we get a relationship between the width and $\wp$ as

$$\Gamma = \alpha(n)\, \wp^{\frac{12}{5}} \tag{6.34}$$

where α is a constant, which depends on n. The numerical values of $\alpha(n)$ corresponding to $n = 1, 2$ and 2 plots are given in the caption of Figure 6.3. The most important feature of equation (6.34) is the universality of the exponent for all the n values.

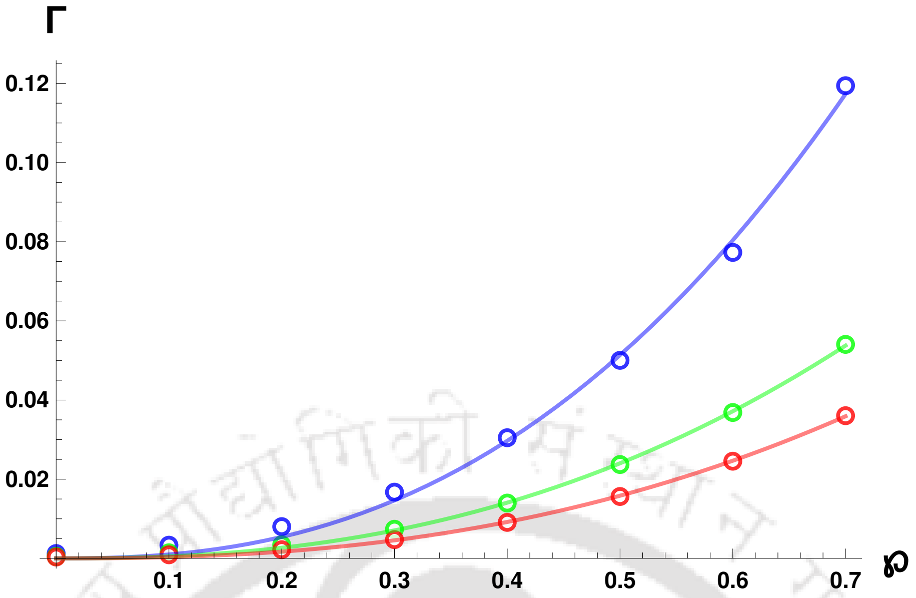

FIGURE 6.3: Variation of quasiparticle's decay width Γ (lifetime $\tau \sim \Gamma^{-1}$) as a function of $\wp$ for $n = 1$(blue), $n = 2$(green) and $n = 3$(red) near $\omega = 0$. The open circular markers correspond to the decay width data, while the solid line are the fitted curves in (6.34) with $\alpha \approx (0.28, 0.12, 0.08)$. Here, fermion mass $m = 0$, charge $q_0 = 1$.

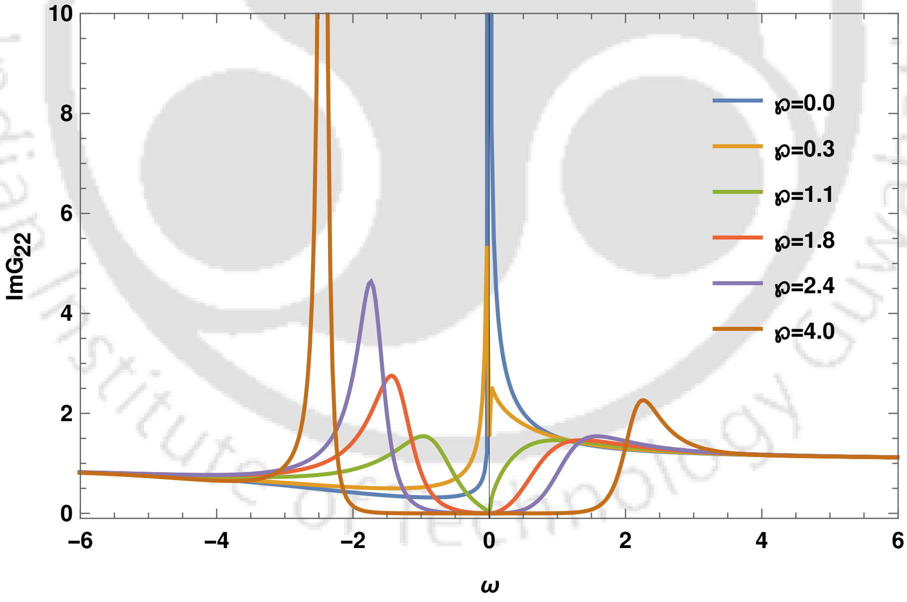

FIGURE 6.4: Gap induced by the coupling $\wp$ near $\omega = 0$. Here, fermion mass $m = 0$, charge $q_0 = 1$, magnetic field $h = 0.38$ and level $n = 1$.

In the above discussion, we have studied the quasiparticle decay width for different n levels for fixed magnetic field h. Now in Figure 6.4 and 6.5, we observed two interesting features. Firstly, there is a transfer of the spectral weight. Secondly we see that a dynamical gap

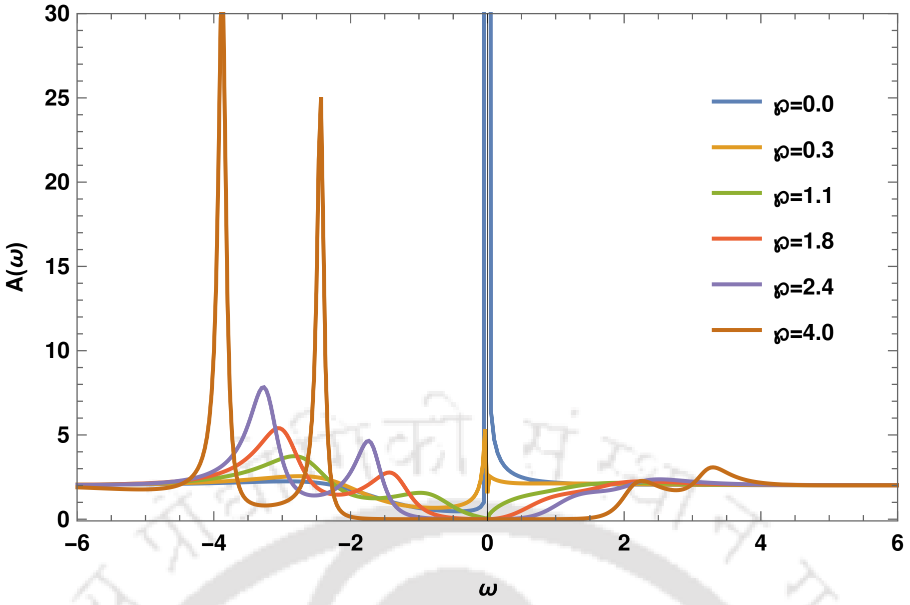

FIGURE 6.5: Spectral function $A(\omega)$ at zero temperature for the fermion mass $m = 0$ and charge $q_0 = 1$. We fix $n = 1$, and with $h = 0.38$.

is induced because of the coupling parameter $\wp$. In both ImG_{22} and the full spectral function $A(\omega)$, the appearance of the gap at $\omega = 0$ is visible on increasing the value of $\wp$ with a fixed $h = 0.38$. The fermionic spectra in this case is way more complicated than that at zero coupling. On comparing the plots for various strengths of $\wp$ in Figure 6.5, for a fixed h there is a splitting in the spectrum into multiple peaks when one increases $\wp$. This is a new feature that does not appear in a non-dyonic case. This splitting is unique and can only be seen in the presence of a magnetic field with the dipole coupling term introduced in the Fermionic action. From the condensed matter perspective, for low temperatures this was found to be originated from a quadrupole interaction, which implies that there is a change in the local charge distribution [169]. On the other hand, on increasing the coupling constant from $\wp = 0.2$, to 4 as shown in Figure 6.5, apart from splitting in a region near $\omega = 0$ when parameter $\wp$ is increased, we also see a dynamical gap as pointed out earlier. We want to study the phenomena of opening of the gap as a function of the dipole parameter $\wp$. In Figure 6.6, we showed for three n values, the zero temperature gap opening up at some critical value of $\wp \approx 1.8$ and the gap increases with increasing $\wp$. So far there are few main differences between the fermionic spectral properties in a dyonic and a non dyonic background. In the case of a dyonic black hole, apart from a spectral weight transfer and opening of a Mott gap, we see the splitting of spectrum into multiple peaks, which is a signature of the magnetic field effects.

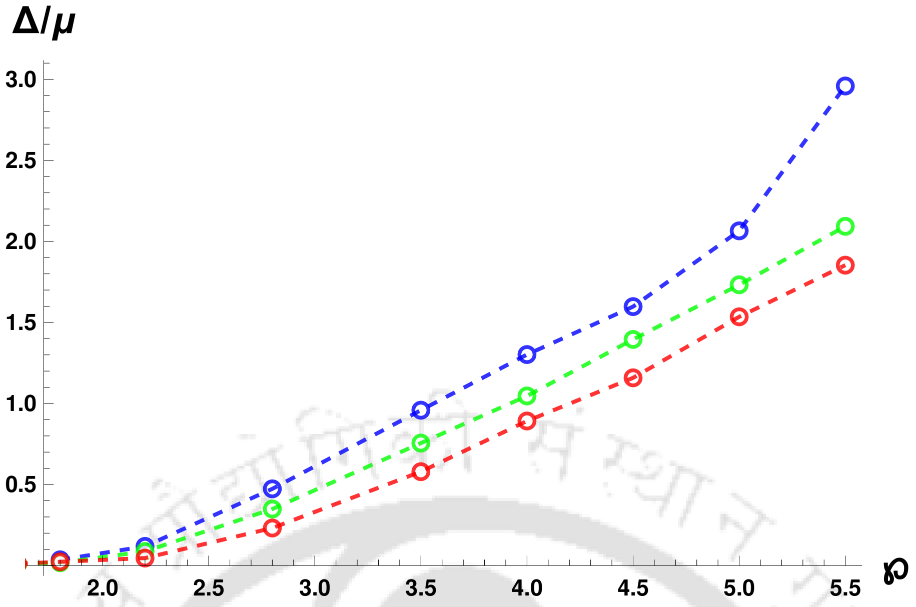

FIGURE 6.6: Zero temperature Gap Δ near $\omega = 0$ plotted vs coupling $\wp$ for $n = 1$(blue), $n = 2$(green) and $n = 3$(red). Here magnetic field h is taken from Figure 6.2, which corresponds to the location of the quasiparticle peak and the fermion mass $m = 0$ and charge $q_0 = 1$.

6.4 Conclusions

In this Chapter, we have studied the holographic fermionic spectral function, taking into account the effects of an external magnetic field along with a non-minimal coupling. We also find the Landau's levels arising from the quantization of electron orbits. We observed that the results are different from the case of zero magnetic field. From our results, we have observed some interesting phenomena like the disappearance of the quasi particles for large magnetic field, the splitting of spectral function for large coupling constant, which we have not seen in a non magnetic systems. In addition, we also see a spectral weight transfer from upper band to a lower band by inducing a gap at the Fermi level for different Landau levels n. Further, we studied the decay width of the quasiparticles, which shown to have a unique scaling exponent for all n levels. Finally, we studied the variation of the zero temperature gap parameter Δ versus coupling parameter $\wp$ for the levels $n = 1\,2$ and 3 respectively.

In our analyses, we have left out some important aspects, such as transport properties. One can further extend our study with this type of coupling to examine other interesting properties such as the Quantum Hall Effect [170, 171], computation of resistivity and conductivity in this system. It would be also interesting to study other intriguing phenomena induced by magnetic field, such as the de-Haas-van Alphen effect, but for now we leave these analyzes for future exploration.

Chapter 7

Summary and Future scopes

This thesis explores the intriguing phenomena in condensed matter physics related to strongly correlated systems using the holographic framework as a mathematical tool. We summarize the results and findings of these studies below.

We started with two introductory chapters that contain some motivations from condensed matter and a brief review of the AdS/CFT correspondence with a discussion on the holographic principle and its application to various systems. We reviewed a few examples, which are considered as pioneering works towards this direction, based on the holographic method. In the first example, we presented some important calculations to compute the retarded Green's function. We discussed the non-Fermi liquid behaviour in the strongly correlated fermionic system [3]. Secondly, we reviewed the steps for computing the conductivity based on the original work in [4] and then compared the results to those of real condensed matter systems. Then, in the final example, we reviewed an application of AdS/CFT to the evolution of Fermi arcs from the Mott insulator [5]. The primary purpose of all those introductory chapters was to familiarise ourselves with the techniques and tools used in both analytical and numerical computations.

In Chapter 3, which is our first technical chapter, we discussed the Fermi arcs, which are disconnected contours of the Fermi surface observed in the pseudo-gap phase of high-temperature superconductors. Since we aimed to understand the pseudo-gap phenomena, we studied a holographic Fermionic system coupled with a massive scalar field in the Reissner–Nordström AdS black hole background. Depending on the boundary conditions of the scalar field mode, we discussed two possible scenarios; (i) when the scalar condenses below a critical temperature T_c, the Fermi surface deforms when transition from normal phase to a pseudo-gap phase happens. Hence, T_c can be reminiscent of the well-known cross over temperature, T^* in cuprates superconductors, below which a pseudo-gap appears at constant doping. (ii) In the second scenario, we discussed a case when the bulk scalar develops a non-normalisable profile at an arbitrary temperature for a non-zero source at the boundary. Therefore, we can tune the Fermi spectrum by tuning a dual-source at the boundary. The dual-source, in this case, can be reminiscent of hole doping in the real cuprate superconductor. In both cases, we studied the Fermi spectrum, and observed an anisotropic gap in the spectral function depending on the model parameter and studied the properties of Fermi arcs across different phases.

This is followed by Chapter 4, where we studied the low energy fermionic properties in the framework of the holographic Mott-Insulator system. The holographic properties of a finite density fermionic system have been shown to exhibit many interesting behaviours. We mainly studied a deformation of the Fermi surface and its evolution by tuning two types of dipole coupling parameters in the bulk. We further introduced a complex scalar field that breaks translational symmetry, which is also coupled with the fermion field ψ. The symmetry breaking background induced by the scalar field is known as the Q-lattice. We calculated the fermionic spectral function, which captures the low energy behaviour of the system. By changing the temperatures, tuning the dipole parameters and the non-normalisable component of the scalar field, we observed interesting phenomena, such as spectral weight transfer, Fermi arcs, Fermi surface smearing, and the presence of secondary Fermi surfaces, which have already been reported in various real condensed matter experiments.

With a similar procedure, in Chapter 5, we modified the fermion interaction terms considered in Chapter 4. We again studied a holographic toy model by considering a probe fermion of finite charge density in the same anisotropic Q-lattice background. We introduced non-minimal interaction terms in the action for holographic fermions along with a complex scalar field but neglecting the back-reaction of the fermion field on the background. We computed the fermionic spectral function numerically and we found that the system here also exhibits similar behaviours in the nature of the Fermi surface and its evolution when tuning the controlling parameters. Suppression in the spectral weight and deformation of Fermi surface is also seen, which are reminiscent of the results seen in different condensed matter experiments in real materials.

In Chapter 6, which is our last one, we devoted to the study of possible effects by a magnetic field in the presence of modified dipole couplings. We consider a fermionic system with interaction terms in the AdS$_4$ dyonic black hole background. We found that in the probe limit, the magnetic holographic system can be reduced to non-magnetic one, with momenta being quantised into Landau levels. For a large magnetic field, we observed a gradual disappearance of the Fermi surface and quasi-particle peaks. We also found the transfer of spectral weight when we tuned the coupling parameter and computed the zero temperature gap. We further tune the coupling parameter and study its effect on the Fermi level and the quasiparticle width. We found an interesting scaling relation between the decay width and the coupling parameter, with a universal scaling exponent which is independent of the Landau levels n.

In recent years, application of holographic principle have become more popular and a very active field for young researchers. Because of this, it has also caught the attention of many in other branches of physics as well. One cannot say for sure whether this Holographic principle will be able to solve all the challenging and interesting phenomena posed by the strongly correlated systems, which we discussed in this thesis. Nevertheless, we must never say never. Along the same path of what we already tried to address, there are some immediate generalisations that we can study in near future. Some of which include a study of these models in higher dimensions to capture both the bulk and surface phenomena related to the $3D-$Dirac and Weyl materials. Recently, there have been other holographic models too, such as those in [144–146], which attempted to address these interesting and rich phenomena observed in topological insulators, and semi-metals. Computation of the conductivity for the models proposed in this thesis is also one of the important aspects for the fermionic system in both magnetic and non-magnetic background. Another aspect is to explore the fermion spectral function in the so-called ionic holographic lattices with periodic chemical potential [38], which mimic the crystal lattice in real materials. For this, one can explore the types of coupling terms that we already studied in this thesis.

Appendix A

Appendix to Chapter 1

A.1 Infinitesimal transformation

Since a conformal transformation is a coordinate transformation that effect the metric as a rescaling

$$\frac{\partial x'^{\rho}}{\partial x^{\nu}}\frac{\partial x'^{\lambda}}{\partial x^{\nu}}\, g_{\rho\lambda} \; = \Omega(x)\, g_{\mu\nu} \tag{A.1}$$

For infinitesimal transformation

$$x'^{\mu} = x^{\mu} + \epsilon^{\mu} \tag{A.2}$$

we get

$$\begin{aligned} \Omega(x)\, g_{\mu\nu} = &\; g_{\rho\lambda}(\delta^{\rho}_{\mu} + \partial_{\mu}\epsilon^{\rho})(\delta^{\lambda}_{\nu} + \partial_{\nu}\epsilon^{\lambda}) \\ = &\; g_{\mu\nu} \; + \partial_{\mu}\epsilon_{\lambda} + \partial_{\nu}\epsilon_{\rho} + O(\epsilon^{2}) \\ = &\; g_{\mu\nu} \; + \partial_{\mu}\epsilon_{\nu} + \partial_{\nu}\epsilon_{\mu} + O(\epsilon^{2}) \end{aligned} \tag{A.3}$$

This show that the tensorial part must be proportional to $g_{\mu\nu}$, let

$$\partial_{\mu}\epsilon_{\nu} + \partial_{\nu}\epsilon_{\mu} = k(x) g_{\mu\nu} \tag{A.4}$$

Now to determine the factor $k(x)$, we can contract by $g_{\mu\nu}$ to give

$$\begin{aligned} g^{\mu\nu}(\partial_{\mu}\epsilon_{\nu} + \partial_{\nu}\epsilon_{\mu}) &= g^{\mu\nu}\, k(x) g_{\mu\nu} \\ (\partial_{\mu}\epsilon^{\mu} + \partial_{\nu}\epsilon^{\nu}) &= \; k(x)\delta^{\mu}_{\mu} \; = d\, k(x) \\ k &= \frac{2}{d}\,\partial_{\mu}\epsilon^{\mu} \end{aligned} \tag{A.5}$$

Now we have

$$\partial_{\mu}\epsilon_{\nu} + \partial_{\nu}\epsilon_{\mu} = \frac{2}{d}\,\partial_{\mu}\epsilon^{\mu}\, g_{\mu\nu} = \frac{2}{d}\,(\partial.\epsilon)\, g_{\mu\nu} \tag{A.6}$$

Taking derivative of this equation by ∂^ν, we have

$$\begin{aligned}\partial^\nu\Big[\partial_\mu\epsilon_\nu + \partial_\nu\epsilon_\mu\Big] &= \frac{2}{d}\,\partial^\nu(\partial.\epsilon)\ g_{\mu\nu}\\ \Big[\partial_\mu(\partial.\epsilon) + \Box\ \epsilon_\mu\Big] &= \frac{2}{d}\,\partial_\mu(\partial.\epsilon)\end{aligned} \tag{A.7}$$

Contract again by ∂_ν we get

$$\partial_\nu\partial_\mu(\partial.\epsilon) + \Box\ \partial_\nu\epsilon_\mu = \frac{2}{d}\,\partial_\nu\,\partial_\mu(\partial.\epsilon) \tag{A.8}$$

using $(\partial_\mu\epsilon_\nu + \partial_\nu\epsilon_\mu) = \frac{2}{d}\,(\partial.\epsilon)\ g_{\mu\nu}$, we get

$$\begin{aligned}\partial_\nu\partial_\mu(\partial.\epsilon) + \Box\ \frac{1}{d}\,(\partial.\epsilon)\ g_{\mu\nu} &= \frac{2}{d}\,\partial_\nu\,\partial_\mu(\partial.\epsilon)\\ (\partial_\nu\partial_\mu + \Box\ \frac{1}{d}\ g_{\mu\nu} - \frac{2}{d}\,\partial_\nu\,\partial_\mu)(\partial.\epsilon) &= 0\\ g^{\mu\nu}(\partial_\nu\partial_\mu + \Box\ \frac{1}{d}\ g_{\mu\nu} - \frac{2}{d}\,\partial_\nu\,\partial_\mu)(\partial.\epsilon) &= 0\\ (\Box\ + \Box\ \ - \frac{2}{d}\,\Box)(\partial.\epsilon) &= 0\\ (d\ - 1\,)\Box(\partial.\epsilon) &= 0\end{aligned} \tag{A.9}$$

This implies that ϵ is up to quadratic order which can be written as

$$\epsilon_\mu\ \ =\ \ a_\mu + \ b_{\mu\nu}\,x^\nu\ + c_{\mu\nu\rho}x^\nu x^\rho\ . \tag{A.10}$$

We see that the constant term a_μ has no constraint, so putting back in $x'^\mu = x^\mu + \epsilon^\mu$, setting b and c to zero gives

$$x'^\mu = x^\mu + a^\mu \tag{A.11}$$

Now the linear term $b_{\mu\nu}$, substituting in $\partial_\mu\epsilon_\nu + \partial_\nu\epsilon_\mu = \frac{2}{d}\,\partial_\mu\epsilon^\mu\ g_{\mu\nu}$ and setting a and c to zero gives

$$\begin{aligned}\partial_\mu b_{\nu\rho}x^\rho + \partial_\nu b_{\mu\rho}x^\rho &= \frac{2}{d}\,b^{\mu\rho}\,g_{\mu\lambda}\partial^\lambda x_\rho\ g_{\mu\nu}\\ b_{\nu\rho}\delta^{\ \rho}_\mu + b_{\mu\rho}\delta^{\ \rho}_\nu &= \frac{2}{d}\,b^{\mu\rho}\,g_{\mu\lambda}\ \delta^{\lambda}_{\ \rho}\ g_{\mu\nu}\\ b_{\nu\mu} + b_{\mu\nu} &= \frac{2}{d}\,b^{\mu\rho}\,g_{\mu\rho}\ g_{\mu\nu} = \frac{2}{d}\,b_\rho^{\ \rho}\ g_{\mu\nu}\end{aligned} \tag{A.12}$$

This means that if $b_{\mu\nu}$ is symmetric then it is proportional to $g_{\mu\nu}$. If $b_{\mu\nu}$ is not symmetric then the antisymmetric part would correspond to Lorentz transformations and the symmetric will correspond to a dilatation. Explicitly we can write the symmetric part

$$b^{\mu\nu} = \lambda \, g^{\mu\nu} \tag{A.13}$$

Therefore

$$x'^{\mu} = x^{\mu} + b^{\mu\nu} x_{\nu} = x^{\mu} + \lambda \, g^{\mu\nu} x_{\nu} = x^{\mu} + \lambda \, x^{\mu} \tag{A.14}$$

For antisymmeric part,

$$x'^{\mu} = x^{\mu} + b^{\mu\nu} x_{\nu} = x^{\mu} + M^{\mu}_{\nu} x^{\nu} = \left(\delta^{\mu}_{\nu} + M^{\mu}_{\nu}\right) x^{\nu} \tag{A.15}$$

Appendix B

Appendix to Chapter 2

B.1 Example - 1 code

Mathematica Code to solve the flow equation (2.20)

```
In[1]:= (*  Numerical solution. *)

        (* constants *)
        m = 0; Q = N[Sqrt[3]]; mu = N[Sqrt[3]]; small = 10^-6;

        (* BCs *)
        bc1[k_]:=( m - Sqrt[k^2 + m^2 - mu^2/6 - I*small])/( mu/Sqrt[6] + k );
        bc2[k_]:=( m - Sqrt[k^2 + m^2 - mu^2/6 - I*small])/( mu/Sqrt[6] - k );

        (* Known functions *)
        f[r_]:= 1 + (Q^2)/r^4 - (1 + Q^2)/r^3;
        u[r_,omega_,q_]:= 1/Sqrt[f[r]]* ( omega + mu*q* (1 - 1/r));

        (* Flow Equations*)
        Xi11[k_,omega_,q_]:= r^2 Sqrt[f[r]] Xi1'[r]+(k - u[r,omega,q])-(k + u[r,omega,q])Xi1[r]^2;

        Xi22[k_,omega_,q_]:= r^2 Sqrt[f[r]] Xi2'[r]-(k + u[r,omega,q])+(k - u[r,omega,q])Xi2[r]^2;

        (*Using NDSolve *)

        sol1[k_,omega_,q_]:=
        NDSolve[{Xi11[k,omega,q] == 0, Xi1[1 + small]] == I (1 - KroneckerDelta[omega, 0]) +
                KroneckerDelta[omega, 0] bc1[k]}, Xi1, {r, 1 + small,10000}, MaxSteps -> Infinity,
                InterpolationOrder -> All,Method -> "StiffnessSwitching"]

        G11[k_,omega_,q_]:= Evaluate[Xi1[r]]/.sol1[k,omega,q] /.r -> 10000;

        sol2[k_,omega_,q_]:=
        NDSolve[{Xi22[k,omega,q] == 0, Xi2[1 + small] == I (1 - KroneckerDelta[omega,0]) +
                KroneckerDelta[omega, 0] bc2[k]}, Xi2, {r, 1 + small,10000}, MaxSteps -> Infinity,
                InterpolationOrder -> All,Method -> "StiffnessSwitching"]

        G22[k_,omega_,q_]:= Evaluate[Xi2[r]] /.sol2[k,omega,q] /.r -> 10000;

        (*Test plot the Imaginary part of G22*)
                Plot[Im[G22[1.2, x, 1]], {x, -2, 2}, PlotRange -> All]
```

```
(* //////////////////////////////////////////////////////////////////////////////// *)
```

B.2 Example - 2 code

Derivation of the perturbation equation using Mathematica package `EDCRGTCcode.m`.

```
In[2]:= Unprotect[Laplacian];
        << EDCRGTCcode.m;
        xIN = {z, t, x, y}; (* coordinates *)

        g0 = 1/z^2*DiagonalMatrix[{1/f[z], -f[z], 1, 1 }];  (* unperturb matric *)
```

```
In[3]:= deltag = E^(-I omega t)/z^2 *gtx[z] SparseArray[{{2, 3} -> 1, {3, 2} -> 1}, 4];
        g = Series[g0 + ep*deltag , {ep, 0, 1}];


        RGtensors[g, xIN];
```

```
In[4]:= Ad = Series[ {0, At[z], 0, 0} + ep*E^(-I omega t)* {0, 0, ax[z], 0}, {ep, 0, 1}];

        Fdd = -covD[Ad] + Transpose[covD[Ad]];
        FUU = Raise[Fdd, 1, 2];
        FdU = Raise[Fdd, 2];
        FUd = Raise[Fdd, 1];

        F2 = multiDot[Fdd, FUU, {1, 1}, {2, 2}];
```

```
In[5]:= EU =  covDiv[FUU, {2, {1}}];


        Einsdd = Rdd - 1/2 R gdd - 3 gdd  - 1/2 (multiDot[Fdd, FdU, {2, 2}] - 1/4 F2 gdd );
```

Check for RN solution if it satisfies Einstein-Maxwell's equations :

```
In[6]:= RNsol = {At -> Function[z, mu (1 - z) ], f -> Function[z, (1 - z) (1 + z + z^2 - (mu^2 z^3)/4) ]};

In[7]:= Simplify[  {EU, Einsdd} /. ep -> 0  /. RNsol ]

Out[7]=  0, 0, 0, 0, 0, 0, 0, 0, 0, 0, 0, 0, 0, 0, 0, 0, 0, 0, 0, 0
```

Further simplify the equations of motion to get equation (2.28)

```
In[8]:= vars = Flatten[ Table[ D[{ ax[z], gtx[z] }, {z, i}] , {i, 0, 2}]];

        eq1 = Collect[ E^(I omega t )*D[ EU[[3]], ep] /. ep -> 0 , vars, Simplify]


        eq2 = Collect[ E^(I omega t )*D[ Einsdd[[1,3]], ep] /. ep -> 0 , vars, Simplify]

In[9]:= Finaleqn = Collect[ (eq1/z^4 + (2 I f[z] D[ At[z],z])/( omega) *eq2) , vars, Simplify ]

Out[9]= ax[z] (omega^2/f[z] - z^2 At'[z]^2) + ax'[z] f'[z] + f[z] ax''[z]
```

B.3 Example - 3 code

Mathematica Code to solve the matrix flow equation (2.52)

```
In[10]:=  (* Putting r0 = L = q = 1 and m = 0 respectively *)

          small = 1/10000; delta = 1/100000;

          f[z_] := 1 - z^3;
          Wp[p_, omega_, mu_]:= Sqrt[1/f[z]] (omega + (1 - z) mu) + (p * mu * z);
          Wm[p_, omega_, mu_]:= Sqrt[1/f[z]] (omega + (1 - z) mu) - (p * mu * z);

          G[z_]:= {{G11[z], G12[z]},{G21[z], G22[z]}} ;

          eqnG[omega_, p_, kx_, ky_, z_, mu_]:=
                  Sqrt[f[z]] G’[z] + ({{ Wp[p, omega, mu] - kx , ky},{ ky, Wm[p, omega, mu] + kx} } )-

                  G[z].( { {-Wm[p, omega, mu] - kx , ky },{ ky, -Wp[p, omega, mu] + kx} } ).G[z]
```

Integrating the flow equation using `NDSolve` from horizon (z=1) to the boundary $z \to 0$. We have defined $z \equiv 1/r$ in the equations above for convenience in setting the boundary. To avoid the singularity at $z = 1$, we put some offset by subtracting with `small` from the horizon as shown in the code above.

```
In[11]:=  solG[omega_, p_, kx_, ky_, mu_]:=
                 NDSolve[{eqnG[omega_, p_, kx_, ky_, z_, mu_][[1]][[1]] == 0,
                          eqnG[omega_, p_, kx_, ky_, z_, mu_][[1]][[2]] == 0,
                          eqnG[omega_, p_, kx_, ky_, z_, mu_][[2]][[1]] == 0,
                          eqnG[omega_, p_, kx_, ky_, z_, mu_][[2]][[2]] == 0,
                          G11[1 - small] == I, G12[1 - small] == 0, G21[1 - small] == 0,
                          G22[1 - small] == I}, {G11, G12, G21, G22}, {z_, 1 - small, delta},

                          Method -> "StiffnessSwitching"]
```

The spectral function is computed through the following line of code :

```
In[12]:=          A[omega_, p_, kx_, ky_, mu_]:=

                            Evaluate[Tr[Im[G[z]]]] /. solG[omega_, p_, kx_, ky_, mu_] /.z -> delta
```

Test output

```
In[13]:=          A[0.001, 1, 1, 1, Sqrt[3]]


Out[13]=          1.40888
```

Appendix C

Appendix to Chapter 3

C.1 The Dirac equation and flow equation

In this appendix, we provide some of the calculations involved for deriving the flow equation in Chapter 3. For the RN-AdS$_4$ background in Chapter 3, the metric is given by

$$\frac{ds^2}{L^2} = -g_{tt}dt^2 + g_{rr}dr^2 + g_{xx}dx^2 + g_{yy}dy^2\,, \tag{C.1}$$

where

$$g_{tt} = r^2 f(r)\ ,\ g_{rr} = r^{-2} f^{-1}(r) \text{ and } g_{xx} = g_{yy} = r^2, \tag{C.2}$$

with

$$f = 1 + \frac{3\gamma}{r^4} - \frac{1+3\gamma}{r^3}\ ,\quad A_t = \mu(1-\frac{1}{r})\,dt \tag{C.3}$$

Spin connection formula:

$$\mathbf{\Gamma}_\mu = \frac{1}{8}\Big[\gamma^a,\gamma^b\Big]e^\nu_a\Big(\partial_\mu e_{b\nu} - \Gamma^\alpha_{\mu\nu}e_{b\alpha}\Big) \tag{C.4}$$

The relations between vielbeins and the metric are given by

$$g^{\mu\nu} = e^\mu_a e^\nu_b \eta^{ab}, \qquad g_{\mu\nu} = e^a_\mu e^b_\nu \eta_{ab}\,.$$

Using these relations we get

$$e^r_{\underline{r}} = \frac{1}{\sqrt{g_{rr}}},\quad e^t_{\underline{t}} = \frac{1}{\sqrt{-g_{tt}}},\quad e^x_{\underline{x}} = \frac{1}{\sqrt{g_{xx}}},\quad e^y_{\underline{y}} = \frac{1}{\sqrt{g_{yy}}}\,.$$

Below are the non-zero Christoffel symbol for the metric (C.1) computed with a `diffeo.m` package in `Mathematica`.

$\Gamma^{x}_{r\,x}, \Gamma^{x}_{x\,r}$ $\Gamma^{y}_{r\,y}, \Gamma^{y}_{y\,r}$	$\frac{1}{r}$
$\Gamma^{r}_{x\,x}, \Gamma^{r}_{y\,y}$	$-r^3 f(r)$
$\Gamma^{r}_{t\,t}$	$r^3 f(r)\ \left(r f'(r) + 2 f(r)\right)/2$
$\Gamma^{r}_{r\,r}$	$-\frac{f'(r)}{2f(r)} - \frac{1}{r}$
$\Gamma^{t}_{t\,r}, \Gamma^{t}_{r\,t}$	$\frac{f'(r)}{2f(r)} + \frac{1}{r}$

We will take the following matrices to evaluate the Dirac equation.

$$\gamma^{\underline{r}} = \begin{pmatrix} -\sigma_3 & 0 \\ 0 & -\sigma_3 \end{pmatrix}, \gamma^{\underline{t}} = \begin{pmatrix} i\sigma_1 & 0 \\ 0 & i\sigma_1 \end{pmatrix} \gamma^{\underline{x}} = \begin{pmatrix} -\sigma_2 & 0 \\ 0 & \sigma_2 \end{pmatrix} \text{ and } \gamma^{\underline{y}} = \begin{pmatrix} 0 & \sigma_2 \\ \sigma_2 & 0 \end{pmatrix} \tag{C.5}$$

Let us first evaluate $\mathbf{\Gamma}_t$

$$\begin{aligned}
\mathbf{\Gamma}_t &= \frac{1}{8}\Big[\gamma^{a}, \gamma^{b}\Big] e^{\nu}_{a}\Big(\partial_t e_{b\nu} - \Gamma^{\alpha}_{t\nu} e_{b\alpha}\Big) \\
&= -\frac{1}{8}\Big[\gamma^{a}, \gamma^{b}\Big] e^{\nu}_{a}\Gamma^{\alpha}_{t\nu} g_{\alpha\beta} e^{\beta}_{b} \\
&= -\frac{1}{8}\left(\Big[\gamma^{\underline{r}}, \gamma^{\underline{t}}\Big] e^{r}_{\underline{r}}\Gamma^{t}_{tr} g_{tt} e^{t}_{\underline{t}} + \Big[\gamma^{\underline{t}}, \gamma^{\underline{r}}\Big] e^{t}_{\underline{t}}\Gamma^{r}_{tt} g_{rr} e^{r}_{\underline{r}}\right)
\end{aligned}$$

Since ,$\Big[\gamma^{\underline{r}}, \gamma^{\underline{t}}\Big] = -\Big[\gamma^{\underline{t}}, \gamma^{\underline{r}}\Big] = 2\sigma_2 \otimes \mathbb{1}$. Therefore,

$$\begin{aligned}
\mathbf{\Gamma}_t &= -\frac{1}{4}\sigma_2 \otimes \mathbb{1}\left[-r^2 f\left(\frac{1}{r} + \frac{f'}{2f}\right) - r^2\left(\frac{f}{r} + \frac{f'}{2}\right)\right] \\
&= \frac{1}{2}\sigma_2 \otimes \mathbb{1}\left[r^2\left(\frac{f}{r} + \frac{f'}{2}\right)\right] \\
\implies e^{t}_{\underline{t}}\gamma^{\underline{t}}\mathbf{\Gamma}_t &= r\sqrt{f}\left(\frac{1}{2r} + \frac{f'}{4f}\right)\gamma^{\underline{r}}
\end{aligned}$$

$\mathbf{\Gamma}_r$ can be shown in a similar way that it is equal zero.

$$\begin{aligned}
\mathbf{\Gamma}_x &= \frac{1}{8}\Big[\gamma^{a}, \gamma^{b}\Big] e^{\nu}_{a}\Big(\partial_x e_{b\nu} - \Gamma^{\alpha}_{x\nu} e_{b\alpha}\Big) \\
&= -\frac{1}{8}\Big[\gamma^{a}, \gamma^{b}\Big] e^{\nu}_{a}\Gamma^{\alpha}_{x\nu} g_{\alpha\beta} e^{\beta}_{b} \\
&= -\frac{1}{8}\left(\Big[\gamma^{\underline{x}}, \gamma^{\underline{r}}\Big] e^{x}_{\underline{x}}\Gamma^{r}_{xx} g_{rr} e^{r}_{\underline{r}} + \Big[\gamma^{\underline{r}}, \gamma^{\underline{x}}\Big] e^{r}_{\underline{r}}\Gamma^{x}_{xr} g_{xx} e^{x}_{\underline{x}}\right) \\
&= \frac{1}{4}\Big[\gamma^{\underline{x}}, \gamma^{\underline{r}}\Big] r\sqrt{f}
\end{aligned}$$

Since $\left[\gamma^{\underline{x}},\gamma^{\underline{r}}\right]=-2\begin{pmatrix}-i\sigma_1 & 0\\ 0 & i\sigma_1\end{pmatrix}$, therfore

$$e^{x}_{\underline{x}}\gamma^{\underline{x}}\mathbf{\Gamma}_x=\frac{r\sqrt{f}}{2r}\gamma^{\underline{r}}.$$

Similarly for $\mathbf{\Gamma}_y$

$$e^{y}_{\underline{y}}\gamma^{\underline{y}}\mathbf{\Gamma}_y=\frac{r\sqrt{f}}{2r}\gamma^{\underline{r}}.$$

Now summing all the terms of spin connection, we have

$$\begin{aligned}S.C&=e^{t}_{\underline{t}}\gamma^{\underline{t}}\mathbf{\Gamma}_t+e^{r}_{\underline{r}}\gamma^{\underline{r}}\mathbf{\Gamma}_r+e^{x}_{\underline{x}}\gamma^{\underline{x}}\mathbf{\Gamma}_x+e^{y}_{\underline{y}}\gamma^{\underline{y}}\mathbf{\Gamma}_y\\&=r\sqrt{f}\left(\frac{3}{2r}+\frac{f'}{4f}\right)\gamma^{\underline{r}}\end{aligned}$$

The Dirac equation of motion from Chapter 3 is given by

$$\left(\not{D}-m-i\,p\mathbf{\Gamma}\Phi(r)\not{F}\right)\psi=0, \tag{C.6}$$

where $\mathbf{\Gamma}\equiv\Gamma^{\underline{r}}\Gamma^{\underline{t}}(\hat{n}\cdot\vec{\Gamma})$ and $\vec{\Gamma}\equiv(\Gamma^{\underline{x}},\Gamma^{\underline{y}})$. We shall take $\hat{n}=\hat{x}$ and $\not{F}$ evaluates to

$$\not{F}=\begin{pmatrix}\sigma_2 & 0\\ 0 & \sigma_2\end{pmatrix}\frac{\mu}{r^2}$$

On simplification of equation(12) one arrives to two coupled equations

$$r^2\sqrt{f}\left(\partial_r+\frac{6f(r)+rf(r)}{4rf(r)}\right)\psi_1=\left(-\frac{\sigma_2}{\sqrt{f}}(\partial_t-iqA_t)+i\sigma_1\partial_x-\sigma_3 m\,r+\sigma_1\frac{p\,\mu\Phi(r)}{r}\right)\psi_1-i\sigma_1\partial_y\psi_2 \tag{C.7}$$

$$r^2\sqrt{f}\left(\partial_r+\frac{6f(r)+rf(r)}{4rf(r)}\right)\psi_2=\left(-\frac{\sigma_2}{\sqrt{f}}(\partial_t-iqA_t)-i\sigma_1\partial_x-\sigma_3 m\,r-\sigma_1\frac{p\,\mu\Phi(r)}{r}\right)\psi_2-i\sigma_1\partial_y\psi_1 \tag{C.8}$$

We simultaneously Fourier transforming and rescaling the bulk spinor

$$\psi_{1,2}(r,x)=r^{-\frac{3}{2}}f^{-\frac{1}{4}}e^{-i\omega t+ik.x}\psi_{1,2}(r,k)$$

Now the spin connection cancelled out because of the scaling and the Dirac equations (C.7) and (C.8) above can be packed into a single equation,

$$r^2\sqrt{f(r)}\partial_r\psi_j = \frac{i\sigma_2}{\sqrt{f(r)}}\left(\omega + q\mu\left(1-\frac{1}{r}\right)\right)\psi_j - \sigma_3 m\,r\psi_j - (-1)^j\sigma_1\left(\frac{p\,\Phi(r)\mu}{r} - k_x\right)\psi_j + \sigma_1 k_y\psi_i. \tag{C.9}$$

Strictly for $i \neq j$ with the spinor $\psi = (\psi_1, \psi_2)^T$. Breaking the Dirac equation by writing the two-component bulk spinors as $\psi_j = (\beta_j, \alpha_j)^T$, we have

$$r^2\sqrt{f}\partial_r\beta_1 = \frac{1}{\sqrt{f}}(\omega + qA_t)\alpha_1 - m\,r\,\beta_1 + \frac{p\,\mu\Phi(r)}{r}\alpha_1 - k_x\alpha_1 + k_y\alpha_2\ , \tag{C.10}$$

$$r^2\sqrt{f}\partial_r\alpha_1 = -\frac{1}{\sqrt{f}}(\omega + qA_t)\beta_1 + m\,r\,\alpha_1 + \frac{p\,\mu\Phi(r)}{r}\beta_1 - k_x\beta_1 + k_y\beta_2\ , \tag{C.11}$$

$$r^2\sqrt{f}\partial_r\beta_2 = \frac{1}{\sqrt{f}}(\omega + qA_t)\alpha_2 - mr\beta_2 - \frac{p\,\mu\Phi(r)}{r}\alpha_2 + k_x\alpha_2 + k_y\alpha_1\ , \tag{C.12}$$

$$r^2\sqrt{f}\partial_r\alpha_2 = -\frac{1}{\sqrt{f}}(\omega + qA_t)\beta_1 + mr\alpha_2 - \frac{p\,\mu\Phi(r)}{r}\beta_2 + k_x\beta_2 + k_y\beta_1. \tag{C.13}$$

Rearranging $\beta' s$ and $\alpha' s$ equations

$$r^2\sqrt{f}\partial_r\beta_1 = \frac{1}{\sqrt{f}}(\omega + qA_t)\alpha_1 - mr\beta_1 + p\frac{\mu\Phi(r)}{r}\alpha_1 - k_x\alpha_1 + k_y\alpha_2\ , \tag{C.14}$$

$$r^2\sqrt{f}\partial_r\beta_2 = \frac{1}{\sqrt{f}}(\omega + qA_t)\alpha_2 - mr\beta_2 - p\frac{\mu\Phi(r)}{r}\alpha_2 + k_x\alpha_2 + k_y\alpha_1\ . \tag{C.15}$$

Which can be group further as

$$\begin{aligned} \frac{r^2}{L^2}\sqrt{f}\partial_r\beta_1 &= (v_+ - k_x)\alpha_1 - mr\beta_1 + k_y\alpha_2\ , \\ \frac{r^2}{L^2}\sqrt{f}\partial_r\beta_2 &= (v_- + k_x)\alpha_2 - mr\beta_2 + k_y\alpha_1\ . \end{aligned} \tag{C.16}$$

Similarly,

$$\frac{r^2}{L^2}\sqrt{f}\partial_r\alpha_1 = -\frac{1}{\sqrt{f}}(\omega + qA_t)\beta_1 + mr\alpha_1 + p\frac{\mu\Phi(r)}{r}\beta_1 - k_x\beta_1 + k_y\beta_2\ , \tag{C.17}$$

$$\frac{r^2}{L^2}\sqrt{f}\partial_r\alpha_2 = -\frac{1}{\sqrt{f}}(\omega + qA_t)\beta_1 + mr\alpha_2 - p\frac{\mu\Phi(r)}{r}\beta_2 + k_x\beta_2 + k_y\beta_1\ . \tag{C.18}$$

or,

$$
\begin{aligned}
\frac{r^2}{L^2}\sqrt{f}\partial_r\alpha_1 &= (-v_- - k_x)\beta_1 + mr\alpha_1 + k_y\beta_2 \ , \\
\frac{r^2}{L^2}\sqrt{f}\partial_r\alpha_2 &= (-v_+ + k_x)\beta_2 + mr\alpha_2 + k_y\beta_1 \ . \qquad \text{(C.19)}
\end{aligned}
$$

In all of the above equations, $v_\pm$ is given by

$$
v_\pm = \frac{1}{\sqrt{f}}(\omega + qA_t) \pm p\mu\Phi(r)\frac{1}{r}
$$

Now we will derive the matrix flow equation (3.18). We start by defining the following matrices

$$
Y = \begin{pmatrix} \beta_1^I & \beta_1^{II} \\ \beta_2^I & \beta_2^{II} \end{pmatrix}, \quad Z = \begin{pmatrix} \alpha_1^I & \alpha_1^{II} \\ \alpha_2^I & \alpha_2^{II} \end{pmatrix}, \quad GZ = Y \ . \qquad \text{(C.20)}
$$

Taking derivatives of the last equality w.r.t r, we have

$$
\begin{pmatrix} \partial_r G11 & \partial_r G12 \\ \partial_r G21 & \partial_r G22 \end{pmatrix} . \begin{pmatrix} \alpha_1^I & \alpha_1^{II} \\ \alpha_2^I & \alpha_2^{II} \end{pmatrix} + \begin{pmatrix} G11 & G12 \\ G21 & G22 \end{pmatrix} . \begin{pmatrix} \partial_r\alpha_1^I & \partial_r\alpha_1^{II} \\ \partial_r\alpha_2^I & \partial_r\alpha_2^{II} \end{pmatrix} = \begin{pmatrix} \partial_r\beta_1^I & \partial_r\beta_1^{II} \\ \partial_r\beta_2^I & \partial_r\beta_2^{II} \end{pmatrix}
$$

or,

$$
A\begin{pmatrix} \partial_r G_{11} & \partial_r G_{12} \\ \partial_r G_{21} & \partial_r G_{22} \end{pmatrix} . \begin{pmatrix} \alpha_1^I & \alpha_1^{II} \\ \alpha_2^I & \alpha_2^{II} \end{pmatrix} = A\begin{pmatrix} \partial_r\beta_1^I & \partial_r\beta_1^{II} \\ \partial_r\beta_2^I & \partial_r\beta_2^{II} \end{pmatrix} - \begin{pmatrix} G_{11} & G_{12} \\ G_{21} & G_{22} \end{pmatrix} .A\begin{pmatrix} \partial_r\alpha_1^I & \partial_r\alpha_1^{II} \\ \partial_r\alpha_2^I & \partial_r\alpha_2^{II} \end{pmatrix}
$$

Here, we have multiplied by $A = r^2\sqrt{f}$. Now using equations (C.16) and (C.19), as set I, we have

$$
L.H.S = A.\begin{pmatrix} \partial_r G_{11}.\alpha_1^I + \partial_r G_{12}.\alpha_2^I & \partial_r G_{11}.\alpha_1^{II} + \partial_r G_{12}.\alpha_2^{II} \\ \partial_r G_{21}.\alpha_1^I + \partial_r G_{22}.\alpha_2^I & \partial_r G_{21}.\alpha_1^{II} + \partial_r G_{22}.\alpha_2^{II} \end{pmatrix} \qquad \text{(C.21)}
$$

and

$$R.H.S = \begin{pmatrix} (v_+ - k_x)\alpha_1^I - mr\beta_1^I + k_y\alpha_2^I & (v_+ - k_x)\alpha_1^{II} - mr\beta_1^{II} + k_y\alpha_2^{II} \\ \\ (v_- + k_x)\alpha_2^I - mr\beta_2^I + k_y\alpha_1^I & (v_- + k_x)\alpha_2^{II} - mr\beta_2^{II} + k_y\alpha_1^{II} \end{pmatrix}$$
$$- \begin{pmatrix} G_{11} & G_{12} \\ G_{21} & G_{22} \end{pmatrix} . \begin{pmatrix} (-v_- - k_x)\beta_1^I + mr\alpha_1^I + k_y\beta_2^I & (-v_- - k_x)\beta_1^{II} + mr\alpha_1^{II} + k_y\beta_2^{II} \\ \\ (-v_+ + k_x)\beta_2^I + mr\alpha_2^I + k_y\beta_1^I & (-v_+ + k_x)\beta_2^{II} + mr\alpha_2^{II} + k_y\beta_1^{II} \end{pmatrix} \tag{C.22}$$

Define the following non-vanishing ratio

$$G_{11} = \frac{\beta_1^I}{\alpha_1^I} \ , \quad G_{12} = \frac{\beta_1^{II}}{\alpha_2^{II}} \ , \quad G_{21} = \frac{\beta_2^I}{\alpha_1^I} \ , \quad G_{22} = \frac{\beta_2^{II}}{\alpha_2^{II}} \ .$$

Equating the elements of matrices, we proceed as follows:

First diagonal element, let's call a_{11}

$$\begin{aligned} A.\Big[\partial_r G_{11}.\alpha_1^I + \partial_r G_{12}.\alpha_2^I\Big] =& (v_+ - k_x)\alpha_1^I - mr\beta_1^I + k_y\alpha_2^I - G_{11}\Big[(-v_- - k_x)\beta_1^I + mr\alpha_1^I + k_y\beta_2^I\Big] \\ & - G_{12}\Big[(-v_+ + k_x)\beta_2^I + mr\alpha_2^I + k_y\beta_1^I\Big] \end{aligned}$$

First off diagonal element, a_{12}

$$\begin{aligned} A.\Big[\partial_r G_{11}.\alpha_1^{II} + \partial_r G_{12}.\alpha_2^{II}\Big] =& (v_+ - k_x)\alpha_1^{II} - mr\beta_1^{II} + k_y\alpha_2^{II} - G_{11}\Big[(-v_- - k_x)\beta_1^{II} + mr\alpha_1^{II} + k_y\beta_2^{II}\Big] \\ & - G_{12}\Big[(-v_+ + k_x)\beta_2^{II} + mr\alpha_2^{II} + k_y\beta_1^{II}\Big] \end{aligned}$$

Second off diagonal element, a_{21}

$$\begin{aligned} A.\Big[\partial_r G_{21}.\alpha_1^I + \partial_r G_{22}.\alpha_2^I\Big] =& (v_- + k_x)\alpha_2^I - mr\beta_2^I + k_y\alpha_1^I - G_{21}\Big[(-v_- - k_x)\beta_1^I + mr\alpha_1^I + k_y\beta_2^I\Big] \\ & - G_{22}\Big[(-v_+ + k_x)\beta_2^I + mr\alpha_2^I + k_y\beta_1^I\Big] \end{aligned}$$

Second diagonal element, a_{22}

$$\begin{aligned} A.\Big[\partial_r G_{21}.\alpha_1^{II} + \partial_r G_{22}.\alpha_2^{II}\Big] =& (v_- + k_x)\alpha_2^{II} - mr\beta_2^{II} + k_y\alpha_1^{II} - G_{21}\Big[(-v_- - k_x)\beta_1^{II} + mr\alpha_1^{II} + k_y\beta_2^{II}\Big] \\ & - G_{22}\Big[(-v_+ + k_x)\beta_2^{II} + mr\alpha_2^{II} + k_y\beta_1^{II}\Big] \end{aligned}$$

When using the ratios given above, taking into account that other possible ratios are equal zero then we have

$$\begin{aligned} a_{11} \implies A\partial_r G_{11} = (v_+ - k_x) - mr\,G_{11} - G_{11}\Big[(-v_- - k_x)G_{11} + mr + k_y G_{21}\Big] \\ - G_{12}\Big[(-v_+ + k_x)G_{21} + k_y G_{11}\Big] \end{aligned} \tag{C.23}$$

$$\begin{aligned} a_{12} \implies A\partial_r G_{12} = -mr\,G_{12} + k_y - G_{11}\Big[(-v_- - k_x)G_{12} + k_y G_{22}\Big] \\ - G_{12}\Big[(-v_+ + k_x)G_{22} + mr + k_y G_{12}\Big] \end{aligned} \tag{C.24}$$

$$\begin{aligned} a_{21} \implies A\partial_r G_{21} = -mr\,G_{21} + k_y - G_{21}\Big[(-v_- - k_x)G_{11} + mr + k_y G_{21}\Big] \\ - G_{22}\Big[(-v_+ + k_x)G_{21} + k_y G_{11}\Big] \end{aligned} \tag{C.25}$$

$$\begin{aligned} a_{22} \implies A\partial_r G_{22} = (v_- + k_x) - \frac{r}{L} m G_{22} - G_{21}\Big[(-v_- - k_x)G_{12} + k_y G_{22}\Big] \\ - G_{22}\Big[(-v_+ + k_x)G_{22} + mr + k_y G_{12}\Big] \end{aligned} \tag{C.26}$$

Grouping back into matrix form, we get

$$\begin{aligned} r^2\sqrt{f}\begin{pmatrix} \partial_r G_{11} & \partial_r G_{12} \\ \partial_r G_{21} & \partial_r G_{22} \end{pmatrix} = -2mr\begin{pmatrix} G_{11} & G_{12} \\ G_{21} & G_{22} \end{pmatrix} + \begin{pmatrix} (v_+ - k_x) & k_y \\ k_y & (v_- + k_x) \end{pmatrix} \\ - \begin{pmatrix} a_{11} = G_{11}\Big[(-v_- - k_x)G_{11} + k_y G_{21}\Big] + G_{12}\Big[(-v_+ + k_x)G_{21} + k_y G_{11}\Big] \\ a_{12} = G11\Big[(-v_- - k_x)G_{12} + k_y G_{22}\Big] + G_{12}\Big[(-v_+ + k_x)G_{22} + k_y G_{12}\Big] \\ a_{21} = G_{21}\Big[(-v_- - k_x)G_{11} + k_y G_{21}\Big] + G_{22}\Big[(-v_+ + k_x)G_{21} + k_y G_{11}\Big] \\ a_{22} = G_{21}\Big[(-v_- - k_x)G_{12} + k_y G_{22}\Big] + G_{22}\Big[(-v_+ + k_x)G_{22} + k_y G_{12}\Big] \end{pmatrix} \end{aligned} \tag{C.27}$$

On further simplification, we have

$$r^2\sqrt{f}\begin{pmatrix}\partial_r G_{11} & \partial_r G_{12}\\ \partial_r G_{21} & \partial_r G_{22}\end{pmatrix} = -2mr\begin{pmatrix}G_{11} & G_{12}\\ G_{21} & G_{22}\end{pmatrix} + \begin{pmatrix}(v_+ - k_x) & k_y\\ k_y & (v_- + k_x)\end{pmatrix}$$
$$- \begin{pmatrix}G_{11} & G_{12}\\ G_{21} & G_{22}\end{pmatrix}\cdot\begin{pmatrix}(-v_- - k_x) & k_y\\ k_y & (-v_+ + k_x)\end{pmatrix}\cdot\begin{pmatrix}G_{11} & G_{12}\\ G_{21} & G_{22}\end{pmatrix} \tag{C.28}$$

Finally, we get the desired equation (3.18)

$$r^2\sqrt{f}\,\partial_r G + 2m\,r\,G = M_+ - GM_-G\ , \tag{C.29}$$

where

$$M_\pm = \begin{pmatrix}\pm v_\pm - k_x & k_y\\ k_y & \pm v_\mp + k_x\end{pmatrix}\ .$$

C.2 AdS$_2$ for Fermi arcs model-A

Since bulk scalar field condensates below the critical temperature which is very small, the black hole near horizon geometry can be approximated as AdS_2. With this assumption we derive the boundary Green's function considering the horizon value of the scalar field to be temperature dependent and show the evolution of Fermi arc with temperature. Therefore, we begin by expanding the equation (3.14) in the near horizon limit and focus only the effects of scalar field. Near the horizon$(r = 1)$, $f(r) \approx 6(r-1)^2$, $A_t \approx \mu(r-1)$, also we will set $L = 1$. Thus we arrive with the equation given by

$$\chi\partial_\chi\psi_I = L_2\left[\sigma_3 m + (-1)^I\sigma_1 m_k\right]\psi_I - i\sigma_2\left(\chi + q\mu L_2^2\right)\psi_I - \sigma_1 k_y L_2\psi_J, \tag{C.30}$$

with $m_k = (\Phi(r_0)\mu - k_x)$ and usual scaling given by $\chi = \kappa\frac{\omega L_2^2}{(r-1)}$. Here we note the dependence of effective mass m_k on the horizon value of the scalar field which in turn will be dependent upon the black hole temperature.

In the low frequency limit $\chi \to 0$, equation (C.30) becomes

$$\chi \partial_\chi \psi_I = L_2 \left[\sigma_3 m + (-1)^I \sigma_1 m_k\right] \psi_I - i\sigma_2 q e_d \psi_I - \sigma_1 k_y L_2 \psi_J, \tag{C.31}$$

where, L_2 is the AdS_2 radius given by $L_2{=}\frac{1}{\sqrt{6}}$ and $\mu L_2^2 = e_d$. Further we can write the above equation in a matrix form as

$$\chi \partial_\chi \psi = U\psi. \tag{C.32}$$

Here U is a real constant matrix, with ψ written as $(\psi_1, \psi_2)^T$. The exact form of the matrix is given by

$$U = \begin{pmatrix} mL_2 & -m_k L_2 - qe_d & 0 & -k_y L_2 \\ -m_k L_2 + qe_d & -mL_2 & -k_y L_2 & 0 \\ 0 & -k_y L_2 & mL_2 & m_k L_2 - qe_d \\ -k_y L_2 & 0 & m_k L_2 + qe_d & -mL_2 \end{pmatrix}.$$

Also U is a matrix with four eigenvalues $\mp\lambda^I$ (I=1,2). Note that there are two eigenvalues with negative sign for first I component and positive sign for second component with $\lambda = \sqrt{m^2 L_2^2 + m_k^2 L_2^2 + k_y^2 L_2^2 - q^2 e_d^2}$. The presence of non zero k_y in this case changes the dimension of the IR CFT operator.

When block diagonalise equation (C.30) we can write as

$$\left[\chi \partial_\chi + i\sigma_2 \left(\chi + qe_d\right) - (-1)^I u_k \sigma_1\right] \psi_{1,2} = 0 \tag{C.33}$$

with $u_k = L_2 \sqrt{m^2 + (\Phi_0 \mu - k_x)^2 + k_y^2}$. Since in equation (C.30) we have a mixing of four spinors, therefore by following the well known methods in [66, 104] the retarded AdS_2 Green's function is expressed as

$$\begin{aligned} \mathcal{G}_R(\omega, k) =& e^{-i\pi\nu_k} \frac{\Gamma(-2\nu_k)\Gamma(1+\nu_k - iqe_d)}{\Gamma(2\nu_k)\Gamma(1-\nu_k - iqe_d)} \\ & \times \frac{(m - iu_k)L_2 - \nu_k - iqe_d}{(m - iu_k)L_2 + \nu_k - iqe_d} (2\omega)^{2\nu_k}. \end{aligned} \tag{C.34}$$

where,

$$\nu_k = \sqrt{m^2 L_2^2 + m_k^2 L_2^2 + k_y^2 L_2^2 - q^2 e_d^2}$$

ν_k plays the role of conformal dimension of dual infrared conformal field theory operator. One can generalise for the finite temperature AdS$_2$ Green's function as in appendix C.4. But the operator dimension ν_k would still have the same form . Further it is important see that the dimension is dependent on the temperature through the scalar field condensation, which is related to the scalar field horizon value $\Phi(r_0)$. To construct the AdS_4 Green's function one needs to match the solutions in AdS_2 usually called inner region and AdS_4 called outer region at their common boundary.

C.3 Details calculations for model-B

With the Fermions action given in (3.9)

$$\mathcal{S}^{(2)}_{Fermion} = \int d^4x \sqrt{-g} i\bar{\psi}\left(\not{D} - m - ip\Phi\not{F}\right)\psi \tag{C.35}$$

where,

$$\begin{aligned} \not{D} =& e^{\mu}_{c}\Gamma^{c}\left(\partial_\mu + \omega^{ab}_{\mu}\Gamma_{ab} - iqA_\mu\right) \\ \not{F} =& \frac{1}{2}\Gamma^{ab}e^{\mu}_{a}e^{\nu}_{b}F_{\mu\nu}. \end{aligned} \tag{C.36}$$

The parameter p is a Pauli coupling, $e^{\mu}_{a}, \omega^{ab}_{\mu}$ are vielbeins and spin connection. Here, $\{a, b\}$ are tangent space indices and $\{\mu, \nu\}$ are for the bulk. Simplifying the Dirac equation from the above action with appropriate choice of gamma matrices, followed by rescaling $\psi(r, \vec{x_i}) = (-gg^{rr})^{-\frac{1}{4}} e^{-i\omega t + ik.x}\tilde{\psi}(r, k)$ and rewrite $\tilde{\psi} = (\tilde{\psi}_1, \tilde{\psi}_2)^T$, because of symmetry we can also set $k_y = 0$, then we have the following equation

$$\begin{aligned} r^2\sqrt{f(r)}\partial_r\tilde{\psi}_I =& \frac{i\sigma_2}{\sqrt{f(r)}}\left(\omega + q\mu\left(1 - \frac{r_0}{r}\right)\right)\tilde{\psi}_I \\ &- \sigma_3 m r\tilde{\psi}_I - \sigma_1\left(p\Phi(r)\mu\frac{r_0}{r} \pm k_x\right)\tilde{\psi}_I. \end{aligned} \tag{C.37}$$

for $I \,\epsilon\, \{1,2\}$. We can further write $\tilde{\psi}_I = (\beta_I, \alpha_I)^T$ and define the ratios $\zeta_\pm = (\beta_{1,2}/\alpha_{1,2})$, from equation (C.37), we get the following flow equation

$$r^2\sqrt{f}\partial_r\zeta_\pm + 2m\,r\zeta_\pm - (X_- \mp k) - (X_+ \pm k)\zeta_\pm^2 = 0 \tag{C.38}$$

where,

$$X_\pm = \frac{1}{\sqrt{f}}\left(\omega + q\mu(1-\frac{1}{r})\right) \pm \frac{p\Phi\,\mu r_0}{r}$$

Finally the Green's function is given by

$$G_R(\omega,k) = \lim_{r\to\infty}\frac{1}{r^{2m}}\begin{pmatrix}\zeta_+ & 0\\ 0 & \zeta_-\end{pmatrix} \tag{C.39}$$

with in-falling boundary conditions at horizon for $\omega \neq 0$ as $\zeta_\pm(r=1) = i$. We will define the spectral function as

$$A(\omega,k) \;=\; Tr\left[Im\left(G_R(\omega,k_x)\right)\right]. \tag{C.40}$$

C.4 Finite temperature AdS_2 Green's function

For finite temperature the $\mathrm{AdS}_2 \times S^2$ metric is given by

$$ds^2 \;=\; \frac{L_2^2}{\zeta^2}\left(-f(\zeta)d\tau^2 + \frac{d\zeta^2}{f(\zeta)}\right) + \frac{r_*^2}{L^2}d\vec{x}^2 \quad, A_\tau \;=\; \frac{e_d}{\zeta}\left(1-\frac{\zeta}{\zeta_0}\right)d\tau$$

where, $f(\zeta) \;=\; 1-\frac{\zeta^2}{\zeta_0^2}$. Now the Dirac equation obtained from C.35 with this metric becomes

$$\partial_\zeta\,\tilde{\Psi} - \frac{i\sigma_2(\omega+qA_\tau)}{f(\zeta)}\,\tilde{\Psi} \;=\; \frac{L_2}{\zeta\,f(\zeta)}\left(m_{k\pm}\sigma_1 + m\sigma_3\right)\,\tilde{\Psi}\;. \tag{C.41}$$

where,$m_{k\pm} \;=\; \sqrt{3}p\,\Phi(r_0) \pm\, k\,.$

Now this equation is exactly the equation in [66], and solution is given by

$$\mathcal{G}_R(\omega, T) = (4\pi T)^{2\nu_k} c_{k\pm} \tag{C.42}$$

where

$$c_{k\pm} = \frac{\Gamma(-2\nu_{k\pm})}{\Gamma(2\nu_{k\pm})} \frac{\Gamma(1+\nu_{k\pm} - iqe_d)}{\Gamma(1-\nu_{k\pm} - iqe_d)} \frac{\Gamma(\frac{1}{2}+\nu_{k\pm} - \frac{i\omega}{2\pi T} + iqe_d)}{\Gamma(\frac{1}{2}-\nu_{k\pm} - \frac{i\omega}{2\pi T} + iqe_d)} \frac{(m - im_{k\pm})L_2 - iqe_d - \nu_{k\pm}}{(m - im_{k\pm})L_2 - iqe_d + \nu_{k\pm}} \tag{C.43}$$

Now, the conformal dimension of the operators in the IR $= \nu_{k\pm} + \frac{1}{2}$, with $\nu_{k\pm}$ given by

$$\nu_{k\pm} = \sqrt{m^2 L_2^2 + m_{k\pm}^2 L_2^2 - q^2 e_d^2 - i\epsilon}$$

Appendix D

Appendix to Chapter 4

D.1 Derivation of Equations of motion for Q-lattice

We will show how to use the `EDCRGTCcode.m` package in `Mathematica`. Beginning from equation 4.2 with the chosen ansatz 4.3, one can implement the package as follows:

```
In[14]:= Unprotect[Laplacian];
         << EDCRGTCcode.m;
         xIN = {z, t, x, y}; (* coordinates *)

         g = 1/z^2*DiagonalMatrix[{1/U[z], -U[z], V1[z], V2[z] }];  (*Metric ansatz*)
```

Then run the following line

```
In[15]:= RGtensors[g, xIN];
```

This will compute the tensors such as Riemann and Einstein tensor, Ricci tensor and Ricci scalar, Christoffel symbols etc. First let us set up the Maxwell's field $F_{\mu\nu} = \partial_\mu A_\nu - \partial_\nu A_\mu$.

```
In[16]:=        Ad = {0, At[z], 0, 0};
                AU = Raise[Ad, 1];

                A2 = multiDot[AU, Ad, {1, 1}];

                Fdd = -covD[Ad] + Transpose[covD[Ad]];
                FUU = Raise[Fdd, 1, 2];
                FdU = Raise[Fdd, 2];
                FUd = Raise[Fdd, 1];

                F2 = multiDot[Fdd, FUU, {1, 1}, {2, 2}];
```

where in the above lines, Ad = A_μ, AU = A^μ, A2 = $A^\mu A_\mu$, Fdd = $F_{\mu\nu}$, FUU = $F^{\mu\nu}$, FdU = $F_\mu{}^\nu$, FUd = F^μ_ν and F2 = $F_{\mu\nu}F^{\mu\nu}$. Now for the scalar field $\phi = e^{ik\,x}\chi(z)$:

```
In[17]:= T = k x; X = chi[z];
```

```
dthed = covD[T];
dchid = covD[X];

Dthe2 = multiDot[ Raise[dthed , 1] , dthed , {1, 1} ];

Dchi2 = multiDot[ Raise[dchid , 1] , dchid , {1, 1} ];
```

Now the stress tensor $T_{\mu\nu}$

```
In[18]:= tchidd = Outer[Times, covD[X], covD[X]] - 1/2 gdd* multiDot[Raise[covD[X], 1], covD[X], {1, 1}] - m/2 gdd X^2;

         thedd = X^2 Outer[Times, covD[T], covD[T]] - 1/2 X^2 gdd* multiDot[Raise[covD[T], 1], covD[T], {1, 1}];

         tlattdd = ( tchidd + thedd  );
```

Einstein equations:

```
In[19]:= Einsdd = Rdd - 1/2 R gdd - 3 gdd  - tlattdd - 1/2 (multiDot[Fdd, FdU, {2, 2}] - 1/4 F2 gdd ) ;

         EinsUd = Raise[Einsdd, 1];
```

Klein-Gordon equation for the scalar field

```
In[20]:= KGchi = covDiv[Raise[covD[X], 1], {1}] - X Dthe2 - m X ;
         KGthe = X covDiv[Raise[covD[T], 1], {1}]  + 2 multiDot[  dchid , Raise[dthed , 1] , {1, 1}];
```

Maxwell equation

```
In[21]:= EU = covDiv[FUU, {2, {1}}];
```

Simplification to get the five ODEs :

```
In[22]:= e1aux = Simplify[ KGchi];
         e2aux = Simplify[ EU[[2]] ];
         e3aux = Simplify[  Einsdd[[1, 1]] ];
         e4aux = Simplify[ Einsdd[[2, 2]] ];
         e5aux = Simplify[ Einsdd[[3, 3]] ];
         e6aux  = Simplify[ Einsdd[[4, 4]] ];

         vars = {(chi''[r], V1''[r], V2''[r], U''[r],At''[r], chi'[r], chi[r], U'[r], U[r],
                V1'[r], V1[r], V2'[r], V2[r], At'[r]} /. r -> z;

         Collect[ 1/U[z] e1aux , vars, Simplify] ; (*eqn for chi*)
```

```
Collect[- e2aux, vars, Simplify]  (*eqn for At*)

Collect[  e3aux , vars, Simplify]  (*eqn for U*)

Collect[ g4 e4aux + g5 e5aux + g6 e6aux /.{g4 -> -(V1[z]/U[z]^2),g5 -> -(1/U[z]), g6 -> V1[z]/(U[z] V2[z])},
vars, Simplify ]        (*eqn for V1*)

Collect[ g4 e4aux + g5 e5aux + g6 e6aux /.{g4 -> -(V2[z]/U[z]^2),g5 -> V2[z]/(U[z] V1[z]), g6 -> -(1/U[z])},
 vars, Simplify ]  (*eqn for V2*)

                  (* ---------------------------------------------------------------------------*)
```

Bibliography

[1] J. M. Maldacena, *The Large N limit of superconformal field theories and supergravity*, *Int. J. Theor. Phys.* **38** (1999) *Adv. Theor. Math. Phys.***2** (1998) 231

[2] E. Witten, "Anti-de Sitter space and holography," Adv. Theor. Math. Phys. **2**, 253-291 (1998)

[3] H. Liu, J. McGreevy and D. Vegh, *Non-Fermi liquids from holography*, *Phys. Rev. D* **83** (2011) 065029,

[4] S. A. Hartnoll, "Lectures on holographic methods for condensed matter physics," Class. Quant. Grav. **26**, 224002 (2009)

[5] G. Vanacore, S. T. Ramamurthy and P. W. Phillips, *Evolution of Holographic Fermi Arcs from a Mott Insulator*, *JHEP* **1809** (2018) 009,

[6] S. Chakrabarti, D. Maity and W. Wahlang, "Probing the Holographic Fermi Arc with scalar field: Numerical and analytical study," JHEP **07**, 037 (2019) doi:10.1007/JHEP07(2019)037

[7] S. Chakrabarti, D. Maity and W. Wahlang, "Studying the holographic Fermi surface in the scalar induced anisotropic background," doi:10.1016/j.physletb.2022.136990

[8] W. Wahlang, "Evolution of holographic Fermi surface from non-minimal couplings," [arXiv:2112.05097 [hep-th]].

[9] S. Chakrabarti, D. Maity and W. Wahlang, "A note on the effects of magnetic field on holographic fermions with dipole-like coupling," [arXiv:2204.06756 [hep-th]].

[10] A. Donos and J. P. Gauntlett, "Holographic Q-lattices," JHEP **04** (2014), 040

[11] M. Edalati, R. G. Leigh and P. W. Phillips, *Dynamically Generated Mott Gap from Holography*, *Phys. Rev. Lett.* **106** (2011) 091602,

[12] M. Edalati, R. G. Leigh, K. W. Lo and P. W. Phillips, *Dynamical Gap and Cuprate-like Physics from Holography*, Phys. Rev. D **83** (2011)

[13] G. Vanacore and P. W. Phillips, "Minding the Gap in Holographic Models of Interacting Fermions," Phys. Rev. D **90** (2014) no.4, 044022

[14] J. Alsup, E. Papantonopoulos, G. Siopsis, K. Yeter, *Duality between zeroes and poles in holographic systems with massless fermions and a dipole coupling,Phys. Rev. D* **90** (2014) 126013, 10.1103/PhysRevD.90.126013.

[15] J. M. Luttinger, *Fermi Surface and Some Simple Equilibrium Properties of a System of Interacting Fermions,Phys. Rev.* **119** 1153 (1960).

[16] T. Faulkner, N. Iqbal, H. Liu, J. McGreevy and D. Vegh, "From Black Holes to Strange Metals," [arXiv:1003.1728 [hep-th]].

[17] Charles Kittel, "Introduction to Solid State Physics", 8th Edition, *John Wiley & Sons, Inc* (2004)

[18] Henrik Bruus, Karsten Flensberg - "Many-Body Quantum Theory in Condensed Matter Physics", *Oxford University Press* (2016)

[19] K. S. Bedell (Ed.) Strongly Correlated Electronic Materials, Addison Wesley, New York (1989).

[20] C. M. Varma, P. B. Littlewood, et al. Phenomenology of the normal state of Cu-O high-temperature superconductors . *Phys. Rev. Lett.* **63**, (1996). `https://doi.org/10.1103/PhysRevLett.63.1996`

[21] C. M. Varma, Abrahams Elihu, What angle-resolved photoemission experiments tell about the microscopic theory for high-temperature superconductors. *PNAS* **97**, (2000). `https://doi.org/10.1073/pnas.100118797`

[22] J. Bardeen, L. N. Cooper, and J. R. Schrieffer, Theory of Superconductivity . *Phys. Rev.* **108**, (1957). `https://doi.org/10.1103/PhysRev.108.1175`

[23] J. Zaanen, Y-W Sun, and Y. Liu and K. Schalm, *Holographic duality in Condensed Matter Physics*; *Cambridge Univ. Press* (2015)

[24] Andrea Damascelli, Zhi-Xun Shen, and Zahid Hussain. Angle-resolved photoemission spectroscopy of the cupratesuperconductors. *Rev. Mod. Phys.* **75**, 473, 2003. 10.1103/RevModPhys.75.473

[25] I. M. Vishik, Photoemission perspective on pseudogap, superconducting fluctuations, and charge order in cuprates, *Reports on Progress in Physics* **81**, `https://doi.org/10.1088/1361-6633/aaba96`

[26] Lv, B., Qian, T. & Ding, H. Angle-resolved photoemission spectroscopy and its application to topological materials. *Nat Rev Phys* **1**, 609–626 (2019). `https://doi.org/10.1038/s42254-019-0088-5`

[27] Ding, H., Yokoya, T., et al. Spectroscopic evidence for a pseudogap in the normal state of underdoped high-Tc superconductors. *Nature* **382**, 51–54 (1996). `https://doi.org/10.1038/382051a0`

[28] Norman, M., Ding, H., Randeria, M. et al. Destruction of the Fermi surface in underdoped high-Tc superconductors. *Nature* **392**, 157–160 (1998). `https://doi.org/10.1038/32366`

[29] Kanigel, A., Norman, M., Randeria, M. et al. Evolution of the pseudogap from Fermi arcs to the nodal liquid. *Nature Phys* **2**, 447–451 (2006). `https://doi.org/10.1038/nphys334`

[30] Su-Yang Xu, Chang Liu et al. Observation of Fermi arc surface states in a topological metal. *Science.* **347**, (2015).

[31] Miao, H., Fabbris et al., Charge density waves in cuprate superconductors beyond the critical doping, *npj Quantum Mater*, **6**, 31 (2021), `https://doi.org/10.1038/s41535-021-00327-4`

[32] Hawking, S. Black holes explosion?. *Nature*, **248**,(1974)

[33] J.D Bekenstein, Black Holes and Entropy. *Phys. Rev. D*, **6**,(1973), `https://link.aps.org/doi/10.1103/PhysRevD.7.2333`

[34] S. W. Hawking, Particle creation by black holes. *Commun. Math. Phys*, **43**,(1975),

[35] G. 't Hooft, "Dimensional reduction in quantum gravity," Conf. Proc. C **930308** (1993)

[36] L. Susskind, "The World as a hologram," J. Math. Phys. **36** (1995)

[37] R. Bousso, The holographic principle, *Rev. Mod. Phys.*, **74**,3(2002), `https://link.aps.org/doi/10.1103/RevModPhys.74.825`

[38] G. T. Horowitz, J. E. Santos and D. Tong, "Optical Conductivity with Holographic Lattices," *JHEP* **07** (2012), 168

[39] G. T. Horowitz, J. E. Santos and D. Tong, "Further Evidence for Lattice-Induced Scaling," *JHEP* **11** (2012), 102

[40] G. T. Horowitz and J. E. Santos, "General Relativity and the Cuprates," *JHEP* **06** (2013), 087

[41] A. Donos and S. A. Hartnoll, "Interaction-driven localization in holography," *Nature Phys.* **9** (2013), 649-655

[42] S. S. Gubser, J. Ren, *Analytic fermionic Green's functions from holography , PhysRevD* **86** (2012).

[43] Makoto Natsuume, AdS/CFT Duality User Guide, *Lect. Notes Phys.*, 903:pp.1–294, 2015.

[44] H. Nastase, Introduction to AdS/CFT Correspondence,. *Cambridge University Press*, 2015.

[45] A. Zaffaroni. Introduction to the AdS-CFT correspondence. *Class. Quant. Grav.*, 17:3571–3597, 2000.

[46] A. V. Ramallo, "Introduction to the AdS/CFT correspondence," *Springer Proc. Phys.* **161** (2015), 411-474

[47] W. Muck, "Studies on the AdS/CFT correspondence," Thesis, *SIMON FRASER UNIVERSITY*

[48] C. Charmousis, E. Papantonopoulos, "From Gravity to Thermal Gauge Theories: The AdS/CFT Correspondence," *Springer* , (2011)

[49] M. Hanada, Y. Hyakutake, G. Ishiki and J. Nishimura, "Holographic description of quantum black hole on a computer," Science **344** (2014), 882-885

[50] Katrin Becker , Melanie Becker , and John H. Schwarz, "String Theory and M-Theory: A Modern Introduction," *Cambridge U. Press, New York* , (2007)

[51] S.S. Gubser, I.R. Klebanov, A.M. Polyakov, "Gauge theory correlators from non-critical string theory," *Physics Letters B* ,**428** (1998)

[52] K. Skenderis, "Lecture notes on holographic renormalization," *Class. Quant. Grav.* **19**, 5849 (2002)

[53] S. de Haro, S. N. Solodukhin and K. Skenderis, “Holographic reconstruction of spacetime and renormalization in the AdS / CFT correspondence,” *Commun. Math. Phys.* **217**, 595 (2001)

[54] M. Henningson and K. Skenderis, *JHEP* **9807**, 023 (1998) doi:10.1088/1126-6708/1998/07/023

[55] D. T. Son and A. O. Starinets, “Minkowski space correlators in AdS / CFT correspondence: Recipe and applications,” JHEP **09** (2002), 042

[56] M. Baggioli, “Applied Holography : A Practical Mini-Course,” doi:10.1007/978-3-030-35184-7

[57] Hong Liu. 8.821 String Theory and Holographic Duality. Fall 2014. https://ocw.mit.edu. License: Creative Commons BY-NC-SA.

[58] Mans Henningson and Konstadinos Sfetsos. Spinors and the AdS / CFT correspondence. *Phys. Lett. B*, **431**, 1998.

[59] W.Muck and K.S.Viswanathan Conformal field theory correlators from classical field theory on anti–de Sitter space: Vector and spinor fields. *Phys. Rev. D*, **58**, 1998.

[60] M. Henneaux, “Boundary terms in the AdS/CFT correspondence for spinor fields,” arXiv:hep-th/9902137.

[61] N. Iqbal and H. Liu, “Real-time response in AdS/CFT with application to spinors,” *Fortsch. Phys.* **57** (2009), 367-384

[62] Z. Li, E. Henriksen, Z. Jiang , “Dirac charge dynamics in graphene by infrared spectroscopy”, *Nature Phys* **4** (2008), `https://doi.org/10.1038/nphys989`

[63] Marel, D., Molegraaf, H., Zaanen, J. et al , “Quantum critical behaviour in a high-Tc superconductor”, *Nature* **425** (2003), `https://doi.org/10.1038/nature01978`

[64] T. Faulkner, G. T. Horowitz, J. McGreevy, M. M. Roberts and D. Vegh, *Photoemission ‘experiments’ on holographic superconductors*, *JHEP* **1003** (2010) 121

[65] S. Bhattacharyya, V. E. Hubeny, S. Minwalla and M. Rangamani, *Nonlinear Fluid Dynamics from Gravity*, *JHEP* **0802** (2008) 045

[66] T. Faulkner, H. Liu, J. McGreevy and D. Vegh, *Emergent quantum criticality, Fermi surfaces, and AdS(2)*, *Phys. Rev. D.* **83** (2011) 125002.

[67] M. Cubrovic, J. Zaanen and K. Schalm, *String Theory, Quantum Phase Transitions and the Emergent Fermi-Liquid*, *Science* **325** (2009) 439.

[68] C. P. Herzog, P. Kovtun, S. Sachdev and D. T. Son, *Quantum critical transport, duality, and M-theory*, *Phys. Rev. D.* **75** (2007) 085020

[69] S. A. Hartnoll, C. P. Herzog and G. T. Horowitz, *Building a Holographic Superconductor*, *Phys. Rev. Lett.* **101** (2008) 031601.

[70] S. A. Hartnoll, C. P. Herzog and G. T. Horowitz, *Holographic Superconductors*, JHEP **0812** (2008) 015.

[71] G. T. Horowitz, *Introduction to Holographic Superconductors*, *Lect. Notes Phys.* **828** (2011) 313.

[72] C. P. Herzog, *Lectures on Holographic Superfluidity and Superconductivity*, *J. Phys. A* **42** (2009) 343001.

[73] J. McGreevy, *Holographic duality with a view toward many-body physics*, *Adv. High Energy Phys.* **2010** (2010) 723105.

[74] S. A. Hartnoll, A. Lucas and S. Sachdev, *Holographic Quantum Matter*; *MIT Press* (2018)

[75] S. S. Lee, *A Non-Fermi Liquid from a Charged Black Hole: A Critical Fermi Ball*, *Phys. Rev. D* **79** (2009) 086006.

[76] J. G. Bednorz and K. A. Muller, *Possible high Tc superconductivity in the Ba-La-Cu-O system*, *Z. Phys. B* **64** (1986) 189.

[77] A. Damascelli, Z. Hussain and Z.-X. Shen, *Angle-resolved photoemission studies of the cuprate superconductors*, *Rev. Mod. Phys.* **75** (2003) 473.

[78] M. R. Norman et.al.,*Destruction of the Fermi surface in underdoped high-T_c superconductors*, *Nature* 392 (1998) 157

[79] T. Yoshida et.al., *Doping Evolution of the Underlying Fermi Surface in $La_{2-x}Sr_xCuO_4$*, *Phys. Rev. B* **74** (2006) 224510

[80] P. D. C. King et.al., *Structural origin of apparent Fermi surface pockets in angle-resolved photoemission of* $Bi_2Sr_{2-x}La_xCuO_{6+\delta}$, *Phys. Rev. Lett.* **106** (2011) 127005

[81] S. Cremonini, L. Li and J. Ren, "Holographic Fermions in Striped Phases," JHEP **1812**, 080 (2018)

[82] Y. Seo, G. Song, Y. H. Qi and S. J. Sin, "Mott transition with Holographic Spectral function," JHEP **1808** (2018) 077

[83] Y. Wu et.al.,*Fragility of Fermi arcs in Dirac semimetals*, *Phys. Rev. B* **99** (2019).

[84] Yang, L., Liu, Z., Sun, Y. et al. *Weyl semimetal phase in the non-centrosymmetric compound TaAs. Nature Phys* **11**, 728-732 (2015).

[85] Eric Brillaux and Andrei A. Fedorenko, *Fermi arcs and surface criticality in dirty Dirac materials*, arXiv:2009.12138 [cond-mat.mes-hall].

[86] Su-Yang Xu et al., *Discovery of a Weyl Fermion semimetal and topological Fermi arcs* , *Science***349**, (2015) 613.

[87] M. Kargarian, M. Randeria and Y-Mi Lu, *Are the surface Fermi arcs in Dirac semimetals topologically protected?* , *PNAS***113** (2016) 8648.

[88] M. Z. Hasan and C. L. Kane, *Colloquium: Topological insulators*, *Rev. Mod. Phys.***82** (2010) 3045.

[89] B. Yan and C. Felser, *Topological Materials: Weyl Semimetals*, *Ann. Rev. Cond. Matt. Phys.***8** (2017) 337.

[90] X. Wan, A. M. Turner, A. Vishwanath, and S. Y. Savrasov, *Topological semimetal and Fermi-arc surface states in the electronic structure of pyrochlore iridates,Phys. Rev. B* **83** (2011) 205101.

[91] M. R. Norman, A. Kanigel, M. Randeria, U. Chatterjee and J. C. Campuzano, *Modeling the Fermi arc in underdoped cuprates*, *Phys. Rev. B* **76** (2007) 174501

[92] K.-Y. Yang, T. M. Rice and F.-C. Zhang, *Phenomenological theory of the pseudogap state*, *Phys. Rev. B* **73** (2006) 174501

[93] S. Hong and P. Phillips, *Towards the standard model for Fermi arcs from a Wilsonian reduction of the Hubbard model*, *Phys. Rev. B* **86** (2012) 115118

[94] T. D. Stanescu and G. Kotliar, *Fermi arcs and hidden zeros of the Green function in the pseudogap state*, *Phys. Rev. B* **74** (2006) 125110.

[95] D. Vegh, *Fermi arcs from holography*, arXiv:1007.0246 [hep-th].

[96] F. Benini, C. P. Herzog and A. Yarom, *Holographic Fermi arcs and a d-wave gap*, *Phys. Lett. B* **701** (2011) 626

[97] N. Trivedi, R. T. Scalettar and M. Randeria, *Superconductor-insulator transition in a disordered electronic system*, *Phys. Rev. B* **54** (1996) R3756.

[98] M. Randeria and N. Trivedi, *Pairing correlations above* T_c *and pseudogaps in underdoped cuprates*, *J. Phys. & Chem. Solids* **59** (1998) 1754.

[99] N. Iqbal, H. Liu, M. Mezei and Q. Si, *Quantum phase transitions in holographic models of magnetism and superconductors*, *Phys. Rev. D* **82** (2010) 045002,

[100] S. S. Gubser and A. Nellore, “Ground states of holographic superconductors,” Phys. Rev. D **80** (2009), 105007

[101] G. T. Horowitz and M. M. Roberts, “Zero Temperature Limit of Holographic Superconductors,” JHEP **11** (2009), 015

[102] J. P. Gauntlett, J. Sonner and T. Wiseman, “Holographic superconductivity in M-Theory,” Phys. Rev. Lett. **103** (2009), 151601

[103] J. P. Gauntlett, J. Sonner and T. Wiseman, “Quantum Criticality and Holographic Superconductors in M-theory,” JHEP **02** (2010), 060

[104] David Guarrera and John McGreevy. Holographic Fermi surfaces and bulk dipole couplings. 2011. https://arxiv.org/abs/1102.3908

[105] T. Faulkner, N. Iqbal, H. Liu, J. McGreevy and D. Vegh, *Holographic non-Fermi liquid fixed points*, *Phil. Trans. Roy. Soc. A* **369** (2011) 1640

[106] T. Faulkner, N. Iqbal, H. Liu, J. McGreevy and D. Vegh, *Charge transport by holographic Fermi surfaces*, *Phys. Rev. D* **88** (2013) 045016

[107] Y. Ling , P. Liu , C. Niu ,J.P. Wu , and Z.Y. Xian, *Holographic fermionic system with dipole coupling on Q-lattice*, *Journal of High Energy Physics* **12** (2014), 10.1007/JHEP12(2014)149

[108] C. P. Herzog and D. T. Son, "Schwinger-Keldysh propagators from AdS/CFT correspondence," JHEP **0303**, 046 (2003)

[109] E. D' Hoker and D. Z. Freedman, "Supersymmetric gauge theories and the AdS/CFT correspondence," arXiv:hep-th/0201253.

[110] J. Casalderrey-Solana and D. Teaney, "Heavy quark diffusion in strongly coupled N = 4 Yang Mills," Phys. Rev. D **74**, 085012 (2006)

[111] S. S. Gubser, "Momentum fluctuations of heavy quarks in the gauge-string duality," Nucl. Phys. B **790**, 175 (2008)

[112] J. Casalderrey-Solana and D. Teaney, "Transverse momentum broadening of a fast quark in a N = 4 Yang Mills plasma," JHEP **0704**, 039 (2007)

[113] J. de Boer, V. E. Hubeny, M. Rangamani and M. Shigemori, "Brownian motion in AdS/CFT," arXiv:0812.5112 [hep-th].

[114] D. T. Son and D. Teaney, "Thermal Noise and Stochastic Strings in AdS/CFT," arXiv:0901.2338 [hep-th].

[115] G. C. Giecold, E. Iancu and A. H. Mueller, "Stochastic trailing string and Langevin dynamics from AdS/CFT," arXiv:0903.1840 [hep-th].

[116] P. M. Chesler and L. G. Yaffe, "Horizon formation and far-from-equilibrium isotropization in supersymmetric Yang-Mills plasma," arXiv:0812.2053 [hep-th].

[117] G. C. Giecold, "Heavy quark in an expanding plasma in AdS/CFT," arXiv:0904.1874 [hep-th].

[118] A. Akhavan, M. Alishahiha, A. Davody and A. Vahedy, "Fermions in non-relativistic AdS/CFT correspondence," arXiv:0902.0276 [hep-th].

[119] R. G. Leigh and N. N. Hoang, "Real-Time Correlators and Non-Relativistic Holography," arXiv:0904.4270 [hep-th].

[120] B. C. van Rees, "Real-time gauge/gravity duality and ingoing boundary conditions," arXiv:0902.4010 [hep-th].

[121] C. P. Herzog, M. Rangamani and S. F. Ross, "Heating up Galilean holography," JHEP **0811**, 080 (2008)

[122] J. Maldacena, D. Martelli and Y. Tachikawa, “Comments on string theory backgrounds with non-relativistic conformal symmetry,” JHEP **0810**, 072 (2008)

[123] A. Adams, K. Balasubramanian and J. McGreevy, “Hot Spacetimes for Cold Atoms,” JHEP **0811**, 059 (2008)

[124] M. Le Bellac, “Thermal Field Theory,” CUP (1996).

[125] N. P. Landsman and C. G. van Weert, “Real- and Imaginary-Time Field Theory at Finite Temperature and Density,” Phys. Rept. **145**, 141 (1987).

[126] L. P. Kadanoff and G. Baym, “Quantum Statistical Mechanics: Green’s Function Methods in Equilibrium and Nonequilibrium Problems,” W. A. Benjamin, Inc. (1962).

[127] N. Iqbal and H. Liu, “Universality of the hydrodynamic limit in AdS/CFT and the membrane paradigm,” Phys. Rev. D **79**, 025023 2009 [arXiv:0809.3808 [hep-th]].

[128] C. W. Misner, K. S. Thorne and J. A. Wheeler, “Gravitation,” W. H. Freeman and Cie (1973).

[129] J. Polchinski, “String theory, Volume 2: Superstring theory and beyond,” CUP (2004).

[130] R. Penrose and W. Rindler, “Spinors and space-time: Volume 2, Spinor and twistor methods in space-time geometry,” CUP (1988).

[131] R. Penrose and W. Rindler, “Spinors and space-time: Volume 1, Two-spinor calculus and relativistic fields,” CUP (1988).

[132] E. Newman and R. Penrose, “An Approach to Gravitational Radiation by a Method of Spin Coefficients,” J. Math. Phys. **3**, 566 (1962).

[133] W. G. Unruh, “Second quantization in the Kerr metric,” Phys. Rev. D **10**, 3194 (1974).

[134] M. Srednicki, “Quantum field theory,” CUP (2007).

[135] A. Iliasov, A. A. Bagrov, M. I. Katsnelson and A. Krikun, *Anisotropic destruction of the Fermi surface in inhomogeneous holographic lattices, JHEP* **01** (2020) 065.

[136] H. Jeong, K. Y. Kim, Y. Seo,S. J. Sin and S. Wu, *Holographic spectral functions with momentum relaxation* , *PhysRevD* **102** (2020).

[137] Sera Cremonini, Li Li, Jie Ren, *Spectral Weight Suppression and Fermi Arc-like Features with Strong Holographic Lattices*, *JHEP* **09** (2019) 014.

[138] F. Balm, et.al., *Isolated zeros destroy Fermi surface in holographic models with a lattice*, *JHEP* **01** (2020) 151.

[139] L. N. Trefethen, *Spectral methods in MATLAB*, *SIAM*, Philadelphia, (2000).

[140] J. P. Boyd, *Chebyshev and Fourier spectral methods,* Lecture Notes in Engineering, *S*pringer (1989).

[141] T. Andrade, *Holographic Lattices and Numerical Techniques*, arXiv:1712.00548 [hep-th].

[142] A. Krikun, *Numerical Solution of the Boundary Value Problems for Partial Differential Equations. Crash course for holographer,*

[143] D. Marchenko, D. V. Evtushinsky, E. Golias, A. Varykhalov, Th. Seyller, and O. Rader, *Extremely flat band in bilayer graphene, Sci. Adv.***4** (2018) 11.

[144] R. Rodgers, E. Mauri, U. Gürsoy and H. T. C. Stoof, "Thermodynamics and transport of holographic nodal line semimetals," JHEP **11** (2021), 191 doi:10.1007/JHEP11(2021)191

[145] K. Landsteiner, Y. Liu and Y. W. Sun, "Holographic topological semimetals," Sci. China Phys. Mech. Astron. **63** (2020) no.5, 250001

[146] E. Oh, Y. Seo, T. Yuk and S-J. Sin, *Ginzberg-Landau-Wilson theory for flat band, Fermi-arc and surface states of strongly correlated systems. JHEP***01** (2021) 053.

[147] K. Yang, *Exactly solvable model of Fermi arcs and pseudogap, Phys. Rev. B* **2** (2021).

[148] A. Chikamatsu *et al.*, *Gradual disappearance of the Fermi surface near the metal-insulator transition in* $\mathrm{La_{1-x}Sr_xMnO_3}$ *thin films*, *Phys. Rev.***B76**, 201103 (2007).

[149] H. C. Robarts *et al.*, *Extreme Fermi Surface Smearing in a Maximally Disordered Concentrated Solid Solution, Phys. Rev. Lett.***124** (2020) 046402.

[150] S. Y. Xu, I. Belopolski *et al.*, "Discovery of a Weyl Fermion semimetal and topological Fermi arcs", *Science* **349** (2015),

[151] Noam Morali *et al.*, "Fermi-arc diversity on surface terminations of the magnetic Weyl semimetal $Co_3Sn_2S_2$", *Science* **365** (2019),

[152] Peng Zhang *et al.*, "Observation of topological superconductivity on the surface of an iron-based superconductor", *Science* **360** (2018),

[153] Matteo Baggioli and Oriol Pujolas. On Effective Holographic Mott Insulators. *JHEP*, 12:107, 2016.

[154] Norihiro Iizuka, Nilay Kundu, Prithvi Narayan, and Sandip P. Trivedi. Holographic Fermi and Non-Fermi Liquids with Transitions in Dilaton Gravity. *JHEP*, 01:094, 2012.

[155] P. W. Anderson. *Phys. Rev. Lett.*, 64:1839, 1990.

[156] Varma, Littlewood, Schmitt-Rink, Abrahams, and Ruckenstein. *Phys. Rev. Lett.*, 63:1996, 1989.

[157] E. Gubankova, J. Brill, M. Cubrovic, K. Schalm, P. Schijven and J. Zaanen, Phys. Rev. D **84**, 106003 (2011) doi:10.1103/PhysRevD.84.106003

[158] P. Basu, J. He, A. Mukherjee and H. H. Shieh, "Holographic Non-Fermi Liquid in a Background Magnetic Field," Phys. Rev. D **82**, 044036 (2010) doi:10.1103/PhysRevD.82.044036

[159] T. Andrade, M. Baggioli and A. Krikun, "Phase relaxation and pattern formation in holographic gapless charge density waves," JHEP **03** (2021), 292 doi:10.1007/JHEP03(2021)292

[160] S. Cremonini, L. Li and J. Ren, "Spectral Weight Suppression and Fermi Arc-like Features with Strong Holographic Lattices," JHEP **09** (2019), 014 doi:10.1007/JHEP09(2019)014

[161] F. Balm, A. Krikun, A. Romero-Bermúdez, K. Schalm and J. Zaanen, "Isolated zeros destroy Fermi surface in holographic models with a lattice," JHEP **01** (2020), 151 doi:10.1007/JHEP01(2020)151

[162] Y. Ling, C. Niu, J. P. Wu, Z. Y. Xian and H. b. Zhang, "Holographic Fermionic Liquid with Lattices," JHEP **07** (2013), 045 doi:10.1007/JHEP07(2013)045

[163] Y. Ling, C. Niu, J. P. Wu and Z. Y. Xian, "Holographic Lattice in Einstein-Maxwell-Dilaton Gravity," JHEP **11** (2013), 006 doi:10.1007/JHEP11(2013)006

[164] T. Andrade, A. Krikun, K. Schalm and J. Zaanen, "Doping the holographic Mott insulator," Nature Phys. **14** (2018) no.10, 1049-1055 doi:10.1038/s41567-018-0217-6

[165] S. Cremonini, L. Li and J. Ren, JHEP **12** (2018), 080 doi:10.1007/JHEP12(2018)080

[166] Soo-Jong Rey and Dongsu Bak. String theory on thin semiconductors: Holographic realization of Fermi points and surfaces. *Progress of Theoretical Physics Supplement*, 177:128, 2009.

[167] Tameem Albash and Clifford V. Johnson. Holographic Aspects of Fermi Liquids in a Background Magnetic Field. 2009, 0907.5406.

[168] P. Basu, J. He, A. Mukherjee and H. H. Shieh, "Holographic Non-Fermi Liquid in a Background Magnetic Field," Phys. Rev. D **82**, 044036 (2010) doi:10.1103/PhysRevD.82.044036

[169] Lu, L., Song, M., Liu, W. et al. Magnetism and local symmetry breaking in a Mott insulator with strong spin orbit interactions. *Nat Commun* **8**, 14407 (2017).

[170] Joshua L. Davis, Per Kraus, and Akhil Shah. Gravity Dual of a Quantum Hall Plateau Transition. *JHEP*, 11:020, 2008, 0809.1876.

[171] Esko Keski-Vakkuri and Per Kraus. Quantum Hall Effect in AdS/CFT. *JHEP*, 09:130, 2008, 0805.4643.